

**INVESTIGATION OF OPTIMUM PROCESS PARAMETERS  
FOR COLD SPRAY COATING ON METAL COATED 3D  
PRINTED PART**

Thesis Submitted For the Award of the Degree of

**DOCTOR OF PHILOSOPHY  
in**

**Mechanical Engineering**

**By**

**Harpinder Singh Sandhu**

**41800999**

**Supervised By**

**Dr. Gurpreet Singh Phull (12174)**

**Professor**

**School of Mechanical Engineering**

**Lovely Professional University**

**Co-Supervised by**

**Dr. Tarun Goyal**

**Asst Professor**

**Department of Mechanical Engineering**

**Punjab Technical University**



**L**OVELY  
**P**ROFESSIONAL  
**U**NIVERSITY

*Transforming Education Transforming India*

**LOVELY PROFESSIONAL UNIVERSITY**

**PUNJAB**

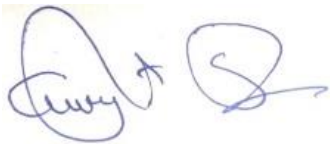
**2023**

## DECLARATION

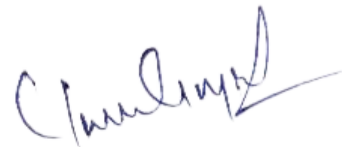
I hereby **certify** that the work which is being presented in the dissertation entitled, **“Investigation of Optimum Process Parameters for Cold Spray Coating on Metal Coated 3D Printed Part”**, by Harpinder Singh Sandhu Registration Number **(41800999)** in partial fulfillment of requirement for the award of the degree of Ph.D. (Mechanical Engineering) submitted in Lovely Professional University, Phagwara, Punjab (India) is an authentic record of my own work carried out during a period from Dec 2018 to Nov 2022 under the supervision of Dr. Gurpreet Singh Phull, Professor and Head of School, School of Mechanical Engineering and Dr. Tarun Goyal, Professor, Mechanical Engineering Department. The matter presented in this thesis has not been submitted by me to any other University / Institute in India or abroad for the award of any degree or diploma.

Signature of the Student

This is to certify that the above statement made by the candidate is correct to the best of my/our knowledge.



Signature of the Supervisor



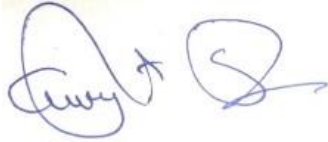
Signature of the Co-Supervisor

## CERTIFICATE

**University Reg. Number: 41800999**

**Name:** Harpinder Singh Sandhu

**Title of Dissertation: Investigation of Optimum Process Parameters for Cold Spray Coating on Metal Coated 3D Printed Part.** We the below signed, after checking the dissertation mentioned above and the official record book (s) of the student, hereby state our approval of the dissertation submitted in partial fulfillment of the requirement of the degree of Doctor of Philosophy in Mechanical Engineering at Lovely Professional University, Phagwara, Punjab (India). We are satisfied with the volume, quality, correctness, and originality of the work.



Signature of the Supervisor



Signature of the Co-Supervisor

## ACKNOWLEDGEMENTS

First and Foremost, I would like to express my sincere gratitude with pride and pleasure to my supervisor **Prof. Dr. Gurpreet Singh Phull and Dr. Tarun Goyal**, for introducing me to the research topic **Investigation of Optimum Process Parameters for Cold Spray Coating on Metal Coated 3D Printed Part** and enlightening me about research. His engagement in my learning process with patience and motivation throughout the course of this research work is thankfully acknowledged. His thoughtful guidance helped me in all the time of research and writing of this thesis. I am very grateful to Dr. Vijay Kumar, Head of the School, Mechanical Engineering, Lovely Professional University for extending the facilities which needed at various stages of this work. Also special thanks to all my colleagues of School of Mechanical Engineering for their extensive discussions around my work and moral support.

Besides my major advisor, I would like to thank the Dr. Sumit Shoor, Rajeev Dhiman, Dr. Swastih Pradhan, Dr. Jaiinder Preet Singh Dr. Piyush Gulati and Dr. Jaspreet Singh for helping me for preparation of experimental set up from design to fabrication. I also would like to thank the rest of my research advisory committee for insightful comments and valuable advice during my progress evaluations. I am extremely grateful to my parents and family for their love, prayers, caring and sacrifices for educating and preparing me for my future.

I express our sincere thanks and gratitude to university authority for allowing me to undergoing my research work.

Harpinder Singh Sandhu  
Lovely Professional University



## ABSTRACT

With the increase in demand for faster production, new product developments and different materials, conventional mode of machining is proved inefficient in meeting the new challenges of manufacturing. In conventional manufacturing process production of a tool would require multiple stages such as designing, programming and machining where each stage would consume time individually and only one tool can be produced at a given point of time. Conventional machining consumes more time in this fast-paced production requirements. The industry is continuously looking to bring down the lead time and cost of production. From past few years research is being carried out to develop various standalone and hybrid manufacturing processes to meet the challenges of Industry4.0.

In this present research work, a new hybrid approach combining the advantages of 3D printing, electroplating process and cold spray for production of multiple parts at a given point of time simultaneously and in least possible time is explored. This research also provides data which can be used to manufacture best products by changing some machine parameters.

In 3D printing the parts are created by depositing the material layer by layer, without any constraint for the shape, dimension and size. The material actually added step by step in a 2-dimensional plane, one upon another to generate final 3-dimensional shape. The machines are developed to create a part from any material, ranging from wax, plastic, metal, cement, food and tissue cells, etc. The major processes evolved in 3D printing so far are fusion deposition modelling, stereolithography, selective laser sintering and laminated object manufacturing.

The FDM process is selected for this work owing to its economical and accessibility advantages over the other 3D printing process. The ABS parts were produced on Ultimaker FDM machine at the optimum settings suggested by literature to get the best part in terms of strength and surface finish parameters.

On 3D printed part metallization is done using a well-known technique of electroplating. The electroplating process requires two electrodes (anode and cathode) immersed in a conducting electrolyte containing metallic salts and a source of electric (DC) power. As current flows through the circuit, metal ions in the solution are converted into atoms and deposited on the cathode (3D part in this case) creating a

metal layer. The electroplated component maintains the accuracy for the shape as of 3D printed part. Previous researches demonstrated that this technique has high potential in the field of rapid tooling due to the following advantages like reproducibility of even the smallest detail of the model surface and strict control over the physical and mechanical properties of the part by selecting the composition of the solution and process conditions. The electroplated part lacks the strength to be used as an option for production tooling, so further strengthening is required by depositing thick layers of metal onto it.

One such method to deposit thick layer is further extension of electroplating to electroforming process. In this case, the metallic shell is grown-up by electroforming around the model or prototype of desired polymer part fabricated by 3D printing or machining. However, the disadvantage of this technique is a long operation time needed for creating of thick layers. For example, deposition of layer with thickness about 3 mm takes several days. It could be suggested that the possible way to decrease the fabrication time of such object is to apply another coating deposition technique for deposition of thermo-conductive copper layer. In other words, one can consider the following procedure of fabrication of tool. Firstly, the 3D part is metalized using electroplating in order to reproduce with high precision geometry of prototype. After that, the copper layer is thickened rapidly using some high productive rate coating deposition technology in this case Cold spray coating. Cold gas dynamic spray technique commonly called as cold spray is a thermal spray coating process whereby the coating formation is achieved by using cold particles on cold substrate that is why name, cold spray. Other thermal spray techniques use the particle temperature as the criterion for achieving bonding with the substrate where as cold spray uses particle velocity as the principle. As the cold-spray process does not normally involve the use of a high-temperature heat source, it generally offers a number of advantages over the thermal-spray material deposition technologies such as high velocity oxy-fuel, detonation gun, plasma spray, and arc spray. Other than eliminating the deleterious high temperature effects, cold sprayed coatings have good electrical and thermal conductivities. Cold spray of the materials like copper, solder and polymeric coatings offers exciting new possibilities for cost-effective and environmentally friendly alternatives to technologies such as electroplating, soldering and painting.

Copper electroplating parameters and their ranges for this research were selected on the basis of the recommendations of the literature and industry. Setup parameters optimization was conceded out by using L9 orthogonal array of Taguchi experimental design. The first experiment for optimization of copper electroplating had voltage, CuSO<sub>4</sub> solution concentration and time as input process parameters to establish the orthogonal array. All the process parameters were tested with a set of nine experiments as per orthogonal array. The response parameters observed under the experimentation were surface roughness and metal deposition thickness.

It was found that deposition rate is mostly affected by voltage (45.24%) followed by the CuSO<sub>4</sub> concentration (39.65%) as the second major contributor in case of copper electroplating. The surface roughness has CuSO<sub>4</sub> concentration as a major contributor (68.75 %) with no significant effect by voltage and time.

After metallization of 3D printed part, the thickness of the shell is increased by exposing a metallic substrate to a high velocity (300–1200 m/s) jet of small 50 $\mu$ m particles accelerated by a supersonic jet of compressed gas. Cold spray coating parameters and their ranges for this research were selected on the basis of the recommendations of the literature. Setup parameters optimization was conceded out by using L9 orthogonal array of Taguchi experimental design. The experiment for optimization of copper cold spray coating had temperature, pressure and standoff distance as input process parameters to establish the orthogonal array. All the process parameters were tested with a set of nine experiments as per orthogonal array. The response parameters observed under the experimentation were surface roughness and hardness.

It was found that surface roughness is affected equally by all the parameters considered for study i.e. Gas Temperature (30.10 %), Pressure (37.25 %) and Standoff Distance (31.07%). The Standoff Distance (75.05%) found to be most influential process parameters as far as hardness of the coating is concerned, followed by Gas Temperature (24.16%) and Pressure has the negligible impact on hardness.

The surface morphology shows the growth of the grains during the deposition in the SEM images from coarse grains to fine grains. The SEM images of plastic and metal interface reveal proper bonding. EDS of the sample in three regions reveal the material weight percentage. The XRD analysis confirms that the composition of the

electroplated and spray coated copper is confirming to the standard pattern list of copper and the peaks are matched with the standard.

It can easily be concluded that this method of fabricating is less time consuming and economical even in case of complex geometries.

## **ORGANIZATION OF THESIS**

The research work has been presented as per the following chapters:

### **Chapter 1: Introduction**

This chapter discusses the need for rapid tooling, gives an introduction to the rapid tooling manufacturing methods. Research gaps have been identified in the context of indirect tooling requirements. Objectives, scope and overall methodology of the experimental work have been outlined.

### **Chapter 2: Literature Review**

In this chapter published works of various researchers working in the domain of additive manufacturing has been reviewed and presented. The literature review has been divided into three segments explaining about developments in (a) rapid prototyping (b) electroplating (c) cold spray coating

### **Chapter 3: Experimental Setup and Process Parameter Selection**

This chapter gives a detailed account of the experimental setup and the equipment used for measurement of different performance characteristics of FDM and electroforming (Bath concentration, Temperature, Current, Voltage, Current Density and pH) and their evaluation criterion.

### **Chapter 4: Experimental Design Methodology**

This chapter gives a detailed account of the design of study, Taguchi approach for design of experiments and the selection of various input process parameters and response characteristics.

### **Chapter 5: Experimentation**

This chapter is comprised of results obtained in experimentation in linear study & optimization of electroforming process. The process of mould manufacturing after the process optimization is also presented in this chapter.

## **Chapter 6: Analysis and Discussion of the Results**

The chapter describes the detail discussion on the results obtained from various tests and about material characterization using SEM, XRD and hardness analysis. The results of FEM analysis on conformal cooling has also been presented.

## **Chapter 7: Conclusions and Scope for Future Work**

The conclusions of the research work and results obtained are presented. Recommendations and scope for the future research have also been reported.

# CONTENTS

<u>TITLE</u>	<u>PAGE NO.</u>
DECLARATION	i
CERTIFICATE	ii
ACKNOWLEDGEMENT	iii
ABSTRACT	iv
ORGANIZATION OF THESIS	viii
CONTENTS	x
LIST OF FIGURES	xiv
LIST OF TABLES	xviii
NOMENCLATURE AND ACRONYMS	xx
CHAPTER 1: INTRODUCTION	1-26
1.1    RAPID PROTOTYPING	2
1.2    RAPID PROTOTYPING TECHNIQUES	3
1.2.1    STEREOLITHOGRAPHY	3
1.2.2    SELECTIVE LASER SINTERING	3
1.2.3    DIRECT METAL LASER SINTERING	4
1.2.4    THREE DIMENSIONAL PRINTING	4
1.2.5    LAMINATED OBJECT MANUFACTURING	5
1.2.6    FUSED DEPOSITION MODELING	5
1.2.6.1    PROCESS OF FUSED DEPOSITION MODELING	6
1.3    RAPID TOOLING METHODS	7
1.3.1    DIRECT TOOLING	7
1.3.2    INDIRECT TOOLING	12
1.3.2.1    SOFT TOOLING	12
1.3.2.2    HARD TOOLING	13
1.4    ELECTROPLATING	14
1.4.1    PROCESS OF COPPER ELECTROPLATING	15
1.5    THERMAL SPRAYING	15
1.5.1    FLAME SPRAYING	16
1.5.2    PLASMA SPRAYING	16

1.5.3	WIRE ARC SPRAYING	17
1.5.4	DETONATION SPRAYING	17
1.5.5	HIGH VELOCITY OXYGEN FUEL SPRAYING (HVOF)	17
1.5.6	WARM SPRAYING	17
1.5.7	COLD SPRAY	18
1.5.7.1	SYSTEMS OF COLD SPRAYING	18
1.5.7.2	EQUIPMENT OF COLD SPRAYING	19
1.5.7.3	MECHANISM OF COLD SPRAY	20
1.5.7.4	PROCESS PARAMETERS EFFECTING DEPOSITION	22
1.5.7.4.1	Particle Velocity	22
1.5.7.4.2	Nozzle Geometry	23
1.5.7.4.3	Carrier Gas	23
1.5.7.4.4	Pressure and Temperature	24
1.5.7.4.5	Particle Size	25
1.6	MOTIVATION FOR WORK	25
1.7	OBJECTIVES	25
1.8	RESEARCH METHODOLOGY	26
CHAPTER 2:	LITERATURE REVIEW	27-66
2.1	RAPID PROTOTYPING AND RAPID TOOLING	27
2.2	ELECTROPLATING	42
2.3	COLD SPRAY	49
CHAPTER 3:	EXPERIMENTAL SETUP AND PROCESS PARAMETER SELECTION	67-88
3.1	3D CAD MODEL OF SELECTED SAMPLES	68
3.1.1	3D CAD MODEL OF SELECTED SAMPLES	69
3.1.2	FUSED COATING MODELING 3D PRINTING APPARATUS	69
3.1.3	ABS MATERIAL	73
3.2	ELECTROPLATING OF 3D PRINTED PART	74
3.2.1	SURFACE PREPARATION FOR COATING	74



3.2.2	ELECTROPLATING PROCESS ELEMENTS AND SOLUTIONS	76
3.2.3	FUNDAMENTALS OF ELECTROCHEMISTRY	78
3.2.3.1	OXIDATION AND REDUCTION	78
3.2.3.2	REACTIONS AT ANODE AND CATHODE	79
3.2.3.3	ELECTROPLATING SETUP	79
3.2.4	PROCESS PARAMETERS	82
3.3	COLD SPRAY COATING ON METALIZED PARTS	82
3.3.1	DESIGN OF COLD SPRAY GUN NOZZLE	82
3.3.2	DESIGN OF COLD SPRAY GUN GAS HEATER	83
3.3.3	DESIGN OF COLD SPRAY GUN CASING AND MOUNTINGS	84
3.3.4	DESIGN OF COLD SPRAY GUN MACHINING TOOLS	86
3.3.5	FABRICATION OF APPARATUS	86
3.3.6	PROCESS PARAMETERS	88
CHAPTER 4:	EXPERIMENTAL DESIGN METHODOLOGY	89-108
4.1	DESIGN METHODOLOGY	89
4.1.1	TAGUCHI APPROACH FOR DOE	90
4.1.2	DESIGN OF EXPERIMENTS STRATEGY	91
4.1.3	SELECTION OF ORTHOGONAL ARRAY	93
4.1.4	SIGNAL TO NOISE RATIO FOR RESPONSE PARAMETERS	95
4.1.5	ANALYSIS OF VARIANCE (ANOVA)	98
4.2	DATA MEASUREMENT	100
4.2.1	MEASUREMENT OF THICKNESS	100
4.2.2	SURFACE ROUGHNESS MEASUREMENT	103
4.2.3	HARDNESS TESTING	104
4.2.4	MICROSTRUCTURE	105
CHAPTER 5:	EXPERIMENTATION	109-149
5.1	OPTIMIZATION OF COPPER ELECTROPLATING PROCESS PARAMETERS	109

5.1.1	EXPERIMENTAL STUDY OF COPPER ELECTROPLATING FOR DEPOSITION THICKNESS	110
5.1.2	EXPERIMENTAL STUDY OF COPPER ELECTROPLATING FOR SURFACE ROUGHNESS	121
5.2	OPTIMIZATION OF COPPER COLD SPRAY COATING PROCESS PARAMETERS	130
5.2.1	EXPERIMENTAL STUDY OF COLD SPRAYED COPPER COATING SURFACE ROUGHNESS	130
5.2.2	EXPERIMENTAL STUDY OF COLD SPRAYED COPPER COATING HARDNESS	140
CHAPTER 6: ANALYSIS AND DISCUSSION OF THE RESULTS		150-170
6.1	SURFACE MORPHOLOGY STUDIES USING SEM	150
6.1.1	SURFACE ENHANCEMENT OF THE FDM PART	151
6.1.2	SURFACE MORPHOLOGY OF ELECTROPLATING COPPER DEPOSITION	152
6.1.3	SURFACE MORPHOLOGY OF COLD SPRAY COPPER DEPOSITION	165
6.2	XRD ANALYSIS OF COPPER DEPOSITION	169
CHAPTER 7: CONCLUSIONS AND SCOPE FOR FUTURE WORK		171-176
7.1	CONCLUSIONS	171
7.2	SCOPE FOR FUTURE WORK	173
REFERENCES		175
APPENDIX A		199
APPENDIX B		200
APPENDIX C		202

## LIST OF FIGURES

<b>Figure No.</b>	<b>Title</b>	<b>Page No.</b>
<b>Fig. 1.1</b>	Stages of Rapid Prototyping Process	2
<b>Fig. 1.2</b>	Equipment for Fused Deposition Modelling	7
<b>Fig. 1.3</b>	Classifications of Rapid Tooling	9
<b>Fig. 1.4</b>	Epoxy Moulds	10
<b>Fig. 1.5</b>	Engine Intake Manifold, Made Using DSPC	10
<b>Fig. 1.6</b>	Micro Cast Die	11
<b>Fig. 1.7</b>	Metal Tooling Process Chain	11
<b>Fig. 1.8</b>	Silicon Mould	12
<b>Fig. 1.9</b>	Metal Spray Technique	14
<b>Fig. 1.10</b>	Schematic of Electroplating Process	15
<b>Fig. 1.11</b>	Schematic of Thermal Spraying Process	16
<b>Fig. 1.12</b>	Cold Spray Apparatus	20
<b>Fig. 1.13</b>	Particle's Effect on the Substrate at Different Times	21
<b>Fig. 1.14</b>	Energy Dispersive Spectrometry Image of Copper Coating on Aluminium	22
<b>Fig. 3.1</b>	Process Flow Chart of Cold Spray Coating of Metallized 3D Printed Parts	68
<b>Fig. 3.2</b>	CAD Model of Sample Component for Copper Electroplating	69
<b>Fig. 3.3</b>	CAD Model of Sample Component for Cold Spray Coating	70
<b>Fig. 3.4</b>	FDM Apparatus used in Experimentation	71
<b>Fig. 3.5</b>	Feed System for Model and Support Material	72
<b>Fig. 3.6</b>	Chemical Formula of ABS	74
<b>Fig. 3.7</b>	Activation of Plastic with Conductive Paint	75
<b>Fig. 3.8(a)</b>	Chemically Treated Components	76
<b>Fig. 3.8(b)</b>	Components after Conductive Paint Coat	76
<b>Fig. 3.9</b>	Schematic of Electroplating Setup	77
<b>Fig. 3.10</b>	Copper Electroplating Setup	80
<b>Fig. 3.11</b>	Titanium Plating Racks	81
<b>Fig. 3.12</b>	Direct Current Rectifier	82

<b>Fig. 3.13</b>	Sketch Showing Optimal Parameters of De-Laval Nozzle Core	83
<b>Fig. 3.14</b>	Fluid Flow Simulation of De-Laval Nozzle Performed In CAE Software	83
<b>Fig. 3.15</b>	CAD Model of Gas Heater	83
<b>Fig. 3.16</b>	CAD Models of Gun Casing and Mountings	84
<b>Fig. 3.17</b>	CAD Models of Complete Assembly	84
<b>Fig. 3.18</b>	Fluid Flow Simulation on Gun Assembly	85
<b>Fig. 3.19</b>	Fluid Flow Simulation on Nozzle and Gun Assembly	85
<b>Fig. 3.20</b>	CAD Models Showing The Nozzle and The EDM Tooling Design	86
<b>Fig. 3.21</b>	Photograph of Tools for Electro-Discharge Machining of De-Laval Nozzle	86
<b>Fig. 3.22</b>	Photograph of Manufactured De-Laval Nozzle	87
<b>Fig. 3.23</b>	Photograph of Manufactured Gas Heater	87
<b>Fig. 3.24</b>	Photograph of Gun Casing and Mountings	87
<b>Fig. 3.25</b>	Photograph of The Complete Cold Spray System	88
<b>Fig. 4.1</b>	Process Flow Chart for Taguchi DOE	93
<b>Fig. 4.2</b>	Taguchi Quadratic Loss Function	96
<b>Fig. 4.3</b>	Smaller-the-Better and Larger-the-Better Loss Function	97
<b>Fig. 4.4</b>	Thickness Measurement by Screw Gauge Micrometer	101
<b>Fig. 4.5</b>	Thickness Measurement by Eddy Current Probe	102
<b>Fig. 4.6</b>	Roughness Testing Equipment	104
<b>Fig. 4.7</b>	Vickers-Hardness Tester	105
<b>Fig. 4.8</b>	Inverted Metallurgical Microscope	106
<b>Fig. 4.9(a)</b>	FE-Scanning electron Microscope (SEM)	107
<b>Fig. 4.9(b)</b>	Gold Sputtering Coater	107
<b>Fig. 4.9(c)</b>	X-Ray Diffractometer	108
<b>Fig. 5.1</b>	FDM Produced ABS Component for Copper Deposition	109
<b>Fig. 5.2 (a)</b>	Effect of Voltage on Deposition Thickness and its S/N Ratio	112
<b>Fig. 5.2 (b)</b>	Effect of CuSO <sub>4</sub> Concentration on Deposition Thickness and its S/N Ratio	113
<b>Fig. 5.2 (c)</b>	Effect of Time on Deposition Thickness and its S/N Ratio	113
<b>Fig. 5.3</b>	Interaction Plot for Means of Deposition Thickness	116

<b>Fig. 5.4</b>	Residual Plots for Mean Data of Deposition Thickness	120
<b>Fig. 5.5</b>	Residual Plots for S/N Data of Deposition Thickness	120
<b>Fig. 5.6 (a)</b>	Effect of Voltage on Surface Roughness and its S/N Ratio	123
<b>Fig. 5.6 (b)</b>	Effect of CuSO <sub>4</sub> Concentration on Surface Roughness and its S/N Ratio	123
<b>Fig. 5.6 (c)</b>	Effect of Time on Surface Roughness and its S/N Ratio	124
<b>Fig. 5.7</b>	Interaction Plot for Means of Surface Roughness	126
<b>Fig. 5.8</b>	Residual Plots for Means Surface Roughness	129
<b>Fig. 5.9</b>	Residual Plots for S/N Surface Roughness	129
<b>Fig. 5.10 (a)</b>	Effect of Temperature on Surface Roughness and its S/N Ratio	132
<b>Fig. 5.10 (b)</b>	Effect of Gas Pressure on Surface Roughness and its S/N Ratio	133
<b>Fig. 5.10 (c)</b>	Effect of Standoff Distance on Surface Roughness and its S/N Ratio	133
<b>Fig. 5.11</b>	Interaction Plot for Means of Surface Roughness	135
<b>Fig. 5.12</b>	Residual Plots for Means of Surface Roughness	139
<b>Fig. 5.13</b>	Residual Plots for S/N Ratios Surface Roughness	139
<b>Fig. 5.14 (a)</b>	Effect of Temperature on Hardness and its S/N Ratio	142
<b>Fig. 5.14 (b)</b>	Effect of Gas Pressure on Hardness and its S/N Ratio	142
<b>Fig. 5.14 (c)</b>	Effect of Standoff Distance on Hardness and its S/N Ratio	143
<b>Fig. 5.15</b>	Interaction Plot for Means of Hardness	145
<b>Fig. 5.16</b>	Residual Plots for Means of Hardness	148
<b>Fig. 5.17</b>	Residual Plots for S/N Ratios of Hardness	149
<b>Fig. 6.1</b>	SEM Image of FDM Part as Fabricated	151
<b>Fig. 6.2</b>	SEM Image of FDM Part after Treatment	151
<b>Fig. 6.3 (a)</b>	SEM Image of Sample at 2.0 mm	152
<b>Fig. 6.3 (b)</b>	SEM Image of Sample at 500 $\mu$ m	153
<b>Fig. 6.4</b>	SEM Image of Specimen of Inside Area	153
<b>Fig. 6.5</b>	EDS Image of the Specimen of Inside Area	154
<b>Fig. 6.6</b>	SEM Image of Specimen at the Merging Zone	155
<b>Fig. 6.7</b>	EDS Image of the Specimen of Merging Zone	155
<b>Fig. 6.8</b>	SEM Image of the Copper Area	156
<b>Fig. 6.9</b>	EDS Image of the Copper Area	157

<b>Fig. 6.10</b>	Mapping of the Elements in the Inside Area of the Specimen	158
<b>Fig. 6.11</b>	Mapping of the Element in the Merging Zone of the ABS Plastic and Copper	159
<b>Fig. 6.12</b>	Mapping of Elements Present in the Copper Deposition Zone	160
<b>Fig. 6.13</b>	SEM Image of the Top Surface of the Electroplated Specimen	161
<b>Fig. 6.14</b>	EDS of Top Surface of the Electroplated Specimen	161
<b>Fig. 6.15</b>	Mapping of the Element in the Top Surface of the Electroplated Specimen	163
<b>Fig. 6.16</b>	SEM Image at Different Magnification of Top Surface of Electroplated Surface	164
<b>Fig. 6.17</b>	SEM Image of Samples at Interface Zone of Copper Plating and ABS	165
<b>Fig. 6.18</b>	SEM Image of Cold Spray Copper Coating	166
<b>Fig. 6.19</b>	SEM Images of Bonding between Cold Sprayed Copper Coating and Electroplated Interface	166
<b>Fig. 6.20</b>	Mapping of the Element in the Cold Sprayed Region of the Specimen	167
<b>Fig. 6.21</b>	EDS of the Cold Sprayed Region of the Specimen	167
<b>Fig. 6.22</b>	SEM Image of Top Surface of Different Cold Spray Coated Samples	168
<b>Fig. 6.23</b>	XRD Image of Copper Deposition	170

## LIST OF TABLES

<b>Table No.</b>	<b>Title</b>	<b>Page No.</b>
<b>Table 1.1</b>	Properties of Stereolithography	3
<b>Table 1.2</b>	Properties of Selective Laser Sintering	3
<b>Table 1.3</b>	Properties of Direct Metal Laser Sintering	4
<b>Table 1.4</b>	Properties of Three Dimensional Printing	5
<b>Table 1.5</b>	Parameters for Laminated Object Manufacturing	5
<b>Table 1.6</b>	Parameters for Fused Deposition Modeling	6
<b>Table 1.7</b>	Cold Spraying Techniques at Low and High Pressure	19
<b>Table 2.1</b>	The Process Parameters for Minimum Surface Roughness	38
<b>Table 2.2</b>	Machine Parameters and Their Effect on Mechanical Properties	41
<b>Table 2.3</b>	Cold Spraying Parameters for Different Materials and Substrate	59
<b>Table 2.4</b>	Properties of Cold Sprayed Layer and The Testing Method	64
<b>Table 3.1</b>	Specifications of the FDM Machine	72
<b>Table 3.2</b>	Copper Electroforming Bath Solutions	78
<b>Table 3.3</b>	Parameters for Copper Electroplating	82
<b>Table 3.4</b>	Parameters for Cold Spray Coating	88
<b>Table 4.1</b>	Orthogonal Array	91
<b>Table 4.2</b>	Standard Design of Experiments for Taguchi's L9 Orthogonal Array	94
<b>Table 4.3</b>	DOE Employing Taguchi's L9 Orthogonal Array for Copper Electroplating	95
<b>Table 4.4</b>	DOE Employing Taguchi's L9 Orthogonal Array for Cold Spray Copper Coating	95
<b>Table 4.5</b>	ANOVA Table	99
<b>Table 5.1</b>	Parameters for Copper Electroforming	110
<b>Table 5.2</b>	Thickness Deposition observation and calculated S/N ratios	111
<b>Table 5.3</b>	Mean Values by Factor Level for Deposition Thickness	112
<b>Table 5.4</b>	Deposition Thickness Confirmatory Experiment Observation	114
<b>Table 5.5</b>	ANOVA Table	116
<b>Table 5.6</b>	ANOVA Table for Copper Coating Thickness	117

<b>Table 5.7</b>	ANOVA Table of S/N Data for Copper Deposition Thickness	119
<b>Table 5.8</b>	Copper Electroplating Surface Roughness Observation and Calculated S/N Ratios	122
<b>Table 5.9</b>	Copper Electroplating Mean Values by Factor Level for Surface Roughness	122
<b>Table 5.10</b>	ANOVA Table of S/N Data for Copper Electroplating Surface Roughness	126
<b>Table 5.11</b>	ANOVA Table of Mean Data for Copper Electroplating Surface Roughness	128
<b>Table 5.12</b>	Cold Spray Surface Roughness observation and Calculated S/N Ratios	131
<b>Table 5.13</b>	Mean Values by Factor Level for Cold Spray Surface Roughness	132
<b>Table 5.14</b>	ANOVA Table of Mean Data for Cold Spray Surface Roughness	136
<b>Table 5.15</b>	ANOVA Table of S/N data for Cold Spray Surface Roughness	138
<b>Table 5.16</b>	Hardness Observation and Calculated S/N Ratios	141
<b>Table 5.17</b>	Mean Values by Factor level for Hardness	141
<b>Table 5.18</b>	Confirmatory Experiment for Hardness Observation	144
<b>Table 5.19</b>	ANOVA Table for Mean Data for Hardness	145
<b>Table 5.20</b>	ANOVA Table of S/N Data for Hardness	148
<b>Table 6.1</b>	Weight Percentage Distribution of the Element of Inside Area	154
<b>Table 6.2</b>	Weight Percentage Distribution of the Element of Merging Zone	156
<b>Table 6.3</b>	Weight Percentage Distribution of the Copper Area of Specimen	157
<b>Table 6.4</b>	Weight Percentage distribution of the Elements on the Top Surface of the Specimen Electroplating Operation	162
<b>Table 6.5</b>	Weight Percentage Distribution of the Elements in the Cold Sprayed Surface	168



## NOMENCLATURE AND ACRONYMS

---

### NOMENCLATURE

Symbol	Notation	Unit
Ra	Average Surface Roughness Number	$\mu m$
HV	Vickers Hardness Scale	---
$I$	Current	Ampere(A)
$\delta$	Deposition Thickness	cm
$\rho$	Density	gm/cm <sup>3</sup>
$n$	Number of electrons	
$F$	Faraday's Constant	C/mole
t	time	sec
$M_w$	Atomic Weight	gm/mole
W	Weight	gm
$S_a$	Surface Area	cm <sup>2</sup>
A <sub>3</sub> B <sub>2</sub> C <sub>1</sub>	Factors at different Levels of treatments	
$\eta_{opt}$	S/N Ratios at Optimum Levels	dB
m	Overall Mean of S/N ratio	mm for deposition thickness $\mu m$ for Surface Roughness
$m_{A3}$	Mean of S/N data for factor A at level 3	mm for deposition thickness $\mu m$ for Surface Roughness
$y_{opt}$	Calculated Response	mm for deposition thickness $\mu m$ for Surface Roughness

## **ACRONYMS**

3DP	Three Dimensional Printing
ABS	Acrylonitrile Butadiene Styrene
AM	Additive Manufacturing
ANOVA	Analysis of Variance
CS	Cold Spray
CuSO <sub>4</sub>	Copper Sulphate Solution
CVS	Cold Vapour Smoothing
DC	Direct Current
DOF or DF	Degree of freedom
DOE	Design of Experiments
DMLS	Direct Metal Laser Sintering
EDM	Electrical Discharge Machining
FDM	Fused Deposition Modelling
H <sub>2</sub> SO <sub>4</sub>	Sulphuric Acid
LOM	Laminated Object Manufacturing
L1, L2, L3	Levels of Input Process Parameters
MS	Mean of square
P %	Percentage Contribution
PVC	Polyvinyl Chloride
RP	Rapid Prototyping
RT	Rapid Tooling
SEM	Scanning Electron Microscope
SLA or SL	Stereo-lithography
SLS	Selective Laser Sintering
S/N	Signal-to-Noise Ratio
SS	Sum of squares
XRD	X-Ray Diffraction

The focus of all industries in today's rapidly evolving and developing world is product life management. As the life span of any product is shortening in the market, customer is always in the search of new better product at even lesser price that was paid for the previous product.

This puts a lot of pressure on the product development team to introduce new products one after another to the market. To meet these challenges fast methods of designing development and manufacturing are being explored by industry, researchers or academia. Last few decades has seen a lot of advancement of CAD, CAE and CAM systems to reduce the development cycle of the product. As far as product development at digital level is concerned many optimized CAD and CAE solutions are available. But the problem which is still challenging is the manufacturing of the prototype. One area which is growing since last two decades or so is the additive manufacturing (AM), known as rapid prototyping.

There are various methods for developing rapid prototypes such as Fused Deposition Modeling (FDM), Stereo-lithography (SLA), Laminated Object Manufacturing (LOM), Selective Laser Sintering (SLS), 3D printing (3DP) among others. These methods are quite effective at creating prototypes out of a range of materials, including Nylon, ceramic, ABS, metal, and aluminium, among others but they are not the economical options for mass production of components. Another limitation of direct RT technology is the ranges of materials available are limited and there are few issues with the mechanical properties of the pattern or moulds. For mass production still the traditional processes like casting, die casting, injection moulding or investment casting are being used.

In recent years, rapid prototyping machines have been utilized for creating tooling necessary for conventional processes. These rapid tooling (RT) development techniques help in reducing the cycle time for the development of patterns, moulds, cores etc. Direct fast tooling and indirect rapid tooling are the two options currently being investigated or employed for the development of rapid tooling. Despite the lack of development in direct metal part fabrication with additive manufacturing, indirect

processes were identified and proven workable with the integration of AM with conventional fabrication process.

### 1.1 RAPID PROTOTYPING

Rapid prototyping is a technique that uses part created by computer-aided design to quickly produce a physical model of a part or assembly. Additive manufacturing is the current term used to refer to rapid prototyping. RP technologies have the ability to produce physical prototypes from computer-aided design (CAD) data automatically. It has most recently been generally categorised as additive manufacturing. The system's greatest benefit is its ability to manufacture practically any shape. These methods use solid free-form fabrication approaches that use CIM (computer automated manufacturing). The part is constructed by layering small sections of the CAD model on top of one another.

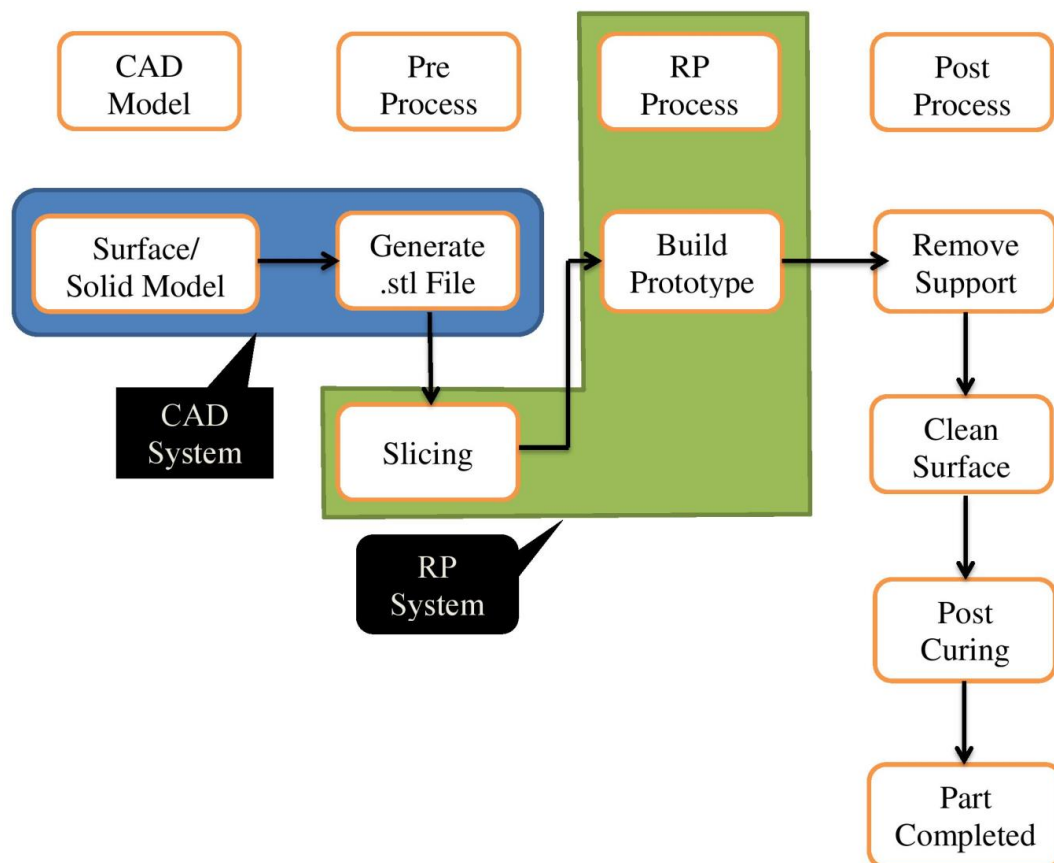


Figure 1.1 Stages of Rapid Prototyping Process

There are four basic stages CAD model generation, pre-processing, 3D printing and post processing as shown in figure 1.1. The majority of fast prototyping processes

employ plastics; however, there are others that also directly use metals in the form of powders and strips.

## 1.2 RAPID PROTOTYPING TECHNIQUES

The different categories of rapid prototyping methods include Stereo Lithography (SLA), Fused Deposition Modeling (FDM), Selective Laser Sintering (SLS), 3D Printing (3DP), Direct metal laser sintering (DMLS), and Laminated Object Manufacturing (LOM).

### 1.2.1 STEREOLITHOGRAPHY

The extensively used prototyping technology is stereo lithography. It is capable of producing incredibly accurate and detailed polymer components. The earliest method for quick prototyping was stereo lithography. In 1988, 3D Systems Inc. got a patent. In stereo lithography, a three-dimensional object is produced in a photosensitive liquid polymer vessel using a low-power, highly concentrated ultraviolet laser.

Table 1.1 Properties of Stereolithography (Hashmi, 2014)

Material type:	Liquid (Photopolymer)
Materials:	Thermoplastics (Elastomers)
Minimum layer thickness:	0.02mm
Surface finish:	4 $\mu$ m
Build speed:	720 mm/hr

### 1.2.2 SELECTIVE LASER SINTERING

Similar to stereolithography, selective laser sintering technology operates on a fundamental level. In 1989, a patent was granted for a method that utilizes a laser beam to selectively sinter metal, composite, and/or polymer powders by following the tool's path.

Table 1.2 Properties of Selective Laser Sintering (Maamoun et al., 2018)

Material type:	Powder (Polymer)
Materials:	Nylon, Polyamide, Polystyrene and Composites
Minimum layer thickness:	0.10mm
Surface finish:	6 $\mu$ m
Build speed:	60 mm/min

### 1.2.3 DIRECT METAL LASER SINTERING

DMLS was the initial commercially accessible method for producing metal items in a single step during prototyping. It was developed in 1994 by Rapid Prototyping Innovations in tandem with EOS GmbH. By skimming a powerful laser beam over the metal powder, this method melts the metal powder without using any binders. In comparison to other additive methods, direct metal laser sintering generates high density parts that can reach 98%. Additionally, because the raw material particles are so tiny, this technology enables the production of parts with incredible levels of detail.

Table 1.3 Properties of Direct Metal Laser Sintering (Yu, 2005)

Material type:	Metal Powder
Materials:	Aluminum, Bronze, Cobalt-chrome Steel alloys, Stainless Steel, Tool Steel, Titanium, Ceramics.
Minimum layer thickness:	0.02mm
Surface finish:	8.75 $\mu\text{m}$
Build speed:	7.0 m/s

### 1.2.4 THREE DIMENSIONAL PRINTING

Similar to SLS and 3DP it uses an ink-jet printing head to deposit a liquid adhesive that fuses the material together rather than utilizing a laser to sinter it. The MIT is where three-dimensional printing technology was created.

Three-dimensional printing has the benefit of being somewhat more affordable than other additive techniques, despite the fact that the material options are limited. A quick technology, three-dimensional printing can print two to four layers per minute. It performs worse than other rapid prototyping techniques in terms of the part's tensile strength, precision, and surface polish. Furthermore, sealant reinforcement is necessary to improve the finished component's strength and surface gloss.

Table 1.4 Properties of Three-Dimensional Printing

Material type:	Powder
Materials:	Stainless steel, Bronze, Composites, Elastomers, Ceramics
Minimum layer thickness:	0.05mm
Surface finish:	25 $\mu$ m
Build speed:	3.0 m/min

### 1.2.5 LAMINATED OBJECT MANUFACTURING

The feeding mechanism for the laminated object production system places a thin film sheet on the work bed, and a heated cylindrical roller generate pressure to glue top layer to the bottom layers. The edges of the portion in each layer of sheets are cut with a laser.

Table 1.5 Properties of Laminated Object Manufacturing (Polydoras, 2001)

Material type:	Solid sheets
Materials:	PVC, Paper, Composites, Ferrous metals, Ceramics
Minimum layer thickness:	0.05mm
Surface finish:	Rough
Builds peed:	Fast

The platform is moved down by an amount equivalent to the sheet thickness. When each cut is complete until the part is finished, the laser trims the edges of each layer. The additional material is left behind after a layer is sliced in order to sustain the item.

### 1.2.6 FUSED DEPOSITION MODELING

In FDM technique, plastic is extruded from a nozzle that layer-by-layer matches the part's periphery shape. Stratasy was the one that created it. A moving head on the FDM machine places the plastic filaments that are extruded from molten plastic on a surface. Because it solidifies immediately after extrusion and sticks to the preceding layers, the building material is heated 0.5 degree above its melting temperature. The rate of material extrusion, nozzle speed, and head speed all have a negative impact on the overall layer thickness.

Table 1.6 Properties of Fused Deposition Modeling (Liu, 2021)

Material type:	Solid Filaments
Materials:	ABS, Polyphenylsulfonite, Polycarbonate, Elastomers
Minimum layer thickness:	0.15mm
Surface finish:	18 $\mu\text{m}$
Build speed:	30 mm/sec

### 1.2.6.1 PROCESS OF FUSED DEPOSITION MODELING

Similar to most rapid prototyping methods, fused deposition modeling commences with a software process where the CAD model of the prototype is transformed into Sliced Thin Layer (STL) format. The process of mathematically slicing and orienting the model for the building process is referred to as STL conversion. When converting into STL format, the software also generates the support structures according to the specifications.

Figure 1.2 shows various part of FDM machine. The part is created by extruding tiny thermoplastic blobs to create layers, which immediately solidify after leaving the nozzle. The device has the ability to dispense two types of materials: one to form the sculpture and the other as a delicate support framework. Plastic fibres are pushed into a hot extruder nozzle, where heat causes them to melt. The filament is typically pushed into the nozzle using a worm-drive at a controlled pace. After that, the extrusion head deposits the molten blobs. A numerical control mechanism allows the stimulation of the nozzle to be done both vertically and horizontally. It follows a tool-path that was produced by a CAM software programme. The part is fabricated layer by layer, starting at the bottom.

The technology of fused deposition modelling is quite light. Through the use of the backing from bottom layers, it can produce pieces with very slight overhangs.



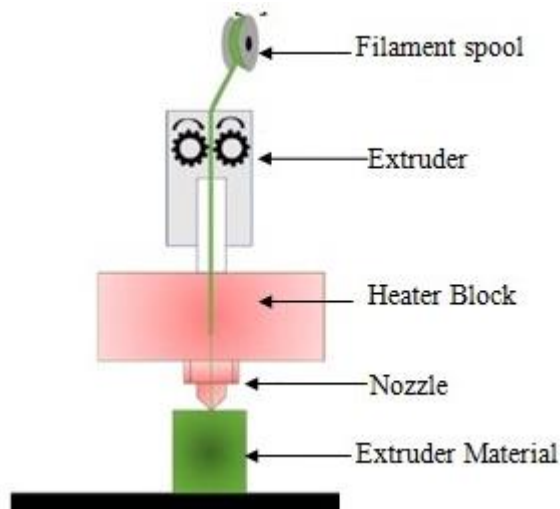


Figure 1.2 Equipment for Fused Deposition Modelling (Pandzic, 2019)

### 1.3 RAPID TOOLING METHODS

Rapid Tooling (RT) is using a technological method to quickly generate patterns, cores, moulds, mould inserts, electrodes, etc. for sand casting, injection moulding, or investment casting. The bigger quantities of components and a extensive range of materials that the RT procedures may provide is the major advantage of the technique. However, the value of RT goes much further assessing component performance. RT is a crucial component of the larger problem of quick part creation. (Rosochowski and Matuszak, 2000). There is a tendency to put RT approaches into categories because their number is growing. The classification of RT is given in the figure.1.3.

#### 1.3.1 DIRECT TOOLING

Direct tooling refers to the patterns, moulds, cores, etc. produced as a first step using SLS, FDM, Stereo-lithography, and LOM. The majority of RP techniques employ soft-built materials, which are unsuitable for direct tooling. Wax patterns have been used as injection moulding patterns with SLA epoxy prototype (Figure 1.4). This makes it an intriguing aspect for investment casting because the epoxy resin moulds can easily withstand the low melting temperature of wax (50-550 C). SLS, FDM, SLA, and model maker II can all directly manufacture the wax patterns (MMII).The shortcomings of utilising wax as a pattern include its fragility, which causes pattern

destruction during transit to the foundry. This method is not appropriate for casting parts with thin walls.

SLS can process a wide variety of unique powders, particularly metals. This makes it possible to produce metal injection moulds directly from CAD models. The SLS RT method uses thermoplastic-bound iron-based powders. To consolidate the metal powder, the binder is only partially heated. The process involves infusing the second metal into the green half after sintering to form a completely solid component. Finally, the cycle is completed by polishing and integrating it into a mold base. This procedure creates moulds that are strong enough and capable of producing more than 50,000 pieces. Another alternate material that can be used to directly produce investment casting patterns using SLS processes is polystyrene.

Ceramic moulds or shells can be directly produced by 3DP. By eliminating the procedures of creating wax patterns, making ceramic shells, autoclaving, and burning moulds, this technology has an advantage over traditional investment casting and other rapid investment casting methods. The process of direct shell production casting (DSPC) is capable of virtually producing any shape.

Utilizing a ceramic shell allows for negative draughts, absence of separation lines, and absence of core prints. The 3DP method utilizes a digital model of the mold, which includes an internal gating mechanism and cores for producing hollow components. For prototypes and quick manufacturing runs, DSPC is employed. Instead of taking weeks or months, it is said to produce working metal parts in just a few days (Figure 1.5).

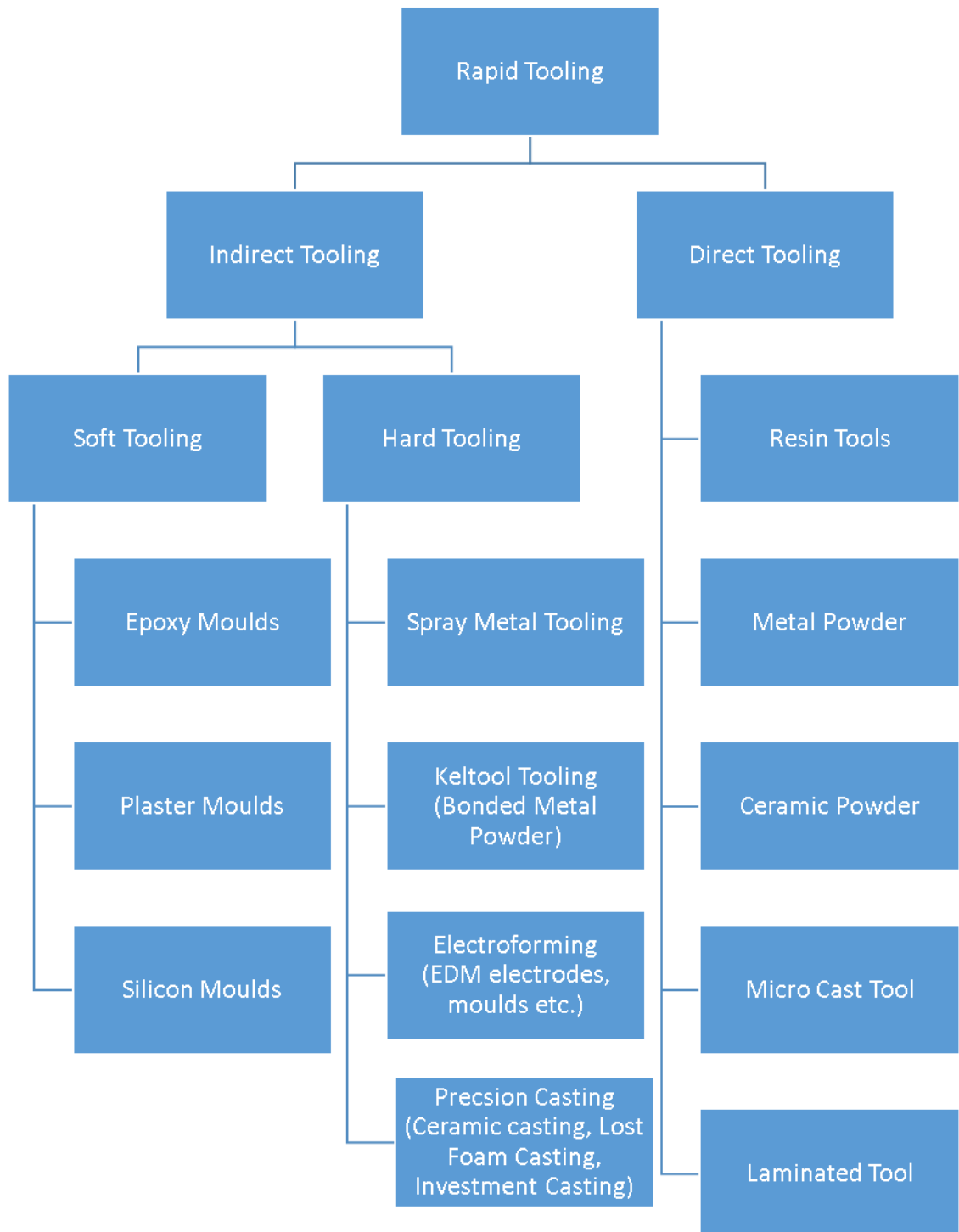


Figure 1.3 Classifications of Rapid Tooling (Rosochowski and Matuszak, 2000)



Figure 1.4 Epoxy Moulds (Rahmati, 2014)

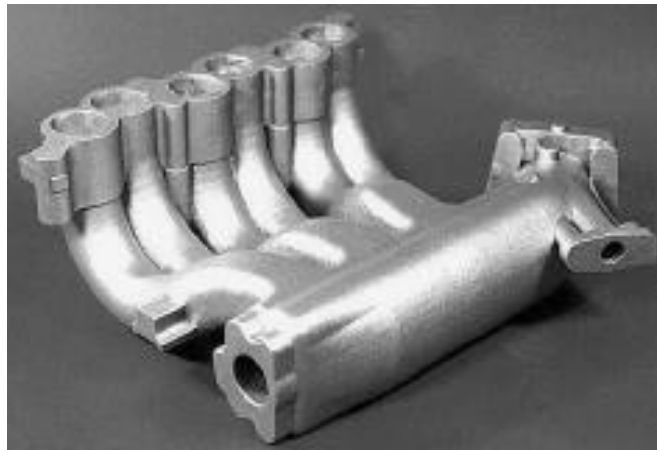


Figure 1.5 Engine Intake Manifold, Made Using DSPC  
(Rosochowski and Matuszak, 2000)

Microcasting, the droplet-based shape deposition manufacturing process, comprises of four processing stations - thermal deposition, shot peening, CNC machining, and cleaning.

The use of microcasting as a direct tool manufacture technology found productive in many fields. Microcasting was utilized to manufacture an injection molding die for the automotive component in Figure 1.6 from low carbon steel, with significant and varying layer thicknesses ranging from 1.15mm to 1.49mm. The support material employed was steel powder, which was subsequently eliminated using an air/water jet. 530 MPa was the reported tensile strength (Rosochowski and Matuszak, 2000).

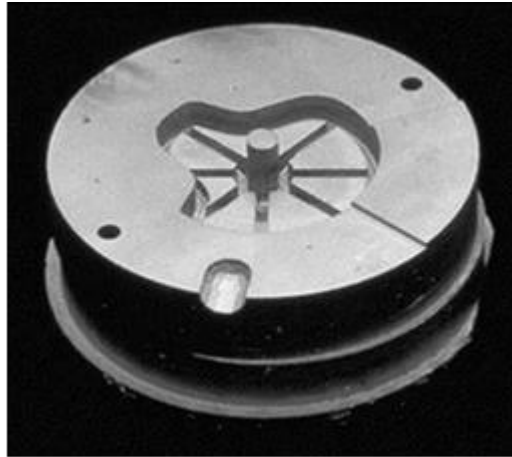


Figure 1.6 Micro Cast Die (Rosochowski and Matuszak, 2000)

Die casting or injection moulding tools can be produced using the Metal Laminated Tooling process. The three-dimensional CAD data of the tool to be manufactured is imported into the CAD system utilizing standard interface formats (such as IGES or STL), as depicted in Figure 1.7. The tool is then divided into individual cross-sections, and the layer thickness must be determined beforehand, taking into consideration metal sheet tolerances and shrinkage of the soldering metal. After slicing, the individual cross-sections are placed on a metal sheet panel.

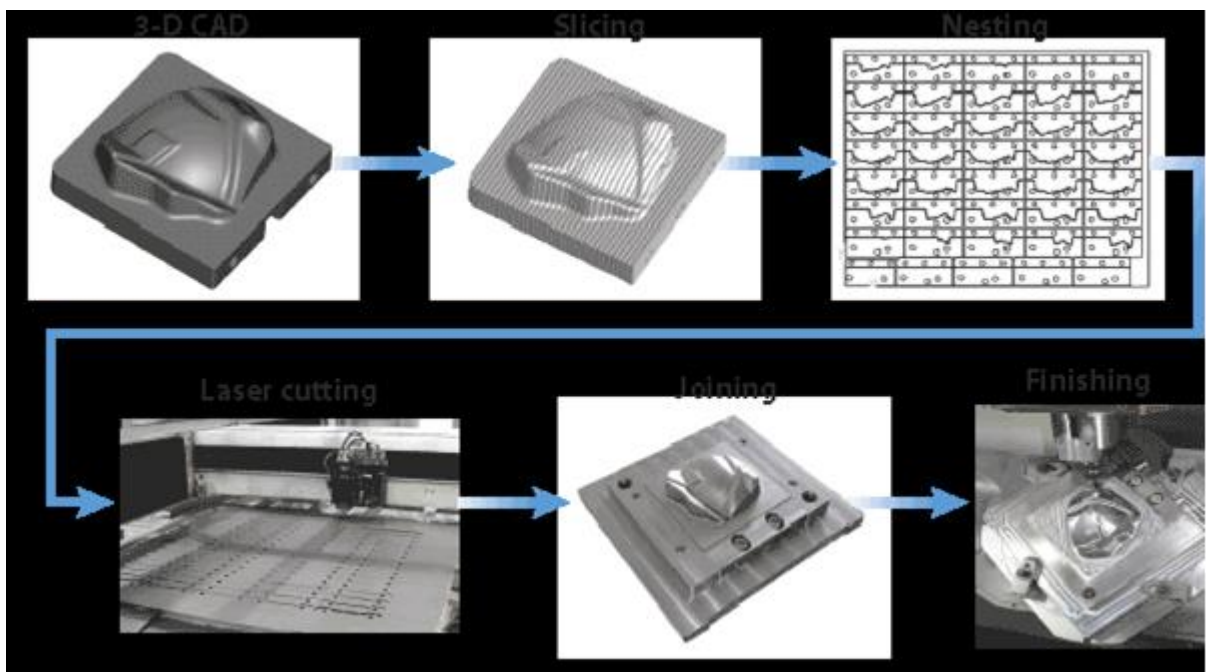


Figure 1.7 Metal Tooling Process Chain (Himmera et al., 1999)

The cross-sections are cut out using a laser beam and then bonded using a variety of bonding techniques. To improve the durability and strength of tools, laser beam build-

up welding can be used to reinforce critical areas. The final steps in finishing the tool include heat treatment, polishing, EDM, and milling, as described by Himmera et al., 1999.

### 1.3.2 INDIRECT TOOLING

In indirect tooling the moulds, patterns, electrodes etc. are prepared by RP in conjunction with other processes such as casting, metal spray, chemical bonding, silicon rubber, epoxy materials or electroplating etc. Further the indirect tooling is classified as soft tooling and hard tooling.

#### 1.3.2.1 SOFT TOOLING

Soft tooling can be referred as the tooling suitable for low pressure, low temperature and low volume polymeric tools. Silicone mould as shown in figure 1.8 and epoxy moulds are being used and explored extensively in this category. Plastic or low melting-point metal pieces, wax patterns, can be created using silicone moulding. RTV or "Room Temperature Vulcanizing" silicones, which are combined in two parts (a base and a catalyst to promote curing), are the silicone compounds most frequently used for mould production. A prepared model or specimen is covered with the silicone mixture, which is then reinforced with gauze or another type of reinforcing material in between layers for greater strength and tear resistance.



Figure 1.8 Silicon Mould (<http://www.techok.com/rtv-molding.html>)

Epoxy molds are the most efficient way to produce short runs of functional items using injection molding. The process involves covering the positive master up to the parting line with clay or plaster, which can be a SLA, SLS, FDM, or LOM model. After coating the master with a release agent, epoxy resin is poured into the mold box and left to dry. The same process is used to complete the second half of the part.

Runners and gates are added to the master before casting, and they can also be machined after casting. To enhance tool durability and strength, the tool can be finished with laser beam build-up welding, heat treatment, polishing, EDM, and milling. To increase heat transfer and lessen tool wear, aluminium is typically added to the epoxy resin. Similar to sand casting, plaster mould casting uses plaster of Paris as the mould material instead of sand in the metal working casting process. The process of plaster mold casting is a type of expendable mold process that resembles sand casting, but it is restricted to the use of non-ferrous materials. It is used for castings ranging in size from 30 g to 45 kg. The form is often ready in less than a week. Plaster moulds may produce items at rates of 1–10 per hour.

#### 1.3.2.2 HARD TOOLING

The tools produced by depositing the metals on the RP produced master are considered in the category of hard tools. These tools are capable of producing high volume production and can withstand relatively higher pressures and temperatures. Some of the hard tools under study are spray metal tooling, electroplating of nickel, Keltool tooling etc.

The process of metal spraying as shown in figure 1.9 involves melting a raw material in the form of wire or powder and then shooting the atomized material in the direction of the workpiece at a high rate of speed to produce a metal coating. For creating the spray metal tooling Rapid prototype model has many advantages. Manufacturing soft tooling, particularly flexible moulds, uses metal spraying.. Producing soft tooling, particularly flexible moulds, involves spraying. It entails spraying an epoxy resin-backed thin shell with a thickness of roughly 2 mm over a pattern to give it stiffness. Metal utilised, in its structure, and support type for the metal shell all affect the properties of metal spray moulds. A tool typically lasts for several hundred injection-molded components. Chua et al., (2003) reported that using a nickel shell with a hardness of HRC 50-58 provides excellent abrasion resistance and improves the tool life for high-volume manufacturing.

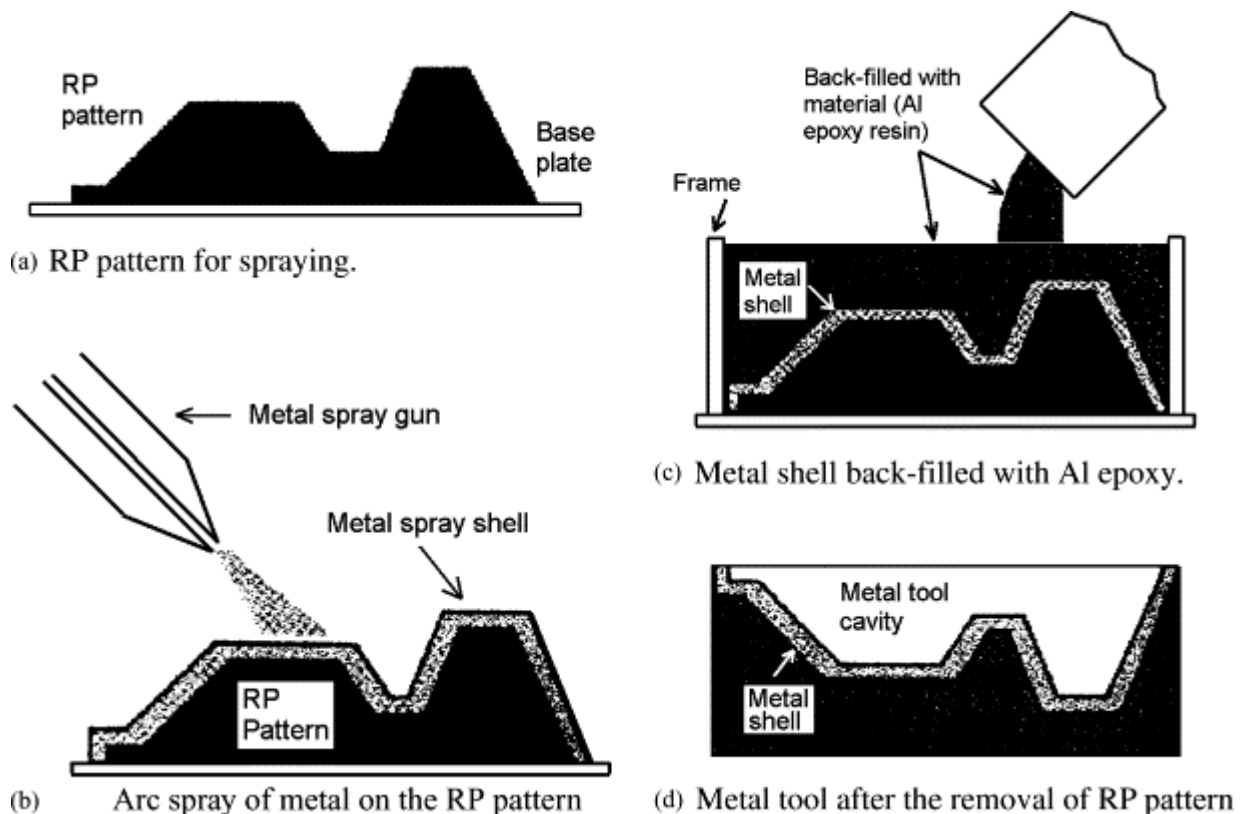


Figure 1.9 Metal Spray Technique (Wang et al., 2004)

The process of using metal powders with the plastic binders for the RT was introduced by Keltool. A silicon mould made from a negative pattern in which powder is poured to get the component shape. Or, the powder can be used to cover the positive master. At 100° C of initial heating results in a green part. Hard tool inserts are produced by final sintering and copper infiltration (HRC 35-55). Tool steel-made Keltool inserts can withstand at least a million rounds. Small pieces parts well with the procedure.

#### 1.4 ELECTROPLATING

By dissolving one electrode into its salt and depositing the dissolved metal ions onto another electrode of equal or greater nobility, electroplating is a process. Similar to a galvanic cell, but operating in the other way, is this procedure. The electrolytic solution, which is normally composed of the salt of the material that has to be plated (for example, copper sulphate for copper plating), is applied to both electrodes. The part which is required to be plated is the cathode (+) and the material of plating is the



anode (-) in the circuit. It is required that the part which is to be coated should either be equal or greater in terms of nobility in the galvanic series. A direct current power supply is attached to the circuit which causes reduction at the cathode and oxidation at the anode. Electric current dissolves the metal from anode into the electrolytic solution and deposits it on the cathode workpiece. The rate of oxidation and reduction reactions are always equal which ensures the replenishment of ions in the solution bath.

#### 1.4.1 PROCESS OF COPPER ELECTROPLATING

By providing two electrons to the power source, the copper anode in the electrolytic  $\text{CuSO}_4$  solution oxidise to  $\text{Cu}^{2+}$  as a result, the  $\text{Cu}^{2+}$  ions relax and dissolve in the solution, where they then join with the anion  $\text{SO}_4^{2-}$  to produce  $\text{CuSO}_4$ .  $\text{Cu}^{2+}$  is converted to metallic Cu at the cathode thanks to the addition of two electrons from the power source. This results in a coating of Cu metal plate over the cathode and the system's total amount of electrons,  $\text{Cu}^{2+}$ , and  $\text{SO}_4^{2-}$  ions being renewed.

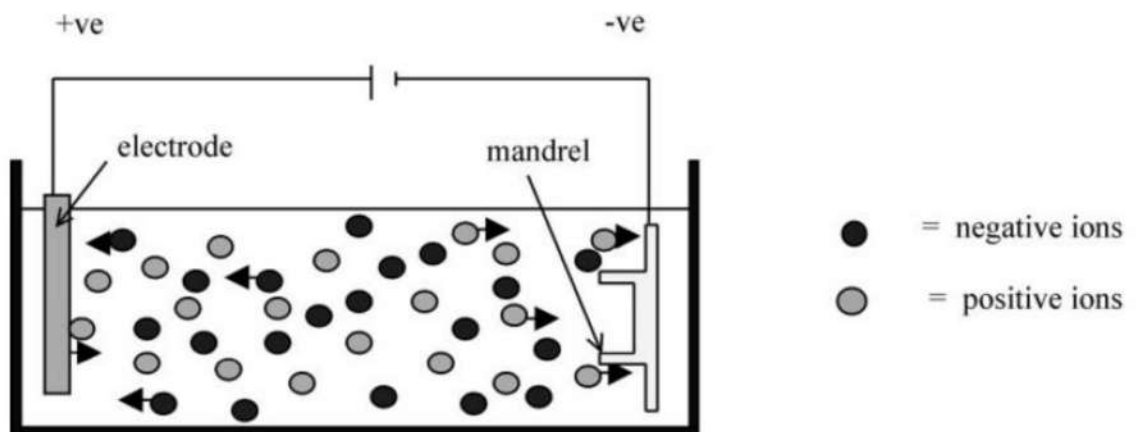


Figure 1.10 Schematic of Electroplating Process (Rennie et al., 2001)

#### 1.5 THERMAL SPRAYING

Thermal spraying technologies are constituents of the group of coating technologies that are used to deposit thick layers of ceramic, metallic, cermet, alloys, plastics, or even composite materials. Unlike other coating methods like cladding, electroplating, glazing, and vapor deposition, thermal spraying may produce thick coatings over a vast area at a rapid rate of deposition. These coatings can range in thickness from 50

m to 1 mm. The ingredients are furnished in the form of powder or wire, heated to molten, semi-molten, or solid state, and then accelerated in the direction of substrates in the pattern of microscopic particles. Particles attack the substrate, and as a result of the blow, it flattens and forms tiny splats that resemble and stick to the substrate surface and to one another. Thermal spray coating is created as the sprayed particles build up, splat by splat, to produce a laminar structure on the surface as shown in figure 1.11. Various type of thermal spray coating are: Flame thermal spraying, Plasma thermal spraying, Wire arc thermal spraying, Detonation thermal spraying, High velocity oxy-fuel thermal spraying, Warm thermal spraying and Cold spraying.

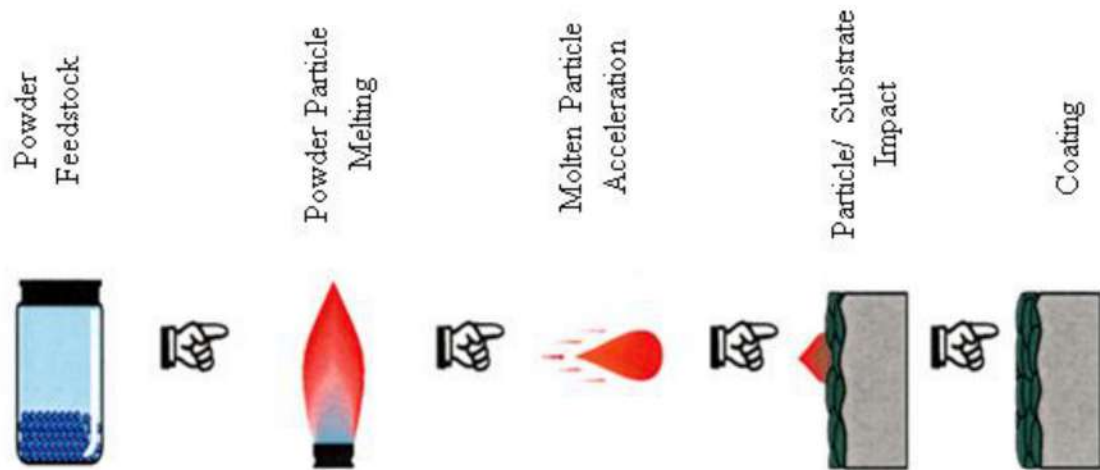


Figure 1.11 Schematic of Thermal Spraying Process

### 1.5.1 FLAME SPRAYING

The feed stock is constantly melting at the center of oxy-acetylene gas flame while using wire or rod flame spraying. The molten metal hence formed is sprayed in the form of droplets with the use of an atomizing gas like nitrogen or compressed air. The particles in molten state are released from the melting zone and bombard onto the substrate surface. Flame spraying using wire as its material is extensively used in the automotive industry to smear a very high superiority coating of molybdenum over gear selectors, piston rings and the synchronizing rings.

### 1.5.2 PLASMA SPRAYING

Plasma spraying method in which the substance to be deposited is either provided in the form of powder or wire in plasma jet that is emitted by plasma torch. The substance melts and is propelled toward the substrate by the jet's temperature, which is typically in the 10,000K range. The molten metal droplets flatten down at the

substrate surface and quickly solidify to create a deposit, which sticks to the substrate as a coat. By removing the substrate after spraying, plasma spraying is used to create free-standing components.

### **1.5.3 WIRE ARC SPRAYING**

In this method two metal wires used as feedstock are continuously fed to bring them closer so as to passing high currents from them to form an arc. At the tip of the arc, the wires are melted off and are pushed onto the surface of the workpiece by the use of an atomizing gas, such as compressed air. This method is a high-performance coating process. Wire arc spraying, uses electrically conductive materials as a feedstock. Wire arc spraying finds their applications in anti-corrosion protection, vessels coating, bond coatings, liners in cylinders.

### **1.5.4 DETONATION SPRAYING**

In this process, a charge of powder is fed into the barrel along with oxygen and fuel. A spark ignites the mixture to create detonation in the chamber. The ensuing detonation warms and propels the powder through the barrel at supersonic speeds. After each detonation, the barrel is purged with a pulse of nitrogen. Typically, the process is performed several times in a second. Very strong and dense coating is achieved due to high kinetic energy of hot particles.

### **1.5.5 HIGH VELOCITY OXYGEN FUEL SPRAYING (HVOF)**

High velocity oxygen fuel spraying technology, a combination of oxygen and gas fuel is served into a combustion chamber, leading to ignition. As a result, high pressure that can reach 1 MPa develops and escapes through a nozzle. At the barrel exit, the jet's speed reaches supersonic levels. When metal powder is added into the gas stream it accelerates up to 800m/s. The heated gas and particle-filled stream is directed at the substrate's surface. Powder melts partially in the stream, and coats the substrate with a low-porosity, high-bonding layer. Fuels that can be used in HVOF can be gases or liquids.

### **1.5.6 WARM SPRAYING**

It is an alteration in HVOF spraying. In warm spraying, nitrogen gas is mixed with the combustion gas to lower down its temperature. The mixture gas usually contains much unreacted hydrocarbons water vapor, and oxygen but still, the coating efficiency is higher as compared to that of HVOF. The chemical reactions and melting

of the feed powder are largely reduced due to lower temperatures in the process. Warm spraying is advantageous for coating such materials as Titanium, metallic glasses, and plastics which are vulnerable to oxidization and deterioration at elevated temperatures.

### **1.5.7 COLD SPRAY**

Singh et al., 2012 explain the cold spray as a type of thermal spray technology, in which metallic or sometimes even non-metallic particles are deposited over the substrate in solid state form. Instead of deposition by solidification of molten or semi-molten particles as in previous thermal spray methods, this approach accumulates solid-state particles in a coat employing supersonic velocity impact..

Cold spray or more precisely, Gas dynamic cold spray (GDCS) is a solid state coating deposition method. The solid powders of diameter up to 60 micrometers in supersonic gas jets, are accelerated to velocities up to 400–1000 m/s. The particles undergo plastic deformation, during impact with the substrate, and due to transition of kinetic energy into strain energy, bonds to the surface. Metals, composite materials, and polymers can be deposited using this technology. The supplied kinetic energy by the expansion of the gas, of the particles, is transformed to plastic deformation energy during bonding.

#### **1.5.7.1 SYSTEMS OF COLD SPRAYING**

The high-pressure cold spray system and the low-pressure cold spray system are two different sorts of systems that make up cold spray technology as discussed in Table 1.7. The operating principle for both the systems is very similar irrespective of the distinction of construction and the gas pressure.

Table 3.7 Cold Spraying Techniques at Low and High Pressure (Pattison et al., 2008)

Characteristics	Low Pressure Cold Spray	High Pressure Cold Spray
Gas Temperature ( $^{\circ}\text{C}$ )	Up to 550	550-1000
Gas Velocity (m/s)	300 to 600	1000 to 1400
Gas Pressure (bar)	5 to 25	25 to 30
Particle size ( $\mu\text{m}$ )	1 to 50	5 to 50
Particle Velocity (m/s)	300–600	500-1200
Splat Size ( $\mu\text{m}$ )	1 to 50	5 to 50
Nozzle distance (mm)	5-25	5-25
Coating Thickness (mm)	0.5-30	0.5-50
Spray Rate (kg/h)	3-15	10-30

#### 1.5.7.2 EQUIPMENT OF COLD SPRAYING

The Cold Spray equipment can be either portable (manual) or fixed (robotic). Whatever the system, a gas heater must be connected together in order to heat the gas beforehand and compensate for the cooling caused by the nozzle's quick expansion.

The main components of Cold Spray apparatus are shown in figure 1.12 (for both low pressure and high pressure cold spray systems) include:

- Supersonic nozzle (De-Laval nozzle)
- Gas compressor
- Gas heater
- Powder feeder mechanism



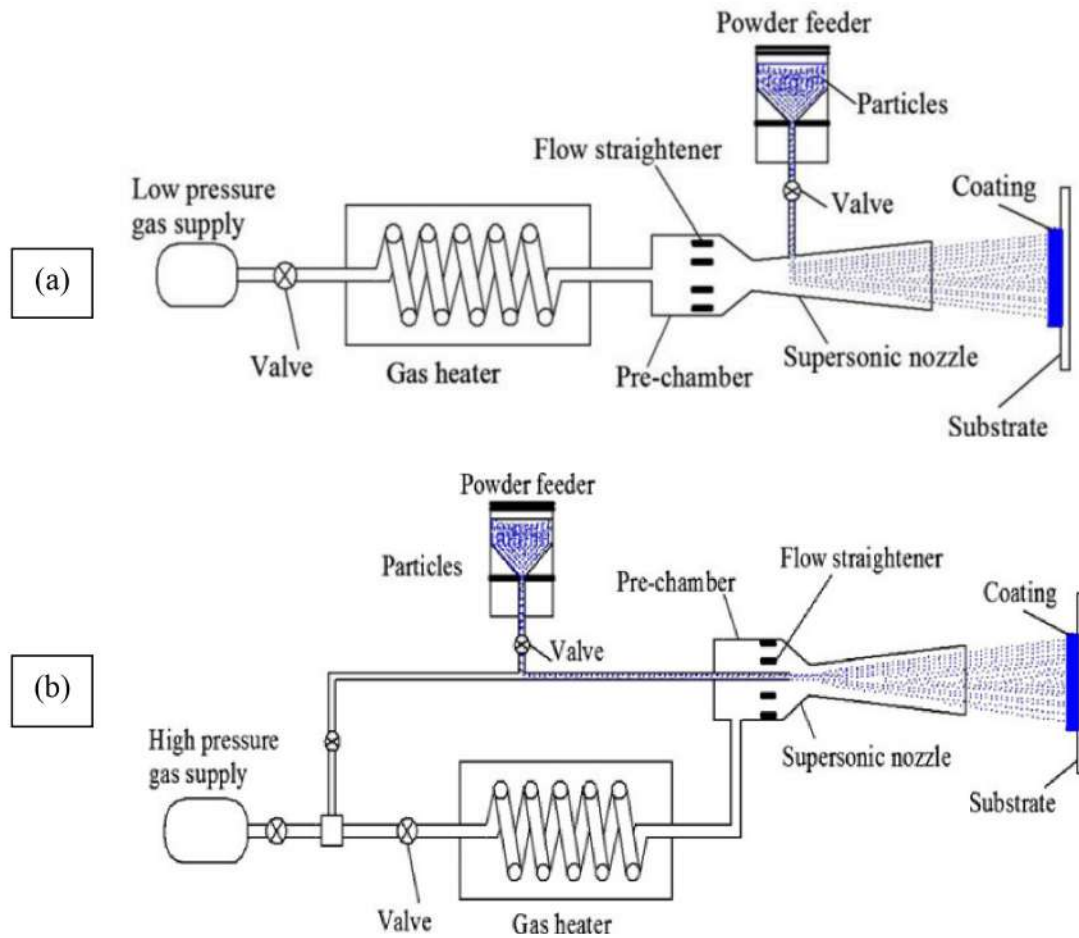


Figure 1.12: Cold Spray Apparatus (a) Low Pressure Cold Spray Setup (Maev and Leshchynsky, 2008), (b) High Pressure Cold Spray Setup (Grujicic et al., 2004)

### 1.5.7.3 MECHANISM OF COLD SPRAY

The principle behind cold spray process could easily be understood by the following explanation: A high velocity gas jet of order 350 to 1200 m/s is formed using a converging-diverging nozzle (usually a de Laval nozzle). The jet of gas thus formed is used to accelerate the tiny powder particles of diameter 1 to 60  $\mu\text{m}$  in order to spray them onto a substrate. The substrate is required to be located 15-30 mm from nozzle's exit. Due to the powder particles' ability to deform plastically into splats and bombard the substrate, the splats stick to the surface and to one another. Kinetic energy rather than the high temperatures thereby minimizing the inadequacies associated with conventional thermal spray approaches such as oxidation, melting, evaporation, recrystallization, and residual stresses. The gasses with aerodynamic properties such as Helium, Nitrogen, mixture of Helium and Nitrogen or sometimes dry air; are

largely used to propel the powder particles over the substrate. The bonding mechanism in the process can be easily understood by means of the most putative theory that during the impact, plastic deformation of solid particles occurs. Bombarding particles upsets reedy surface layers, which usually are of metal oxide, to attain close conformal contact. The high contact pressure involved indorses coalescence with the substrate surface. Champagne et al., 2005 in his experimentation observed the common phenomena during spraying onto numerous substrates, that the deformation of the substrate and the particle occurs showing viscous fluid-like behavior. On collision of spray material particles, metal jet formation is evident as a consequence of occurrence of interfacial waves, roll-ups, and vortices over the substrate. The figure 1.13 could more easily comprehend this: -

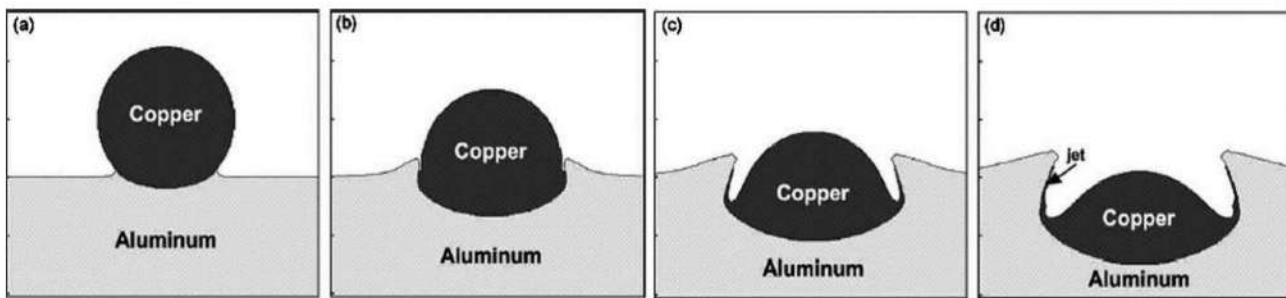


Figure 1.13 Particle's Effect on the Substrate at Different Times (Grujicic et al., 2004)

H. Singh and M. E. Dickinson suggests through their research work that the particles' adhesion-strength of the in the process is exclusively dependent upon the kinetic energies at the impact time. The kinetic energies of the particles is characteristically much lower than the energy of melting and therefore cold spray is considered to be a process in solid-state. The notion is clarified by the energy dispersive spectrometry image as shown in figure 1.14 of copper coating by cold spray on aluminum substrate, inspected by Champagne et al., 2005. It demonstrates that between the deposited copper (the light region) and the aluminum substrate (the darker region) forced mixing occurs, and that can only be attained by deep-impact infiltration of the copper particles into aluminum.

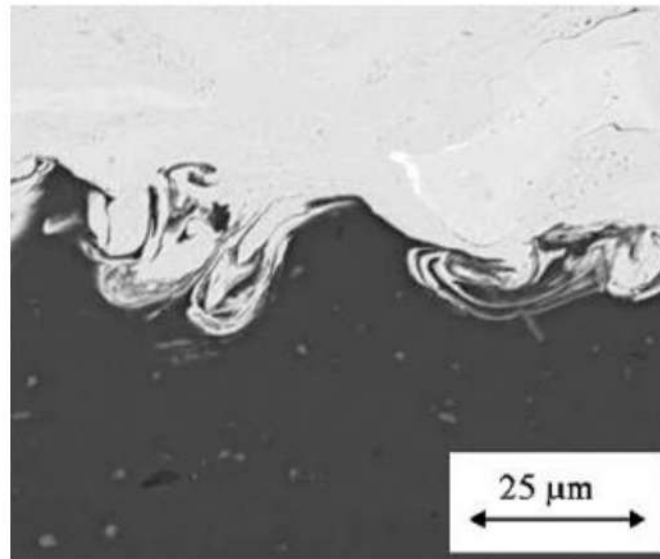


Figure 1.14 Energy Dispersive Spectrometry Image of Copper Coating on Aluminium  
(Champagne et al., 2005)

This model also elucidate the minimum particle velocity that is essential to achieve deposition. In order to deform the solid material plastically, a sufficient amount of kinetic energy is vital to be supplied and with the knowledge of adequate amount of kinetic energy, one can determine the minimum particle velocity required for coalescence. The empirical model devised by Champagne demonstrates that substrate coating interfacial depends upon the hardness of substrate and the density of coating material, solely with the velocity of particle (m/s)  $V_p$  required for the achievement of mixing at interfacial level.

#### 1.5.7.4 PROCESS PARAMETERS EFFECTING DEPOSITION

The important process parameters for cold spray are particle velocity, nozzle geometry, carrier gas, pressure and temperature, particle size and substrate surface roughness.

##### 1.5.7.4.1 Particle Velocity

Jodoin et al., 2002 investigated that particle velocity ( $V_p$ ) is a function of jet velocity which dependent on the size, morphology, and mass of the particles. The degree of plastic deformation at the particle/substrate bonding and substrate surface erosion are both governed by particle velocity. The critical velocity ( $V_c$ ) is the lowest particle speed necessary to achieve particle/substrate adhesion in a specific medium. The feedstock particles are easily reflected off the surface and do not form a continuous



coating or deposit when the particle velocity ( $V_p$ ) is too low for a specific coating/substrate combination. Much like shot blasting of surfaces, solid particle erosion of the surface may happen at greater values of particle velocity ( $V_p$ ). Particles start to plastically deform, stick to the substrate, and create an overlay layer when particle velocity ( $V_p$ ) surpasses a critical value. Particle material such as Al, Ni, Fe, and Cu have critical velocity in the range of 680–700, 620–640, 620–6400 and 560–580 m/s respectively.

Li et al., 2008 acknowledged that faster particle velocities lead to shorter dwell durations, which means less time for particle heating. Converging/diverging nozzles are frequently used in gun designs to generate supersonic expansion, which boosts particle velocity.

#### 1.5.7.4.2 Nozzle Geometry

The velocity of the gas depends on the geometry of the nozzle used for cold spray. The particle's velocity as it impacts the substrate surface is significantly influenced by the nozzle shape. Heated gas flows through the De-Laval nozzle and material particles are pushed to attain the supersonic speed due to the converging and diverging geometry of the nozzle. There is a maximum Mach number for any nozzle design that is unaffected by environmental factors like pressure and temperature. The nozzle geometry limits the Mach number. To accomplish a superior Mach number, the diverging portion of the nozzle is to be enlarged. However, shocks caused by air incursion due to low static pressure near the nozzle outlet prevent the diverging region of the nozzle from enlarging much further. These shocks can lead to reduction in the velocity of particles hence resulting to a lower Mach number with increased density, entropy, static pressure, and temperature of the system (Lee et al., 2011, Li et al., 2012).

#### 1.5.7.4.3 Carrier gas

Carrier gas like helium, nitrogen and air is used in cold spray process. Selection of carrier gas affects the impact energy of the particles by controlling the particle velocity there by affect the microstructure of the coatings. High gas constant and low molecular weight and of the carrier gas is the major influencer for the particle

velocity. Helium is most suited because of its low molecular weight and greater gas constant characteristic. More efficiently than nitrogen or air, whose velocity is low due to a low value of the gas constant, helium is used to propel the gas at high velocity (Tabbara et al., 2011, Sova et al., 2013). Helium is suggested for metals that need extremely high critical velocities and for premium materials. In addition, although having various benefits including improved deposit densification, high productivity, and an increase in working temperature, use of helium is not commercially feasible and is not easy to get as compared to nitrogen and air. But the major issue is the cost of helium gas. So, to decrease the cost at same time provide high particle velocity a mixture of helium and nitrogen/air is used and it is found out to be fruitful (Sou et al., 2015).

#### 1.5.7.4.4 Pressure and temperature

The cold spray process is categorized in low pressure cold spraying process and high pressure cold spraying process. Generally, when pressure is above 1.5 MPa the process is called high-pressure cold spraying and in this case the gases like helium and nitrogen are used as the carrier gases. In low pressure cold spraying process the pressure used will be in a range of 0.5 MPa to 1 MPa and the carrier gas used would be compressed air (Faizan et al., 2016). In case of High-pressure cold spraying, a pre-chamber zone is there where the feed stock powders are combined with the carrier gas and afterwards, they can enter the upstream of the nozzle. The carrier gas in this process is heated in another heating section before entering the gun and then in the spray gun. But in low pressure cold spraying method the materials are introduced normal to diverging segment of the nozzle and the gas can get heated in the spray gun (Rokni et al., 2017).

For cermet compounds, such as titanium, copper, inconel, tungsten carbide cobalt and MCrAlY compound, had to be deposited at high pressure above 3MPa and temperatures between 500 and 1000 degrees celsius. Aluminum, tin and oxides, had to be deposited at pressure less than 3MPa and temperatures between 20 and 750 degrees Celsius (Srikanth et al., 2020).

#### 1.5.7.4.5 Particle size

Particles smaller than 100  $\mu\text{m}$  are typically easier to accelerate and deposit, however particles larger than this range are generally difficult to accelerate. Therefore, choosing the right particle size is of the utmost importance. The ideal range of particle sizes can be achieved by controlling the deposition efficiency and particle velocity. With the exception of aluminium and zinc, which have been utilised with up to 100 and 90  $\mu\text{m}$ , the maximum particle size for most of material varies between 20 and 60  $\mu\text{m}$ . Very low temperature and pressure are used for particle size from 1 to 20  $\mu\text{m}$  to satisfactorily deposit (Raoelison et al., 2018).

### **1.6 MOTIVATION FOR WORK**

Despite the fact that additive manufacturing is a four-decade-old technology that is still in development, researchers are demonstrating interest in the technology and showing the possibility for improvement in the methodology and techniques. One of the main advance technology is the additive manufacturing used for product development but unable to be fully functional in main stream production. Presently in conventional manufacturing process production of tool required multiple stages such as designing, programming and machining (subtractive manufacturing) is required. Which is time consuming, capital and resource intensive, adverse effected by complexity.

The research is based on rapid tooling, that enable to produce tooling that are directly or indirectly fabricated using 3d printing techniques, where material is added (additive manufacturing) rather than being removed hence having potential to reduce lead time, reduce production cost, Virtual Independence for complexity.

### **1.7 OBJECTIVES**

The current study aims to examine the impact of key parameters on process performance, with the following objectives.

1. Substrate preparation for the Cold spray using 3D printing and metallizing with optimized process parameters.
2. To establish optimum process parameters for cold metal spray coating on metallized 3D printed part.

3. Characterization of surface morphology after the cold metal spraying process.

## **1.8 RESEARCH METHODOLOGY**

The whole research is categorized into different phases to achieve the various objectives defined. The phases are discussed below:

### **Phase -I**

The CAD models of test components will be made using CREO parametric software and then the test components will be fabricated using FDM.

The staircase effect of the 3D printing process will be reduced by vapour smoothing process using dymethyle ketone vapours.

### **Phase –II**

Experimental setup for the electroplating of copper and nickel material on 3D printed component will be developed.

The 3D printed component will be activated for electroplating using electroless plating.

### **Phase –III**

Electroplating process parameters such as current, voltage, temperature, pH level, time, copper sulphate solution concentration and nickel chloride concentration and nickel sulphate concentration will be selected from literature or industries.

The activated 3D printed parts will be coated for different electroplating (copper and nickel) thickness.

### **Phase –IV**

➤ Cold Spraying of bulk metal on the surface of electroplated material.

### **Phase –V**

Study of mechanical properties and surface morphology after the cold metal spraying process using micro hardness, surface roughness, SEM, EDS and XRD.

This Chapter explores the literature associated with the different fields applied and used in the current research. Primarily the research is about the development of the mould using the rapid tooling concepts. The whole literature review is subdivided into three sections. First section developments in rapid prototyping, rapid tooling, 3D printed parts. Second section discusses about electroplating and third section discuss about cold gas dynamic spray. The last section is the compilation of conclusions from the findings of the literature in the form of literature gaps.

### **2.1 RAPID PROTOTYPING AND RAPID TOOLING**

The rapid prototyping technology began with the invention of Stereolithography by Chuck Hull on March 1986, which also leads to the foundation of 3D systems. The first StereoLithography machine (SLA-1) produced parts were brittle, not accurate and of mediocre surface finish. However, by 1990s, after four years of inception of concept, the development in software, hardware, resins and process improvement leads to a drastic improvement in the quality of the build part. During 1990s, another technology fused deposition modelling for producing ABS components using layer-by-layer deposition technology was commercialized by Stratasys Corporation. Then, during 1993s the 3D printing using powder materials in conventional inkjet print heads was developed by MIT and commercialized by Z Corporation. Around the same time high precision polymer jet fabrication system was developed by a company Solidscape followed by the development of metal printing machines such as selective laser sintering and direct metal laser sintering. In last few decades' lots of experimentation and developments are carried out to enhance the potential of additive manufacturing by exploring different materials, processes and machines. The technology today is being explored for applications in wide range of aspects of life, like, product development, medical implants, tissues, cells, tooling, replacement parts, fashion accessories and 3D printed foods etc. In this section the review is done for rapid prototyping and rapid tooling.

**Denton and Jacobs (1994)** explored probably the first application of rapid prototyping for the generation of injection moulding tool through indirect tooling method for Ford Motor Company. The 3D system QuickCast used to make

stereolithographic patterns for the investment casting of the mould. From this first experience with investment cast tooling, the groundwork was definitely being laid. They found three areas of concerns, which are needed to be optimized before it can be used as an alternative for the existing tooling making processes. First, the surface finish of the patterns produced from SL, second, the hardness of the investment casted mould along with the cooling rate and third the optimization of the time and cost, as in the presented work substantial machining and finishing work was required before the final use of the tool.

**Pham and Gault (1998)** offered an outline of rapid prototyping methods with emphasis on their advantages and disadvantages. Data for typical process parameters such as layer thickness, component orientation, system accuracy, and operation speed were provided. This study provided a clear image of the procedure to be chosen based on the prototype's final usage.

**Kruth et al. (1998)** compiled the progress of the RP in its initial decade of development, they have also compared the material removal manufacturing with material addition manufacturing for physical and chemical phenomenon. The key developments in rapid prototyping, as well as improvements on a process-by-process basis, are thoroughly covered. The development of materials for various processes was also discussed, with the suggestions for handling the problems like crack formation, internal stresses and delamination at the substrate and coating between different materials. The paper also touched upon the major development in the new applications of the RP with the focus to turn additive manufacturing into a production technique.

**Jayanthi et al. (1999)** studied the stereo lithography core and cavity for identifying and optimizing the issues for low volume direct tooling applications. The solution for the problems of trapped volume geometries and heat deflection temperature were also discussed. It was found that thermal post curing of the high temperature materials improves upon the heat deflection temperature and physical properties. The effect of mould design features like the draft, venting, cooling channels and stair stepping discussed for their possible defects in the mould making using SL. It was recommended to use a 3 degree to 5 degree of draft angle to minimize the undercut effect of the stair step effects. The SL mould may lead to longer cycle time due to

longer cooling cycle, suggestions were made of using cooling channels for optimizing the cycle time. The need to study the variation in the physical properties of injection moulded parts using the SL tools and conventional hardened steel tools was also stressed upon.

**Rosochowski and Matuszak (2000)** described RP applications referred to as rapid tooling that include the fabrication of prototype and production tooling. The paper briefly discusses various RP techniques along with secondary operations. The work establishes the classification of the rapid tooling techniques based on the outcome of the process such as soft tooling vs hard tooling, indirect tooling vs direct tooling and production tooling vs prototype tooling etc.

**Karunalaran et al. (2000)** proposed an alternative RP process to eliminate the problem of staircase effect and poor accuracy of the metallic parts. The proposed method employs adaptive slicing with first order edge approximation. The concept explores the two level processing, by hybrid of the high speed CNC machining for net shaping after near net building of the layers using MIG welding process. The proposed process was primarily for the use of mould making, for intricate parts and tools this process yet to be developed.

**Yarlagadda et al. (2001)** approached two techniques for rapid tooling of sheet metal drawing tool by using a combination of stereolithography (SL) and nickel electroforming processes. In first approach they created a SL master model followed by silicon rubber mould then to silicon tool mandrel and finally the electroformed nickel shell is produced to fit into the die set. The second approach was to use the die and punch made directly through SL with back filling by aluminium filled epoxy to provide the strength. It was concluded that the direct tool made by SL has less durability than nickel electroformed tool. The process of making a tool by electroforming using SL patterns was lengthier than the direct tool generation of SL.

**King and Tansey (2002)** used direct rapid tooling method using selective laser sintering and CNC machining to fabricate modular injection tool inserts. The mould tools were fabricated by using different materials, like, copper polyamide, Rapid Steel, Cibatool board, Ureol and Araldite.

**Song et al. (2002)** created automobile deck part die using RP and RT, The three step process developed using laminated object manufacturing to produce the prototype,

then the ceramic mould was prepared through unbaked ceramic technology. Finally the casting was obtained by precise casting and polished for good surface quality. The method of three dimensional nonlinear coupled thermo-mechanical FEM analysis was also performed to analyse the dimension accuracy. The whole work emphasis on the importance of the conversion of non-metallic prototype into metallic component for longer duration of the tool life. The method discussed is found to be very useful for developing the tools for long parts.

**Pal et al. (2003)** investigated the use of rapid prototype technology for creating a sacrificial pattern for investment casting. Various RP processes were found to be capable of producing wax patterns, but the limitation with these methods was the brittleness of the wax along with the problem in transportation. They experimented with non-wax patterns produced using SLS, FDM and thermojet. Some problems such as the expansion of the RP parts leads to the cracking of the shell, additional attention and skill required to handle non-wax patterns and the staircase effect were exposed. The need to make it cost effective by reducing the cost of RP pattern for more samples also discussed.

**Rosen et al. (2004)** used a DFM technique Material Process Geometric Tailoring (MPGT) to overcome the limitations of SL moulds, such as low strength, poor thermal conductivity and short life of the tool. MPGT is the alteration of non-critical feature geometry and production process variables in order to save fabrication costs and time while also producing functioning prototypes that resemble the characteristics of production parts.

**Dunne et al. (2004)** researched about two different rapid tooling process; bolstered silicon moulding and sand moulding. In the enhanced silicon moulding, mould was created by pouring a mixture of silicon rubber and 50 wt. % iron powder over master pattern. In the foundry sand moulding, 3% phenolic resin coated zircon sand was used to cast around a RP master pattern to prepare a mold. The molds such created required to be cured for 24 hrs to harden the surfaces. They addressed and suggested the improvements during the pre-processing, processing and post processing demands, such as the surface finish, dimensional stability, thermal susceptibility, surface porosity and thermal expansions.



**Zhou et al. (2004)** compared different infiltration methods and materials for a rapid tool produced by sintering techniques. It was observed that the sintered tools has 30-40 % porosity and 70-60% metal. This porosity leads to the poor performance of the rapid tools, hence three infiltration methods suggested in the proposed work. The methods suggested were based on the curing conditions of the resins used for infiltration. It has been found that the strength and hardness of polymer infiltration were less than that of copper, brass bronze infiltration. The need to find new resins and curing methods was felt for better product life.

**Ding et al. (2004)** established a rapid tooling integrated manufacturing system for reduction in cycle time and tool development cost. The integrated manufacturing system consists of four different building blocks: digital prototyping, virtual prototyping, physical prototyping and rapid tooling system. The digital prototyping includes the data capturing for 3D model generation using technologies such as a laser scanner, MRI, CMM and computer tomography, etc. Virtual prototyping validate the 3D CAD models using various software in lieu of physical parts. The physical prototype can be produced by rapid prototyping techniques or high speed machining processes. It was suggested to use the RP pattern to create the rapid tooling.

**Pal et al. (2004)** described a synergistic approach of minimizing the lead time for the development of casting by use of reverse engineering, RP and casting process simulation. The generation of an aluminium alloy impeller using these methods suggested more predictable and consistent results. In the study the scanned model after converting into solid models were rapid prototyped as non-expandable patterns with SLA, FDM, Thermojet and LOM RP techniques. The results for the cost, dimensional accuracy and surface finish were compared for different processes. The proposed approach was useful for complex parts required in small numbers.

**Pal and Ravi (2007)** developed a methodology by implementing in the software using the C++ programming for the RT route selection and evaluation of two different type of casting i.e sand casting and investment casting. Using suitable cost models, the technique entailed selecting tooling qualities, assessing compatibility, and calculating the cost of quick and traditional tooling.

**An and Chen (2007)** studied a different aspect of demoulding of stereolithography tooling for injection moulding. The demoulding stresses were studied against hold

pressure, cooling time and mould temperature. The demoulding stresses increases with the increasing hold pressure, reduction in mould temperature, and with increasing cooling time.

**Ma S. (2007)** investigated particulate reinforced epoxy composites for rapid tooling. The reinforced epoxy composites of different compositions of Al powder, Al<sub>2</sub>O<sub>3</sub> powder, Si<sub>3</sub>N<sub>4</sub> powder and CaSO<sub>4</sub>.2H<sub>2</sub>O powder were tested for hardness, compressive strength, wear rate and thermal expansion. It was found that 20 % alumina powder worked best for the tested parameters. It was also established that the tools produced were more suited for injection molding of wax and polymers.

**Rahmati and Dickens (2007)** tested an epoxy backed stereolithography injection tool for the causes of failure. The impact of injection pressure and temperature for flexure and shear stress was measured and elaborated. It was found that the SL tool has better life, if the temperature of the tool to be maintained around 45 °C. The forced air convection cooling was also suggested to shorten the cycle time, although the cycle time was higher as compared to conventional tooling. It was concluded from the findings that tool failure was independent of the plastic temperature, rather flexural stresses during the injection process were the major factor.

**Kechagias et al. (2008)** published the compilation of the research conducted by various researchers in the field of rapid electrode manufacturing of stereolithography models. Both the approaches direct and indirect tool generation by electroplating, electroforming, metal spray and cast methods discussed and compared. It was suggested that most convenient method to make non-conductive plastic to conductive is electroplating. Electroformed electrodes tended to perform better in rough EDM than electroplated electrodes in finishing applications. The cast made electrodes requires further CNC machining for the surface finish. The development of a suitable software to manipulate STL file for scaling, cutting or joining for the EDM electrode and CNC programming was suggested as the scope for future work.

**Yang and Hannula (2008)** upgraded spray forming machine from a single nozzle to double nozzle machine. The objective was to use this machine for bigger moulds/die up to 400 mm in diameter. The melted tool steel sprayed on the ceramic mould to create a mould. It was observed that the mould such produced has up to 61 HRC hardness and exhibited over 25% longer life than the conventional tools. Spray

forming techniques of generating moulds also has the capability to create conformal cooling channels and shapes of 0.5 mm thin and 5.5 mm deep in the moulds.

**Lokesh and Jain (2010)** elaborated the lack of benchmark standards and industry experience for the picking of the RP technology and presented a systematic approach to the selection of the technology. On the basis of issues and sub issues involved in RP technology selections, a structured hierarchical model was designed. Grand rating approach was used to suggest the appropriate technology using Eigen values and consistency ratios, higher the rating better the technology.

**Yan et al. (2010)** introduced multiphase polymeric materials for rapid prototyping and tooling technologies. High impact polystyrene was blended with epoxy and wax blend was produced for SLS found to have increased in the tensile strength, flexural strength and impact strength. The multiphase mixture of polystyrene (80%), polyamide (20%) and compatilizer (5%) yielded SLS parts with high tensile strength of 14.4 MPa. Organically modified rectorite was blended with polyamide-12 to produce high strength SLS component.

**Singamneni et al. (2011)** experimented with the possibility of light metal casting using 3D printing technology. The variations in pouring temperature, mold material and coatings studied for the variation in the responses such as tensile strength, microstructure and surface finish using Taguchi L9 OA. Mold materials selected were ZP131, ZCAST, SILICA and mold coatings done of ISOMOL, ZIRCOAT and MAGCOAT. The casting was done using two Mg alloys and one Al alloy. The patternless mold of ZP131 were found to be best suited with a MgO coating at 690<sup>0</sup>C temperature for pouring. There were no loss in the mechanical characterization of the castings using rapid prototype molds made in 3D printing.

**Sivadasan et al. (2012a)** compared the pattern for investment casting produced by FDM and selective laser sintering process. A set of tests using RP patterns were performed out, as well as a set of steel castings for testing fabricated, to determine feasibility. The fabrication medium was ABS. Investigators also looked into shell cracking using SLS patterns. The critical factor noticed was the thermal expansion of the ABS, which needed to be controlled through the manipulation in the size during ABS build. A need to establishment of the scale factor also proposed in the work.

**Sivadasan et al. (2012b)** explored the possibilities of ABS patterns for investment casting using FDM process. The ABS pattern after burning from the ceramic shells, leaves loose and brittle residues around 1.5 %, which needed to be cleaned as after the process. It was proposed to develop a surface finish process to remove the staircase effect from the ABS pattern. The ABS pattern found to be 7-8 times less expanding than the Duraform patterns, results in the less cracks as compared to the Duraform.

**Noble et al. (2014)** explored and compared three different methods of mould fabrication required for optical components. The methods explored were CNC machining of aluminium, CNC machining of plastics and inkjet style 3D printer. Furthermore, 3D printed items have extremely rough surfaces was improved by exploring three different methods, hot pressing, coating with printer resin and mechanical polishing. Conventional polishing and hot-pressing required shorter time and were easier to regulate than coating.. Based on initial finding, 3D printing shows potential as a way for generating rapid tooling for injection moulding.

**Nuñeza et al.(2015)** FDM is majorly used in low cost printers which provide information on layer thickness, but these do not provide any information on dimensional accuracy or surface characteristics. In this paper research has been done on two different dense modules with two layer thickness 0.178, 0.254mm. With the maximal layer thickness and solid density of 100%, good dimensional patterns were found. Solid density (100%) and minimum layer thickness (0.178mm) were used to produce the best surface quality and the lowest flat line.

**Maidin et al.(2015)** in this paper they discussed an adaptive way to enhance the surface quality of FDM built components. The author presented that by applying ultrasonic vibration the surface finish of the FDM components can be improved. This research they studied the replica under three different frequencies 11,16,21 khz. Upon research it has been concluded that the replica which is under the influence of 21khz showed less deformation and reduced surface defects.

**Clayton Neff et al.(2016)** AM manufacturing is economical when produced complex geometry prototypes, but the parts produced have low strength and high surface roughness. To compensate with this high surface roughness mechanical finishing or different types of coating techniques are used. Vapour polishing is one of the widely

used polishing technique. This paper compares the strength, ductility and surface roughness of vapour polished ABS specimens.

**Gajdos et al.(2016)** AM techniques decrease the production time and cost and can produce complex geometrical parts. Parts produced by FDM have lo surface finish. The researcher showed the way to improve surface finish of FDM parts. NaHCO<sub>3</sub> and glass beads were blasted onto FDM parts. Roughness test values Ra and Rz were noted and compared respectively.

**Singh et al.(2016)** FDM can fabricate parts with complex geometry. However, poor surface finish limits its use in various industries. In this present study it is proposed to use acetone vapours to improve the surface finish of FDM parts. These parts are exposed to acetone vapour using vapor smoothing station. Design of experiment technique is used to find the effects on different parameters on the fabricated parts.

**Haidiezul et al.(2017)** FDM is one of the economical 3d printing technology. This process uses the principle of layer by layer deposition. This leads to uneven or irregular surface finish. This study investigates how the smooth-on application of XTC-3d coating affects the surface finish. The surface finish of 3D printed components can be improved by reducing the gap between layers.

**Taufik et al.(2017)** AM based FDM helps in manufacturing or fabricating a product or part without any geometrical constraints. But the parts fabricated have finishing issues and rough surfaces. This research provides a strategy of coupling the laser finishing and FDM process to improve the overall surface roughness of the fabricated part. Empirical analysis is used to determine the parameters like laser power and resolution.

**Lalehpour et al.(2017)** AM is a widely used technology with high capability for manufacturing parts with complex geometry. Parts fabricated using AM technology suffers from bad surface finish. Applications of AM manufactured parts depends on the post-processing technique. This technique enhances the surface finish of the fabricated parts with negligible changes in the dimensions. In this case study acetone vapor bath proved to be an effective method to improve the surface roughness. The smoothing parameters are classified to be number of cycles and its duration.

**Jayanth et al. (2018)** FDM, the most abundantly AM technique because of its environmental and cost effective nature. But the downside of FDM is its surface roughness. Due to the large layer resolution the printed parts have high surface roughness. By employing different solvents after the chemical process, this roughness may be smoothed off. This study shows how chemical treatment dissolves the layer of the printed part and gives a smooth surface.

**Kalyana et al. (2018)** In AM operations for the creation of diverse industrial parts, the FDM technology is crucial. But dimensional inaccuracy and rough surface finish limits its range of applications. This research presents the replicas produced by FDM-ABS and their reaction when different parameters are varied and their effect on surface finish, hardness, dimensional accuracy is noted in pre-processing stage. It has been noted that replicas fabricated at 90degree orientation resulted in better surface finish than the replicas fabricated at 0 and 45 degrees. Now these replicas are exposed to acetone vapours and the changes occurred have been noted. This study summarises, the replicas exposed to hot vapours of acetone showed significant improvement in surface finish with negligible variance in dimensions.

**Chohan et al. (2019)** this paper presents the possibility of using ACETONE for finishing the FDM-ABS replicas in controlled environment. Experiments have been carried out to evaluate the impact of number of cycles and its duration on surface finish. Upon performing number of test cases it is deduced that exposure of FDM replicas to ACETONE vapor proved to produce better surface finish, but over exposure resulted in deterioration of surface. The excessive flow of layer resulted in weight imbalance. The upper and lower limit of smoothing duration has been noted. Replicas were exposed to vapours for 15,30 and 45 seconds. The replicas exposed for 45 seconds showed surface finish of 96.52% where 94.33% has been achieved in first cycle. The pieces got a smooth and shiny finish..

**Shahrubudina et al.(2019)** 3D printing is a type of technology which manufactures materials by successive addition of material. 3D printing the most used innovation for mass manufacturing of materials. This 3D printing is used for mass production and customization of various material in different fields like agriculture, manufacturing and production industries.

**Radhwan et al. (2019)** In this research the author analyses the effect of main parameters on surface quality of 3d printed parts and to find the optimum parameters using response surface methodology. Three parameters are chosen namely, layer thickness, print speed & fill density. ANOVA table is used to determine the significance of different factors. Layer thickness played the most significant factor in surface roughness.

**Radhwan et al. (2020)** In this paper they discussed that FDM is a process for developing objects by depositing fused layers of materials. This research has been performed to optimise better roughness for materials and how layer height, outline speed, extruder temperature effects the part roughness. To develop the material CAD has been used and later transferred to STL. FDM will deposit the material from the bottom to top by reading the STL file. To cut down on trial runs, the Taguchi approach based on 1 composite design is applied. Different specimens are compared by using different parameters and their effects are studied.

**Pramanik et al. (2020)** FDM being the popular additive manufacturing technic is used in various engineering application. This article discusses the research works done till now to optimize the surface roughness followed in FDM process. Studying different research finding could help us identify the parameters that affect the surface finish of 3d printed parts.

**Khan and Mishra (2020)** FDM is one of the most abundantly used AM technique using which manufacturing is done economically. ABS material manufactured by FDM has minimum surface finish. The process of improving the surface finish of 3D-printed ABS parts has been discussed. Leaving aside the important parameters for manufacturing a part, some other parameter have been taken into consideration. The importance of several process factors that enhance the overall surface quality has been examined using ANOVA. With the use of the L27 Taguchi experiment design, the parameters were optimized. It was observed that air-gap is having maximum influence over other parameters for part surface roughness.

**Emmanuelle et al. (2020)** In this paper author analysis the surface roughness of 3D printed components by varying the process parameters of 3D printer. The surface roughness was measured by measuring Arithmetic average height and Maximum height of the profile. Surface roughness is analysed through analysis of variance and

subjected to box-behnken design. This analysis was used to determine the significance of the variables. This study showed how changing different aspects during printing can change the outcome of the surface finish.

**Baligheid et al. (2020)** Lack of surface quality and hardness are the reason for the tough development of 3D printing. Controllable, consistent and predictable post processing procedure necessitates enhancing surface finish without affecting the properties of the 3D printed part. This article outlines techniques for upgrading surface quality so that it may be used for an array of high-temperature tasks. This technique takes into account variables including layer thickness, nanoclay content, and immersion duration.

Table 2.1 Process Parameters for Minimum Surface Roughness

Layer Thickness (mm)	Raster Width (mm)	Speed of Deposition (mm/s)	Fill Density (%)	Raster Angle (Degrees)	Air Gap (mm)	Remarks	References
0.254	0.2832	-	-	10°	0.02	Flat surface	Khan et al., 2020
0.254	0.6213	-	-	8°	0.02	Inclined surface	Khan et al., 2020
0.254	0.5102	-	-	37°	0.05	Curved Surface	Khan et al., 2020
0.1152	--	36.3	26.973	-	-	-	Parmanik et al.,2020
0.254	0.508	-	-	45 ° / 90 °	-0.01	ABS M-30i	Kumar et al.,2014
0.178	0.305	-	-	-	-	-	Galantucci et al., 2009
0.1778	(Fine rasters)	-	-	-	-	ABS-400	Horbath et al., 2007
0.254			-	90°	0.02	Stratasys P-400 ABS	Raju et al.,2018



0.007	-	-	-	-	-	-	Sood et al., 2012
0.127	0.407	-	-	-	4E-07	ABS P400	Khan et al., 2019
0.254	0.4564	-	-	0°	0	Ra = 2.10	Dong et al., 2018
0.1788	-	-	-	-	-	Flat surface	Ali et al., 2014
0.254	-	150	-	-	-	Ra = 2.79	Nancharaiah et al., 2010
0.3556	0.537	200	50	45°	-	ABS400	Jaisingh et al., 2020
0.25	-	-	100	45°	0.02	Flat surface	Abeykoom et al., 2020
0.3556	0.537	150	90	45°, 90°	0.01	CFR-ABS and CNT-ABS	SatyadevR. S, 2020
0.2	-	200	80	90°	0.02	ABS	Mora et al., 2019
0.35	-	100	-	30°, 60°	0.02	ABS Round Parts	Saini et al., 2019
0.2	-	80-100	40	-	-	50% ABS and 50% PETG	Yadav et al., 2020
0.1	-	100	-	-	-	(60% ABS + 40% PETG)	Nunez et al., 2015

0.174	-	-	100	-	-	ABS plus P430	Rehman et al.,2018
0.2	-	45	15	-	-	-	Hafsa et al., 2013
0.1778	-	-	-	-	-	ABS	Chung et al.,2007
0.1778	0.7258	-	-	45 <sup>o</sup>	- 0.001	-	Reddy et al.,2016
0.127	0.2032	-	-	45 <sup>o</sup>	0.558 8	Ra = 4.01	Onwubolu and Rayegani ,2014
0.178	-	-	100			Minimum	Nuneza et al.,2015
-	-	-	-	45 <sup>o</sup>	-	Minimum	Singh et al.,2017
0.15	-	40	100	45 <sup>o</sup>	-	Ra= 9.42	Jayanth et al.,2018
0.13	-	45	30	-	-	Ra= 8.828	Randhwan et al.,2019
0.25	-	45	-	-	-	Ra= 7.87	Randhwan et al.,2020
0.12	-	40	25	-	-	Ra= 6.362	Pramanik et al.,2020
-	0.3556	-	-	0 <sup>o</sup>	0	Ra= 0.466	Khan and Mishra, 2020
0.2	-	60	-	-	-	Minimum	Biglete et al.,2020

TABLE 2.2: Machine Parameters and Their Effect on Mechanical Properties

Machine Parameters	Tensile Test	Compression Test	Flexure Test	Reference
	(MPa)	(MPa)	(MPa)	
Layer thickness(0.254mm), Deposition style (Vn), Deposition orientation – Z direction (M), Support style(basic), Deposition orientation – X direction (45°) and Build location (100mm)	23.93	-	-	Wang et al.,2007
Build Angles 90° in XY (for tensile) and Build Angles 0° in the XY plane (for compression and flexure)	10.8	59.3	122	Hernandez et al.,2016
Layer Thickness(0.1270mm), Orientation (30°), Raster Angle (60°), Raster Width(0.4064mm) and Air Gap (0.0080mm)	18.0913	-	39.242	Panda et al.,2009
Raster Orientation 90° (for tensile) and Raster Orientation 0° (for compression and flexure)	25.72	34.69	38.1	Ziemian et al.,2012
Layer Thickness (0.254mm), Sample Orientation (0°), Raster Angle (60°), Raster Width (0.4564mm), Air Gap (0mm)	18.6234	-	37.7666	Sood et al.,2011
Layer Height (0.5 mm) Raster Angle (65°) and Infill Density (80%)	31.57	-	-	Samykan et al.,2019
Layer Thickness (0.1mm), Nozzle Temperature (230°C) and Print Head Speed (70mm/s)	-	-	49.376	Satyadev and Srivastava, 2021

Layer Height(0.1mm), Fill Density (60%), Print Temperature (250°C) and Print Speed(40mm/s)	29	-	63.640	Poondla ,2019
Layer Thickness (0.3mm), Infill Density (100%), Infill Angle (45°) and Infill Pattern (Rectilinear)	36.4	-	-	Fernandez et al.,2016
Layer Thickness (0.1mm), Orientation Angle (0°) and Fill Angle (0°)	27.674	-	-	Nidagundi et al.,2015
Raster Angle 60°, Raster Width (0.554 mm) (for tensile) and Raster Angle (60°), Raster Width (0.479mm) (for flexure)	21.21	-	44.35	Galantucci et al.,2010
Raster Width (0.35), Raster orientation (45°/-45°), Infill Density(Solid), Layer Thickness(0.2mm), Nozzle Temperature (245°C)	-	37.51	-	Brischetto et al.,2017
Raster Orientation (0°) and Layer Thickness(0.2mm)	39.4	-	-	Rankouhi et al.,2016
Raster Orientation 0°	22.4	-	-	Cai et al.,2016
Y-axis, Built up Orientation for Tensile(0°) and X-axis, Built up Orientation for Flexure(0°)	35.45	-	45.2	Alvarez et al.,2016
Print Orientation 0°	20.6	-	-	Rauth et al.,2014
Infill Density(100%), Layer Thickness (0.254mm) and Air Gap(-0.03mm) (negative)	27.27	56.76	43.75	Baich et al.,2015

## 2.2 ELECTROPLATING

The technique of depositing a thin metal coating on a variety of materials is known as electroplating. Since the Italian inventor Luigi V. Brugnatelli invented electroplating

in 1805 and began commercialising it in the 1840s, it has developed into a mature technique and is utilised widely in a variety of applications. Electroplating, which involves depositing a thin layer on a substrate that not more than 400 microns thick, is one of electroplating's other significant applications. Electroplating is used as an additive manufacturing procedure for the creation of tool and dies, fixtures, mandrels, or components is widely accepted and utilized. This section will discuss the research work of various researchers in the domain of electroplating and electroforming for improving the mechanical and chemical properties along with the improvements in the process parameters.

**Heymann et al. (1970)** Electroplated plastics have many advantages of both metals and plastics; they have the shine, toughness, and electrical conductivity of metals as well as the low weight and ease of moulding of plastics. A pretreatment to ensure strong adherence of the metal coating is crucial for the electroplating of polymers. The straight-through approach only needs six phases of pretreatment for etching activation.

**Stein (1996)** discuss the nature of the stresses created during the electroplating process was covered, along with details on how to measure and manage the stresses within the process window. According to the sources included in the article, each of the process-related parameters—including current density, salt concentration, bath temperature, agitation rate, solution pH, cell shape, and many others—contributes to stresses. For improved stress management, it was highlighted that a bath stress profile and process window should be created. Additionally, the significance of recommended post-plating heat treatments to lower electroplating stresses.

**McGeough et al. (2001)** explained the electroforming process's and operating principles, emphasising its benefits and drawbacks. According to the review study, electroforming may be done effectively on metals up to 16 mm thick, including copper, nickel, and iron. With this method, it is possible to attain surface smoothness of 0.05 micrometres and dimensional accuracy under 0.001 millimetres. The work has been done by a number of researchers in the field of micro and macro manufacturing for mould, electrodes, inserts, etc. The electroforming is also being used in the fabrication of micro-electromechanical systems along with lithography and plastic moulding.

**Rennie et al. (2001)** for electro-discharge machining electrodes, mandrels for quick prototyping were electroformed. Complex electrodes may be made in a respectable amount of time by electroforming the RP component. This study described the authors' research in this field and the use of several RP technologies to create these electroforms. The best electrodes for use on electro-discharge machine were discovered to be thin walled (less than or equal to 1.5 mm) electroformed copper electrode backed up by acceptable filler materials.

**Teixeira et al.(2005)** Brushed ABS was treated with less pugnacious and non-contaminating solutions of  $H_2O_2$ ,  $HNO_3$ , and  $H_2SO_4$  as an alternative to the  $Cr(VI)/H_2SO_4$  solutions that are frequently used in industry. To provide excellent metal plating quality for synthetic moulding activation of ABS sheets is necessary—brushing alone is insufficient. Sulfuric/chromic acid combinations are used to etch the surface of polymers prior to metallization. These baths actually function rather well, nevertheless, the presence of Cr causes serious ecological operating challenges.. The current work presents the findings on the surface moulding of ABS using sulfuric acid-based arrangements in which  $H_2O_2$  and  $HNO_3$ , in place of  $H_2CrO_4$ , serve as oxidants.

**McCaskie et al.(2006)** Author presents technical data on the various mechanisms and techniques involved in achieving successful metal coating adhesion to plastic substrates. Surface preparation is a crucial step, with techniques such as mechanical abrasion, chemical etching, and plasma treatment discussed. The review highlights physical and chemical bonding mechanisms involved in adhesion, such as van der Waals forces, hydrogen bonding, and covalent bonding. Adhesion-promoting agents, such as palladium or stannous chloride, are also discussed. The article presents a detailed comparison of the advantages and disadvantages of different plating techniques, including electroless plating, electroplating, and vacuum deposition, and their compatibility with different types of metal coatings.

**Monzon et al.(2006)** Author investigated electroforming as a technique for production of cores for plastic injection moulds. From CAD models, shells were created utilising the FDM method for fast prototyping. Through the use of conductive paint, the FDM design was rendered conductive. The deposit was made using nickel sulfamate at a concentration of 400 ml/L along with the stress-relieving additive

Allbrite SLA (30 cc/L). The operating parameters for the bath were held constant at pH 4.0, current densities between 1 and 22 A/dm<sup>2</sup>, and temperatures between 35 and 55 °C. Results for internal stresses, hardness, and metallographic structure were evaluated at various levels. Due to the epoxy filling of the shell, it was discovered that the mould insert so created exhibits limited heat conductivity.

**Xiang et al. (2006)** Author presented a method for electroplating ABS polymers directly. Despite being a very efficient and cost-effective technique, they noted that electroless copper plating on nonconductive polymers is not environmentally friendly. The solution of palladium chloride and stannous chloride were found to be very effective and accelerated the process of direct electroplating of copper. The deposition rate of direct copper plating found to be 3500 times faster than the traditional copper deposition. The study's calculated deposition rate was 0.07 mm/s. The thickness variation amongst the deposits was less than 0.1 micron metres, and they were homogenous.

**Kulkarni et al.(2006)** A growing trend in recent years has been the replacement of metals with light weight plastics in the production of PCs, commercial machinery, automobile, media transmission and electronic equipment. Low weight plastic component has always been significant in the aircraft business. Weight reduction is more crucial in the market than ever before. For motor vehicles, for instance, switching from plastic to metal has significantly reduced overall weight and improved fuel efficiency. One example of a model for reducing car section weight is ABS chromed components. In order for the electroplating process to be successful, the plastic model must be made completely electrically conductive. In this work, honest try has been done to clarify and explain the improvement of plating ABS plastics through the new improved electroplating setup. These kinds of plating on polymers have been developed and are often used in the production of printed circuit boards, automotive components, and electromagnetic impedance (EMI) protection fields.

**Hsu et al. (2008)** conducted experiment on gypsum powdered electrode prototype made by 3DP underwent electroless plating. After the electroless nickel plating, copper with a thickness of up to 1 mm was electroformed. Using a corrosive mixture of potassium dichromate, sulphuric acid, and water, the surface that would be electroplated was roughened. The corrosion period, which in this case was 3 minutes,

was also optimised.  $\text{NiSO}_4$ ,  $\text{NaPO}_2\text{H}_2$ ,  $\text{C}_2\text{H}_3\text{NaO}_2$  and  $\text{C}_4\text{H}_4\text{Na}_2\text{O}_4$  solutions were used for nickel plating of  $25\mu\text{m}$ . Using an electrolytic bath of  $\text{Cu}_2\text{P}_2\text{O}_7$ ,  $\text{K}_4\text{P}_2\text{O}_7$  and  $\text{NH}_4\text{OH}$  a thickness of  $1\text{mm}$  was reached for the electroforming of copper on the conducting electrode.

**Monzon et al. (2008)** By using rapid prototyping (RP) and electroforming methods, a novel electrical discharge machining (EDM) electrode was produced. Analysis was done on the electrolytic bath additives, model's composition, copper shell structure, hardness, internal stresses, pitting, roughness and dimensional accuracy. For consistent thickness and smoothness, copper acid solution with three organic agents were employed. The recommended temperature range for the bath was  $20\text{ }^\circ\text{C}$  to  $35\text{ }^\circ\text{C}$ . In locations with high current densities, low temperature causes polarisation and burning, whereas high temperature necessitates the use of additional brightener. The addition of the additive clearly improves the hardness, increasing it from  $60\text{ HV}$  to  $130\text{ HV}$ . At lower VDI values, the produced electrode was shown to function better than the traditional electrodes, while at higher VDI values, the findings were the opposite.

**Jahed and Noban (2009)** investigated on nickel electroformed mould for the early fracture. The specimens that were removed from the electroformed mould underwent tensile and fatigue tests. Both at room temperature and  $200\text{ }^\circ\text{C}$ , the mechanical and fatigue characteristics were discovered. The failure was found to be ductile in nature under tensile as well as fatigue testing. The results demonstrate a maximum endurance limit of  $150\text{ MPa}$  at ambient temperature, yield strength of  $253\text{ MPa}$ , a maximum tensile strength of  $375\text{ MPa}$ , and a  $30\%$  percentage elongation. The performance of the mould shows a decline during the elevated temperature. The hardness around  $136.7$  on the Vickers scale of the electroformed found to be uniform across the thickness of the mould. The properties were found to be similar of the pure nickel.

**Pouzada (2009)** gathered the results of several studies conducted over the course of several decades for the production of hybrid mould employing quick tooling techniques. The factors involved in the hybrid tooling like mechanical performance, thermal performance, tribological issues and design issues compiled and elaborated. It



was concluded that most aspects related to hybrid tooling studied needed to be applied to fabricate large moulds.

**Kang et al. (2010)** created a green etching procedure to pre-treat ABS plastic before electroless plating. To improve mechanical adhesion with the plating media, the ABS plastic's surface must be rough. An alternative to the dichromic acid ( $H_2Cr_2O$ ), fluoric hydrogen acid and hydrochloric(HCl) acid etching process was proposed as these causes environmental problems. The chemical foaming agent MS140 D mixed with methanol solvent and dispersed on the surface using 24 kHz ultrasound for three minutes. The foaming was done by using infrared heater at a temperature of 110-120 °C. The grains broke open and released nitrogen gas as a result of the agent's thermal foaming effect, and they later collapsed and were crushed, leaving the sample surface rough with pores and holes. To further increase the surface roughness the samples were subjected to ultrasonically agitated bath. The cross-cutting method was used to assess the adhesion between nickel and the plastic, and the results showed a strong adherence..

**Bazzaoui et al.(2013)** Another instant plating method was used to metallize acrylonitrile butadiene styrene (ABS), which involved first changing the plastic conductor with polypyrrole (PPy) and then directly electroplating copper. PPy and  $FeCl_3$  act as an oxidant to artificially induce the deposition on ABS. PPy is adhesive to the surfaces of plastic. On PPy/ABS, adherent copper films of varying thicknesses have been obtained during the course of several electrolysis cycles. Analyses using EDS show us that copper is depositing onto the surface of ABS. Expanding the electrolysis time results in a thicker copper covering, according to SEM analysis.

**Equbal et al.(2013)** Electroless plating on polymers with minimal cost and time using different methods has a lot of potential, as seen by the expanding possibilities. The properties of the resulting component will be greatly enhanced with a large expansion in its interest in the global market because plastic parts themselves already possess many beneficial characteristics. If metallic features are added to them, the resulting part's properties will also be greatly boosted. One of the best examples of this is a metalized product, which is created by depositing metallic layers over a plastic or composite object. Due to its reduced weight, lower cost, and ability to take on any shape quickly, plastic products are becoming more and more popular as

manufacturing processes become more efficient. The research examines the various metalizing techniques used on plastic components and compares them.

**Bikulcius et al.(2013)** The method for determining if ABS polymers are suitable for metallization is presented in this study. The review's main objective is to determine the most effective method for judging the level of adhesion between the metal coating and the ABS plastic substrate while applying various adhesion-promoting chemicals. The "peel test" is described in the article as a quick and efficient way to assess adhesion performance. In order to shed light on how well certain adhesion-promoting compounds work, the authors give the test findings for those substances. The review is concluded with a discussion of the results' ramifications, including the significance of effective adhesion promotion for ABS polymers' successful metallization.

**Cobley et al. (2014)** devised a technique for improving electroless nickel plating rates by agitating the bath solution with low frequency ultrasounds, employing 1.5% v/v of palladium instead of 3% v/v. The operating temperature was likewise kept within the necessary range of 25–50 °C to conserve energy. Two methods, continuous ultrasonography and delay time ultrasound, were examined; in the latter, the ultrasound was introduced 7 minutes into a 25-minute cycle after the delay. All techniques were shown to show an increase in electroless plating rate with temperature rise, although delay time ultrasound was found to be more efficient. In fact, at 25 °C utilising 40 kHz ultrasonic, electroless copper coverage was similar to 50 °C with traditional agitation. In contrast to the coarse microstructure in traditional electroless plating, fine grain microstructure produced an ultrasonic environment. The electroless plating's finer grain structure also made sure that the surface would be covered uniformly.

**Olivera et al.(2016)** The butadiene is uniformly distributed in ABS, over the acrylonitrile-styrene grid. ABS has great toughness, precise form stability, manageability, chemical immunity, and value for money. Effective descriptions are given of the plating mechanisms and procedures. Plating on ABS can help to increase the material's durability and temperature resistance while also enhancing its strength and structural integrity, giving it metallic qualities. Overall, this review presents valuable information for researchers and engineers seeking to develop efficient methods for plating on ABS plastics.

**Pandey and Suri (2016)** This paper reasoned that ABS like plastics are low weight, low cost and aesthetically improved plan. The above process is eco friendly so no negative effect on climate. plastic is at a phase of replacing metals parts because of its nature of practical, light weight simple to form so great in aesthetic and design. so on Principle issue is its non-conductivity since metals are generally good conductor of heat and power. Plastic is strengthen enough so we done etching on it to make it conductive with a eco-friendly etching process as immediate electroplating isn't simple without any adhesion. So in this paper coating on plastics is examined below as earlier graphite plating with some adhesion was finished. Presently a days because of progression in industry and material we lean toward the copper plating on ABS plastic.

**Uraz (2019)** In this experimental investigation, the effects of ionic liquids were investigated in the electroless metal plating procedure on ABS plastic. For the copper and nickel plating operations on ABS plastic, two alternative electroless baths were created for this purpose utilising ecologically acceptable chemicals (EMIC & DCA). The etching and plating operations were carried out using ecologically benign chemicals, as opposed to the conventional techniques using chromic and sulfuric acids. In the electroless metal plating process on ABS plastic, the analysed factors were plate thickness, plating time, and the influence of sandpaper size on the plating quantity.

### **2.3 COLD SPRAY**

**K. Sakaki Y. Shimizu et al (2000)** in their research, they used numerical simulation and tests to examine the impact of the nozzle's entry shape. They stated that the gas exhibits a substantially higher temperature and flows subsonically at the convergent region near the nozzle's entry. The convergent section at the entrance thus, is best suitable for heating spray particles. Additionally, they noted that the microstructure, hardness, and deposition effectiveness were all significantly impacted by the change in the gun nozzle's entry convergent section length. As the entrance geometry is increased, the deposition efficiency and hardness also increases.

**Stoltenhoff et al. (2001)** their work gives the analysis of cold spray process as an outcome of CFD analysis and wide-ranging spray experiments. In their experiments,

they modeled particle and the gas flow field for different geometries of nozzle and parameters of the process in association with the experimental results. They discover that adhesion that is specific to the material happens when the powder particles exceed a threshold impact velocity. They observed that the critical velocity for spherical Cu powder with a little amount of O<sub>2</sub> was around 570 m/s. They observed deposition capabilities of above 70% using nitrogen as the process gas and particle grain sizes ranging from 5 to 25 microns. Additionally, they stated that : “ the coatings produced by cold spray exhibit negligible porosity and O<sub>2</sub> concentrations similar to the powdered main material”.

**Assadi et al. (2003):** Cold spray is a coating method that does not require the spray powder to be heated significantly. The bonding between particles in cold spray is weak and substrate happens because of particle kinetic energy upon impact. According to the findings, adiabatic shear instabilities that occur at high-velocity particle/substrate or particle/particle interfaces are to blame for the adherence of particles.

**Li et al (2004)** used the computational fluid dynamics programme FLUENT to conduct a numerical study for the accelerating behaviour of spray particles in cold spraying. Based on modelling findings, they were able to build the spray gun nozzle in the best possible way to address the issue of coating the narrow inner surface of a small cylinder or pipe. According to their findings, the nozzle expansion ratio, temperature, operating pressure, accelerating gas type, and particle size were the primary determinants of how quickly spray particles accelerated in a constrained area. By employing experimental findings from the planned small nozzle with a total gun length of around 70 mm, they were able to confirm the viability of the ideal design for a spray gun nozzle.

**Champagne et al. (2005)** in this work goal was to show microstructural proof of a bonding mechanism between a copper substrate that has undergone cold spray deposition and an aluminium substrate. They further explains the various parameters of the same that are taken into considerations. Their study also comprises the comparison of various thermal spray technologies.

**Knight et al. (2005)** in his work he tells about the origination of very first thermal spray technology by Schoop. He explains how the notion grown from the model of a

toy canon to a discovery that has changed the face of coatings in the world. He explains the contribution of Schoop in the development of various types of thermal spray technologies such as HVOF, Plasma and Cold Spray. He also tells about the applications of thermal spray such as wear and corrosion resistance marine and aerospace industry. He also explains the breakthrough that the technology has made in surface engineering.

**Schmidt et al. (2006)** constructed of a generalised parameter window for using cold spray deposition is covered in this study. To allow bonding with a substrate with cold spray, the particle velocity should be higher than the critical velocity. Many factors affect critical velocity, including spray content, powder consistency, particle size, and particle impact temperature.. The generalised window offers enough details to predict the optimal spray conditions for cold spray on various substrates, according to the results.

**Stoltenhoff et al. (2006)** The paper discusses the microstructures and critical properties of copper coatings in cold and thermal spray applications. The outcome demonstrates that cold spray has significant advantages over thermal spray. Cold spray coating has a greater conductivity than thermal spray. Many annealing experiments and studies revealed that in cold- sprayed coatings, recovery and recrystallization are the key determinants of subsequent micro structural innovations.

**François Raletz et al.(2006)** discussed the critical velocity of particles in cold spray (CS) settings. The characteristics of the substrate and the sprayed substance define the particle's critical velocity. The findings reveal that, we can detect the change in impact particle velocity for critical velocity by counting the amount of rebounds on the substrate.

**Li et al. (2006)** study examines the critical velocity for copper(Cu) particle deposition in cold spray. Both theoretically and empirically, the critical velocity of the copper particle for deposition in cold spray was established. On the basis of observations of relative deposition effectiveness at various spray rates, an experimental approach for figuring out a particle's critical velocity was presented. The results show that as particle temperature rises, critical velocity decreases. Its oxidising state has an effect on it as well.

**Fukanuma et al. (2006)** studies Aluminum, Nickel, and Copper coatings deposition by Cold Spray on three different of substrates, copper, aluminum and Steel. They tested the hardness of the substrates and the tensile strength of the coatings. Additionally, they discussed how the hardness of the substrate affected the coating's tensile strength. Additionally, they talked about how the working gas temperature affects tensile strength.

**Pattison et al. (2007)** reports on the progress of a fresh freeform construction technique using cold spray. They also reports that the process is capable of producing functional forms by employment of unique manufacturing strategies for cold spray. The paper gives statistics on the process including details of tactics incorporated during the fabrication of the component. They concludes the possibility for building the components from materials like Ti, which unveiled embedded devices, internal channels and freeform surfaces.

**Hussain et al. (2009)** in their research have found the contribution of the bonding mechanism in the cold spray technique by the comparison of the metallurgical bonding (Substrate + Particle) and mechanical interlocking (particle + sprayed layers with the methodology of using a short heat treatment to promote inter diffusion and intermetallic formation. Low binding strength was observed on the grit-blasted surface due to micro-pores and flaws. Only the initial few layers of coating are affected by the substrate surface roughness, hence the influence on deposition efficiency may be minimal. In their experiment they perform CS using DeLaval nozzle, Cu powder on Al polished and grit blasted, polished and ground substrate and did the bond strength and fracture testing. The bond strength is higher if CS is done on Grit blasted substrate which is annealed prior to CS.

**Jung et al (2009)** To lessen the shockwave, experiments were done on the nozzle's length ratio and expansion ratio in relation to temperature, gas pressure, and nozzle length. They observed that the particle temperature increases and the particle velocity decreases as the convergent length increases. Increases in particle velocity and temperature are accompanied by increases in divergent length. When the nozzle's expansion ratio is 4.27, the particle velocity reaches an extreme of 633.1 m/s, and the shock wave is kept to a minimum. With increases in nozzle length and gas pressure,

the nozzle's ideal expansion ratio rises. The ideal expansion ratio of the nozzle does not alter with a change in gas temperature.

**Li et al (2010)** discovered that in addition to material kinds, particle temperature and oxidation conditions also affect the critical velocity. By isothermal oxidation in the presence of ambient air, they altered the powders' oxygen content. They looked at how oxygen content affected the critical velocity and found that, in addition to material parameters, the critical velocity in cold spray was also menacingly affected by particle oxidation conditions. They claimed that the change in powder oxygen concentration caused the critical velocity of copper particles to vary from around 300 m/s to over 610 m/s. They discovered that the critical velocity was more significantly impacted by the material's characteristics at low oxygen level than at high oxygen content. According to their findings, the oxide on the powder surface tends to influence the critical velocity with a rigorously oxidised powder rather than the characteristics of the materials.

**Ning et al (2010)** used CFD software to create a 2D model of the low pressure cold spray with radial powder feeding. Both the nitrogen and the helium propellant gases' flow fields were modelled. They devised a discrete phase model to describe the interaction of the particle with the supersonic gas jet in order to estimate the in-flight particle velocity and temperature. To verify the estimated velocity for the low-pressure cold spray technique, they employed experimental copper powder of various sizes. Their findings demonstrate that the computer model can accurately anticipate the supersonic gas flow. They discovered that the drag coefficient formulas developed by Morsi and Alexander and Henderson yielded equal velocities. In order to compare the predicted velocity of a non-spherical particle to the experimental findings, the shape factor can be reasonably computed.

**Huang and Fukanuma (2012)** examined the impact of particle velocity on cold spray deposit adhesive strength. They claimed that increasing gas pressure, temperature, or utilising helium instead of nitrogen gas boosted the in-flight particle velocity. The adhesive strength of coatings to surfaces rose along with the particle velocity when gas pressure and temperature were raised or helium was used in place of nitrogen gas. They also observed that, based on plastic deformation, the particle velocity has a significant effect in enhancing adhesive strength. An improved link between the



coating and substrate is produced by the mechanical interlock effect, which is enhanced by increased particle velocity. Discussed how particle velocity affects the bonding strength of cold spray deposition.. A5052, A6063, and copper were used as the substrates for this experiment. Copper metal powder with an average diameter of 18 micrometre was used for the cold spray. Copper powder has a bonding strength of >150 MPa to copper.

**Singh et al. (2012)** in their work concisely labels the various facets of cold spray technology, also explaining the crucial parameters that affects the deposition conduct along with pros and cons; applications and history of advent of cold spraying. They have concluded cold spray technology as an emerging technology to enhance and enlarge the series of uses for thermal spray procedures as a greener auxiliary according to stringent environmental and health safety regulations rather not for the replacement of any of the deep-rooted coating methods. They also frames the future scopes of the study of the technology as designing of optimum parameters like nozzle design, temperature control, nature of gas, and its material and also estimate of critical velocity for different substrate and particle blends.

**Yin et al. (2013)** examine how the spray angle affects how hot or cold the metal substrate is during the cold spraying procedure. To achieve the goal, they worked using a CFD technique. Their modelling results show that the spray angle has a significant impact on the substrate's temperature distribution. They get to the conclusion that when using a perpendicular spray, the temperature gradient contours typically take the shape of an annulus, meaning that the temperature distribution depends exclusively on the radial location. Additionally, they note that the highest value of the surface temperature is somewhat off-center from the geometric centre (the point of stagnation), which may be the result of the flow evolving from a laminar to a turbulent condition. He discovers that moving the nozzle from uphill toward the downhill direction is the optimum technique to warm the substrate at the angle condition.

**Sova et al. (2013)** take into account two situations with powder injection to subsonic and supersonic portions of the nozzle, the effect of powder preheating on the particle impact was numerically examined. They claimed that the particles injected to the nozzle pre-chamber had a lower effect temperature than the artificially warmed 10–50



m copper particles that were axially injected to the supersonic area of the nozzle. They provided an explanation for this phenomenon by pointing out how the position of the powder injection site affected the length and intensity of the gas-particle heat exchange. The implementation of powder preheating might move the particle impact characteristics toward the deposition window in the event of powder injection into the supersonic zone, they added, without raising the working gas stagnation temperature.

**Yin et al. (2013):** The cold spray deposition behavior of preheated and softened copper particles is investigated in this paper. The preheated temperature was set to 300 degrees Celsius. Preheated particles deform more than non-preheated particles, according to the report.

**Sova et al. (2014)** in their research have found the effect of the powder feedstock entry position into the cold spray apparatus that can lead to maximum deposition efficiency. They found that powder entered after throat of nozzle and mix with preheated air have more deposition efficiency than entering it before the throat thus reducing the efficiency and increasing wear and tear of the nozzle because it not only depend on impact velocity but also on impact temperature during coating. Thus injection of the Cu powders in supersonic region after the throat in DeLaval nozzle lead to impact velocity and temperature even in low working gas temperature and more sensitive to thermal advantage of preheat air than if enters in nozzle in sub sonic region i.e. before throat, in this case all favoring parameters will not be effective at all.

**Cai et al. (2014)** examined the connection between the spray distance and the coating profile. A technique for modelling coating profiles was used in this study; in Matlab, a 2D coating profile was fitted as a Gaussian curve. They analyze the connections between the spray distance, scanning step, coating thickness, and deposition efficiency.

**Lemiale et al. (2014)** in their research have described the model which shows combine effect of the strain rate and the temperature as a 3D model as a single Cu particle impacting the Cu substrate using smoothed particle hydrodynamics. The assumption of both particle and substrate at room temperature initially during the impact and using low strain rates are incorrect and provide misleading results because thermal softening can change final attributes of the CS coating. These experiments

enable the investigation of essential elements in the physical mechanics of cold spray and will optimise the procedure based on data not accessible in experimental settings.

**Huang et al. (2014)** in their research have developed the ultra-strong bonding inbetween the particle and substrate and its measurement is done by pull test and corresponding stress and strain graphs are plotted, effect of critical velocity and splat formation effected by impact temperature. The initial applied impact by the powders was used to initiate the jet formation in substrate that will lead to CS coating in effective way.

**Kaur et al. (2015)** in their research have found that the Thermal spray coating of the corrosion-erosion resistant Cr and Ni on the boilers steel tubes which was done earlier for resistance of corrosion and erosion at high temperature have some oxidation and chemical behavior different than estimated. They have taken boiler steel tube material of power plants i.e. T22 and SA516 which are polished then grit blasted to have rough surface and proper material interlocking with powders and used the powder for cold spray as mixture of micro and nano sized Ni and nano sized Cr termed as Ni-20Cr. The nano particle seems to be more effective in coating using square exit DeLaval nozzle than the micro particles due to less density and high resistance to corrosion and erosion.. The adhesion strength, scratch resistance and indentation are found using high tech devices like Ducom, TR-101 etc. The oxidation process is performed by washing the specimen with acetone. The results shows that oxidation of the powder do not take place using XRD/SEM/EDS techniques. Due to introduction of the nano particles in the cold spray along with micro particles the hardness and the erosion-corrosion resistance than the bare boiler steel tubes. Thus cold spray utilized to improve its material quality even at elevated temperature after CS process is being done.

**Grigoriev et al (2015)** in their workthey explains the fundamentals of the process with the mechanism of coating. They also gives the empirical relations associated with the process. Further they explains the construction of the apparatus and the comparison of cold spray with other thermal spraying technologies.

**Li et al. (2015)** The paper provides information on the residual stress analysis of copper coatings applied by cold spray, as well as numerical simulation results. The copper cold sprayed Cu and Al substrates were used for the analysis. The maximum

residual compressive and tensile stresses increase with increasing impact velocity from 300 to 500 m/s, according to the findings. Effect velocity of 500 to 700 m/s, With an increase in velocity in Cu/Cu and a marginal increase in Cu/Al, the residual stress does not shift significantly.

**Kumar et al.(2016)** In any coating operation, the roughness of the substrate is critical. It strengthens the bond between the substrate and the coating. The effect of surface roughness on the cold spray bonding mechanism is the subject of this paper. It explains how surface roughness improves the bonding of the substrate to the cold spray coating. The experiment included a variety of material pairings, including soft/soft, soft/hard, hard/soft, and hard/hard. The ideal roughness size for soft/soft, hard/hard, and soft/hard interactions is R3, 0.75 times the particle size (R2), and between 0.5 and 0.75 times the particle size, respectively (R1 and R2).

**Che et al. (2017)** The paper provides a study on the cold spray-ability of metal powders(Cu, Fe, Su) on different materials (including polymers). The metal powders that are used for the experiment is copper, tin, and iron. polymers that are chosen to cold spray the metal powders are carbon fiber reinforced polymer (CFRP), polyether ether ketone (PEEK), acrylonitrile butadiene styrene (ABS), polyethyleneimine (PEI), mild steel. Results show that Thick copper coatings were successfully deposited on PEEK and PEI at 425°F At low pressures (14 bar and lower), CFRP has significant erosion and ABS deposition efficiency is (less than 5%). At high pressures, CFRP has significant erosion and ABS deposition efficiency is (less than 5%). (20 bar and higher). The best deposition behaviour was observed when tin was coated on ABS at 200°C and 14 bar (1.4 MPa). The coating, however, is not standardised.

**Yin et al. (2018)** presented the advancements in the field of CSAM since the start of 1980s. It's been used as an additive manufacturing method to produce and restore parts in recent years. Cold spary is used to make multimaterial metal composites.

**Che et al. (2018)** Cold spray has proven to be a viable approach for metallizing polymers (metallization is the process of coating polymers with metal) and polymer composites. The effect of a single copper particle on polymers is discussed in this paper. ABS, PEEK, and PEI are the polymers used in the experiment. The copper

particle interlocked well with all three polymers without causing significant particle deformation, according to the findings. PEEK is the only substrate that can achieve a good thick coating.

**Joshi and James (2018)** The main goal is to comprehend the significance of the parameters (impact velocity and angle of impact) in cold spray, as well as their impacts. It also uses MD (Molecular dynamics) simulation to investigate the effect of particle size on the plating consistency of cold spray on an atomistic scale. The study found that impact velocity of 500-700 m/s is ideal for uniform and thick coating. We can reach the maximum deposition height at 90 degree (angle of deposition). However, we can achieve uniform coating at 600, and uniformity improves as particle size increases above 20.

**Rahmati et al. (2020)** The paper investigates how the copper particle deforms during impact. To investigate the shift in deformation behaviour, copper particles of various diameters (5,10,20,30,40 NM) were used. The particle's initial temperature and velocity are 300 k and 1000 m/s, respectively, and the particles are accelerated using cold spray. Particles with a diameter greater than 10 nm have three phases of deformation, according to the findings. The lower half of the particle deforms first, followed by the lower half of the particle, and finally the top of the particle. However, the upper half of the body remained almost unaltered.

**Srikanth et al. (2020)** Cold spray is a cutting-edge technology with a wide range of industrial applications. It became increasingly advanced over time. This paper examines the cold spray coating process in detail, including its operating theory, process parameters, and applications.

**Wu et al. (2021)** in this article discusses several spray trajectories (zigzag, cross, parallel, and spiral) and how they affect the vital characteristics of copper deposits that are cold sprayed. The impacts of the spray trajectory on the related thermal background and residual stress distribution are also described in depth. The results indicate that parallel paths have an effect on surface morphology. However, it has a smaller impact on surface roughness.

Table 2.3 Cold Spraying Parameters for Different Materials and Substrate

Substrate Material	Powder Material	Carrier Gas	Powder Diameter ( $\mu\text{m}$ )	Temperature	Pressure	Reference
				( $^{\circ}\text{C}$ )	(MPa)	
SS347	Ag	Air	15 to 50	250 to 450	1 to 2	Chavan et al., 2011
SS400	Cu	Air	5 to 50	300	3	Fukumoto et al., 2009
SS304	Cu	Air	5 to 15	250 to 650	0.4 to 1	Fukumoto et al., 2007
SS304	Cu	He	5 to 15	20 to 400	0.2 to 1	Fukumoto et al., 2007
SS304	Inconel 625	N <sub>2</sub>	38 to 15	500	3.2 to 3.3	Poza et al., 2014
SS304	Ti	He	<25	20	2.9	Hussain et al., 2011
SS304	Cu	Air+He	-	249 to 399	0.4 to 0.6	Fukumoto et al., 2007
SS316L	Cu	N <sub>2</sub>	10 to 33	150	1	Raletz et al., 2006
SS	Cu	N <sub>2</sub>	15 to 37	220	2	Li et al., 2007
SS	Ti	N <sub>2</sub>	37 to 44	240	2	Ji et al., 2013
SS304	SS316L	He	16 to 44	150 to 300	1.5 to 3	Fukumoto et al., 2006
SS304	Fe101	N <sub>2</sub>	15 to 44	200 to 300	1 to 3	Fukumoto et al., 2006
SS	Cu-Sn	He	48	520	2	Li et al., 2007
SS	WC-12Co	N <sub>2</sub>	9 to 17	750	2.4	Ji et al., 2013
SS304	WC-12Co	N <sub>2</sub>	15 to 45	700	3.4	Kim et al., 2005
SS304	WC-17Co	N <sub>2</sub>	15 to 45	600	1.2 to 1.5	Kim et al., 2005
SS	WC-17Co	He	30	600	3 to 4	Ang et al., 2011
SS316L	Ni/Al- TiB <sub>2</sub>	N <sub>2</sub>	-	250 to 450	2 to 2.2	Chen et al., 2019

Al	Al	He	20	20	1.5 to 2	Morgan et al., 2004
Al	Al	-	2 to 20	-	-	Wang et al., 2011
Al2024 T351	Al	N2	5 to 50	230	3.45	Ziemian et al., 2014
Al 1100	Al1100	He+ N2	1 to 30	227 to 527	2.1	Balani et al., 2005
Al	Al2618	He	25	20	1.7	Ajdlelsztajn et al., 2006
Al6061	Al2618	He	25-38	20	1.4	Jodoin et al., 2006
Al5052	Al7075	N2	-	500	1.6	Ghelichi et al., 2014
Al6061	Cu	N2	-	300	1.5	Richer et al., 2006
Al6082	Cu	He	5 to 25	200	3	Hussain et al., 2005
Al6063	Cu	Air	5 to 15	250 to 650	0.4 to 1	Fukumoto et al., 2007
Al	SS316L	N2	18 to 25	500	4	Sova et al., 2005
Al	SS316L	N2	28 to 45	600	4	Sova et al., 2005
Al	SS316L	N2	36 to 53	720	4	Sova et al., 2005
Al7075 T6	SS316L	N2	20 to 40	600 to 800	2 to 4	Villa et al., 2013
Al	Ta	N2	10 to 30	800	3.8	Bolelli et al., 2010
Al	Ti	N2	-	370 to 480	2.7	Lima et al., 2002
Al6063	Ti	He	22	600	1.5	Moay et al., 2010
Al2O3	Ti	N2	25	450	2.5	Rokni et al., 2015
Al6061	Zn	He	17 to 45	260	2	Robitailli et al., 2009
Al	Al	Air	53 to 75	315	2	Zhao et al., 2006

Al	Zn	Air	45	315	2	Zhao et al., 2006
Al	Al	Air	90	290 to 340	1.5	Van et al., 1999
Al	Fe	Air	≤45	480 to 590	1.5	Van et al., 1999
Al	Cu	Air	≤445	480 to 590	1.5	Van et al., 1999
Al	Cu	N <sub>2</sub>	-	300 to 640	2 to 2.99	Zahiri et al., 2006
Al6061	Al-5Sn	N <sub>2</sub>	20	500	3	Ning et al., 2008
Al6061	Al-10Sn	He/ N <sub>2</sub>	15.2	300	0.7	Ning et al., 2009
Al	Al-13Co-26Ce	He	23	200 to 370	1.7	Sansoucy et al., 2007
AlSi4130	Cu-2Ag-0.5Zr	He	27	500	1.6 to 2.6	Codded et al., 2013
Al6061	Al-Cr-Mn-Co- Zr	N <sub>2</sub>	-	430	3.5	Watson et al., 2017
Al6061	Ti <sub>2</sub> AlC	N <sub>2</sub>	25 to 40	500 to 800	3.8	Rech et al., 2013
Al6061	CoNiCrAlY	He	5 to 37	550	2	Richar et al., 2010
Al7075 T6	WC-12Co	N <sub>2</sub>	10 to 30	800	3	Ji et al., 2013
Al7075 T6	WC-17Co	N <sub>2</sub>	10 to 30	800	4.4	Li et al., 2007
Al7075 T6	WC_25Co	N <sub>2</sub>	32	800	3 to 4	Dosta et al., 2013
Al7075-T6	Al	N <sub>2</sub>	-	1000	2.5 to 4	Silva et al., 2017
Al	WC_CoCr	He	34 ± 17	550	1.7	Yandouzi et al., 2007
Brass	Al	Air	40,60,80	204 to 371	2	Alkhimov et al., 1982
CI	Cu	N <sub>2</sub>	1 to 50	600	2.7	Choi et al., 2010
Bronze	Al	Air	9 to 40	290 to 340	1.5 to 2	Vin et al., 2013
Bronze	Fe	Air	≤445	480 to 590	1.5 to 2	Vin et al., 2013

Bronze	Cu	Air	≤445	480 to 590	1.5 to 2	Vin et al., 2013
Cu	Cu	Air	75	500	2.5	Eason et al., 2013
Cu	Cu	He	1.32	–	–	Eason et al., 2013
Cu	Cu	N <sub>2</sub>	10 to 33	150	1	Raletz et al., 2006
Cu	Ni	N <sub>2</sub>	10 to 33	150	1	Raletz et al., 2006
Cu	Al-10Sn	He/ N <sub>2</sub>	15.2	300	0.7	Ning et al., 2008
MS	Inconel 718	N <sub>2</sub>	33	800	3.2 to 3.4	Levasseur et al., 2012
MS	Ti	N <sub>2</sub>	38 to 44	155 to 263	2	Li et al., 2003
MS	Ti	He	38 to 44	255	1	Li et al., 2003
Fe	Ti	He	<25	20	2.9	Husain et al., 2011
MS	Ti	He	<25	20	2.9	Husain et al., 2011
Fe	Ti	N <sub>2</sub>	44	450	2	Wang et al., 2010
MS	Zn	He	5.2 to 26.4	140	0.5	Li et al., 2008
MS	Zn	N <sub>2</sub>	5.2 to 26.4	165–410	2	Li et al., 2008
MS	Al2319	Air	<63.8	250	2.8	Li et al., 2008
MS	Ti	Air	<38.9	250	2.8	Li et al., 2008
MS	Cu	Air	<98.5	250	2.8	Li et al., 2008
MS	Ti	Air	5 to 45	250	2.8	Li et al., 2007
MS	Ti	N <sub>2</sub>	5 to 45	263	2	Li et al., 2007
MS	Ti6Al4V	Air	5 to 90	520	2.8	Li et al., 2007
MS	Al	Air	5 to 63	520	2.8	Li et al., 2007
MS	Al-10Sn	He/ N <sub>2</sub>	15	300	0.7	Ning et al., 2009
MS	Cu—6Sn	Air	28	500	3	Guo et al., 2007



MS	Cu-8Sn	Air	17	500	3	Guo et al., 2007
MS	Diam alloy	N2	<50	800	–	Cinca et al., 2013
Carbon Steel Alloy	Cu	N2	-	400	3	Silva et al., 2019
Ni	Al	Air	80	280	0.7 to 2.5	Lee et al., 2008
Ni	MCrAiY-Re	N2	10 to 40	800	4	Bonadei et al., 2014
Ni	Cu	Air	-	375 to 400	0.71 to 0.82	Goyal et al., 2012
Ti	Ti	N2	29	300 to 800	3 to 4	Zahiri et al., 2009
Ti	Ti	N2	16 to 22	600	2.4	Zahiri et al., 2009
Ti	Ti	He	16	600	1.5	Zahiri et al., 2009
Ti-6Al-4V	Ti	He	5 to 29	260	1.6	Cizek et al., 2013
Ti64	Ti	N2	-	1000	4.5	Lek et al., 2018
Ti-6Al-4V	Ti	N2	-	780 to 1000	3.8 to 5	Vidaller et al., 2015
Sn	Al	He	15 to 75	20	2.5	Zhang et al., 2009
Zn	Zn	N2	5.2 to 26.4	320	2	Li et al., 2010
Si	WO3	He	30 to 50	300	0.7	Koivuoto et al., 2014
WC-12Co	WC-12Co	N2	9 to 17	750	2.4	Chun et al., 2012
PVC	Cu	N2	-	373 to 573	44564	Ganeshan et al., 2012

CFRP	Cu	N2	-	482	0.41 to 0.48	Fallah et al., 2020
PC/ABS	Cu	N2	-	-	0.5 to 3	Lupoi et al., 2010
PEEK	Ti	N2	-	800	4	Gardon et al., 2009
CFRP, ABS	Fe	N2	-	425	2 to 4.9	Che et al., 2018
CFRP, ABS, PEEK	Cu	N2	-	425	0.3 to 1.4	Che et al., 2018
CFRP, ABS, PEEK	Sn	N2	-	200	0.5 to 1.4	Che et al., 2018

Table 2.4: Properties of Cold Sprayed Layer and The Testing Method

Properties	Testing Method	Description	Reference
Micro Hardness	Berkovich Indenter	<input type="checkbox"/> When the substrate and deposit material are same then hardness depends on the porosity of the deposited layer.	Rokni et al., 2015
	Oliver Method	<input type="checkbox"/> Substrate and deposit material are different then hardness depends on intrinsic material differences.	
	Pharr Method	<input type="checkbox"/> The internal porosity will be high on surface leads to less bonding and finally low hardness value. Hardness increases as we go deep from surface.	
Bond Strength	Tensile Pull Off	<input type="checkbox"/> Bond strength depends on variables such as	Huang et al., 2012,

		a) Velocity of particle	Bhinder et al., 2011, Chun et al., 2012
		b) Temperature and pressure of carrier gas	
		c) Standoff distance	
		d) Surface roughness	
		e) Spray angle	
Tensile Strength and Ductility	ASTM E-8	<input type="checkbox"/> Tensile strength and ductility depend on some variables such as	Bhinder et al., 2011, Ghelici et al., 2012, Assadi et al., 2003, DeForce et al., 2011, Coddet et al., 2015
	ASTM E-290	a) Speed of material	
		b) Gas type, temperature, and pressure	
		c) Surface roughness	
	d) Spray angle		
Fatigue	Stress-Life Method	<input type="checkbox"/> The fatigue in cold-sprayed materials is significantly influenced by the properties of the material and the spraying settings.	Ghelici et al., 2012 Ziemian et al., 2014
	Strain-Life Method	<input type="checkbox"/> The compressive stresses present in cs deposits helps to hold back the crack formation due to fatigue loading.	
	Crack Growth Method	<input type="checkbox"/> The fatigue strength will be increased by surface preparation techniques like shot peening and grit blasting.	
Residual Stress	Hole Drilling Method	<input type="checkbox"/> Cold spray will have compressive residual stresses.	Ghelici et al., 2012, Shayegan et al., 2014
		<input type="checkbox"/> Residual stresses also depend on the various process parameters of cold spray mainly on the substrate material	

		and depositing powders hardness.	
Corrosion	Electrochemical Method	<input type="checkbox"/> The cold spray deposited materials will have high density and the inviolable microstructure leads to high corrosion resistance.	Jones et al., 1996 Koivuluoto et al., 2014
	Weight Loss Coupons	<input type="checkbox"/> The passivation of metals which means the formation of oxide layer reduces the corrosion.	
		<input type="checkbox"/> Passivation potential helps to indicate the corrosion.  <input type="checkbox"/> $E_p$ indicates the critical potential; above the $E_p$ the corrosion decreases and below the $E_p$ the corrosion highly increases.	
Porosity	$\text{Porosity Volume} = (\text{Total Volume}) - (\text{Material Volume})$	<input type="checkbox"/> The particle deposition and particle velocity depend on Pressure and temperature hence the effect of Temperature, pressure and material size varies the porosity	Zahiri et al., 2006, Singh et al., 2020

The 3D printing technology for metal is yet not economical. This work is study towards hybrid additive manufacturing of metal parts using 3D printing, electroplating and cold spray coating.

In the first stage, different geometrical shapes designed through CREO software were converted into the STL files for the fabrication of test samples of ABS using FDM technique. The components were produced for the best settings of layer thickness, build direction, step over and raster angles as suggested in the work of the various researchers and as per the manual provided by the manufacturer of machine.

The second stage was the optimization of the process parameters for copper electroplating along with the fabrication of the setup. Copper coating is the essential process to be done on the plastic substrate before the final coating of copper using cold spray. An experimental study was performed using Taguchi's L9 orthogonal array for the input process parameters such as current density, electrolytic solution concentration and time. The optimization was established against the material coating rate and surface finish of copper on 3D printed part.

The third stage was the creation of the cold spray coating setup and optimization of the cold spray process parameters. A detailed emphasis was given for the optimization of the process to ensure the consistency of the process. The experimental studied was performed by L9 orthogonal array of Taguchis method. In the study, the input process parameters considered were gas temperature, electroplating coating thickness and nozzle. The optimization was established against the material coating rate. and microhardness, adhesive strength, surface roughness of copper coating.

In the fourth stage, the study of surface morphology after the cold metal spraying process was performed through SEM and XRD

The flow chart depicting the process of cold spray coating on metal coated 3D printed part has been shown in Figure 3.1. Chapter illustrates the comprehensive approach for specifications of materials, methods, equipment and measurement instruments, testing techniques and analysis methods used for conducting the present research.

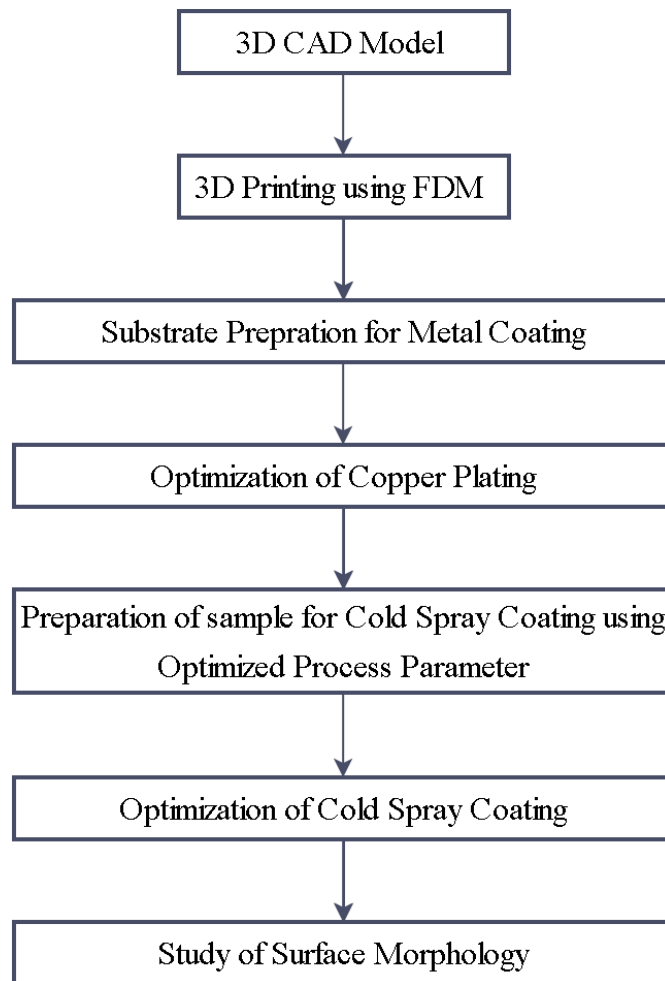


Figure 3.1 Process Flow Chart of Cold Spray Coating of Metallized 3D Printed Parts

### 3.1 3D PRINTING OF ABS SPECIMEN

#### 3.1.1 3D CAD MODEL OF SELECTED SAMPLES

The CAD models of the test samples used for the process optimization selected to represent the primitive shapes of any solid model like cylinders, cube, cone or cuboids, the Creo 2.0 was used to create these CAD models. The cylindrical component (Figure 3.2) was selected for the optimization of copper coating process parameters.

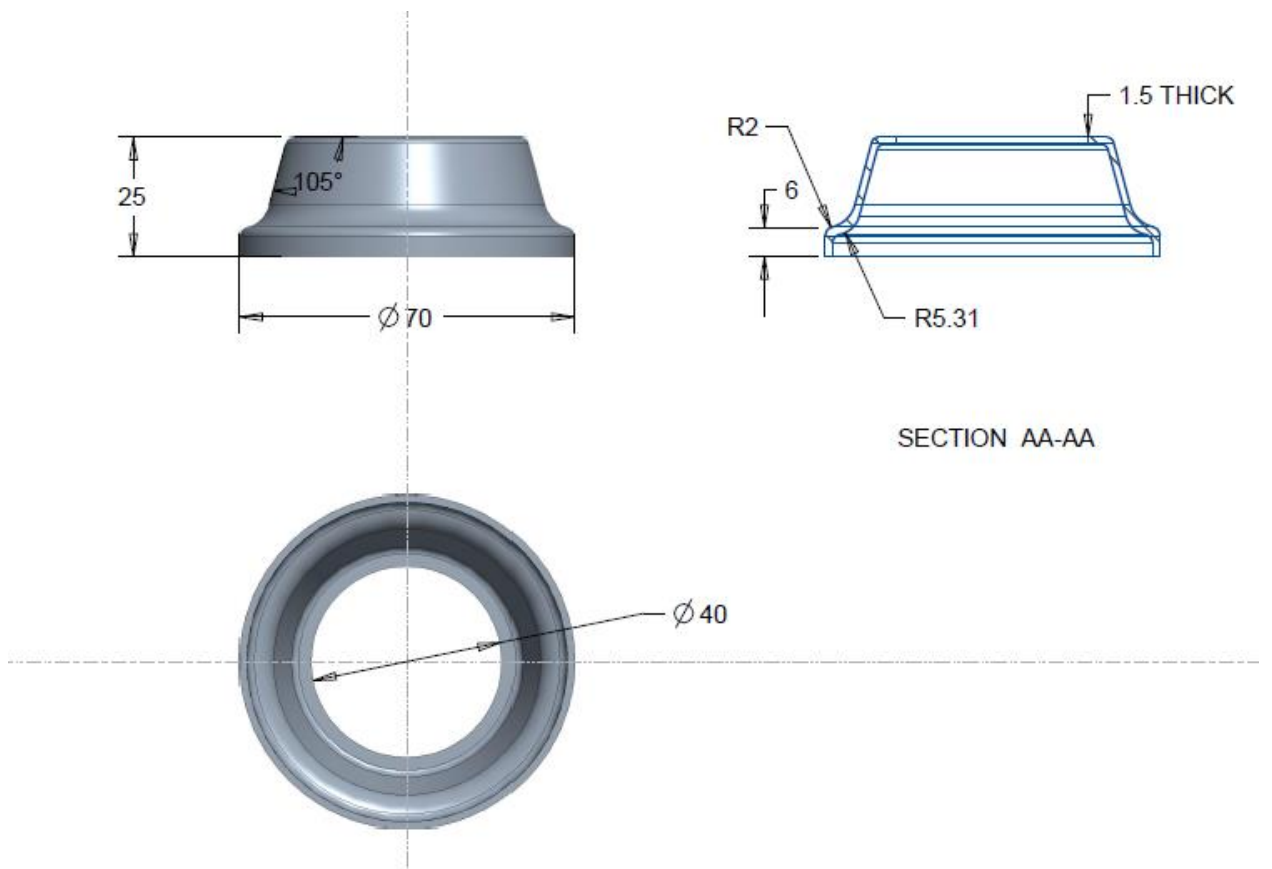


Figure 3.2 CAD Model of Sample Component for Copper Electroplating

One different components selected for design of CAD models, having a rectangular frame for the process optimization of copper cold spray coating on the plastics. The CAD drawings of the components are shown in Figure 3.3.

### 3.1.2 FUSED COATING MODELING 3D PRINTING APPARATUS

The test components and final mould assembly designed by Creo 2.0 were finally produced with ABS material by Ultimaker 3 of Neatherland as in Figure 3.4(a). The facilities available at Lovely Professional University was used to produce the

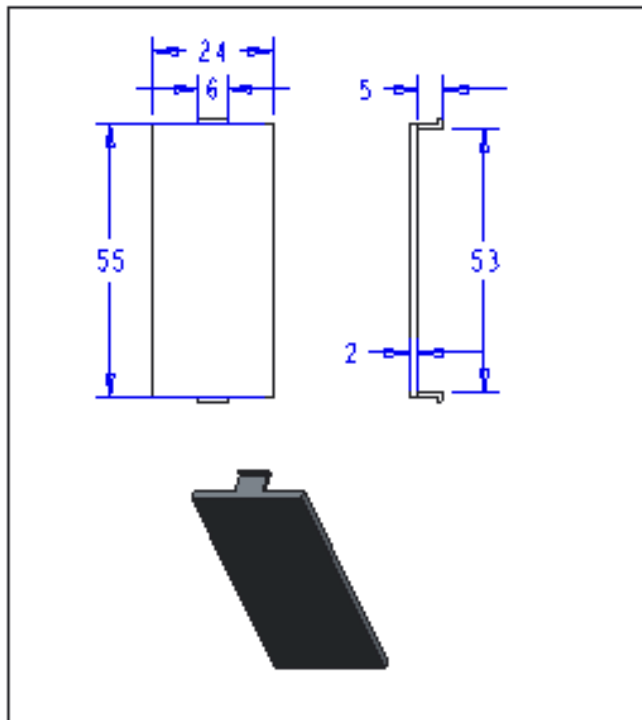


Figure 3.3 CAD Model of Sample Component for Cold Spray Coating

components. The 3D CAD files of models are converted into STL format and exported to the FDM machine system for final slicing of 0.127 mm thickness using Ultimaker Cura software. The printer then builds these sliced cross-sections one after another from the lower part of the component to the upper part with ABS and support material. The ABS and the support material are forced through the two nozzles available at the head of the machine as shown in Figure 3.4(b). Two different spools of wires supply the material to the nozzles using electromechanical devices (as shown in Figure 3.5).

Materials used for support as well as model are polymers made from ABS and the main solubility of these two materials in water is where they differ from one another.. Model material is insoluble, while support material is constructed of a water-soluble substance. The extrusion head can move in horizontal directions designated as x and y direction while





(a)



(b)

Figure 3.4 FDM Apparatus used in Experimentation

the third direction, i.e. z direction is provided by the work table of the machine. Extrusion force is provided by the rollers and the motion to the extrusion head and table is provided through servo motors. The speed control is automatically adjusted by the machine as per the geometry of the component.

FDM machine before executing the command for printing of the components does the self-referencing for x, y and z axes. After calibration is completed, the system needs 3 to 4 minutes to heat the work chamber and extrusion head to 80 and 220 degrees Celsius, respectively. The heated nozzles melt the plastic, and a mechanism helps to control the nozzles and flow of the melted plastic.

The Initial few layers are printed with the support material to fabricate the foundation of the part to be built upon. Additionally, this foundation prevents model material from coming into direct touch with the base platform, which would otherwise make it difficult to separate and risk damaging the table. No additional binding material is

required to keep the layers intact apart from the main material and the support material. The machine's comprehensive specifications are provided in Table 3.1.



Figure 3.5 Feed System for Model and Support Material

Table 3.1 Specifications of the FDM Machine

Part Name	Printing Properties
Print head	Dual-extrusion print head with an auto-nozzle lifting system and
Build volume	215 x 215 x 200 mm
Filament diameter	2.85mm
Layer resolution 0.25 mm nozzle:	150 – 60 micron
XYZ accuracy	12.5, 12.5, 2.5 micron
Print head travel speed	120 mm/s
Build speed	< 24 mm <sup>3</sup> /s
Build plate temperature 20 – 100 °C	80 °C
Supported materials	PLA
Nozzle diameter 0.25 mm, 0.40 mm, 0.80 mm	0.25 mm
Nozzle temperature	220 °C

After fabrication, the components are cleaned in an ultrasonic cleaner for 30 minutes at fifty degrees Celsius, using water and sodium hydroxide solution. Ultrasonic waves cause the burrs and flakes of the support structure to be washed away. The transducer converts electricity into sound waves and further into vibrations which have the capacity to remove microscopic dust particles. The support structure gets dissolved into water while clean ABS parts are received after washing for 30 minutes. Then the part can be post processed further.

### **3.1.3 ABS MATERIAL**

The use of plastics in daily life for various purposes has taken the prime place in the product manufacturing in less than a century. Plastics are instrumental in light weight applications, medical equipment, automotive, household products, packaging and many more products. The plastics are made by linking hydrocarbon atoms indefinitely to form very large molecules through covalent bonds. Broadly the plastics are divided into two categories thermosets and thermoplastics. Thermoplastics are the major contributor to the plastic industry. There is a big family of plastic materials and commonly used plastics for various applications are ABS (Acrylonitrile-Butadiene-Styrene), Acrylics, Cellulosic, Fluorocarbons, Polyamides, Polycarbonates (PC), Polyesters (PET), Polyethylene, Polypropylene, Polystyrenes, Polyurethane (PU), Polyvinyl chloride (PVC) and vinyl. Out of so many available plastics only two polymers ABS and PLA (Poly Lactic Acids) are used as filaments in the additive manufacturing process. PLA is a natural plastic made of corn starch or sugar cane while ABS is made out of oil based resources, non-biodegradable plastic. ABS is preferred over PLA because it is sturdier and can withstand relatively high temperature for the most of the 3D printers. The glass transition temperature of ABS is 105 °C, there is no fix melting point of ABS owing to its amorphous nature. The recommended working temperature for the ABS is between -20 °C to 80 °C.

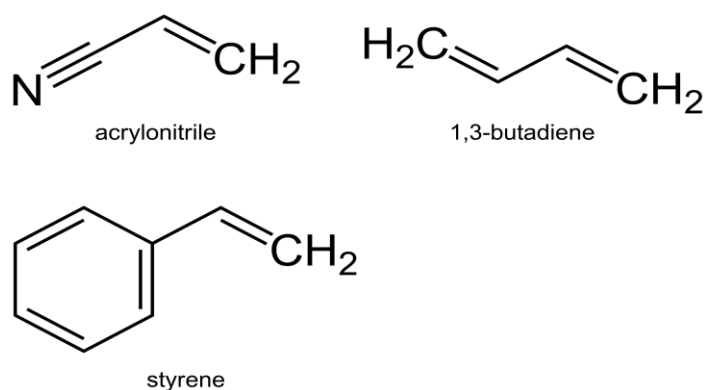


Figure 3.6 Chemical Formula of ABS

ABS polymers show good resistance to aqueous acids, alkalis and concentrated hydrochloric acids while they do not withstand the attack of glacial acidic acids, concentrated sulphuric acid, concentrated nitric acid and carbon tetrachloride. Additionally, thermoplastic polymers provide a positive combination of thermoelectrically and mechanical properties. ABS plastic demonstrates good durability, resilience, and mechanical strength.

### 3.2 ELECTROPLATING OF 3D PRINTED PART

#### 3.2.1 SURFACE PREPARATION FOR COATING

Atomically the surface to be plated differs from the bulk of the material as they are subjected to oxidation, absorption of external substances, such as gas molecules, greases and soils, which generally are organics. These surface films could be retained tenaciously, often making their cleaning difficult. The poor adhesion leads to the poor coating quality. Adhesion of electrodeposits to non-metallic substrates always require some mechanical keying of the deposit to the rough or porous surface. The pores may be created by conditioning with the acids. There are typically three fundamental processes in surface treatment and plating operations.

- Surface preparation or cleaning: The surface is treated with solvents, alkaline and acid cleaners and followed by rinsing in water after each treatment. For mechanical cleaning specially of metals, polishing, brushing and buffing can be performed to attain the clean surface for coating. Other methods available for cleaning are thermal energy, abrasive flow, mechanical vibrator and disc finishing.

- Modification of surface: This involves modifications to the surface's characteristics, such as the introduction of a metal coating or hardening.
- Alkaline wash or similar process is performed just before the plating to provide a hydrophilic surface.

ABS (or any nonconductive material) to be deposited with copper needed to be made conductive to participate in the electroplating process, to achieve this an additional process for the surface preparation is required. The activation of the ABS was achieved by applying a coat of conductive paint. The steps involved to make the component conductive and ready for the electroplating are given in the Figure 3.7.

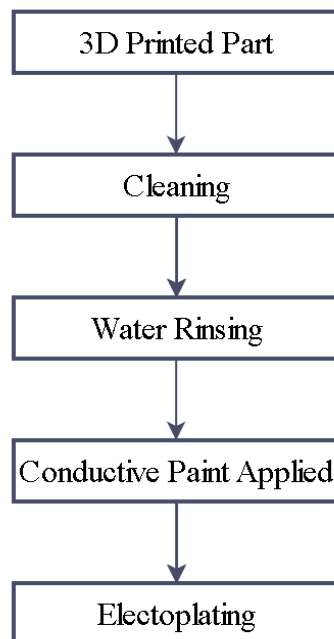


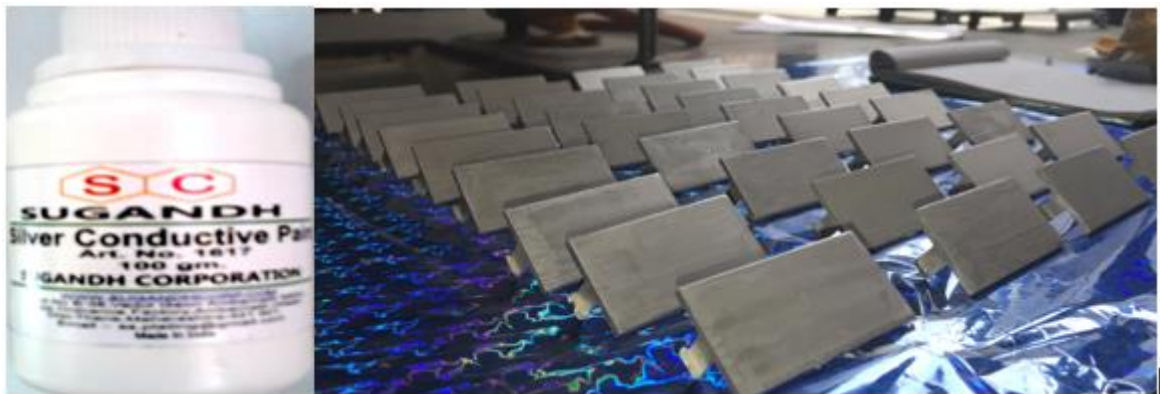
Figure 3.7 Activation of Plastic with Conductive Paint

- Cleaning is done to remove all the contaminants, dust without damaging the original surface to be plated. The cleaning is performed by an industrial degreasing agent of non-silicate mild alkaline soaks degreaser system (Ginplate 452 product of GROWEL) at elevated temperature up to 60-65 °C. The samples are kept in the solution for 4-5 minutes.
- Water rinsing was performed to wipe out the chemicals of the previous process along with the any dust particles before final copper/nickel coating.
- The samples were dried in over at 25°C for 24 hours.

- The samples were plated with silver conductive paint using zero number paint brush. The suspended particles of silver present in the paint, make the plastic component conductive for the coating of copper
- The painted samples were dried for five hours in an air oven at 80 degrees Celsius.



(a)



(b)

Figure 3.8 (a) Chemically Treated Components (b) Components after Conductive Paint Coat

### 3.2.2 ELECTROPLATING PROCESS ELEMENTS AND SOLUTIONS

Electroplating is a fabrication process to form various shapes with the use of electroplating. As per ASTM B734-97(2018), “This specification covers requirements for electrodeposited coatings of copper used for engineering purposes. Examples include surface hardening, heat treatment stop-off, as an underplate for other engineering coatings, for electromagnetic interferences (EMI) shielding in electronic circuitry, and in certain joining operations”electroplating of copper for engineering purpose”.

The electrocoating process consists of the following components (Figure 3.9)

Electrolyte – The conductive bath solution in the electrocoating tank is known as electrolytes. The constituents of the electrolyte are distilled water, salt (of the metal to be deposited) and acids or alkali. Depending upon whether acid or alkali is added to the bath, the solution is called acidic or alkaline.

Anode – Anode is positively charged electrode in the electrolyte solution undergoing the oxidation reaction to sacrifice itself for the metal coating on the cathode. The anode is a metal such as copper, nickel or chromium, etc. which are to be plated. The anode can be of spherical or cuboid shape.

Cathode – Cathode is negatively charged electrode in the electrolytic solution on which the pure metal layer gets deposited through the metal ions from the ionic solution. The material of the cathode can be metal or non-metal.

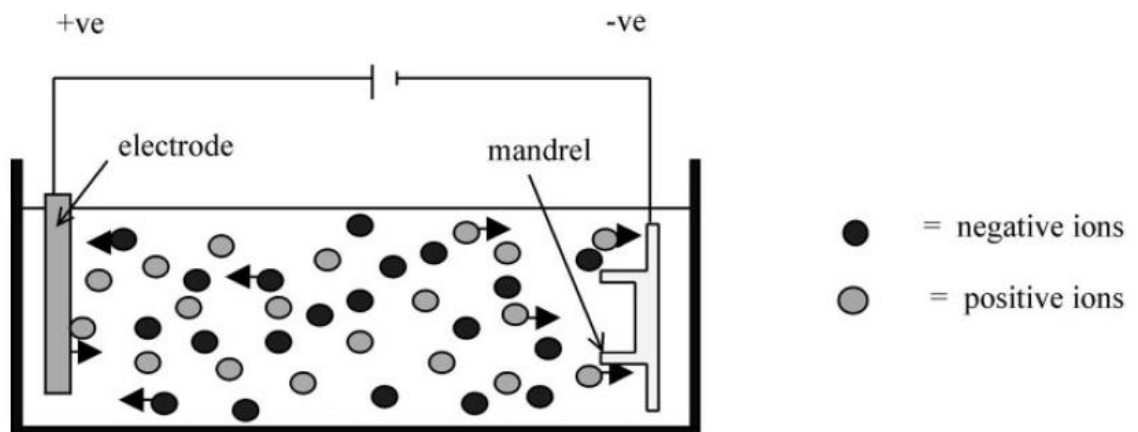


Figure 3.9 Schematic of Electroplating Setup (Rennie et al., 2001)

The electroplating solution selection serves a crucial function in the functional requirements expected from the electrodeposit for a particular application. As such there is not much difference of the solution required for electroplating from the general plating solution. Nickel, copper and chrome electroplating solutions are the ones most widely used in practice. The compositions and operating conditions of copper electroplating solutions is given in Table 3.2

Table 3.2 Copper Electroplating Bath Solutions

<b>Electrolyte Composition, g/L</b>			
<b>Copper Sulphate</b>		<b>Copper Fluoborate</b>	
CuSO <sub>4</sub> .5H <sub>2</sub> O	195-248	Cu(BF <sub>4</sub> ) <sub>2</sub>	225-450
H <sub>2</sub> SO <sub>4</sub>	30-75	HBF <sub>4</sub>	Maintain pH at 0.15-1.5
<b>Operating Conditions</b>			
Temperature	21-32 °C	21-54 °C	
Agitation	Air or mechanical	Air or mechanical	
Cathode Current Density	2-10 A/dm <sup>2</sup>	7.5-12.5 A/dm <sup>2</sup>	
Anodes	Copper	Copper	

The properties of electrodeposits are interdependent as they are dependent upon operating parameters. Operating parameters that control the properties of deposits are temperature and cathode current density. The elements of the solution, if their concentrations are retained within specified limits, can also, have an effect on the properties of the deposits. Current density is measured as amperes of current per unit area of the electrode.

### 3.2.3 FUNDAMENTALS OF ELECTROCHEMISTRY

Chemical reactions happen in the interactions between the circuit and the solution when a direct electric current passes through an electrolyte. The process is referred to as electrolysis and electrolytic cell undergoes electrolysis process. One specific form of electrolysis is known as electroplating. Electroplating is known as one of a particular kind of electrolysis. In addition to electroplating, electrolysis has also been widely employed to produce halogens, chlorine, and to purify metals like copper or zinc. Understanding electrochemical Electro-coating concepts is required for the creation of electroplating concepts.

#### 3.2.3.1 OXIDATION AND REDUCTION

Oxidation and reduction are bound to happen together in all electron transfer reactions. The material attracting electrons (known as oxidizing agent) oxidizes the material which is shedding electrons (known as reducing agent). Along the way, the



oxidizing agent is itself reduced by the reducing agent. As a consequence, the reduction process is sometimes known as electronation, and the oxidation process is known as “de-electronation” (Lou and Hunag 2006).

### 3.2.3.2 REACTIONS AT ANODE AND CATHODE

The general reaction takes place during the reduction process at the cathode, where electrons are transported from the cations to the anodes. is shown in Equation 3.1.



Electrons are given to the anions at the anode, and they move towards the cathode. The reaction at anode takes place as per Equation 3.2.



The work in this research requires the plating of both Ni and Cu metals on the substrate for which salts of nickel sulphate (NiSO<sub>4</sub>) and copper sulphate (CuSO<sub>4</sub>) are used and the reactions involved are represented in the equations from 3.3 to 3.5



### 3.2.3.3 ELECTROPLATING SETUP

As discussed earlier in the process flow shown in Figure 3.7, that the electroplating process involves an extensive number of steps. The processes before the final coating, i.e. from the surface preparation to surface activation were carried out in the plastic containers. The electroplating setup consists of a tank, DC rectifier, agitator, electrode holders, and connection rods etc.

The main requirement of the tank for electroplating setup is, that, it should hold the required bath solution without any leakage or contaminations. The tank geometry, size and material depend upon the metal to be deposited and the size and no of the components to be electroformed. The material used for making the tank was steel with glass container inside (Figure 3.10).



Figure 3.10 Copper Electroplating Setup

The lining was provided to prevent contamination and to insulate the tank from the current flow. The capacity of the tanks was made to accommodate the bath solution up-to 30 litres. At the bottom of the tank the pipes with holes are fitted to supply the air for the agitation of bath solution. As the setup was developed for the experimental work no filtration system was fitted with the tanks, the filtration was performed manually. On the top of the tank rods were fitted to hang the anodes (copper metal strips) and cathodes (component fixture). The rods were made of copper to ensure the effective flow of the current and are insulated from each other. As the solution selected for copper electroplating was of copper sulphate and the suggested temperature range is within the atmospheric conditions (Table 3.2), so no equipment for heating and cooling was provided in the setup. The titanium plating racks as shown in Figure 3.11 were used to support copper electrodes and to hang the work piece.



Figure 3.11 Titanium Plating Racks

The rectifier, which transforms alternating current into low voltage direct current (D.C.) is supplied through the power supply. It rectifier has an inbuilt step down transfer to convert high voltage to low voltage. The rectifier designed to handle range of voltage from 0 to 50 Volt and range of current 0 to 100 Amperes, the control panel includes the digital display meter for voltage and current and the knob to control the required output voltage or current. Figure 3.12 shows the rectifier used in the electroplating setup. The rectifier efficiency can be calculated by the ratio of power output to the power input. The output power is equal to the D.C. volts X D.C. Amps. Owing to the various components of the rectifier, it consumes the electricity even if the output voltage is set to be 0 V. Thus the maximum efficiency of the rectifier is achieved at the higher voltage output. The recent developments in the technology of the rectifier have resulted in to pulse plating rectifiers which can handle a very high range of the voltage.

A stirrer is also fitted in the tank to ensure that the temperature is maintained uniformly throughout the tank.

The inner tank is made of 8 mm thick Teflon glass to contain copper solution bath, the Teflon glass was fixed with silicon adhesive. The adhesive silicon gum ensures that the joints are leak proof. Aquarium pump was placed inside the tank to agitate the solution for the proper flow.

As the current and voltage requirements of copper electroplating process are low so the lab rectifier (Figure 3.12) having a range of voltage 0 to 5 Volt and range of current of 0-5 Ampere was used in the setup.



Figure 3.12 Direct Current Rectifier

The anode and cathode handling system, along with the current distribution system was kept similar to the setup used for copper electroplating.

### 3.2.4 PROCESS PARAMETERS

The coating rate and quality of the plating depends upon various parameters, the major influence as per the literature is found to be of current, current density, pH, bath concentrations and temperature. To establish the optimum parameters for copper electrocoating various parameters were tested in nine sets of experiments with reference to the ranges mentioned in the literature. The nine set of experiments was conducted to establish the optimum parameters for the coating rate and surface finish of copper electroplating, by varying the voltage, copper sulphate solution (CSS) concentration and time of coating. The ranges selected are given in the Table 3.3.

Table 3.3 Parameters for Copper Electroplating

Variable	Range
Voltage	2V to 4 V
CuSO <sub>4</sub> concentration	190 g/L to 210 g/L
Time	120 Minutes to 240 Minutes

## 3.3 COLD SPRAY COATING ON METALIZED PARTS

### 3.3.1 DESIGN OF COLD SPRAY GUN NOZZLE

In the converging part the diameter is reducing linearly till throat from 8 mm to 2mm (10 mm long) while afterwards from throat to diverging section end it is increasing

from 2 mm to 5 mm (40 mm long). As per the optimal attributes of design given by Li and Li, 2005, the stated dimensions (shown in figure 3.13) were taken and performed fluid flow simulation (shown in figure 3.14) upon, applying the optimal boundary conditions (temperature=500°C, pressure=1000000Pa) for low pressure cold spray system. The flow simulation yielded that a velocity of 875.628m/s can be achieved on the parameters.

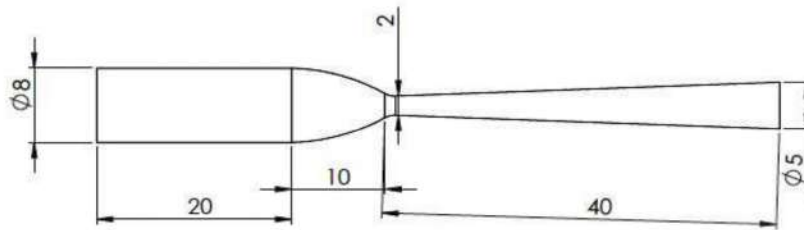


Figure 3.12 Sketch Showing Optimal Parameters Of De-Laval Nozzle Core

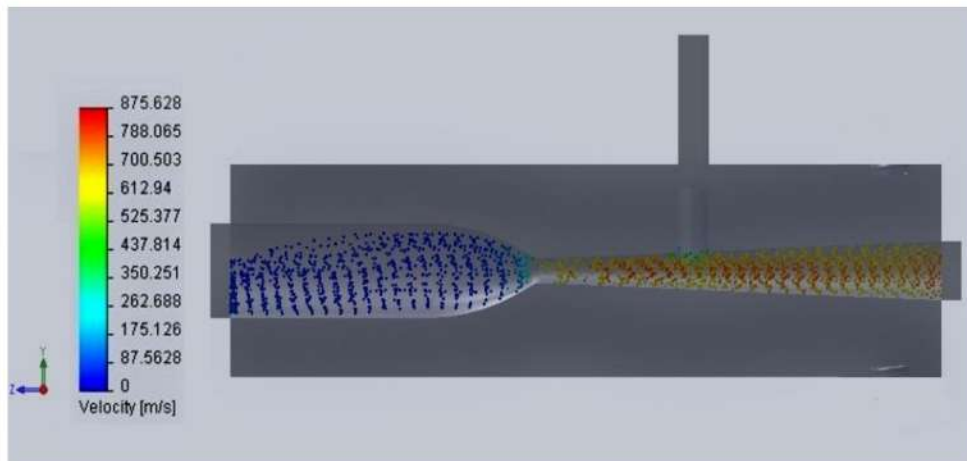


Figure 3.14 Fluid Flow Simulation of De-Laval Nozzle Performed In CAE Software

### 3.3.2 DESIGN OF COLD SPRAY GUN GAS HEATER

The heater is designed in such a way that it heats the pressurized air up to 600°C and

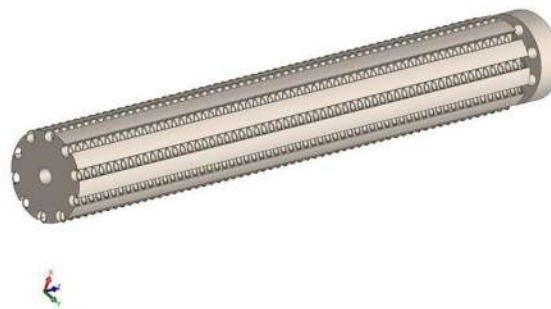


Figure 3.15 CAD Model of Gas Heater



its purpose of heating is such that it should make the air more aerodynamic, less denser and light weight so that it perform its task of carrying the metal powders effectively, without melting them. The required length of articulated ceramic body, for the achievement of the said goals was estimated to be 12 inches. Figure 3.15 shows the CAD model of the gas heater.

### 3.3.3 DESIGN OF COLD SPRAY GUN CASING AND MOUNTINGS

Austenitic stainless steel 304 (18% chromium and 8% nickel) was found most relevant for the application as it has capability to withstand elevated temperatures up to 700°C and its own melting point is 1450°C. The casing was designed 14 inches long tube with 3mm thickness. The flanges and other mountings are designed of the same configurations. Figure 3.16 shows the CAD model of casing and different mountings of cold spray gun whereas Figure 3.17 the CAD models of complete assembly.



Figure 3.16 CAD Models of Gun Casing and Mountings



Figure 3.17 CAD Models of Complete Assembly

In order to determine wholesome aerodynamic performance of the gun, fluid flow simulations were made on the assembly which are shown in the Figures 3.18 and 3.19. The boundary conditions were taken as temperature=500°C, pressure=1000000Pa. The flow simulation yielded that there is velocity drop in the assembly and a final velocity of 625.066m/s can be achieved on the parameters.

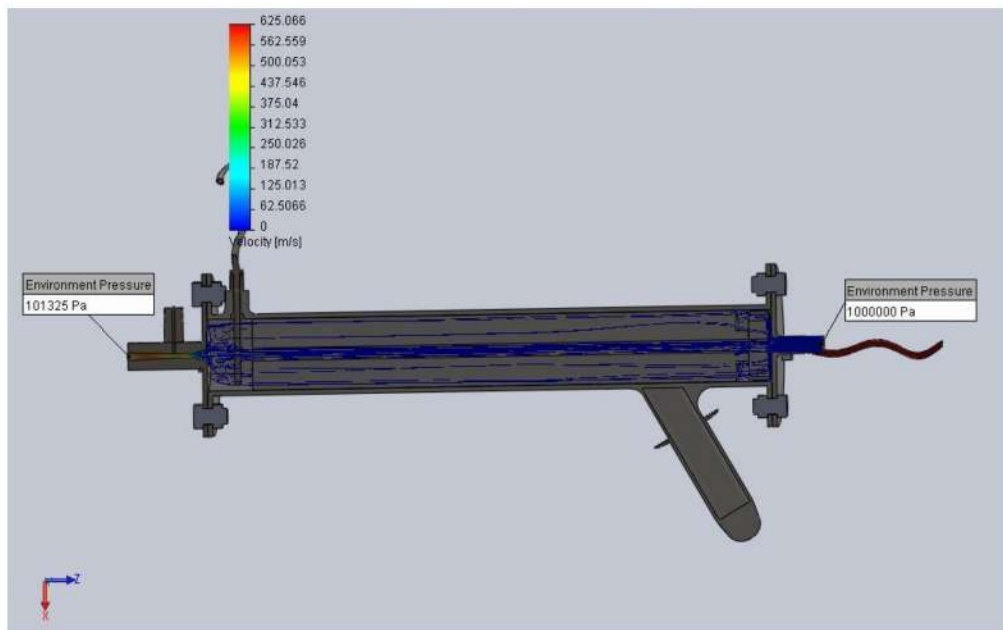


Figure 3.18 Fluid Flow Simulation on Gun Assembly

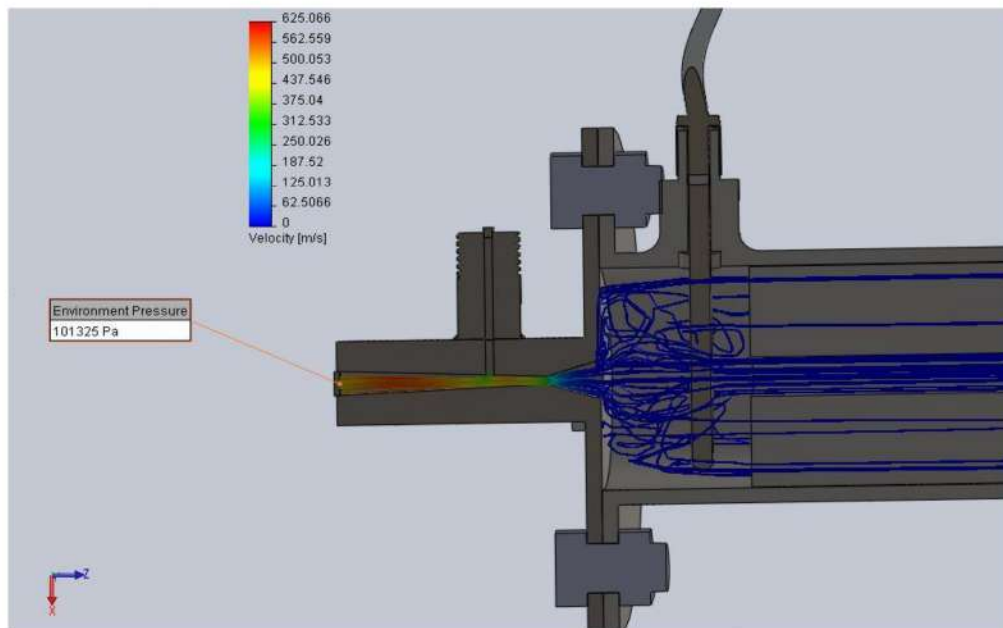


Figure 3.19 Fluid Flow Simulation on Nozzle and Gun Assembly

### 3.3.4 DESIGN OF COLD SPRAY GUN MACHINING TOOLS

Since the nozzle's inner cross-section is intricate and a high accuracy is desired to meet the application needs, Electro-Discharge Machining (EDM) was found most appropriate and most economical. The tool for EDM were designed on CAD as shown in Figure 3.20 so as to be turned on a CNC lathe to achieve higher levels of accuracy.



Figure 3.20 CAD Models Showing The Nozzle and The EDM Tooling Design

### 3.3.5 FABRICATION OF APPARATUS

The fabrication process started with the CNC turning of EDM tools, figure 3.21 shows the photographs of the turned tools.

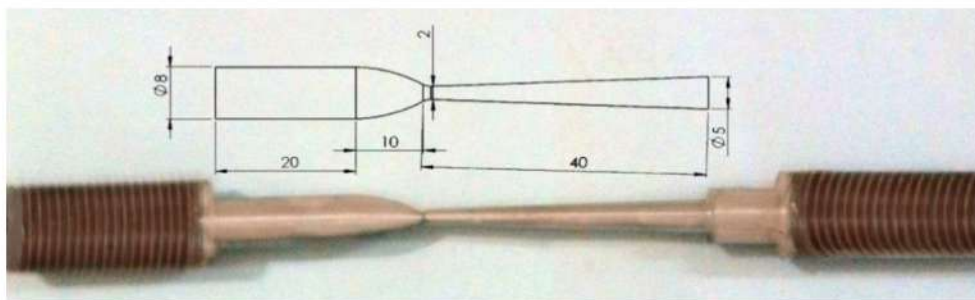


Figure 3.21 Photograph of Tools For Electro-Discharge Machining of De-Laval Nozzle

Performing Electro-Discharge Machining over the straightened EN-38 die steel billet having hole drilled through it led the manufacturing of the nozzle. The nozzle was subjected to induction hardening for improving the abrasion resistance. Figure 3.22 shows the photograph of manufactured De-Laval nozzle.





Figure 3.22 Photograph of Manufactured De-Laval Nozzle

Next to the nozzle, heater fabrication was done. The heating elements are axially fixed at the through holes on the periphery of the nozzle surrounded by the ceramic insulators, having electrical terminal at the end. Figure 3.23 shows the photograph of the heater.



Figure 3.23 Photograph of Manufactured Gas Heater

After having the gas heater built, gun casing and mountings were manufactured from procured stainless steel flats and tube which were put altogether by performing Gas Tungsten Arc Welding (GTAW). Figure 3.24 shows the photograph of gun casing and mountings.



Figure 3.24 Photograph of Gun Casing and Mountings

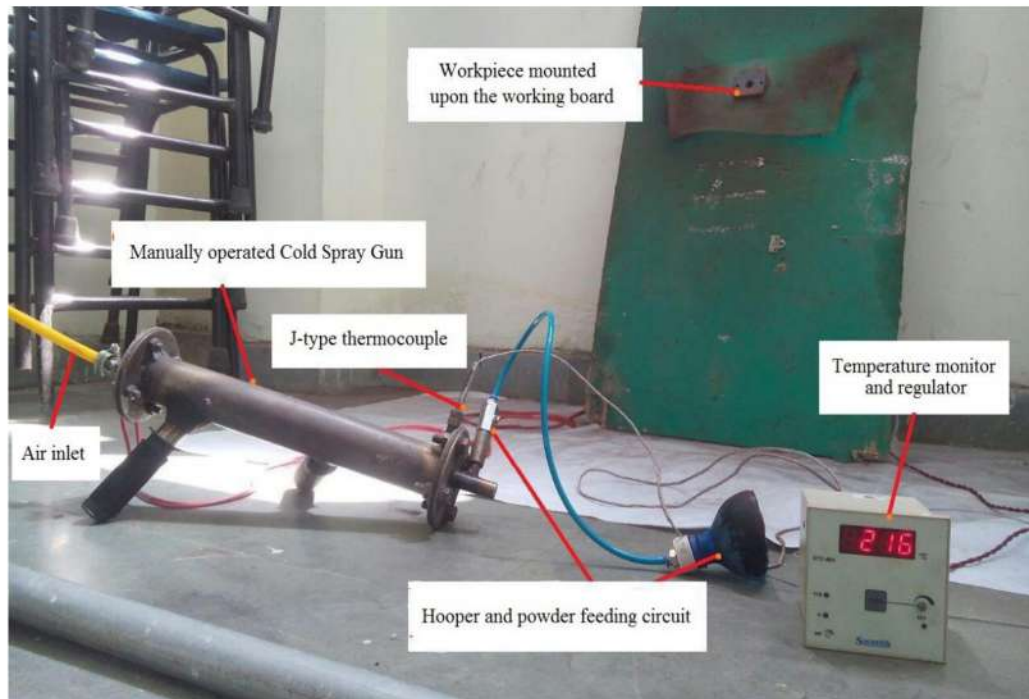


Figure 3.25 Photograph of the Complete Cold Spray System

Figure 3.25 shows the labeled photograph of the complete cold spray system along with the control and feed elements.

### 3.3.6 PROCESS PARAMETERS

While designing the experiments, persistent changes are made to the input variables of a process so that we may observe and identify corresponding effects on the output responses. In this study, 3 factors (Gas temperature, Electroplating thickness and Standoff distance) each at 3 different levels are selected for experimentation to determine their effects upon surface roughness, deposition thickness and hardness.

Table 3.4 Parameters for Cold Spray Coating

Parameter	Level 1	Level 2	Level 3
Gas Temperature, T (°C)	300	350	400
Electroplating Thickness (microns)	100	300	600
Standoff Distance (mm)	15	20	25

## **CHAPTER-4                      EXPERIMENTAL DESIGN METHODOLOGY**

---

The systematic strategy to organize the experimental analysis is essential for the successful conduct of experiments. The statistical design of experiments is undertaken to ensure that relevant data would be collected and analysed by statistical techniques forming legitimate and purposeful findings. When the problems that includes data which are exposed to experimental error, statistical techniques are the primarily unbiased approach to investigation. Therefore, experimental problems have two main components: the design of the experiments (DOE) and the statistical analysis of the data. As the method of study directly depends on the experimentation design adopted, both of these factors are closely associated. Following are the objectives of DOE as provided below (Montgomery, 2017):

- Determining which variables is more influential on the response.
- Minimum numbers of experiments required for the finding optimum parameters.
- Experimental error can be established.
- The interdependence of the process parameters upon each other to influence the outcome can be established.
- Qualitative estimation of the parameters can be established.

The present work of optimization of the process parameters for copper electroplating and cold spray coating of copper was completed using Taguchi's method of orthogonal array, as the full factorial design will demand that more experiments be undertaken.

### **4.1      DESIGN METHODOLOGY**

The robust design is required to achieve the goal of optimization of the variable for the best response and G. Taguchi, discussed the sturdy design as one, which is produce by a structure of the design methods further which minimize anomalies in products and procedures, while concurrently leading the manifestation to optimum setup. Good or service which is stringently designed and guarantees satisfaction of the customer even though exposed to dire situations occur during the production or in the service ecosystem. Taguchi method, DOE and regression analysis are a few of the key

components of robust design that produce parameters for high-quality results at minimal cost.

#### **4.1.1 TAGUCHI APPROACH FOR DOE**

The Taguchi technique depends on performance assessment or experiments to examine the sensitiveness of several response factors to several control variables by contemplating analysis with “orthogonal array” to achieve best settings with control variables. With orthogonal arrays we can achieve a better list of optimum experiments. Table 4.1 displays the number of columns at various levels for the 18 standard orthogonal arrays. The two terms, factors and level needed to be understood first for better exploration of the concepts. Factors are the control elements for variations in the desired output, e.g. in the electroplating operation on a metal, current density, concentration, temperature, electrolyte and agitation are the control parameters to decide about the quality of electroplating, so these become the factors. The range of values to be tested for these factors becomes the levels of the experiment, e.g. minimum cutting speed and maximum cutting speed. The number of trials under each setting is called replica or replicates.

The orthogonal array name such as L4 ( $2^3$ ) gives the information about the experiments to be conducted, number of factors involved and levels of the factors, like in array L4 ( $2^3$ ), four experiments are to be conducted of three factors each at two levels. Similarly, the array L18 ( $2^13^7$ ) has eighteen experiments to be conducted with one factor at two levels and seven factors at three different levels. There should be at least as many experiments as there are degrees of freedom associated with the various factors. The number of DOF allied with a factor is equivalent to the number of levels for the given factor minus one. For example, an experimental study has one factor (M) with “two levels”, and five factors (P, Q, R, S, and T) each with “three levels”. So, the degree of freedom for M as per the above discussion will be two minus one, i.e. one and similarly for the remaining factors, each at three levels the degree of freedom will be two. The total degree of freedom of the experimental study including one for the error in the system will be twelve. The highest number of factors which can be explored using an array is represented by the number of columns in that array.

Table 4.1 Orthogonal Array

Orthogonal array	Number of experiments	Maximum number of factors	Maximum number of factors at these levels			
			Level 2	Level 3	Level 4	Level 5
L4	4	3	3	-	-	-
L8	8	7	7	-	-	-
L9	9	4	-	4	-	-
L12	12	11	11	-	-	-
L16	16	15	15	-	-	-
L16'	16	5	-	-	5	-
L18	18	8	1	7	-	-
L25	25	6	-	-	-	6
L27	27	13	-	13	-	-
L32	32	31	31	-	-	-
L32'	32	10	1	-	9	-
L36	36	23	11	12	-	-
L36'	36	16	3	13	-	-
L50	50	12	1	-	-	11
L54	54	26	1	25	-	-
L64	64	63	63	-	-	-
L64'	64	21	-	-	21	-
L81	81	40	-	40	-	-

#### 4.1.2 DESIGN OF EXPERIMENTS STRATEGY

The success of the DOE depends upon the selection of the relevant orthogonal array, control factors and understanding (or influence) of the noise factors, along with the participation interface inbetween the numerous control factors. Noise factors are frequently functions of environmental circumstances, such as temperature or relative humidity (Montgomery, 2017) or may be the properties of the raw materials or sensitive process parameters. The identification of the controllable or noise factors is the integral part of the DOE strategy to find the settings of the controllable parameters that reduces the variability transmitted through the noise factors. The optimal

condition is determined by investigating the main effects of every parameter. Main effects identify the common tendency of the effects of each parameter. Knowing how a certain parameter is involved is crucial to figure out the type of control that must be established for a production procedure. The statistical method used frequently for assessing the percentage influence of each parameter to the results of studies against a defined degree of confidence is called analysis of variance (ANOVA). Finding which of the parameters has to be commanded is rendered more straightforward by looking at the ANOVA table for a specific research. Taguchi recommends two distinct methods to perform the entire investigation. First, the fundamental approach, which uses main effect and ANOVA analysis to look at the results of a single run or the average of several runs. Administering signal-to-noise ratio (S/N) for the identical phases of the research is the second approach, which Taguchi unequivocally advocates for numerous runs. Irrespective of the methodology the procedure for the DOE can be followed as shown in the Figure 4.1. The basis for the selection of the control factors of the existing process or service can be decided based upon the information available through the literature, design standards, related handbooks or through the text books. For the selection of the influential control factors for a new process or service along with the literature reference, conduct of trial experiment is recommended. The trial (or Pilot) experiment can be conducted with more parameters and then eliminating the parameters which are least influential in the output of the results. For the current research work, the literature base was used to decide upon the control factors and their levels for the optimum deposition of the metal on the substrate in the electroplating process.

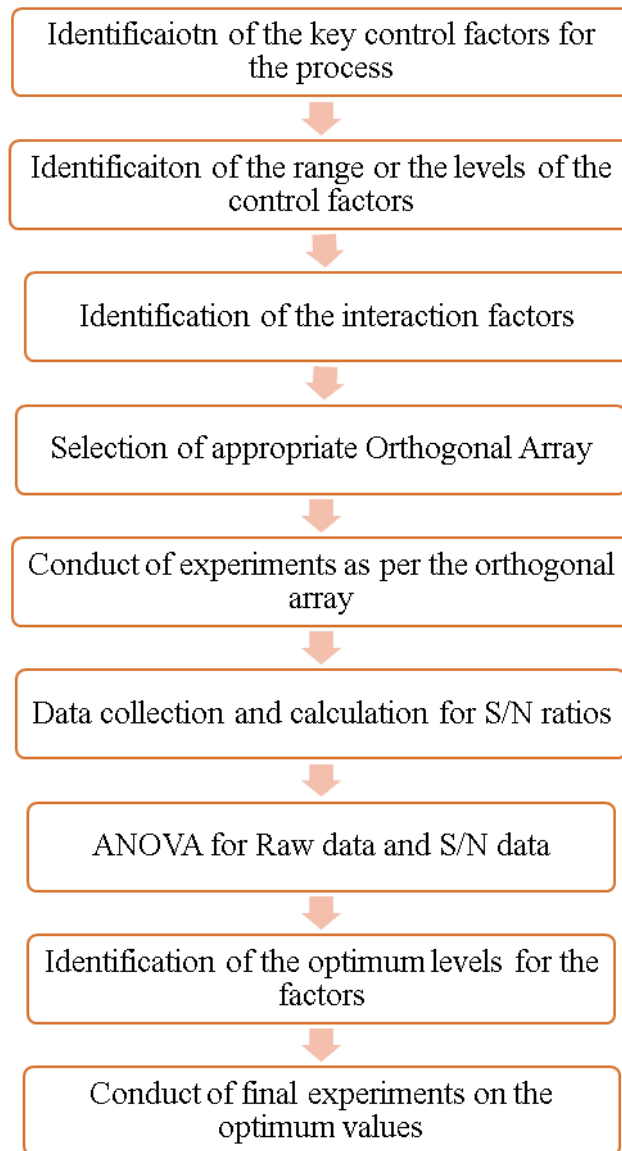


Figure 4.1 Process Flow Chart for Taguchi DOE

### 4.1.3 SELECTION OF ORTHOGONAL ARRAY

The selection of the orthogonal array depends upon some of the following parameters

- No. of factors to be evaluated
- Levels of the factors
- Cost of the experiments
- The time requirement to conduct the experiment etc.

The selection of these parameters can be governed by the brainstorming, flow chart or root cause analysis as suggested by Taguchi. In this work the optimization of operating parameters of the electroplating of the two material, i.e. copper and nickel

was established in the initial phases. The final mould to be produced is of nickel material, hence making it more critical material to be studied for the electrodeposition. Based on the reference of the literature as discussed in the section 3.8, three factors are selected for study the deposition of copper such as temperature, copper sulphate solution concentration and time, for three different levels. Nickel deposition is decided to be studied for five different factors such as current density, temperature, pH, nickel sulphate concentration and nickel chloride concentration each at three levels.

The full factorial method suggests that  $3^3$  (27) and  $5^3$  (125) experiments to be conducted, which will add in the additional cost and time. So the Taguchi approach was explored for the experimentation. As per the Table 4.1 of orthogonal array the options available to test the factors for three levels only are L9, L27 and L81. The application of L27 to copper deposition leads to the full factorial design, owing to the importance of the process, L9 is found to be the suitable orthogonal array. The standard L9 orthogonal array as per Taguchi design for four parameters is given in Table 4.2, where levels are represented as numbers 1, 2, 3.

Table 4.2 Standard DOE for Taguchi's L9 Orthogonal Array

Expt. No.	Column			
	1	2	3	4
1	1	1	1	1
2	1	2	2	2
3	1	3	3	3
4	2	1	2	3
5	2	2	3	1
6	2	3	1	2
7	3	1	3	2
8	3	2	1	3
9	3	3	2	1

Based upon the above standard table the final L9 table for the three factors of copper electroplating of three different levels is represented in Table 4.3.



Table 4.3 DOE Employing Taguchi's L9 Orthogonal Array for Copper Electroplating

Expt. No.	Voltage (v)	CuSO <sub>4</sub> Concentration (g/l)	Time (Min)
1	2	190	120
2	2	200	180
3	2	210	240
4	3	190	180
5	3	200	240
6	3	210	120
7	4	190	240
8	4	200	120
9	4	210	180

Based upon the above standard table the final L9 table for the three factors of copper electroplating of three different levels is represented in Table 4.4.

Table 4.4 DOE Employing Taguchi's L9 Orthogonal Array for Cold Spray Copper Coating

Experiment No.	Gas Temperature ( ° C)	Pressure (Mpa)	Standoff Distance
1	300	1	15
2	300	2	20
3	300	3	25
4	350	1	20
5	350	2	25
6	350	3	15
7	400	1	25
8	400	2	15
9	400	3	20

#### 4.1.4 SIGNAL TO NOISE RATIO FOR RESPONSE PARAMETERS

Taguchi suggested that for the robustness of the process the effect of noise factors needed to be taken into consideration. The noise factors are the uncontrollable variable that can significantly affect the outcome of the results. The atmospheric conditions, contaminations in the salts, power factors, the design of the component,

base material quality, etc., can be considered as few of the noise factors in the current work which may lead to the variability in the desired outcome. Taguchi suggested the loss functions to correct the deficiency in the system. Although Taguchi created more than 68 loss functions, the quadratic function, also known as the nominal-the-best type, approximates numerous circumstances. Following equation described the quadratic loss function.

$$L = k(y - \tau)^2 \quad (4.1)$$

Where L = cost incurred due to quality loss

y= performance characteristic

$\tau$ = target to be achieved

k= quality loss coefficient

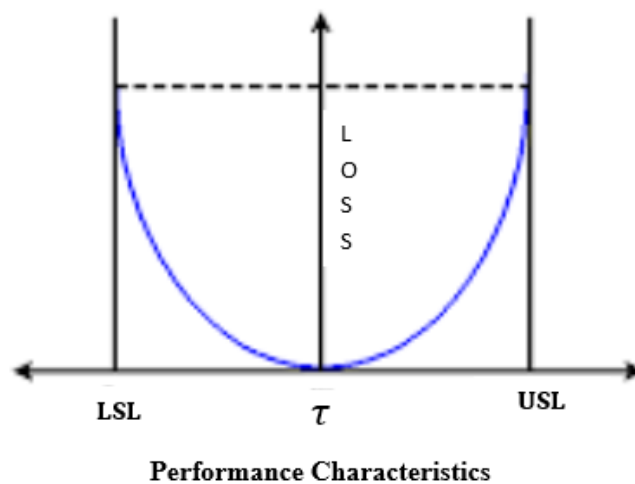


Figure 4.2 Taguchi Quadratic Loss Function

The graph of the quadratic function is shown in the Figure 4.2 and it depicts that as the product's characteristic move away from the target value, the losses increases. The loss is a continuous function. Considering that the data under consideration is not only for the one component, but actual of mass components (or experiments) the concept of average loss is used. The expression for the average loss is given in Equation 4.2.

$$\bar{L} = k[\sigma^2 + (\bar{y} - \tau)^2] \quad (4.2)$$

Where  $\bar{L}$  = the average loss

$\sigma$  = population standard variation

Apart from nominal the best, there are two more quite common loss functions, these are smaller-the-better and larger-the-better Figure 4.3 illustrate the both. The target value for smaller-the-better is zero and whole curve is in the positive domain for the performance characteristics.

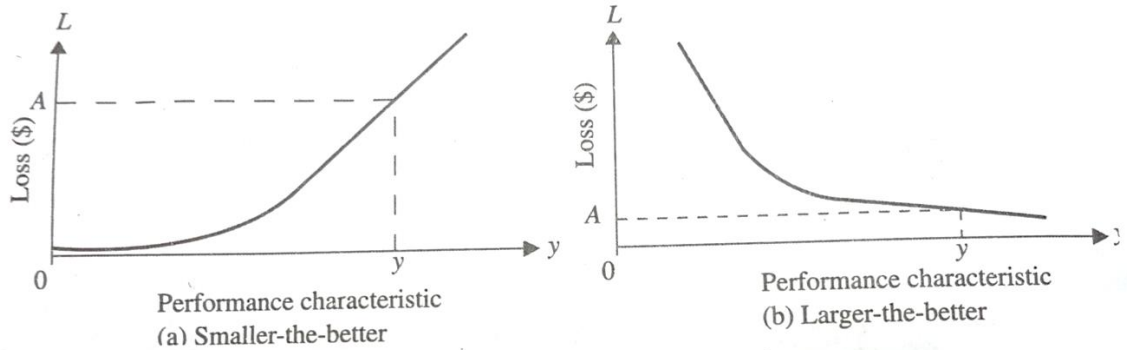


Figure 4.3 Smaller-the-Better and Larger-the-Better Loss Function (Besterfield et al., 2017)

The target value for larger-the-better is infinity with zero loss and whole curve is in the positive domain for the performance characteristics with worst case at zero.

A greater S/N number indicates that the signal outweighs the random effects of noise components by a significant amount. Finding a suitable aim function to enhance an engineering design problem is crucial. The following three sorts of S/N ratios are utilised in practise depending on the type of reaction. (Besterfield et al., 2017):

- Nominal- the-Best (N)

$$(S/N)_N = 10 \log_{10} \left( \frac{\bar{y}^2}{s^2} \right) \quad (4.3)$$

Where  $\bar{y} = \frac{1}{n} \sum_{i=1}^n y_i$  and  $s^2 = \frac{\sum_{i=1}^n (y_i - \bar{y})^2}{n-1}$

- Smaller-the-Better (S)

$$(S/N)_S = -10 \log_{10} [MSD] = -10 \log_{10} \left[ \frac{1}{n} \sum_{i=1}^n y_i^2 \right] \quad (4.4)$$

Where MSD = Mean standard deviation

- Larger-the-Better (L)

$$(S/N)_L = -10 \log_{10}[MSD] = -10 \log_{10} \left[ \frac{1}{n} \sum_{i=1}^n \frac{1}{y_i^2} \right] \quad (4.5)$$

The nominal-the-best equation is to be selected whenever we have a nominal value. The S/N ratio should be maximum for a robust design; this can be achieved with large average and variance. The target value in this case is finite but not zero. For zero target value, smaller-the-better is to be used.

The larger-the-better value is utilized wherever the greatest significance is preferred such as yield of a crop, tool life, or material removal rate. In larger-the-better mode, inverse of every larger value turns into a smaller value as well as again the target value is zero.

#### 4.1.5 Analysis of Variance (ANOVA)

Analysis of variance (ANOVA) is widely used statistical methods for data analysis. Models for the data is useful to describe the observations from an experiment, following is one such model for a totally random design. (Montgomery, 2017):

$$y_{ij} = \mu + \alpha_i + \epsilon_{ij} \quad (4.6)$$

The Equation 4.6 is called fixed effect model and is used as single factor analysis of variance, the stepwise sequence of the analysis is given below

- (1) Find out the total of the readings of individual repetitions:

$$y_{i.} = \sum_{j=1}^n y_{ij} \quad (4.7)$$

Where 'i' is the number of treatments (i =1, 2, 3...a) and 'j' is the number of observations (j= 1, 2, 3...n).

- (2) Let  $\bar{y}_{i.}$  represents the average of the observations under *i*th treatment.

$$\bar{y}_{i.} = \frac{y_{i.}}{n} \quad (4.8)$$

- (3) Let  $y_{..}$  represent the grand total of all observations

$$y_{..} = \sum_{i=1}^a \sum_{j=1}^n y_{ij} \quad (4.9)$$

- (4)  $\bar{y}_{..}$  is the grand average of all the observations

$$\bar{y}_{..} = \frac{y_{..}}{N} \quad (4.10)$$

- (5) Find the total corrected sum of squares (SST) as

$$SS_T = SS_{Treatments} + SS_E$$

$$\sum_{i=1}^a \sum_{j=1}^n (y_{ij} - \bar{y}_{..})^2 = n \sum_{i=1}^a (\bar{y}_{i.} - \bar{y}_{..})^2 + \sum_{i=1}^a \sum_{j=1}^n (y_{ij} - \bar{y}_{i.})^2 \quad (4.11)$$

Where  $SS_{Treatments}$  is called the sum of square due to treatments, and  $SS_E$  is called the sum of square due to errors.

(6) Find out degree of freedom (DOF):

$$\text{Total DOF for SST} = (\text{total number of observation} - 1) = (N-1) \quad (4.12)$$

$$\text{DOF for Treatments} = (\text{number of treatments} - 1) = (a-1) \quad (4.13)$$

$$\begin{aligned} \text{DOF for error} &= \text{number of treatment (no of replicas for each treatment} - 1) \\ &= a(n-1) = (N-a) \end{aligned} \quad (4.14)$$

(7) The test procedure can be accumulated in the Table 4.5, this table is called as analysis of variance (or ANOVA) table.

(8) For the same treatment means these two estimates would be similar otherwise there would be difference in the variances. The variances (mean squares) can be found as follows

$$(9) \quad MS_{Treatments} = \frac{SS_{Treatments}}{a-1} \quad (4.15)$$

$$(10) \quad MS_E = \frac{SS_E}{N-a} \quad (4.16)$$

Table 4.5 ANOVA Table

Source of variation	Sum of squares (SS)	Degree of freedom (DOF)	Mean of square (MS) or variance (V)	F-ratio(F0)
Between treatments	$SS_{Treatments}$	$a - 1$	$MS_{Treatments}$	$F_0 = \frac{MS_{Treatments}}{MS_E}$
Error (Within treatments)	$SS_E$	$N - a$	$MS_E$	
Total	$SS_T$	$N - 1$		

The hypothesis of no difference in the treatments means can be tested by comparing Equation 4.15 and Equation 4.16. According to Cochran's theorem  $SS_{Treatments} / \sigma^2$

and  $SS_E/\sigma^2$  are independently distributed chi-square random variables. To test the null hypothesis for no difference in treatments the following ratio is used and compared.

$$F_0 = \frac{MS_{Treatments}}{MS_E} \quad (4.17)$$

For knowing the percentage of contribution of the each treatment of the experiments the following equation can be used.

$$\text{Percentage contribution (P \%)} = \frac{SS_{Treatments}}{SS_T} \times 100 \quad (4.18)$$

The evaluation of the values for the various tests for ANOVA table is calculated using the software rather than doing the manual calculation for the current work.

## 4.2 DATA MEASUREMENT

The accuracy to collect the data without variation plays important role in establishing the correct conclusions and finalization of the optimum parameters. The recommended tests which may be conducted on the electrodeposited metals are thickness, appearance, porosity, adhesion, stress, hardness, wear and abrasion resistance, tensile strength and ductility. The properties most important in the aspects of the current work are thickness, appearance (surface finish) and hardness. The output response parameters for the set of experiments are thickness of the deposit and surface finish. The hardness and surface morphology was also studied, get greater comprehension of the process parameters on mechanical properties of the deposited metal. The following section will discuss the measuring instruments used for the process.

### 4.2.1 MEASUREMENT OF THICKNESS

Thickness of electrodeposited metal can be measured using micrometer, microscopio cross-sectioning. For highly accurate results double beam interference microscope (interferometry) is preferred, which is mainly used in the calibration of thickness standards. The other methods used for the measurement of thickness is the use of the physical and chemical properties difference in the deposit and substrate. Such methods commonly use the electrical, magnetic and chemical properties. Another

method used to find the thickness of the deposition is the indirect method of measurement of mass per unit area or weight gain through the difference in the weight before and after treatment.

The deposition of the material in this work is measured using screw gauge micrometer of 0.01 mm least count. As the thickness of deposition of copper during electroplating is in the range of 0.1mm to 0.3 mm, so the instrument used is reliable for this measurement. The ABS parts thickness was measured as bare component and then again it was measured with the deposition. The final thickness of the deposit is recorded as the difference of the two values. The Mitutoyo 0-25 mm range micrometer was used for the measurements (Figure 4.4)



Figure 4.4 Thickness Measurement by Screw Gauge Micrometer

The precoating of copper electroplating before cold spray coating was not very thick, so it was measured using eddy current method. The eddy current probe (Figure 4.5) generates a high frequency electric field when in contact with the test specimen. The magnitude of the eddy currents depends upon the distance between the substrate surface and the probe, which is equivalent to the thickness of the metal deposit.

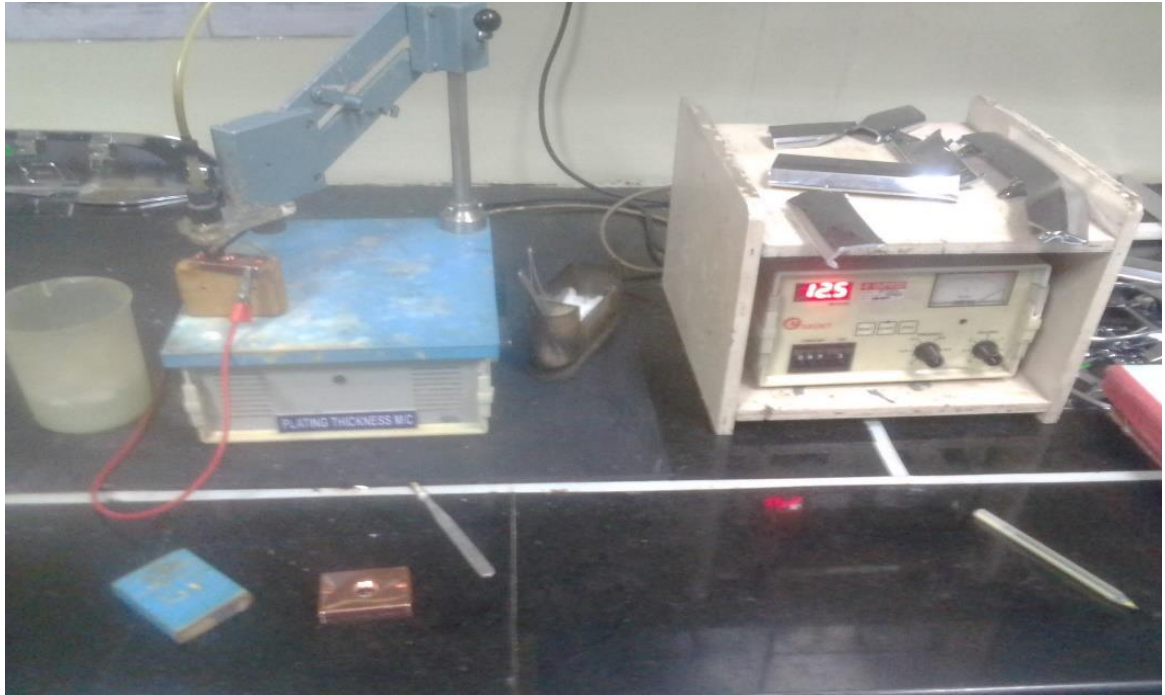


Figure 4.5 Thickness Measurement by Eddy Current Probe

The intensity of the eddy currents is dependent upon the gap between the substrate top surface and the probe, which is usually similar to the deposit's material thickness. The interaction of the magnetic field with the probe coil ultimately determines the intensity of the generated current. Fluctuations in the probe coil are determined with a micro ammeter as they are associated with the coating thickness by utilizing calibrated recommended coating thickness standards. The variance in conductivity between metal deposit and substrate is precisely what, essentially, can make this instrument a thickness gage, by measuring the degree of difference in conductivity between them. This means the instrument is more suitable when the conductive and nonconductive materials are involved.



#### **4.2.2 SURFACE ROUGHNESS MEASUREMENT**

The condition of the ABS surface is responsible for the final surface on the interface of the deposited metal and FDM part, the average surface roughness ( $R_a$ ) have been considered. The average surface roughness ( $R_a$ ) had been recorded for each replica after the electrodeposition (Figure 4.6). The reason for selecting  $R_a$  values in order to measure the surface roughness was that it employs an algorithm that averages the absolute values of the profile height deviations from the mean line on the entire surface within the sampling length and then neutralizes the few outlying points so that the extreme points have no significant impact on the final results (as described in ASME B46.1). Also, it is a simple and effective method for monitoring the surface texture and ensuring consistency in measurement of multiple surfaces. The surface roughness was measured using **MITUTOYO – SJ 201P**. The device has a digital display for the final roughness value and the machine can also be connected to a computer system for the data calculation. During processing, the sensor is positioned on the top surface which uniformly slides along the surface by the powering mechanism inside the instrument. The sensor obtains the information about surface roughness by the pointed integrated diamond probe. This roughness leads to displacement of the probe, producing a change of inductive amount of induction coils. This translates into the analogue signal, which is usually in proportion to the surface roughness at the output end of phase-sensitive rectifier. The inductive changes are evaluated, transformed into a signal proportional to the displacement and logged as a surface dimension. This equipment uses the stylus method of measurement; it has the profile resolution of 12 nm and measure the roughness up to 100 $\mu$ m. It uses tracing length of 4.0mm for analysis. It gives a very accurate value of roughness and evaluate the quality of formed product.



Figure 4.6 Roughness Testing Equipment

#### **4.2.4 HARDNESS TESTING**

The hardness of the deposits was measured using Vickers hardness testing machine as per ASTM-E-384 standard test method for Vickers hardness of metallic materials (shown in Figure 4.7). Technical specifications of testing equipment are given in appendix A. The indentations on each polished sample were performed at a load of 0.1 Kg and at a dwell time of 10 sec. The results of tests were obtained directly through the measurement of indentation scale. The indentations were made using a square based pyramid indenter and size of the hardness impressions was measured precisely with an integral microscope attachment. The surface hardness may vary within the part itself due to various uncontrollable factors. So, in order to minimize this variation, three readings were taken at the selected location for all the electroplated and cold sprayed samples.



Figure 4.7 Vicker-Hardness Tester

The hardness of final mould was measured using Vicker hardness testing equipment at HV scale of 0.1. Minimum scale value of optical micrometer  $0.01\mu\text{m}$  and measuring range of  $200\mu\text{m}$ .

#### **4.2.4 MICROSTRUCTURE**

The internal structure of the metal is made up of crystal (known as grains) which is defined by the arrangements of the atoms. The grains orientation and placement is a major contributing factor for the mechanical properties of the metals. These arrangements of the grains, which are of microscopic level is called the microstructure of the metal. The study of the microstructure of a material could reveal a great piece of information about the composition, properties, processing history and performance of the metal.

The equipment used to study the various information about the substrate or deposit was optical microscope and scanning electron microscope. The optical microscope used in this work was Inverted Metallurgical Microscope model no. RMM-5 (Figure

4.8). It is a self contained portable microscope. Generally used for inspection of microstructure of metals in laboratories. It is having a digital camera and CCD image processing systems and also download the images for data transfer, storage, analysis etc.



Figure 4.8 Inverted Metallurgical Microscope

The standard magnification of RMM-5 inverted metallurgical microscope is 40x to 400x. The magnification of the order of 300x to 400x was used in this work for the recording of copper microstructures at initial level.

For more in depth study of the formation of the deposition pattern and the microstructure the Scanning Electron Microscope, model JSM-840A, make JEOL, Japan has the range of magnification from 10x to 3,00,000x was used. The information about the composition of the materials present in the samples are reported using the XRD and SEM analysis. The XRD and SEM facility available at Lovely Professional University is shown in Figure 4.9 was used for the analyze the composition of Cu deposition. The X-Ray diffractometer was set for  $2\theta$  angle between  $0^{\circ}$  to  $80^{\circ}$  at a scan speed of  $2^{\circ}$  per minute for each specimen.



Fig 4.9 (a)

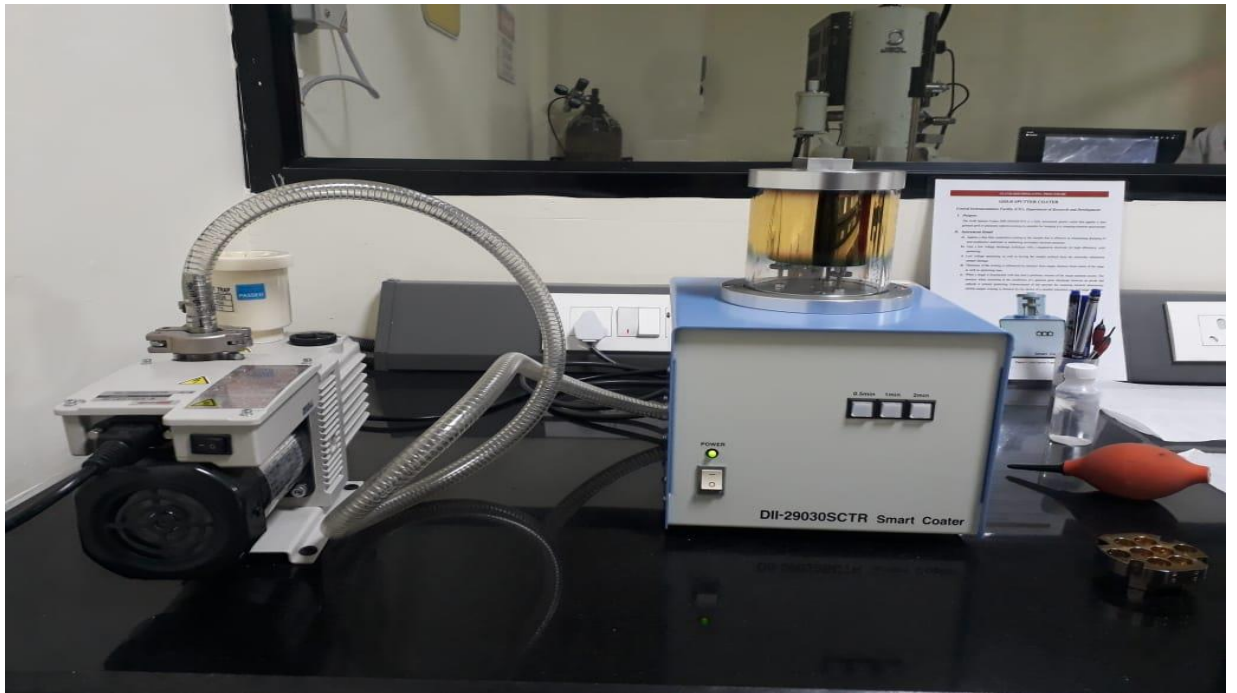


Fig 4.9 (b)

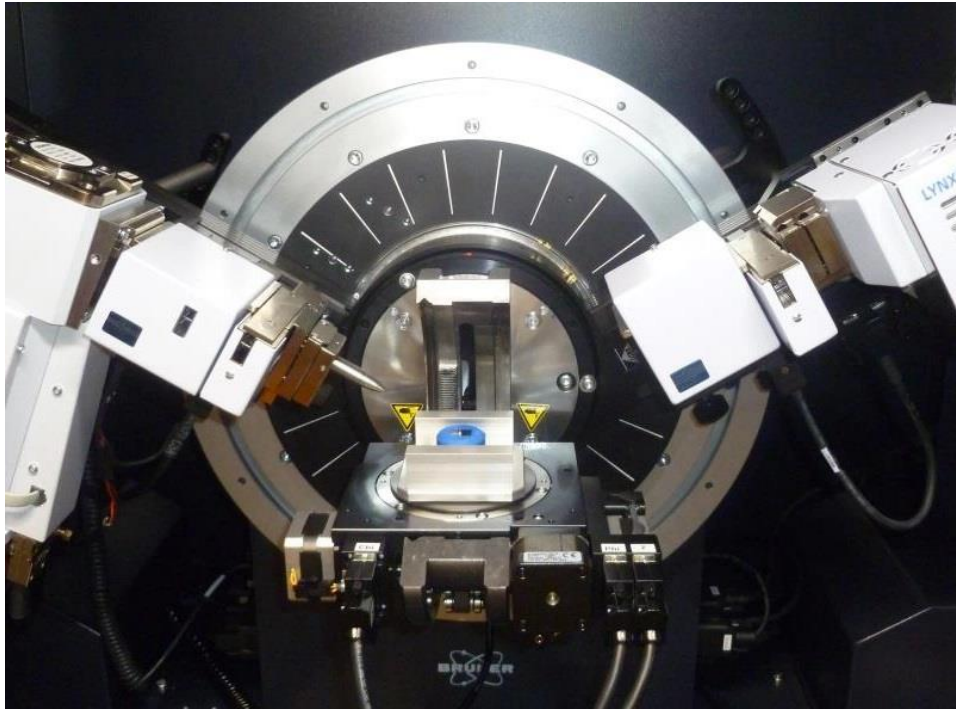


Fig 4.10 (c)

Fig 4.9 : a) FE-Scanning Electron Microscope(SEM) b) Gold Sputtering Coater c)  
X-Ray Diffractometer



## CHAPTER-5 EXPERIMENTATION

---

The experimentation to establish the optimum parameters for cold spray coating on metal coated 3D printed part was conducted in two stages. The first set of experiments was to test the electrodeposition of copper on the ABS plastic test components. The second set of experiments was conducted in establishing optimum process parameters for cold spray coating on electroplated 3D printed parts and finding the optimum levels of these parameters.

### 5.1 OPTIMIZATION OF COPPER ELECTROPLATING PROCESS PARAMETERS

The ABS samples to be electrodeposited with copper were fabricated using FDM process as shown in Figure 5.1. Twenty-seven samples were subjected to surface preparation treatments for copper plating as per the procedure discussed in 3.2.1.



Figure 5.1 FDM Produced ABS Component for Copper Deposition

The 3D printed samples coated with silver conductive were subjected to the process of copper electrodeposition in the electrolytic solution of copper sulphate and sulphuric acid in the setup as explained earlier. Total nine experiments with three replicas of each were conducted as per Taguchi's L9 design of experiments. The responses for the samples were noted for the thickness and surface finish of copper deposit. The process control parameters identified as given in the Table 3.5 taken were copper sulphate concentration, time and voltage for three levels as given in Table 5.1.

Table 5.1 Parameters for Copper Electroplating

Control Parameters	Levels		
	L1	L2	L3
Voltage (V)	2	3	4
CuSO <sub>4</sub> Concentration(g/l)	190	200	210
Time (minutes)	120	180	240

The values of voltage, CuSO<sub>4</sub> concentration and time for each experiment were established from the L9 design of experiments orthogonal array as given in Table 4.3. The effect of three response control factors on deposition thickness and surface roughness have been investigated and results are discussed in this section.

### 5.1.1 EXPERIMENTAL STUDY OF COPPER ELECTROPLATING FOR DEPOSITION THICKNESS

The Taguchi method's "larger-the-better" criterion for deposition thickness has been applied for computing S/N ratios. Experimental data was collected to determine the ideal input control parameters for the best response, the proportion of each factor's contribution using an ANOVA table for S/N ratios, and to project the best theoretical response characteristic values for the optimum parameters.

The confirmation of the optimized parameters was achieved through the set of experiments performed on various components of ABS for copper electroplating. A comparison between the experimental results and the theoretical estimated was also drawn and discussed. The observed values with S/N Ratio as per the orthogonal array for deposition rate are given in Table 5.2.



Table 5.2 Thickness Deposition Observations and Calculated S/N Ratios

Trail No.	Voltage (V)	CuSO <sub>4</sub> Conc. (g/l)	Time (min)	Thickness(( $\mu\text{m}$ ))			Mean Thickness ( $\mu\text{m}$ )	Mean Deposition Rate ( $\mu\text{m}/\text{min}$ )	S/N Ratio (dB)
				S1	S2	S3			
1	2	190	120	215	228	217	220	1.83	46.84
2	2	200	180	267	258	261	262	1.46	48.36
3	2	210	240	357	361	368	362	1.51	51.17
4	3	190	180	149	156	160	155	0.86	43.80
5	3	200	240	319	303	299	307	1.28	49.73
6	3	210	120	254	252	274	260	2.17	48.28
7	4	190	240	119	135	121	125	0.52	41.90
8	4	200	120	230	216	214	220	1.83	46.84
9	4	210	180	148	147	161	152	0.84	43.61

For the three levels of voltage, CuSO<sub>4</sub> concentration, and duration, the mean values of the deposition thickness and the related S/N ratios have been derived from these data and are shown in Table 5.3. The factor impacts of the input factors are represented by these mean values.

Table 5.3 Mean Values by Factor Level for Deposition Thickness

Factors	Voltage (V)		CuSO4 Conc. (g/l)		Time (min)	
Levels	Raw Data	S/N Data	Raw Data	S/N Data	Raw Data	S/N Data
L1	281.33	48.79	166.67	44.18	233.33	47.32
L2	240.67	47.27	263.00	48.31	189.67	45.26
L3	165.67	44.12	258.00	47.69	264.67	47.60

The mean effects of these factors have been plotted and presented in Figure 5.2 (a), (b) and(c)

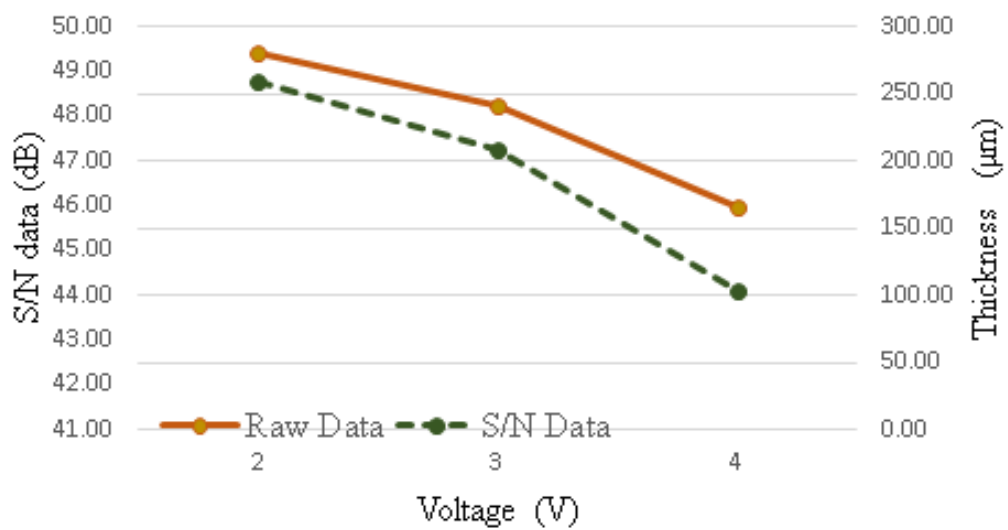


Figure 5.2 (a) Effect of Voltage on Deposition Thickness and its S/N Ratio

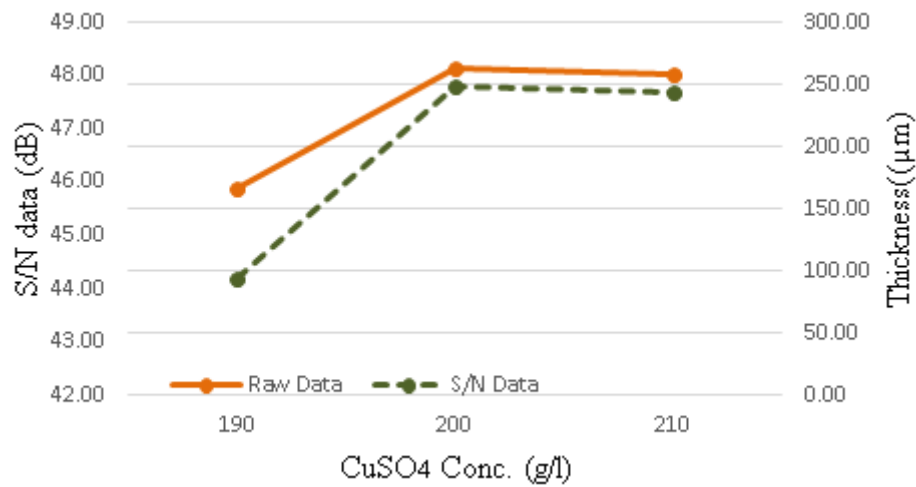


Figure 5.2 (b) Effect of CuSO4 Concentration on Deposition Thickness and its S/N Ratio

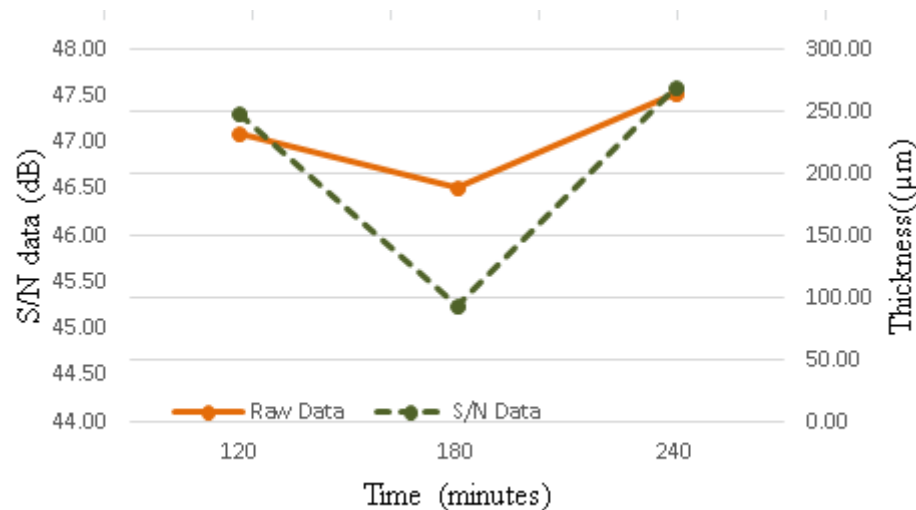


Figure 5.2 (c) Effect of Time on Deposition Thickness and its S/N Ratio

The 'larger-the-better' sort of response characteristic describes metal deposition thickness. High thickness deposition values are therefore regarded as ideal. From the main effects plot of voltage in Figure 5.2 (a), it is interpreted that the rate of deposition decreases as the voltage increases from 2V to 3V followed by a dip by a further change in the voltage. As the high voltage leads to high current density, which limits the ability of depositing atoms to diffuse to epitaxial growth sites on the surface, results in non-epitaxial growth mode and slows down the deposition rate.

Higher voltages also weaken the adhesion properties of the deposition. The deposition rate increases as CuSO<sub>4</sub> concentration increases from 190 g/l to 200 g/l as shown in Figure 5.2 (b), followed by a dip on a further increase in the concentration. One possible reason is the lack of flow of ions owing to high concentrations in the solution.

Time factor also played an important role on the rate of deposition as indicated in the Figure 5.2(c). The deposition rate decreases initially and the least thickness is observed at time setting of 180minutes. The deposition rate increased consistently as the time is increased further from 180minutes to 240 minutes. The lower deposition rate may be due to the fact that after a period of time, distribution of copper tends to be more at the sharp corners. This non-uniform deposition reduces the average thickness growth over the whole surface. From Figure 5.2 (a), (b), and (c) it can be interpreted that all the three process parameters (voltage, CuSO<sub>4</sub> concentration and time) have a direct impact on the deposition rate. Figure 5.2 (a), (b), and (c) show greater values for the deposition rate on the ABS component as a result. They are found to be the first level of voltage (A1), second level of CuSO<sub>4</sub> concentration (B2), and third level of time (C3). Hence, A1B2C3 is the optimum set of input parameters for the best deposition. Since this set of experiments does not exist in the orthogonal array in Table 5.3 so, a confirmatory experiment is required. The result of confirmatory experiment is tabulated in Table 5.4.

Table 5.4 Deposition Thickness Confirmatory Experiment Observation

Trail No.	Voltage (V)	CuSO <sub>4</sub> Conc. (g/l)	Time (min)	Thickness(( $\mu$ m))			Mean Thickness ( $\mu$ m)	Mean Deposition Rate ( $\mu$ m/min)
				S1	S2	S3		
10	2	200	240	356	346	347	349	1.454

The mean value of this confirmatory experiment for the thickness of deposition is 349 $\mu$ m, which, using the Taguchi approach, can be compared to the theoretical value.

The mean of different factors and overall mean of the deposition rate can be used to predict the thickness at these optimum settings. Table 5.3 provides the means for the three thickness and S/N Ratio variables. Equation 5.1 provides the theoretical value of  $\eta_{opt}$  under ideal conditions.

$$\eta_{opt} = m + (m_{A1} - m) + (m_{B2} - m) + (m_{C3} - m) = 50.94 \text{ dB} \quad (5.1)$$

$m$  is the overall S/N data mean,  $m_{A1}$  is the S/N data mean for factor A at level 1,  $m_{B2}$  is the S/N data mean for factor B at level 2, and  $m_{C3}$  is the S/N data mean for factor C at level 3.

The corresponding value of deposition thickness is given by equation 5.2.

$$y_{opt}^2 = \frac{1}{10^{\frac{-\eta_{opt}}{10}}} \quad (5.2)$$

Calculated value of  $y_{opt}$  is 352  $\mu\text{m}$ , which is quite similar to the experimental value of 349  $\mu\text{m}$ .

Means of thickness (Figure 5.3) interaction effects have also been plotted in order to analyse the impact of each parameter with respect to other factors (Figure 5.4). As there are no parallel lines in the entire interaction plot for the means of thickness and S/N ratio, it can be inferred that there is a strong interaction between all the components. It is implied by this that one factor depends on another.

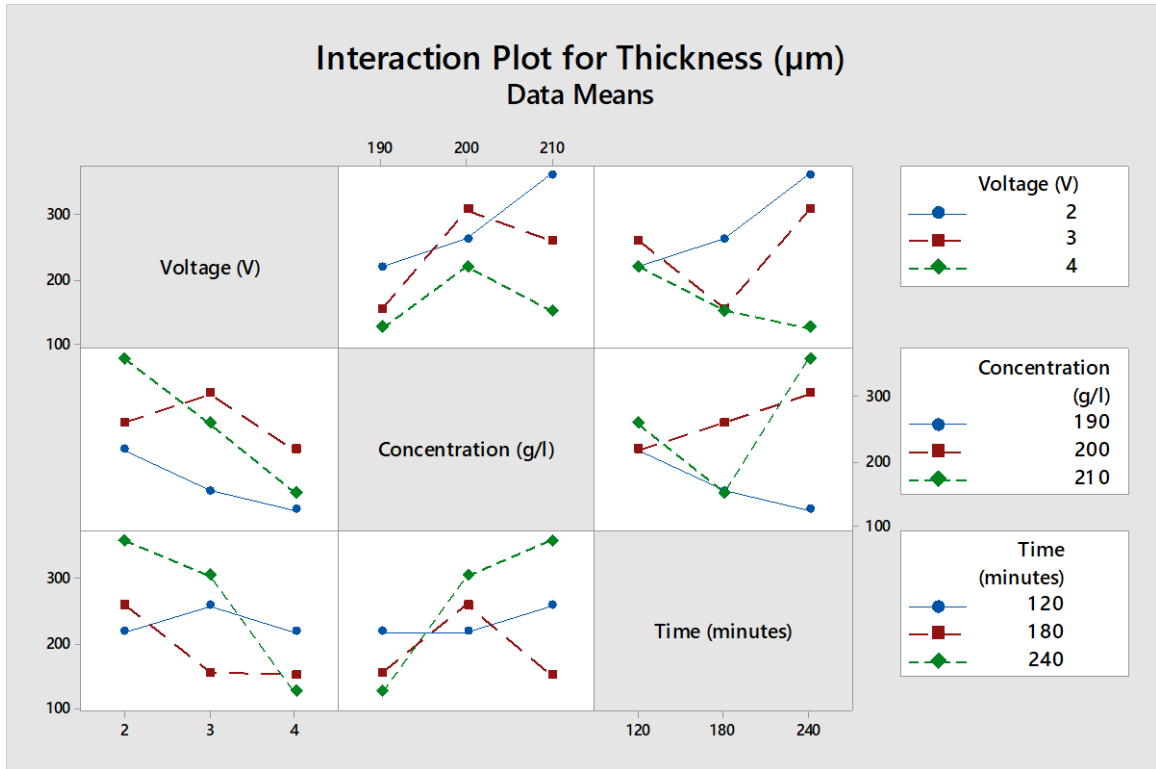


Figure 5.3 Interaction Plot for Means of Deposition Thickness

To determine the percentage contribution of the three components and their significance, analysis of variance (ANOVA) of the mean data was carried out at the 95% confidence level. Table 5.6 illustrates how voltage, concentration, and duration affected the deposition thickness for mean data.

Table 5.5 ANOVA Table

Parameters	D.F	Sum of squares	Mean sum of squares	Variance Ratio	P value
Between Rows	$p_1 - 1$	SSR	$MSR = \frac{SSR}{p_1 - 1}$	$F_{(p_1 - 1), (p_1 - 1)(p_2 - 1)} = \frac{MSR}{MSE}$	$\alpha_1$
Between Columns	$p_2 - 1$	SSC	$MSC = \frac{SSC}{p_1 - 1}$	$F_{(p_2 - 1), (p_1 - 1)(p_2 - 1)} = \frac{MSC}{MSE}$	$\alpha_2$
Error	$(p_1 - 1)(p_2 - 1)$	SSE	$MSE = \frac{SSE}{(p_1 - 1)(p_2 - 1)}$		
Total	$p_1 p_2 - 1$	SST			

Table 5.6 ANOVA Table for Copper Coating Thickness

Source	DF	Sum of squares ( $SS^2$ )	Adj MS	F	P	% Contribution	Significant
Voltage (V)	2	33.83	16.92	23.33	0.041	45.24%	Yes
Concentration(g/l)	2	29.65	14.83	20.45	0.046	39.65%	Yes
Time (minutes)	2	9.85	4.93	6.79	0.140	13.17%	No
Error	2	1.45	0.73			1.94%	
Total	8	74.79	37.39				
		<b>S = 0.8544</b>		<b>R<sup>2</sup> = 98.06%</b>			
<b>Tabular value of F = F(2,2,0.05) = 19</b>							
<b>Degrees of freedom- DF, Adjusted Mean squares measure – Adj MS, Determines significance of a factor at 95% confidence level P &lt; 0.05</b>							

The  $F_{\text{values}}$  are calculated as

$$\text{Sum of square for error} = SSE = 75.069 - (33.83 + 29.65 + 9.85) = 1.44$$

$$\text{Sum of square of mean for Voltage (V)} = MSS_V = \frac{33.830}{2} = 16.915$$

$$\text{Sum of square of mean for Concentration (g/l)} = MSS_C = \frac{29.654}{2} = 14.8272$$

$$\text{Sum of square of mean for Time (minutes)} = MSS_T = \frac{9.830}{2} = 4.915$$

$$\text{Sum of square of means for Error} = \frac{1.45}{2} = 0.73$$

$$F_{\text{Value for Voltage (V)}} = F_V = \frac{MSS_V}{MSE} = \frac{16.92}{0.73} = 23.33$$

$$F_{\text{Value for Concentration (g/l)}} = F_C = \frac{MSS_C}{MSE} = \frac{14.83}{0.73} = 20.45$$

$$F_{\text{Value for Time (minutes)}} = F_T = \frac{MSS_T}{MSE} = \frac{4.93}{0.73} = 6.79$$

The calculated  $P_{\text{Values}}$  are

$$P_{\text{Value for Voltage (V)}} = P_V = \frac{F_{\text{Tabulated}}}{F_V} = \frac{19}{23.33} \times 0.05 = 0.041$$

$$P_{\text{Value for Concentration (g/l)}} = P_C = \frac{F_{\text{Tabulated}}}{F_C} = \frac{19}{20.45} \times 0.05 = 0.046$$

$$P_{\text{Value for Time (minutes)}} = P_T = \frac{F_{\text{Tabulated}}}{F_T} = \frac{19}{6.79} \times 0.05 = 0.140$$

$$S = \sqrt{MSE} = \sqrt{0.73} = 0.8544$$

The coefficient of determination is given as

$$R^2 = 1 - \frac{SSB}{SST} = \left(1 - \frac{1.45}{74.79}\right) \times 100 = 98.06\%$$

The tabulated value of  $F_{(0.05, 2, 2)} = 19$ . When the calculated value of F for voltage (23.33) and Concentration (20.45) is compared with the tabulated value of F, it is observed that these two parameters have a significant effect on the deposition rate of copper whereas the calculated value of F for time (6.79) is less than the tabulated value of F so its effect is insignificant on the rate of copper deposition. Using the p-value of F so its effect is insignificant on the rate of copper deposition. Using the p-value, we can also analyze the significance of the parameters. As p-values for Voltage and concentration are less than 0.05 so these parameters are more significant whereas the p-value of time is more than 0.05 so this parameter is insignificant.

It is evident from the Table 5.6 that the two factors have a significant contribution on the deposition thickness. The effects of voltage and concentration factors are almost equal on the response parameter and time factor is insignificant. To understand the effect of each factor on the deposition rate per minute as a response, Table 5.2 has an additional column in which the calculated mean deposition rate for each experiment is recorded. Table 5.7 has the results of ANOVA for S/N data for three factors against the deposition rate.



Table 5.7 ANOVA Table of S/N Data for Copper Coating Thickness

Source	DF	Sum of squares ( $SS^2$ )	Adj MS	F	P	% Contribution	Significant
Voltage (V)	2	4.009	2.004	23.848	0.040	45.24%	Yes
Concentration(g/l)	2	3.545	1.772	21.086	0.045	39.65%	Yes
Time (minutes)	2	1.368	0.684	8.140	0.117	13.17%	No
Error	2	0.168	0.084			1.94%	
Total	8	9.09	4.545				
$S = 26.89$				$R^2 = 97.12\%$			
Tabular value of $F = F(2,2,0.05) = 19$							
Degrees of freedom- DF, Adjusted Mean squares measure – Adj MS, Determines significance of a factor at 95% confidence level $P < 0.05$							

Residual plots aid in evaluating data for variances caused by control settings. The residual plots for means in (Figure 5.4) and S/N ratio (Figure 5.5) show that they do not deviate much from the projected normal distribution line and follow symmetry in the histograms around the zero value. Residual plots assist in analysing data for variances caused by control settings. Residuals have constant variance because they are randomly distributed around zero in residuals against fitted values. Because residuals show no discernible pattern, there is no inaccuracy owing to time or data collecting order. This suggests that the experimental work using the input parameters of voltage, concentration, and duration has less fluctuation.

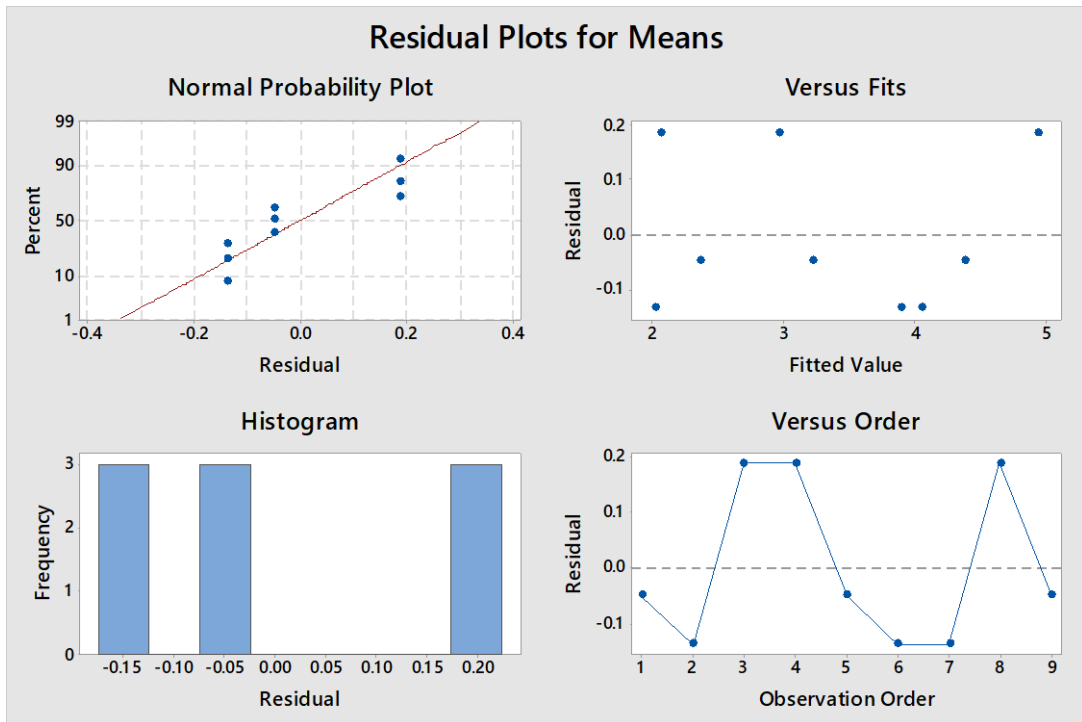


Figure 5.4 Residual Plots for Mean Data of Deposition Thickness

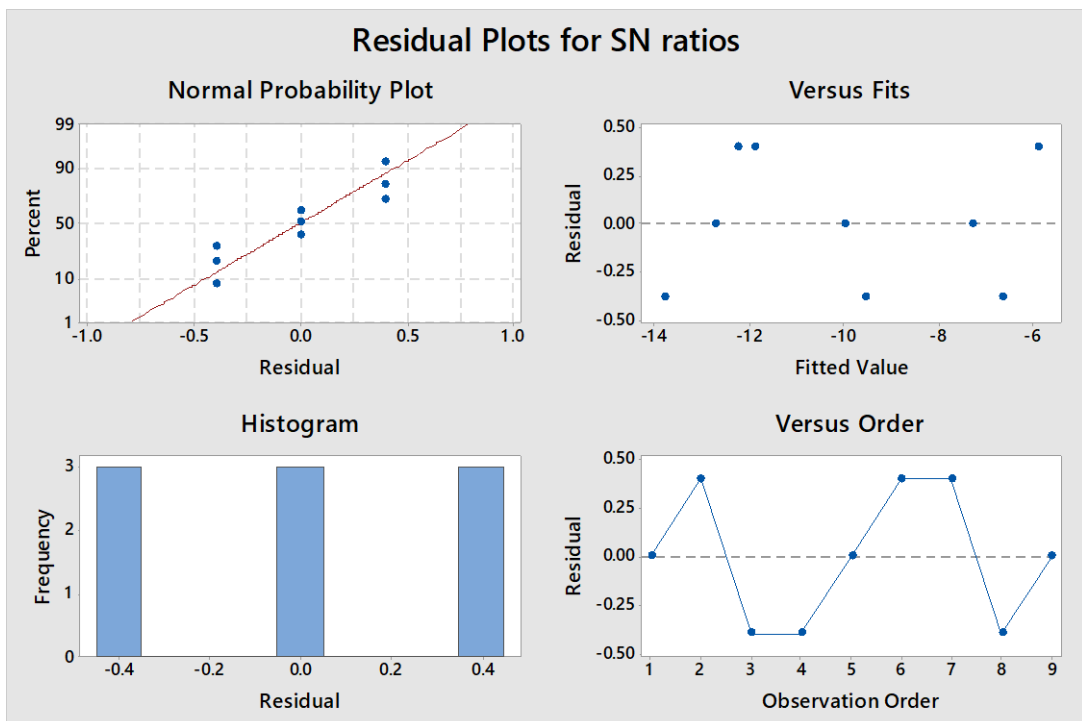


Figure 5.5 Residual Plots for S/N Data of Deposition Thickness

### **5.1.2 EXPERIMENTAL STUDY OF COPPER ELECTROPLATING FOR SURFACE ROUGHNESS**

S/N ratios for surface roughness have been calculated using the Taguchi approach, which advocates "smaller-the-better." The experimental data was gathered to determine the input control parameters that produced the best response, the proportion of each factor's contribution using an ANNOVA table for S/N ratios, and to calculate the best theoretical response characteristics for the determined optimal parameters. A comparison between of experimental results and the theoretical estimated was also drawn and debated. Talysurf is used to measure the surface roughness of electroplated components with a minimum count of 0.0 $\mu$ m. The observed values for the variations in the control parameters such as voltage, CSS concentration and time as per the Taguchi L9 experiments are noted in Table 5.8. From these observed values the calculated values of means of surface roughness and their S/N ratios are also given in Table 5.9

For the three levels of voltage, CuSO<sub>4</sub> concentration, and time, the mean values of surface roughness and related S/N ratios have been derived from these data and are shown in Table 5.9. The factor impacts of the input factors on the surface roughness are represented by these mean values.

Table 5.8 Copper Electroplating Surface Roughness Observation and Calculated S/N Ratios

Trail No.	Voltage (V)	CuSO4 Conc. (g/l)	Time (min)	Surface Roughness ( $\mu\text{m}$ )			Mean Surface Roughness ( $\mu\text{m}$ )	S/N Ratio (dB)
				S1	S2	S3		
1	2	190	120	1.82	1.96	1.86	1.85	-5.3434
2	2	200	180	3.21	3.12	3.08	2.22	-6.9271
3	2	210	240	2.24	2.29	2.41	3.46	-10.782
4	3	190	180	2.17	2.26	2.31	2.22	-6.9271
5	3	200	240	4.39	4.31	4.28	2.75	-8.7867
6	3	210	120	3.76	3.62	3.87	3.14	-9.9386
7	4	190	240	3.09	3.24	3.14	2.86	-9.1273
8	4	200	120	4.05	3.82	3.87	2.28	-7.1587
9	4	210	180	4.22	4.09	4.04	4.11	-12.277

Table 5.9 Copper Electroplating Mean Values by Factor Level for Surface Roughness

Factors	Voltage (V)		CuSO4 Conc. (g/l)		Time (min)	
	Raw Data	S/N Data	Raw Data	S/N Data	Raw Data	S/N Data
<b>L1</b>	2.51	-7.68	2.31	-7.66	2.42	-7.48
<b>L2</b>	2.70	-8.55	2.42	-7.62	2.85	-8.71
<b>L3</b>	3.08	-9.52	3.57	-9.57	3.02	-9.57

The mean effects of these factors have been plotted and presented in Figure 5.6 (a), (b) and(c)

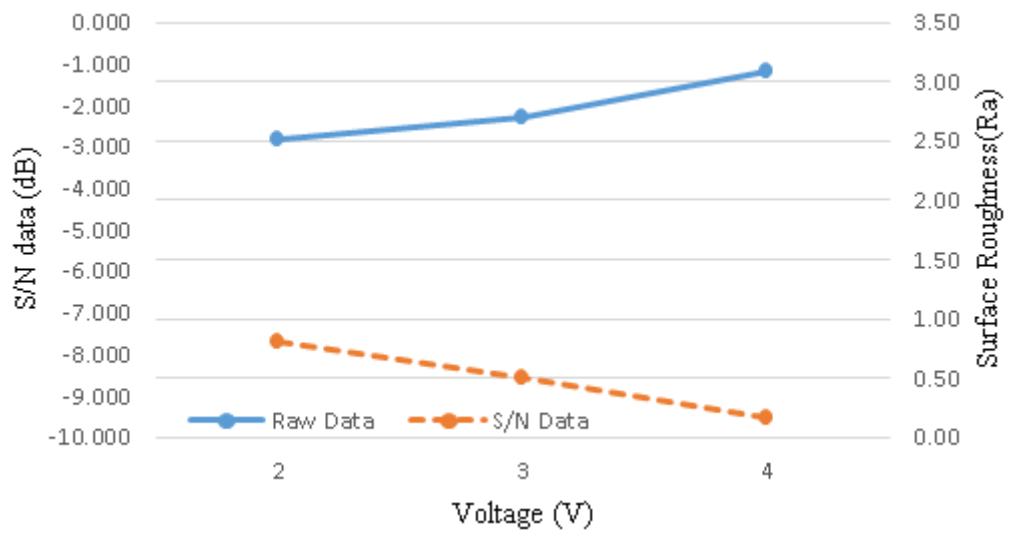


Figure 5.6 (a) Effect of Voltage on Surface Roughness and its S/N Ratio

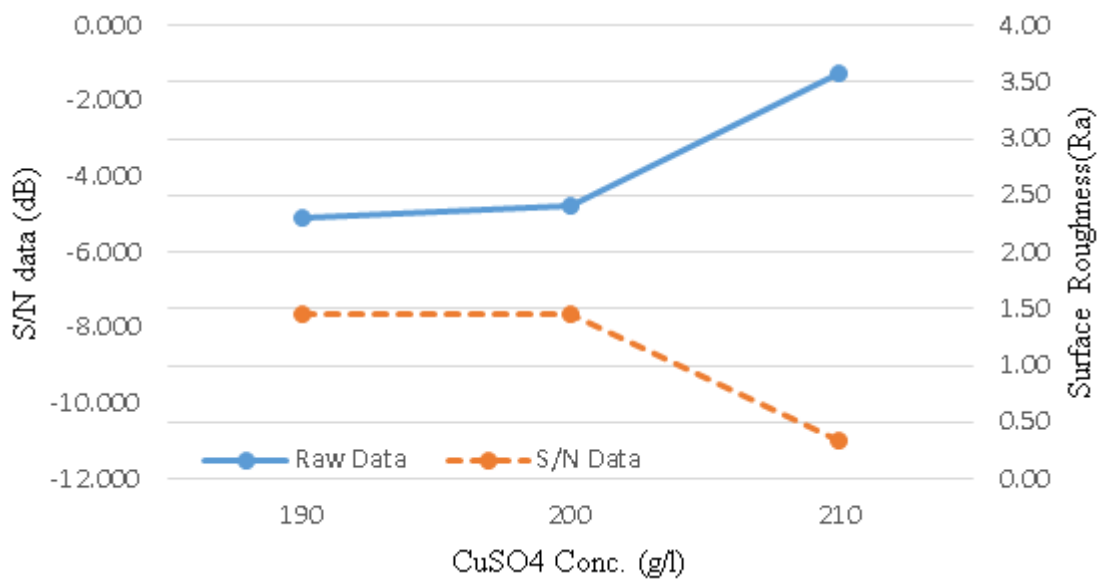


Figure 5.6 (b) Effect of CuSO<sub>4</sub> Concentration on Surface Roughness and its S/N Ratio

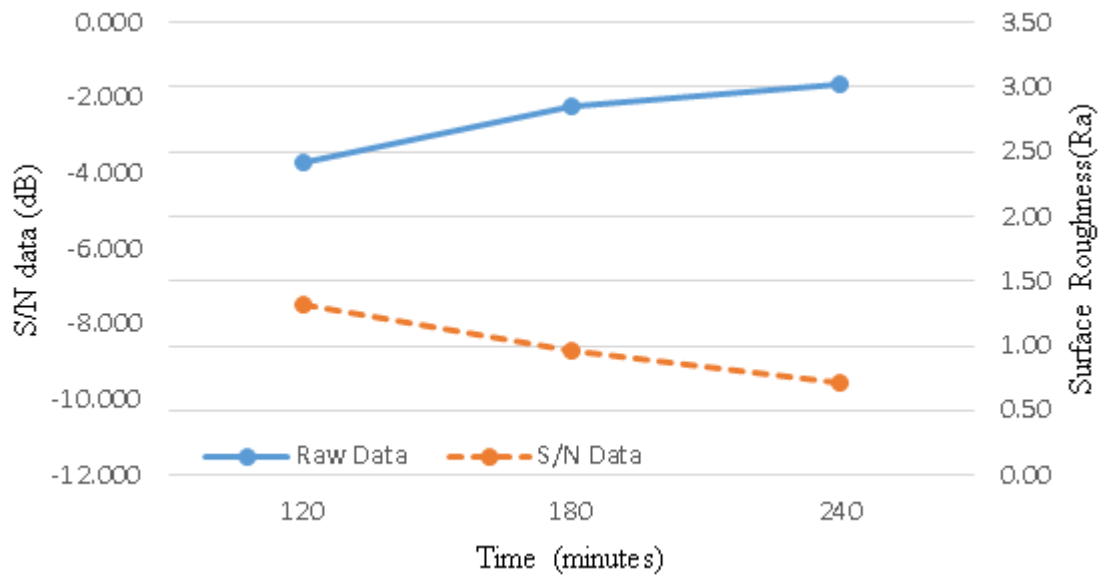


Figure 5.6 (c) Effect of Time on Surface Roughness and its S/N Ratio

Surface roughness is the ‘smaller-the-better’ type of response characteristic. Low surface roughness ratings are therefore regarded as ideal. The surface roughness showed a difference from 1.85  $\mu\text{m}$  to 4.11  $\mu\text{m}$ . From the main effects plot of voltage in Figure 5.6 (a), it is interpreted that the surface roughness increases with the increase in voltage continuously. Higher voltage (more current density) results in a high rate of deposition and heat generation that makes the deposit coarser in nature and gives a poor surface finish. The  $\text{CuSO}_4$  concentration also affects the surface roughness considerably as shown in Figure 5.6 (b). The surface roughness first remains low and constant for 190 g/l and 200 g/l, but the change is rapid as the concentration changes from 200 g/l to 210 g/l. In the more concentration scenario, the deposition is more coarse and powdery due to low acid and chloride content in the solution. According to Figure 5.6(c), time played a significant impact on surface roughness, and the time period of 120 minutes has the lowest surface roughness. The increase in the thickness of plating with time also brings in the non-uniformity in the growth of the plating due to the geometrical shapes, and visual lumps start forming at the edges of the component leading to poor surface finish. Hence there is a continuous decrease in the surface finish with the increase in the time of deposition.

From Figure 5.6 (a), (b), and (c) it can be interpreted that all the three process parameters (voltage,  $\text{CuSO}_4$  concentration and time) have a direct impact on the

surface roughness. Therefore, lower values for surface roughness on ABS component can be observed from Figure 5.6 (a), (b), and (c). They are found to be the first level of voltage (A1), first level of concentration (B1), and first level of time (C1). Hence, A1B1C1 is the optimum set of input parameters for the lowest surface roughness. Since this set of experiments exists in the orthogonal array in Table 5.8 as first experiment, a confirmation experiment is not required. The mean value of this experiment for surface roughness is  $1.85\mu m$ , which can be compared with the theoretical value using Taguchi method. The mean of different factors and overall mean of surface roughness can be used to predict the roughness at these optimum settings. The means for three factors for thickness and S/N Ratio is given in Table 5.9. The theoretical value of  $\eta_{opt}$  under the optimum conditions is given by equation 5.3.

$$\eta_{opt} = m + (m_{A1} - m) + (m_{B1} - m) + (m_{C1} - m) = -5.8 \text{ dB} \quad (5.3)$$

The corresponding value of surface roughness is given by equation 5.4.

$$y_{opt}^2 = 10^{\frac{-\eta_{opt}}{10}} \quad (5.4)$$

Or,  $y_{opt} = 1.9 \mu m$ , which is quite close to the experimental value that was reported.

Surface roughness method have also been plotted to explore the interaction effects between each parameter and other factors (Figure 5.7). Because there are so few parallel lines in the complete interaction plot for the means of surface roughness and S/N ratio, it may be inferred that there is a strong interaction between all the components. It is implied by this that one factor depends on another.

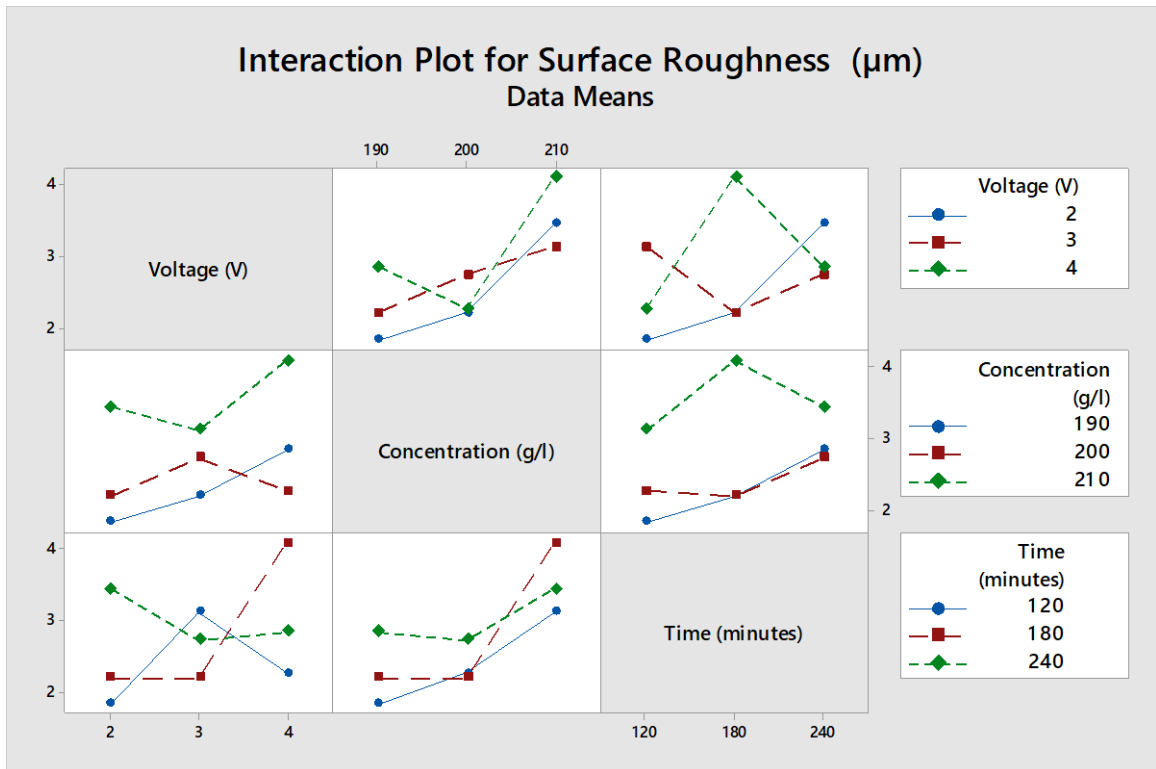


Figure 5.7 Interaction Plot for Means of Surface Roughness

Table 5.10 ANOVA Table of S/N Data for Copper Electroplating Surface Roughness

Source	DF	Sum of squares ( $SS^2$ )	Adj MS	F	P	%Contribution	Significant
Voltage (V)	2	5.0669	2.533	11.973	0.079	13.11%	No
Concentration(g/l)	2	26.5801	13.290	62.807	0.015	68.75%	Yes
Time (minutes)	2	6.5908	3.295	15.574	0.061	17.05%	No
Error	2	0.4232	0.212			1.09%	
Total	8	38.661	19.331				
		S = 0.464		$R^2 = 98.91\%$			
Tabular value of F = F(2,2,0.05) = 19							
Degrees of freedom- DF, Adjusted Mean squares measure – Adj MS, Determines significance of a factor at 95% confidence level P < 0.05							



The F values are calculated as

$$\text{Sum of square for error} = \text{SSE} = 4.108 - (0.51 + 2.929 + 0.572) = 0.097$$

$$\text{Sum of square of mean for Voltage (V)} = \text{MSS}_V = \frac{0.51}{2} = 0.255$$

$$\text{Sum of square of mean for Concentration (g/l)} = \text{MSS}_C = \frac{2.929}{2} = 1.465$$

$$\text{Sum of square of mean for Time (minutes)} = \text{MSS}_T = \frac{0.572}{2} = 0.286$$

$$\text{Sum of square of means for Error} = \frac{0.097}{2} = 0.048$$

$$\text{F\_Value for Voltage (V)} = F_V = \frac{\text{MSS}_V}{\text{MSE}} = \frac{0.255}{0.048} = 5.28$$

$$\text{F\_Value for Concentration (g/l)} = F_C = \frac{\text{MSS}_C}{\text{MSE}} = \frac{1.465}{0.048} = 30.294$$

$$\text{F\_Value for Time (minutes)} = F_T = \frac{\text{MSS}_T}{\text{MSE}} = \frac{0.286}{0.048} = 5.917$$

The calculated P\_Values are

$$\text{P\_Value for Voltage (V)} = P_V = \frac{F_{\text{Tabulated}}}{F_V} = \frac{19}{5.28} \times 0.05 = 0.180$$

$$\text{P\_Value for Concentration (g/l)} = P_C = \frac{F_{\text{Tabulated}}}{F_C} = \frac{19}{20.45} \times 0.05 = 0.037$$

$$\text{P\_Value for Time (minutes)} = P_T = \frac{F_{\text{Tabulated}}}{F_T} = \frac{19}{6.79} \times 0.05 = 0.161$$

$$S = \sqrt{\text{MSE}} = \sqrt{0.048} = 0.2199$$

The coefficient of determination is given as

$$R^2 = 1 - \frac{\text{SSE}}{\text{SST}} = \left(1 - \frac{0.097}{4.108}\right) \times 100 = 97.65\%$$

It is evident from the Table 5.10 that CuSO<sub>4</sub> concentration factors have a significant contribution on the surface roughness. The effects of the factors are almost equal on the response parameter. To understand the effect of each factor on the surface roughness as a response, Table 5.8 has an additional column in which the calculated mean surface roughness for each experiment is recorded. Table 5.11 has the results of ANOVA for three factors against the surface roughness.

The tabulated value of F(0.05, 2, 2) = 19. When the calculated value of F for CuSO<sub>4</sub> concentration (30.29) is compared with the tabulated value of F, it is observed that

the CuSO<sub>4</sub> concentration parameter have a significant effect on the surface roughness of copper whereas the calculated value of F for time (5.280) and voltage (5.917) is less than the tabulated value of F so its effect is insignificant on the surface roughness. Using the p-value, we can also analyze the significance of the parameters. As p-values for CuSO<sub>4</sub> concentration is less than 0.05 so these parameters are more significant whereas the p-value of voltage and time is more than 0.05 so these parameters are insignificant.

Table 5.11 ANOVA Table of Mean Data for Copper Electroplating Surface Roughness

Source	DF	Sum of squares ( $SS^2$ )	Adj MS	F	P	% Contribution	Significant
Voltage (V)	2	0.510	0.255	5.280	0.180	12.43%	No
Concentration(g/l)	2	2.929	1.465	30.294	0.031	71.30%	Yes
Time (minutes)	2	0.572	0.286	5.917	0.161	13.92%	No
Error	2	0.097	0.048			2.35%	
Total	8	4.108	2.054				
$S = 0.2199$				$R^2 = 97.65\%$			
Tabular value of $F = F(2,2,0.05) = 19$							
Degrees of freedom- DF, Adjusted Mean squares measure – Adj MS, Determines significance of a factor at 95% confidence level $P < 0.05$							

It can be seen that residual plots for S/N ratio (Figure 5.9) and means (Figure 5.8) are not deviating far from the predicted normal distribution line and follows symmetry in the histograms about the zero value. These observations imply that the residuals follow a normal distribution. As they are randomly distributed around zero in residuals vs the fitted values, residuals have constant variance. There is no inaccuracy related to time or the order of data collection because residuals don't show any discernible patterns. Which implies that there is less variation in the experimental work with the input parameters which are voltage, CuSO<sub>4</sub> concentration and time.

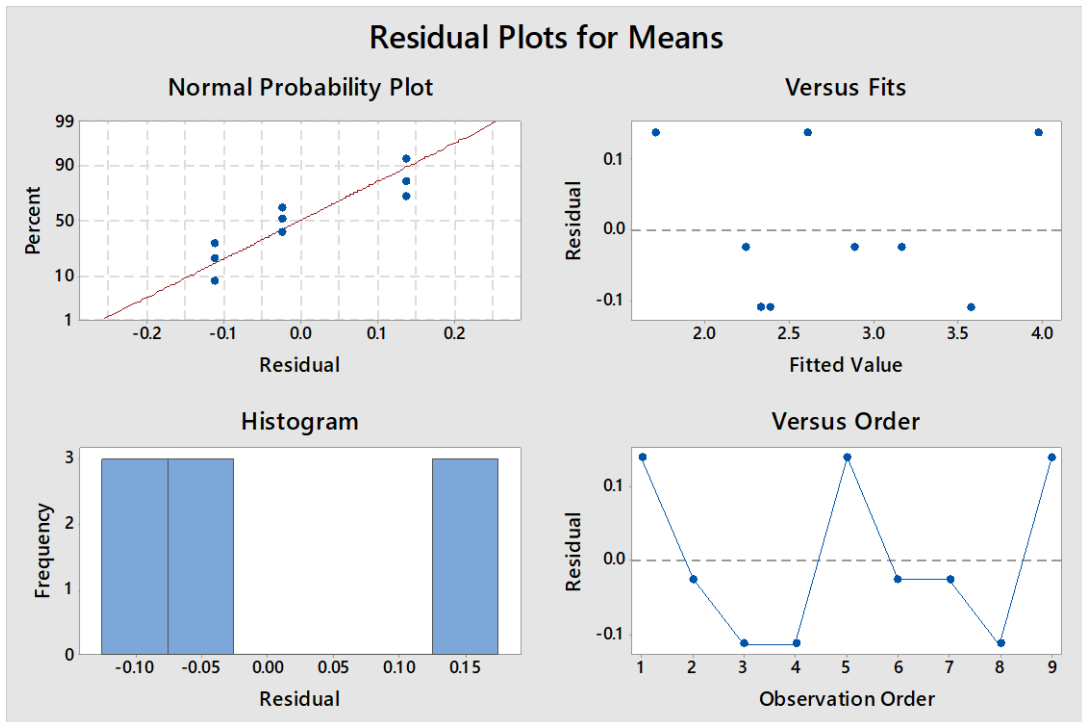


Figure 5.8 Residual Plots for Means Surface Roughness

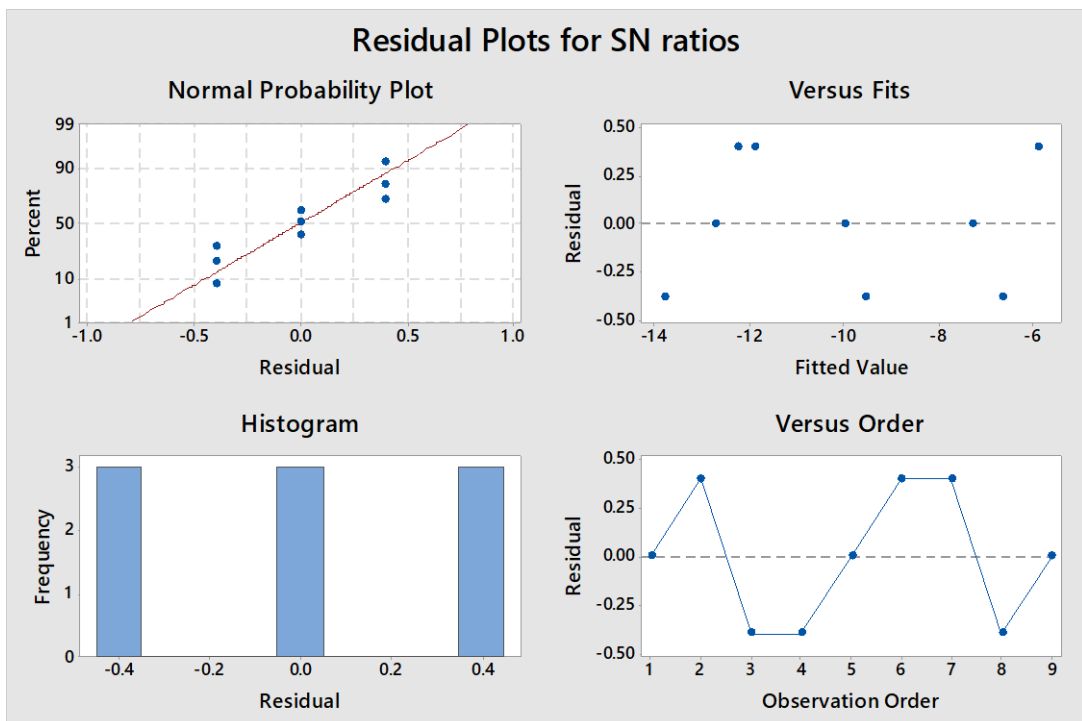


Figure 5.9 Residual Plots for S/N Surface Roughness

## **5.2 OPTIMIZATION OF COPPER COLD SPRAY COATING PROCESS**

### **PARAMETERS**

The impact of various process parameters on the chosen response characteristics has been addressed in this chapter. The recommended standard procedure by Taguchi is used. From experimental data, the mean or average values and the interaction plot of the response characteristics for each parameter at various levels have been determined. To determine the contribution of each factor in each response and to assess the model's significance, an ANOVA was performed on the experimental data. Response curve analysis has been used to determine the most advantageous conditions (optimal settings) for the process parameters in terms of the mean response of the characteristic.

The main effects show the broad patterns of each parameter's influence. The statistical method most frequently used to analyse experimental results and determine the percentage contribution of each parameter to a certain degree of confidence is the analysis of variance (ANOVA). Analyzing the ANOVA table for a particular investigation enables one to decide which parameters require control. Results are divided into three sections on the basis of the three measured output responses.

1. Surface roughness
2. Hardness

### **5.2.1 EXPERIMENTAL STUDY OF COLD SPRAYED COPPER COATED SURFACE ROUGHNESS**

S/N ratios for surface roughness have been calculated using the Taguchi approach, which advocates "smaller-the-better." The experimental data was gathered to determine the input control parameters that produced the best response, the proportion of each factor's contribution using an ANNOVA table for S/N ratios, and to calculate the best theoretical response characteristics for the determined optimal parameters. A comparison between of experimental results and the theoretical estimated was also drawn and debated. The surface roughness of cold spray coated components are measured using Talysurf with least count of 0.01 $\mu$ m. Table 5.12 lists the observed values for changes in the control parameters, such as temperature, gas pressure, and standoff distance, according to the Taguchi L9 tests. Table 5.12 also includes the

computed mean surface roughness values and corresponding S/N ratios based on these observed values.

Based on these findings, Table 5.13 provides the average values of surface roughness and the accompanying S/N ratios for the three levels of temperature, gas pressure, and standoff distance. The factor impacts of the input factors on the surface roughness are represented by these mean values.

Table 5.12 Cold Spray Surface Roughness Observation and Calculated S/N Ratios

Trail No.	Gas Temp. (°C)	Pressure (MPa)	Standoff Distance (mm)	Surface Roughness (µm)			Mean Surface Roughness (µm)	S/N Ratio (dB)
				S1	S2	S3		
1	300	1	15	3.35	3.22	3.25	3.27	-10.301
2	300	2	20	3.87	3.98	3.94	3.93	-11.888
3	300	3	25	6.14	6.18	6.04	6.12	-15.735
4	350	1	20	3.91	4.02	3.86	3.93	-11.889
5	350	2	25	4.89	4.83	4.88	4.87	-13.745
6	350	3	15	5.52	5.62	5.55	5.56	-14.907
7	400	1	25	5.01	5.14	5.04	5.06	-14.089
8	400	2	15	4.08	3.98	4.06	4.04	-12.128
9	400	3	20	7.24	7.3	7.26	7.27	-17.227

Table 5.13 Mean Values by Factor Level for Cold Surface Surface Roughness

Factors	Gas Temp. (°C)		CuSO4 Conc. (g/l)		Standoff Distance(mm)	
	Raw Data	S/N Data	Raw Data	S/N Data	Raw Data	S/N Data
L1	4.44	-12.64	4.09	-12.62	4.29	-12.45
L2	4.78	-13.51	4.28	-12.59	5.04	-13.67
L3	5.46	-14.48	6.32	-14.52	5.35	-14.52

Figure 5.10 (a), (b), and (c) demonstrate the mean effects plot of these parameters.

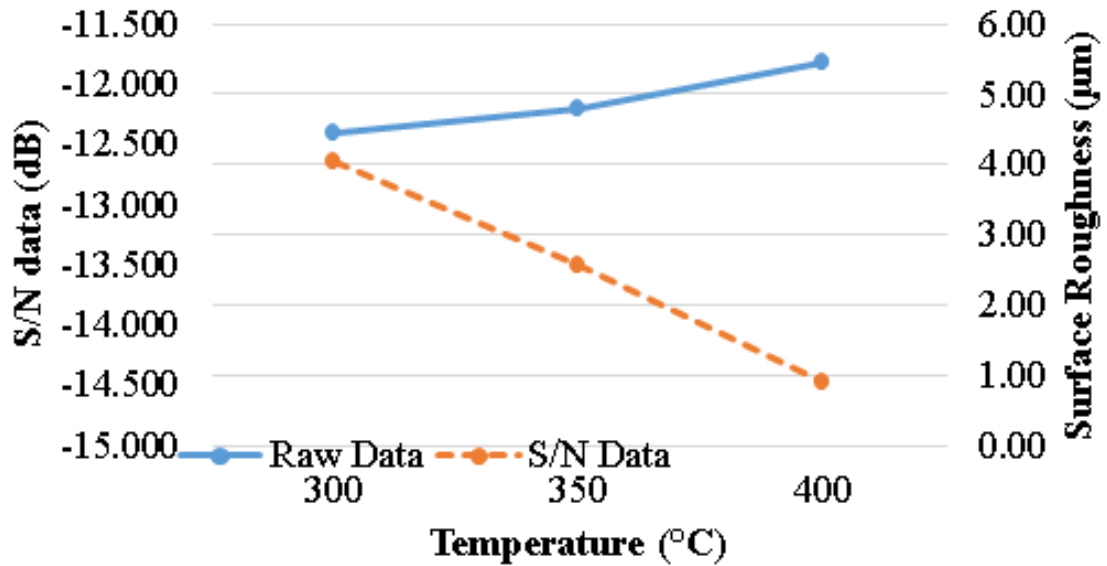


Figure 5.10 (a) Effect of Temperature on Surface Roughness and its S/N Ratio

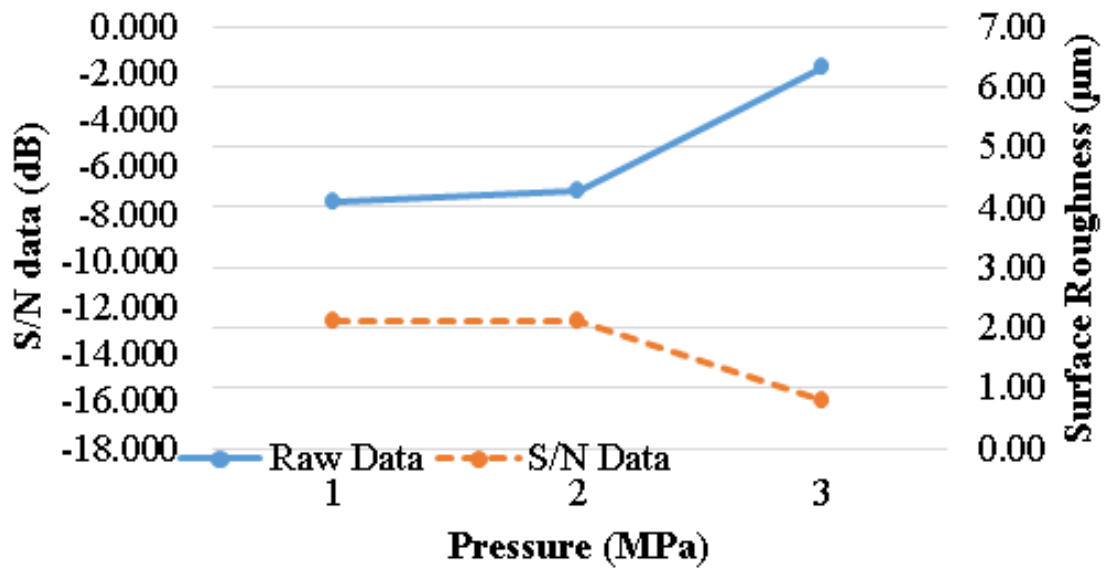


Figure 5.10 (b) Effect of Gas Pressure on Surface Roughness and its S/N Ratio

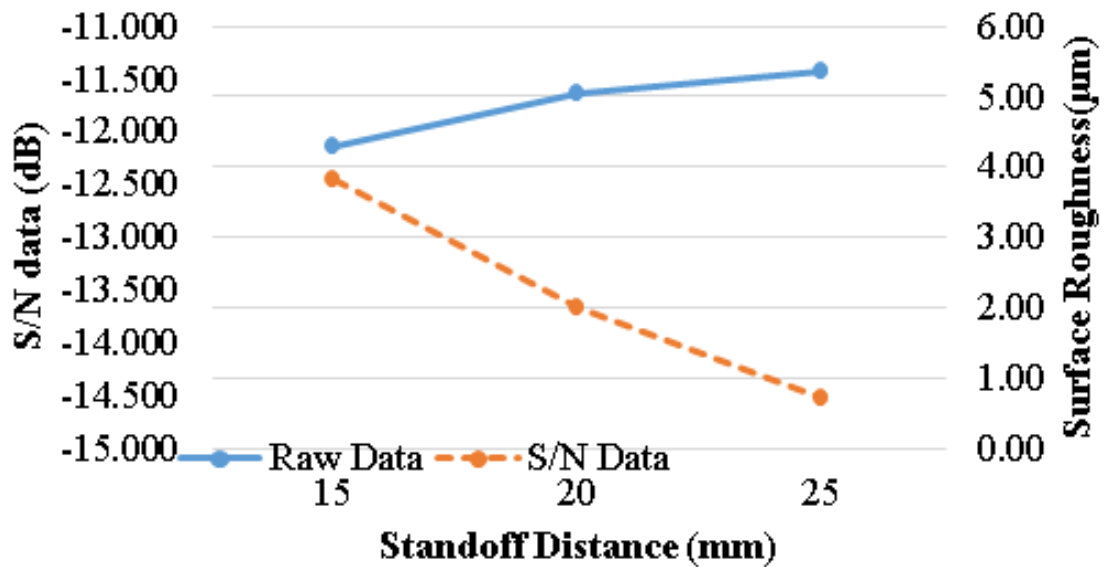


Figure 5.10 (c) Effect of Standoff Distance on Surface Roughness and its S/N Ratio

Surface roughness is the ‘smaller-the-better’ type of response characteristic. Low surface roughness ratings are therefore regarded as ideal. The surface roughness showed a difference from 3.27 µm to 7.27 µm. From the main effects plot of voltage in Figure 5.10 (a), it is interpreted that the surface roughness increases with the increase in temperature continuously. The gas pressure also affects the surface roughness

considerably as shown in Figure 5.10 (b). The surface roughness first remains low and constant for 1 MPa and 2 MPa, but the change is rapid as the pressure changes from 2 MPa to 3 MPa. The standoff distance factor played a significant impact in surface roughness, and Figure 5.10(c) illustrates that the surface roughness is lowest at a standoff distance of 15 mm. The increase in the standoff distance also brings in the non-uniformity in the growth of the coating due to the geometrical shapes, and visual lumps start forming at the edges of the component leading to poor surface finish. Hence there is a continuous decrease in the surface finish with the increase in the standoff distance.

From Figure 5.10 (a), (b), and (c) it can be interpreted that all the three process parameters (temperature, gas pressure and standoff distance) have a direct impact on the surface roughness. Therefore, lower values for surface roughness on Copper cold sprayed component can be observed from Figure 5.10 (a), (b), and (c). The first level of temperature (A1), the first level of pressure (B1), and the first level of standoff distance (C1) are discovered to be these parameters. In order to achieve the lowest surface roughness, A1B1C1 is the ideal set of input values. A confirmation experiment is not necessary because this set of experiments is included in the orthogonal array in Table 5.6 as the first experiment. The Taguchi method was used to compare the experimental surface roughness mean value, which is 3.27  $\mu\text{m}$ , with the theoretical value. The mean of different factors and overall mean of surface roughness can be used to predict the roughness at these optimum settings. The means for three factors for thickness and S/N Ratio is given in Table 5.13. The theoretical value of  $\eta_{opt}$  under the optimum conditions is given by equation 5.5.

$$\eta_{opt} = m + (m_{A1} - m) + (m_{B1} - m) + (m_{C1} - m) = -10.51 \text{ dB} \quad (5.5)$$

The corresponding value of surface roughness is given by equation 5.6.

$$y_{opt}^2 = 10^{\frac{-\eta_{opt}}{10}} \quad (5.6)$$

Or,  $y_{opt} = 3.35 \mu\text{m}$ , which is quite close to the experimental value that was reported.



Surface roughness interaction effects have also been presented in Figure 5.11 in order to analyse the impact of each parameter in relation to other factors. Because there are so few parallel lines in the complete interaction plot for the means of surface roughness and S/N ratio, it may be inferred that there is a strong interaction between all the components. It is implied by this that one factor depends on another.

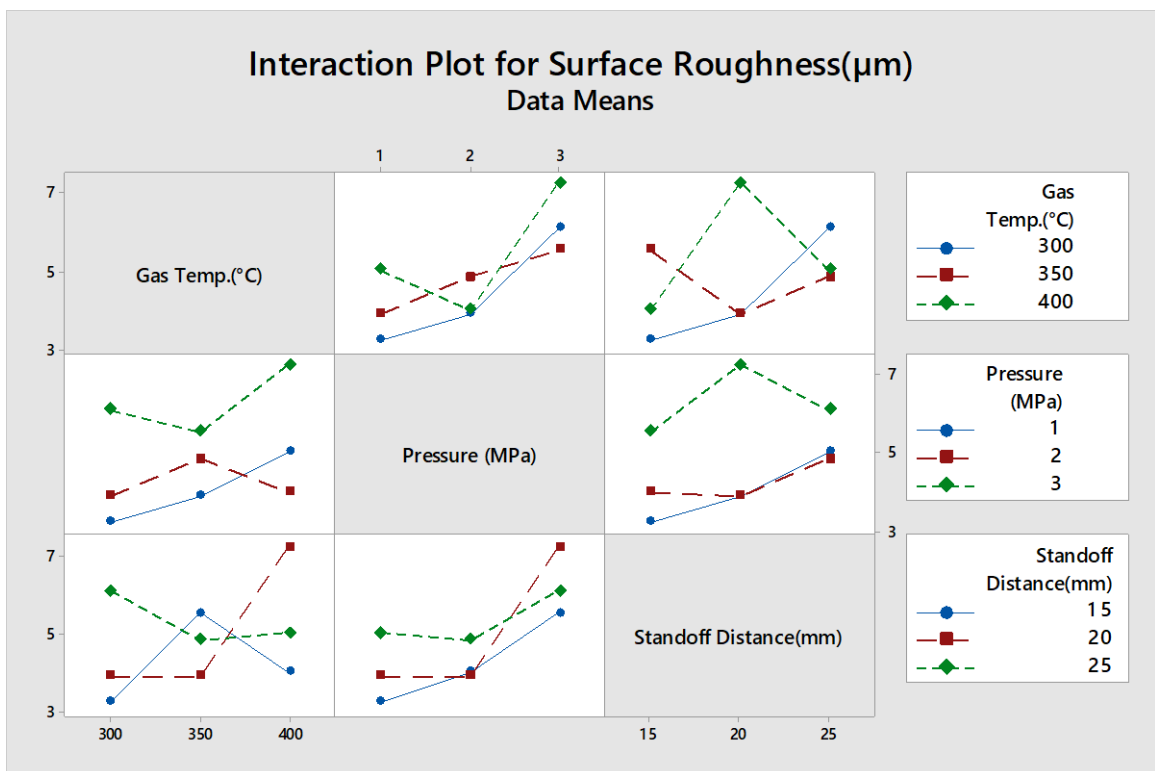


Figure 5.11 Interaction Plot for Means of Surface Roughness

Table 5.14 ANOVA Table of Raw Data for Cold Spray Surface Roughness

Source	DF	Seq SS	Adj MS	F	P	% Contribution	Significant
Gas Temp.(°C)	2	5.799	2.900	19.146	0.050	30.10%	Yes
Pressure(MPa)	2	7.177	3.588	23.694	0.040	37.25%	Yes
Standoff Distance(mm)	2	5.985	2.993	19.760	0.048	31.07%	Yes
Residual Error	2	0.303	0.151			1.57%	
Total	8	19.264	9.632				
S = 0.38858						R-Sq = 98.42%	
Tabular value of F = F(2,2,0.05) =19							
Degrees of freedom- DF, Adjusted Mean squares measure – Adj MS, Determines significance of a factor at 95% confidence level P < 0.05							

The F values are calculated as

$$\text{Sum of square for error} = \text{SSE} = 19.264 - (5.799 + 7.177 + 5.985) = 0.303$$

$$\text{Sum of square of mean for Gas Temperature (°C)} = \text{MSS}_T = \frac{5.799}{2} = 2.9$$

$$\text{Sum of square of mean for Pressure (MPa)} = \text{MSS}_P = \frac{7.177}{2} = 3.588$$

$$\text{Sum of square of mean for Standoff Distance (mm)} = \text{MSS}_D = \frac{5.985}{2} = 2.993$$

$$\text{Sum of square of means for Error} = \frac{0.303}{2} = 0.151$$

$$\text{F\_Value for Gas Temperature (°C)} = F_T = \frac{\text{MSS}_T}{\text{MSE}} = \frac{2.9}{0.151} = 19.146$$

$$\text{F\_Value for Pressure (MPa)} = F_P = \frac{\text{MSS}_P}{\text{MSE}} = \frac{3.588}{0.151} = 23.694$$

$$\text{F\_Value for Standoff Distance (mm)} = F_D = \frac{\text{MSS}_D}{\text{MSE}} = \frac{2.993}{0.151} = 19.760$$

The calculated P\_Values are

$$P\_Value \text{ for Gas Temperature } (^{\circ}\text{C}) = P_T = \frac{F_{\text{Tabulated}}}{F_T} = \frac{19}{19.146} \times 0.05 = 0.050$$

$$P\_Value \text{ for Pressure (MPa)} = P_P = \frac{F_{\text{Tabulated}}}{F_C} = \frac{19}{23.694} \times 0.05 = 0.040$$

$$P\_Value \text{ for Standoff Distance (mm)} = P_D = \frac{F_{\text{Tabulated}}}{F_T} = \frac{19}{19.760} \times 0.05 = 0.048$$

$$S = \sqrt{MSE} = \sqrt{0.151} = 0.38858$$

The coefficient of determination is given as

$$R^2 = 1 - \frac{SSB}{SST} = \left(1 - \frac{0.303}{19.264}\right) \times 100 = 98.42\%$$

It is evident from the Table 5.14 that all the three factors have a significant contribution on the surface roughness. The effects of the factors are almost equal on the response parameter. To understand the effect of each factor on the surface roughness as a response, Table 5.12 has an additional column in which the calculated mean surface roughness for each experiment is recorded. Table 5.915 has the results of ANOVA for three factors against the surface roughness.

The tabulated value of  $F(0.05, 2, 2) = 19$ . When the calculated value of F for temperature is (19.14) and for standoff distance is (19.76), is more than the tabulated value of F, so these parameters are having a significant effect on the surface roughness of cold sprayed copper surface. The calculated value of F for pressure (23.694) is more than the tabulated value of F so its effect is significant on the surface roughness. Using the p-value, we can also analyze the significance of the parameters. As p-values for all parameters are less than 0.05 so these parameters are significant.

Table 5.15 ANOVA Table S/N Data for Cold Spray Surface Roughness

Source	DF	Seq SS	Adj MS	F	P	% Contribution	Significant
Gas Temp.(°C)	2	19.381	9.690	19.323	0.049	31.84%	Yes
Pressure (MPa)	2	21.585	10.793	21.521	0.044	35.46%	Yes
Standoff Distance(mm)	2	18.909	9.455	18.853	0.050	31.06%	Yes
Residual Error	2	1.003	0.501			1.65%	
Total	8	60.878	30.439				
S = 0.38858				R-Sq = 98.35%			
Tabular value of F = F(2,2,0.05) =19							
Degrees of freedom- DF, Adjusted Mean squares measure – Adj MS, Determines significance of a factor at 95% confidence level P < 0.05							

It can be seen that residual plots for S/N ratio (Figure 5.12) and means (Figure 5.13) are not deviating far from the predicted normal distribution line and follows symmetry in the histograms about the zero value. These facts suggest a normal distribution for the residuals. Since residuals are randomly distributed around zero when compared to the fitted values, residuals have constant variance. There is no time or data collection order error because the residuals don't show any discernible patterns. Which implies that there is less variation in the experimental work with the input parameters which are gas temperature, pressure and standoff distance.

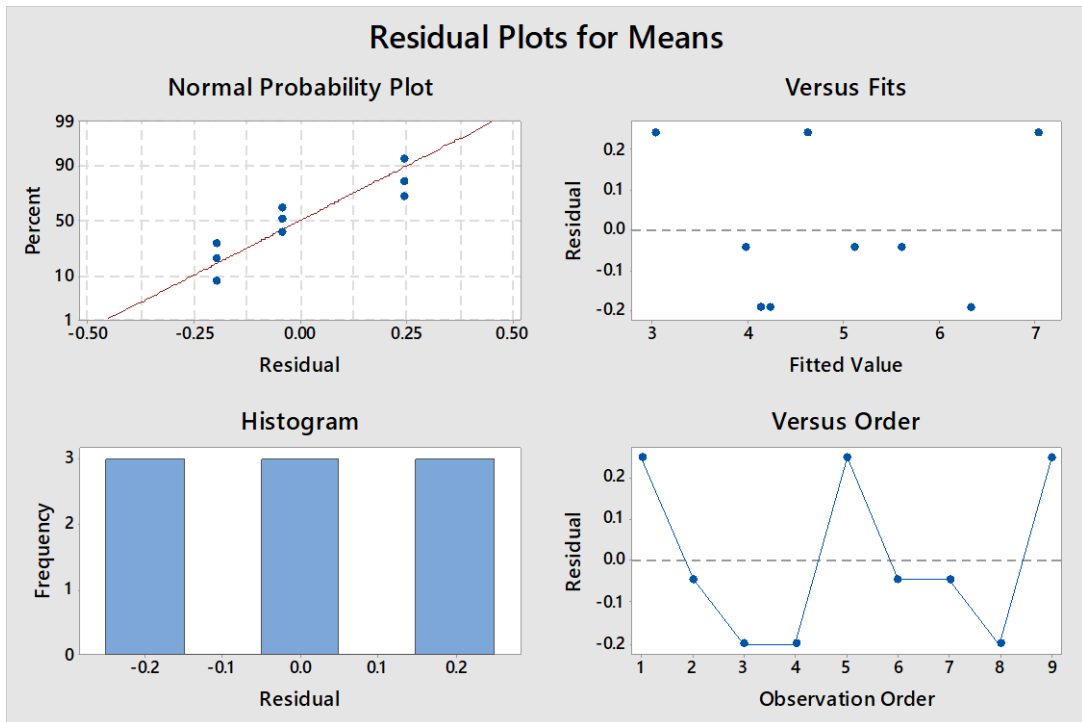


Figure 5.12 Residual Plots for Means Surface Roughness

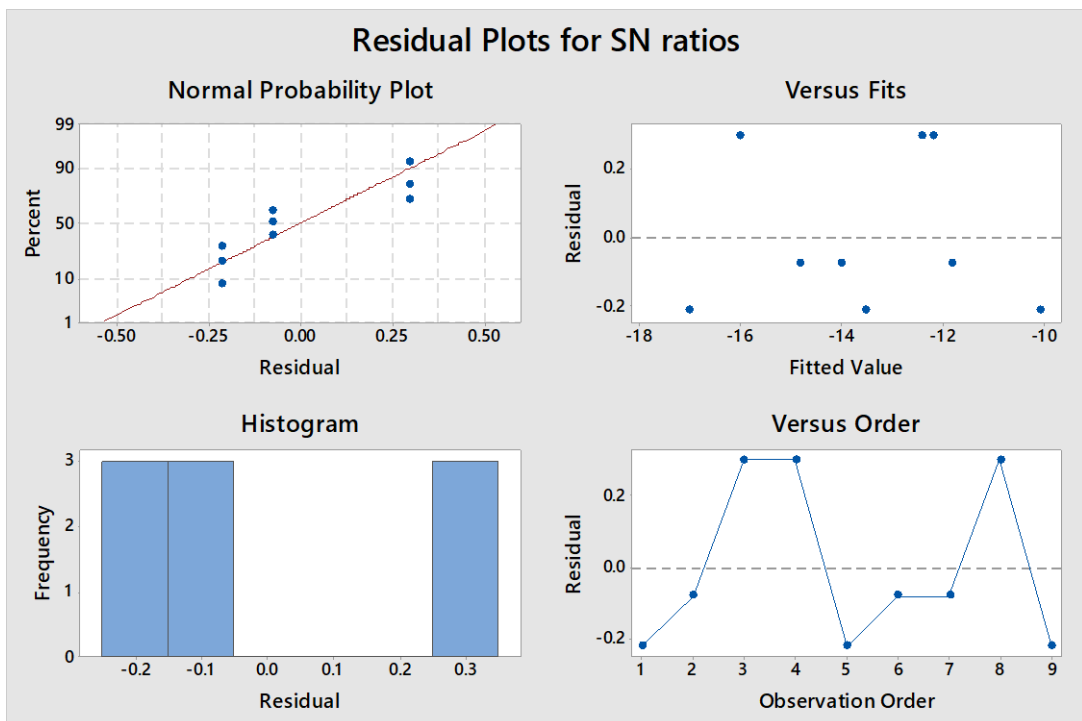


Figure 5.13 Residual Plots for S/N Surface Roughness

### **5.2.2 EXPERIMENTAL STUDY OF COLD SPRAYED COPPER SURFACE HARDNESS**

The Taguchi method's "larger-the-better" criterion for the hardness of the cold sprayed copper layer has been applied for determining S/N ratios. The experimental data was gathered to determine the input control parameters that produced the best response, the proportion of each factor's contribution using an ANOVA table for S/N ratios, and to calculate the best theoretical response characteristics for the determined optimum parameters.

The confirmation of the optimized parameters was achieved through the set of experiments performed on various components cold sprayed copper component. A comparison between the experimental results and the theoretical estimated was also drawn and discussed. The observed values with S/N Ratio as per the orthogonal array for deposition rate are given in Table 5.16.

Table 5.17 shows the computed mean coating hardness values for the three levels of gas temperature, pressure, and standoff distance together with the related S/N ratios. The factor impacts of the input factors are represented by these mean values.

Table 5.16 Hardness Observation and Calculated S/N ratios

Trail No.	Gas Temp. (°C)	Pressure (MPa)	Standoff Distance (mm)	Hardness ( $\mu\text{m}$ )			Mean Hardness (HV)	S/N Ratio
				S1	S2	S3		
1	300	1	15	78	84	81	81	38.17
2	300	2	20	98	94	93	95	39.55
3	300	3	25	112	118	121	117	41.36
4	350	1	20	98	106	108	104	40.34
5	350	2	25	132	130	128	130	42.28
6	350	3	15	92	92	98	94	39.46
7	400	1	25	132	137	136	135	42.61
8	400	2	15	110	102	103	105	40.42
9	400	3	20	112	106	118	112	40.98

Table 5.17 Mean Values by Factor Level for Hardness

Factors	Gas Temp. (°C)		Pressure (MPa)		Standoff Distance(mm)	
	Raw Data	S/N Data	Raw Data	S/N Data	Raw Data	S/N Data
L1	97.67	39.70	106.67	40.37	93.33	40.37
L2	109.33	40.69	110.00	40.75	103.67	40.29
L3	117.33	41.34	107.67	40.60	127.33	42.083

The mean effects of these factors have been plotted and presented in Figure 5.14 (a), (b) and(c)

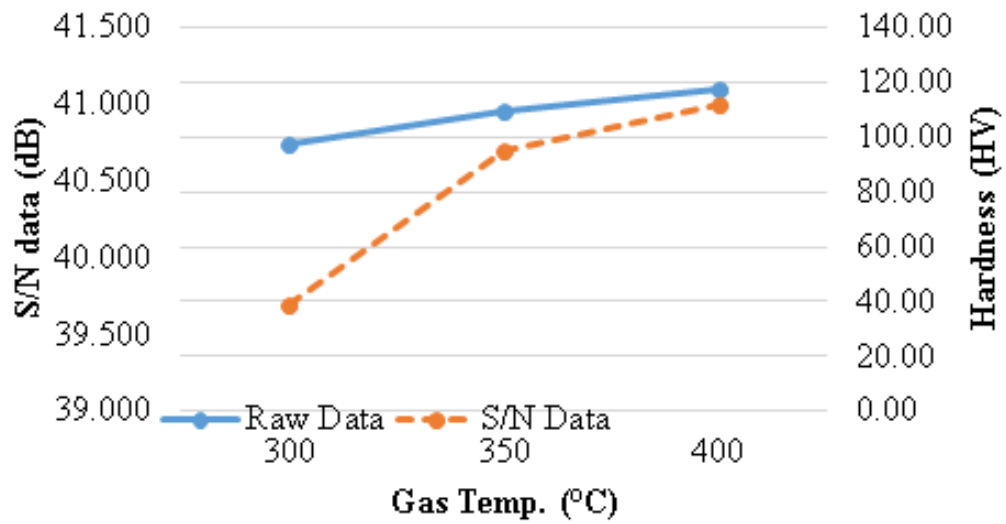


Figure 5.14 (a) Effect of Gas Temperature on Hardness and its S/N Ratio

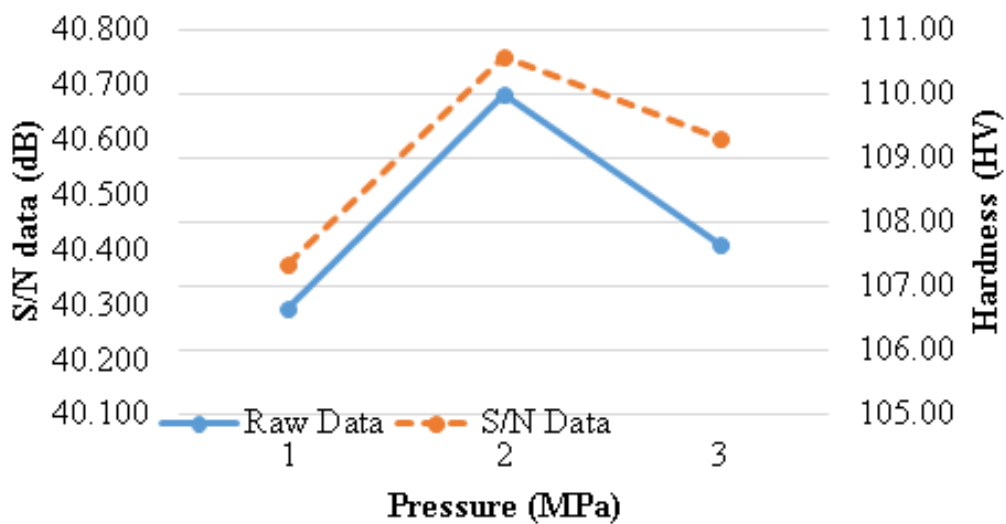


Figure 5.14 (b) Effect of Gas Pressure on Hardness and its S/N Ratio



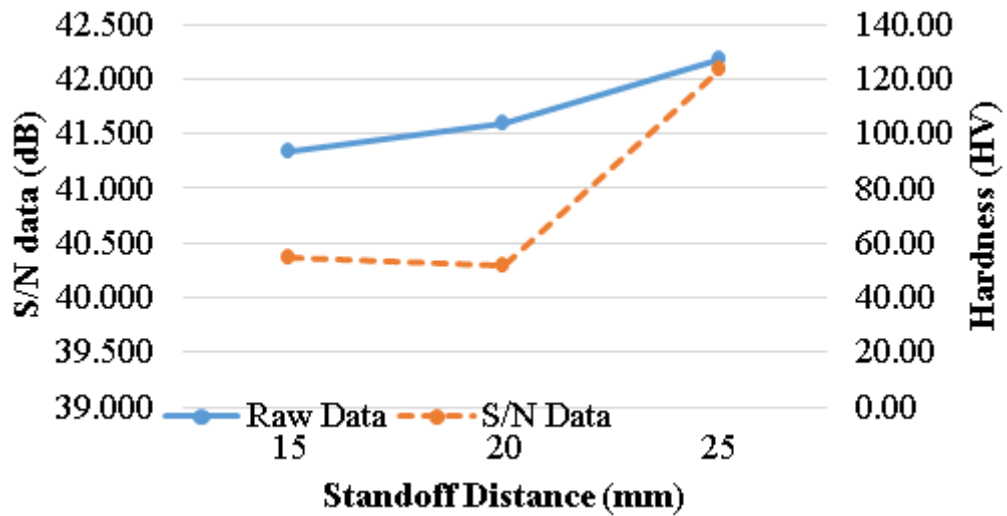


Figure 5.14 (c) Effect of Standoff Distance on Hardness and its S/N Ratio

The 'larger-the-better' sort of response characteristic describes metal hardness. Consequently, a high hardness value is viewed as ideal. From the main effects plot of gas temperature in Figure 5.14 (a), it is interpreted that the hardness increases as the gas temperature increases from 300°C to 350°C and further to 400°C.

Pressure also played an important role on the hardness as indicated in the Figure 5.14(b). The hardness rate increases initially and the maximum hardness was observed at pressure setting of 2MPa. The hardness decreases consistently as the pressure is increased further from 2MPa to 3Mpa.

Standoff distance plays an important role on the hardness as indicated in the Figure 5.14(c). The hardness rate is maximum at a standoff distance of 25mm. Hardness increases constantly as the standoff distance increases from 15mm to 20mm and beyond this the rate of hardness increase is observed as we move from 20mm to 25mm.

From Figure 5.14 (a), (b), and (c) it can be interpreted that all the three process parameters (temperature, pressure and standoff distance) have a direct impact on the hardness. Therefore, higher values for hardness of cold sprayed copper coated surface can be observed from Figure 5.14 (a), (b), and (c). They are found to be the first level of temperature (A1), second level of pressure (B2), and third level of standoff distance (C3).

Hence, A1B2C3 is the optimum set of input parameters for the best hardness. Since this set of experiments does not exist in the orthogonal array in Table 5.17 so, a confirmatory experiment is required.

Table 5.18 Confirmatory Experiment for Hardness Observation

Trail No.	Gas Temp. (°C)	Pressure (MPa)	Standoff Distance (mm)	Hardness (μm)			Hardness (HV)
				S1	S1	S1	
10	300	2	25	114	120	112	116

The mean value of this experiment for the hardness is 116μm, which is comparable with the theoretical value using Taguchi method. The mean of different factors and overall mean of the deposition rate can be used to predict the thickness at these optimum settings. Table 5.17 provides the means for the three factors and S/N Ratio variables. Equation 5.7 provides the theoretical value of  $\eta_{opt}$  under ideal conditions.

$$\eta_{opt} = m + (m_{A3} - m) + (m_{B2} - m) + (m_{C3} - m) = 41.15 \text{ dB} \quad (5.7)$$

The corresponding value of deposition thickness is given by equation 5.8.

$$y_{opt}^2 = \frac{1}{10^{\frac{-\eta_{opt}}{10}}} \quad (5.8)$$

Or,  $y_{opt} = 114 \text{ HV}$ , which is extremely near to the 116HV measured experimental measurement.

As evident from the micro-hardness profile, the coatings exhibited a micro hardness value in the range of 81 – 135 Hv. The measured values of micro hardness are in good agreement with the findings of Borchers et al., (2003) and McCune et al., (2000). However, the hardness value is higher for the coatings sprayed at larger stand-off distance and found to increase with increase in stand-off distance which is found to be in agreement with Gartner et al., (2006) and Li et al., (2008).

Means of hardness (Figure 5.15) interaction effects have also been plotted in order to analyse the impact of each parameter with respect to other parameters. As there are no parallel lines in the entire interaction plot for hardness it may be inferred that there is

a significant interaction between all the parameters. It is implied by this that one factor depends on another.

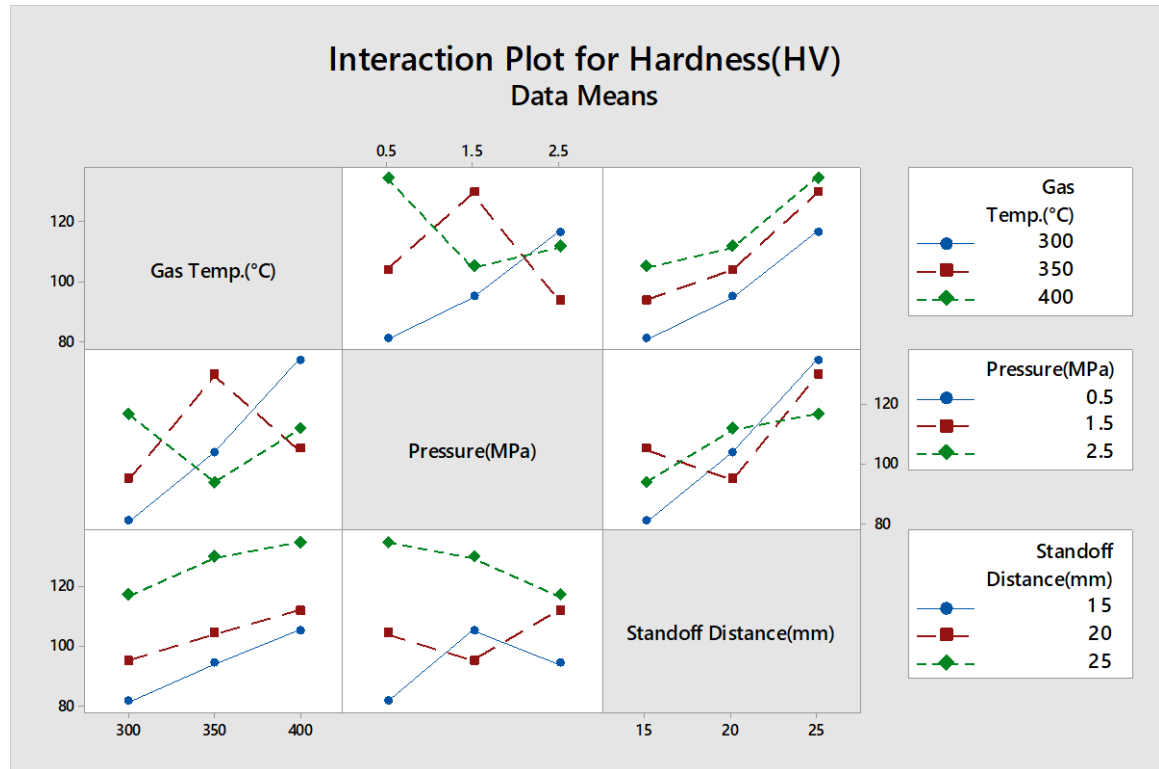


Figure 5.15 Interaction Plot for Means of Hardness

Table 5.19 ANOVA Table for Mean Data for Hardness

Source	DF	Sum of squares ( $SS^2$ )	Adj MS	F	P	%Contribution	Significant
Gas Temp.(°C)	2	586.89	293.445	376.21	0.003	24.16%	Yes
Pressure(MPa)	2	17.56	8.78	11.26	0.084	0.72%	No
Standoff Distance(mm)	2	1822.89	911.445	1168.52	0.001	75.05%	Yes
Error	2	1.56	0.78			0.06%	
Total	8	2428.89					
$S = 0.8819$				$R^2 = 99.94\%$			
Tabular value of $F = F(2,2,0.05) = 19$							
Degrees of freedom- DF, Adjusted Mean squares measure – Adj MS, Determines significance of a factor at 95% confidence level $P < 0.05$							

To determine the percentage contribution of the three components and their significance, analysis of variance (ANOVA) of the S/N data was carried out at the

95% confidence level. Table 5.19 illustrates how standoff distance, gas temperature, and pressure affect the hardness for mean data.

The  $F$ \_values are calculated as

$$\text{Sum of square for error} = \text{SSE} = 2428.89 - (586.89 + 17.56 + 1822.89) = 1.56$$

$$\text{Sum of square of mean for Gas Temperature (}^\circ\text{C)} = \text{MSS}_T = \frac{586.89}{2} = 293.445$$

$$\text{Sum of square of mean for Pressure (MPa)} = \text{MSS}_P = \frac{17.56}{2} = 8.78$$

$$\text{Sum of square of mean for Standoff Distance (mm)} = \text{MSS}_D = \frac{1822.89}{2} = 911.445$$

$$\text{Sum of square of means for Error} = \frac{1.56}{2} = 0.78$$

$$\text{F\_Value for Gas Temperature (}^\circ\text{C)} = F_T = \frac{\text{MSS}_V}{\text{MSE}} = \frac{376.21}{0.78} = 376.21$$

$$\text{F\_Value for Pressure (MPa)} = F_P = \frac{\text{MSS}_C}{\text{MSE}} = \frac{8.78}{0.78} = 11.26$$

$$\text{F\_Value for Standoff Distance (mm)} = F_D = \frac{\text{MSS}_T}{\text{MSE}} = \frac{911.445}{0.78} = 1168.52$$

The calculated  $P$ \_Values are

$$\text{P\_Value for Gas Temperature (}^\circ\text{C)} = P_T = \frac{F_{\text{Tabulated}}}{F_V} = \frac{19}{376.21} \times 0.05 = 0.003$$

$$\text{P\_Value for Pressure (MPa)} = P_P = \frac{F_{\text{Tabulated}}}{F_C} = \frac{19}{11.26} \times 0.05 = 0.084$$

$$\text{P\_Value for Standoff Distance (mm)} = P_D = \frac{F_{\text{Tabulated}}}{F_V} = \frac{19}{1168.52} \times 0.05 = 0.001$$

$$S = \sqrt{MSE} = \sqrt{0.78} = 0.8819$$

The coefficient of determination is given as

$$R^2 = 1 - \frac{SSE}{SST} = \left(1 - \frac{1.56}{2428.89}\right) \times 100 = 99.94\%$$

The tabulated value of  $F_{(0.05, 2, 2)} = 19$ . When the calculated value of F for gas temperature (376.21) and standoff distance (1168.52) is compared with the tabulated value of F, it is observed that these two parameters have a significant effect on the hardness of copper whereas the calculated value of F for pressure (11.26) is less than the tabulated value of F so its effect is insignificant on the hardness of copper deposition. From the % contribution from Table 5.20 we can conclude the standoff distance contribution on hardness is maximum. Using the p-value, we can also analyze the significance of the parameters. As p-values for gas temperature and standoff distance is less than 0.05 so these parameters are more significant whereas the p-value of pressure is more than 0.05 so this parameter is insignificant.

It is evident from the Table 5.19 that the two factors have a significant contribution on the deposition thickness. The effects of voltage and concentration factors are almost equal on the response parameter and time factor is insignificant. To understand the effect of each factor on the deposition rate per minute as a response, Table 5.16 has an additional column in which the calculated mean deposition rate for each experiment is recorded. Table 5.20 has the results of ANOVA for S/N data for three factors against the surface hardness.

Residual plots aid in evaluating data for variances caused by control settings. The residual plots for means in (Figure 5.16) and S/N ratio (Figure 5.17) show that they do not deviate much from the projected normal distribution line and follow symmetry in the histograms around the zero value. Residual plots assist in analysing data for variances caused by control settings. Residuals have constant variance because they are randomly distributed around zero in residuals against fitted values. Because residuals show no discernible pattern, there is no inaccuracy owing to time or data collecting order. This suggests that the experimental work using the input parameters

of gas temperature and pressure has less fluctuation

Table 5.20 ANOVA Table of S/N Data for Hardness

Source	DF	Sum of squares ( $SS^2$ )	Adj MS	F	P	% Contribution	Significant
Gas Temp.(°C)	2	586.89	293.445	376.21	0.003	24.16%	Yes
Pressure(MPa)	2	17.56	8.78	11.26	0.084	0.72%	No
Standoff Distance(mm)	2	1822.89	911.445	1168.52	0.001	75.05%	Yes
Error	2	1.56	0.78			0.06%	
		2428.89					
Total	8	586.89	7.98138				
S = 0.2074				$R^2 = 99.46\%$			
Tabular value of F = F(2,2,0.05) = 19							
Degrees of freedom- DF, Adjusted Mean squares measure – Adj MS, Determines significance of a factor at 95% confidence level P < 0.05							

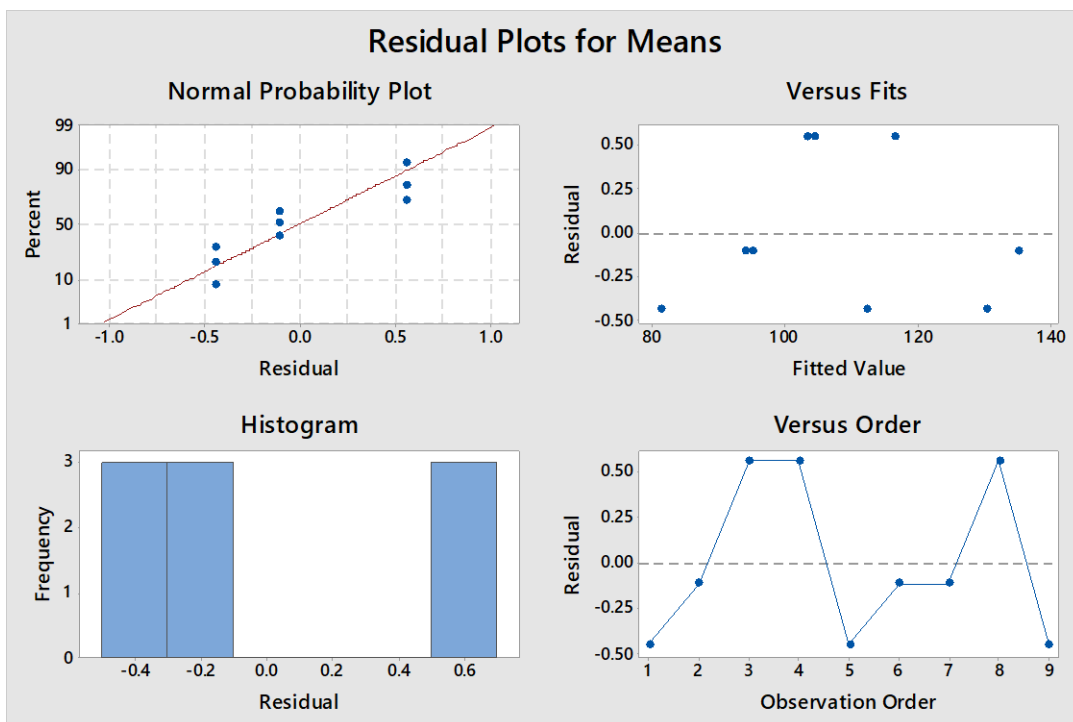


Figure 5.16 Residual Plots for Means of Hardness

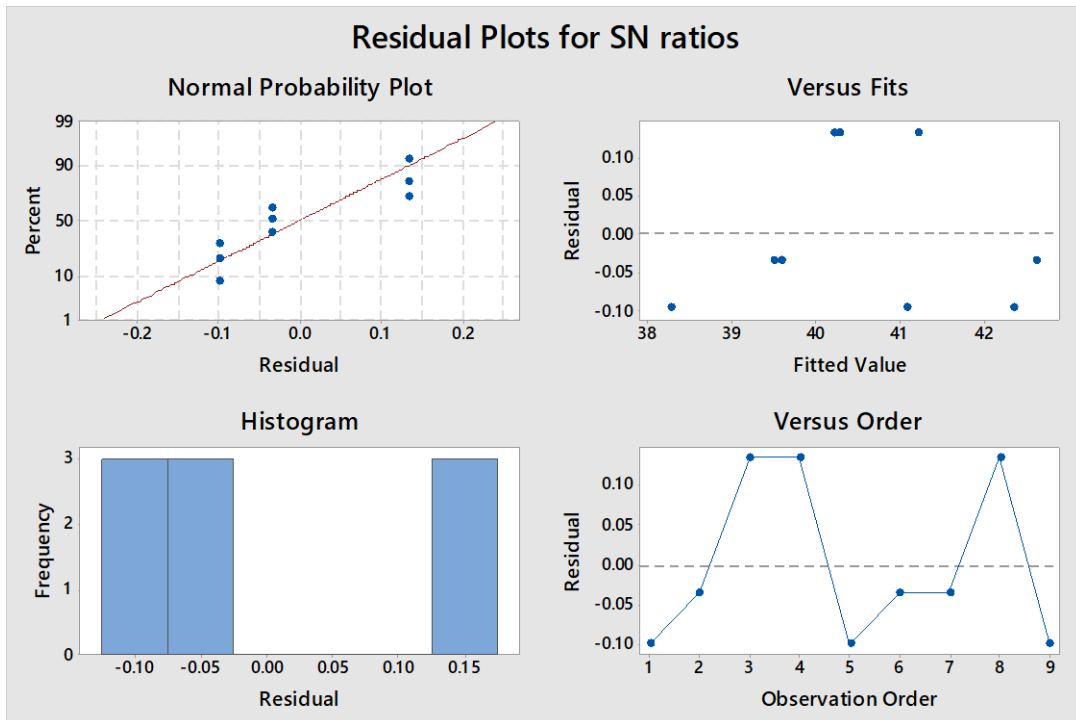


Figure 5.17 Residual Plots for S/N Data of Hardness

## **CHAPTER-6 ANALYSIS AND DISCUSSION OF THE RESULTS**

---

One experiment was conducted to establish the optimum parameters for copper electroplating using L9 orthogonal array of Taguchi design experiments then second set of experiment was conducted to find the minimum thickness of Cu coating that can retain its original shape under selected process parameters of cold spray coating. The Third set of experiment was conducted to find the optimum process parameter for cold spray coating on metal coated 3D parts and elaborated in chapter 5. All the Fuse Deposition Model (FDM) parts were subjected to deposition thickness and surface roughness measurements. For each experiment, the data were analyzed to determine the ideal levels for each of the three input process parameters, as well as their relative importance. Confirmation experiments were carried out to determine the best experimental results, and they were compared with the theoretical values predicted by Taguchi analysis, wherever the desired combination of components in the orthogonal array of the trials did not exist. Chapter 5 also includes the discussion on the process cold spray coating using the optimized process parameters. Further analysis of the electroplated components after confirmation experiments was done to find out surface composition and microstructure and it has been presented in this chapter. Surface composition was determined with the help of X-ray diffraction (XRD) analysis. Microstructural studies were carried out on a Scanning Electron Microscope (SEM).

### **6.1 SURFACE MORPHOLOGY STUDIES USING SEM**

The SEM images of the various samples of FDM, copper deposition electroform were taken using the facilities available at Lovely Professional University. The following sections will discuss the findings related to surface morphology of various test samples. The aim of the study is to know the surface enhancement due to the smoothening process and the pattern of growth of the metal deposition as it progress. The effect of the progress in the growth of their impact on the grain sizes is also discussed.



### 6.1.1 SURFACE ENHANCEMENT OF THE FDM PART

The component produced using any additive manufacturing process has the staircase step marks as a result of the method of producing parts layer by layer. The SEM image shown in Figure 6.1 clearly display the layers of the FDM component, resulting to poor surface finish.

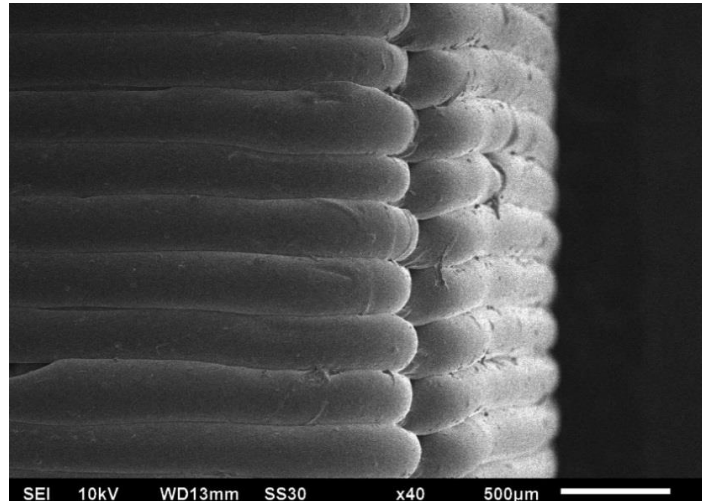


Figure 6.1 SEM Image of FDM Part as Fabricated

The post processing opted in this research work for the improvement of the surface treatment was cold vapour smoothening using acetone. Figure 6.2 shows the SEM image of the FDM part after treatment, the staircase marks, which are prominent in the Figure 6.1 are clearly improved to provide a smooth clean surface.

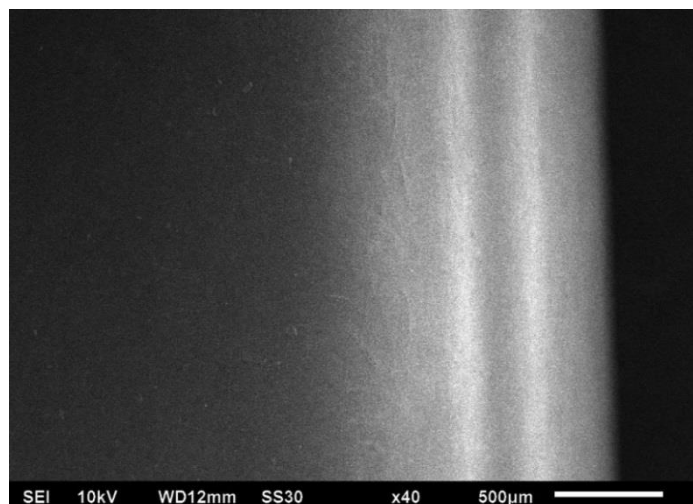


Figure 6.2 SEM Image of FDM Part after Treatment

This enhancement was brought about by the material's reflow, which forms thin ABS layers on the surface of created patterns, reducing the roughness of the surface. As a result of this treatment there was no significant dimensional distortion in the component. The improvement in the surface finish was quite evident, measured as 5.63  $\mu\text{m}$  before treatment and 0.25  $\mu\text{m}$  after treatment.

### 6.1.2 Surface Morphology of Copper Deposition Using Electroplating

The microstructure of the copper that was deposited was captured in a SEM photograph. In order to analyze the structural nature of the copper deposition on the substrate. Figure 6.3 (a) and (b) show that as the thickness of the deposited layer grows, the grain size of the deposited copper shifts from coarse to fine. As the substrate was made of ABS plastic, which has a lesser thermal conductivity causes the coarse grain size. Fine grain size was achieved with increase in the thickness which was due to more heat conduction in the deposited metal. Furthermore, with finer grain sizes compared to coarse grain sizes, the voids in the grains decrease the surface integrity. From the results it can be concluded that electrolytic bath is necessary to dissipate the heat generated uniformly and to improve grain size and strength of the electroformed component.

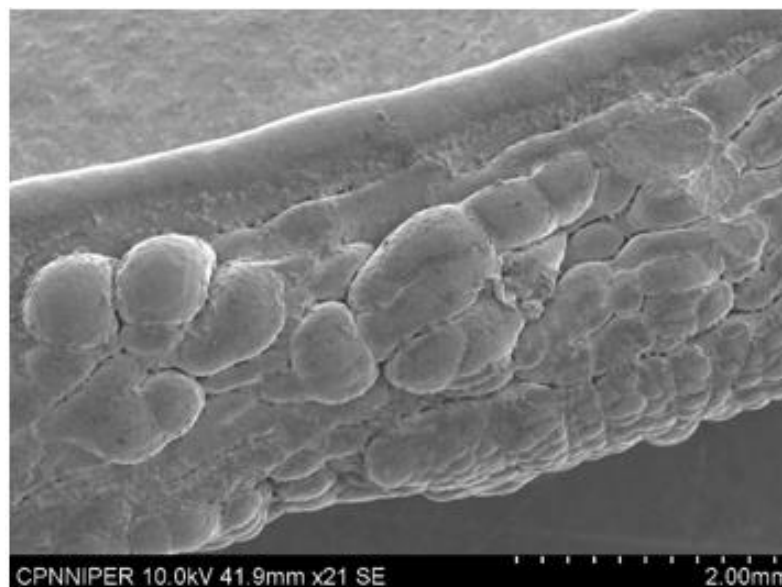


Figure 6.3 (a) SEM Image of Sample at 2.0 mm

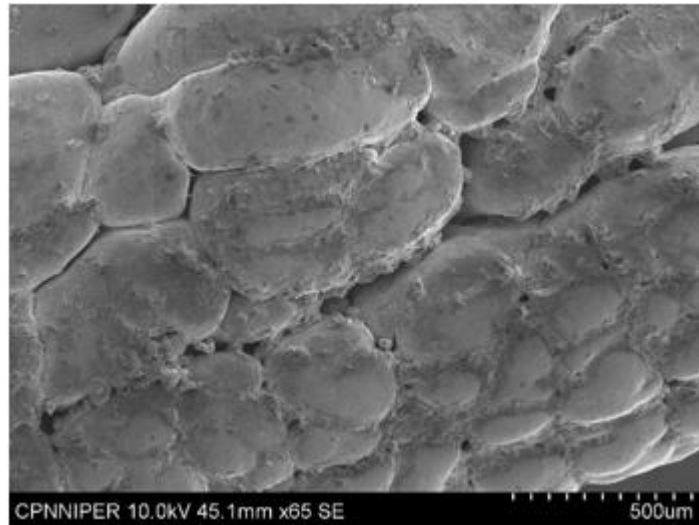


Figure 6.3 (b) SEM Image of Sample at 500  $\mu\text{m}$

Figure 6.4 and 6.5 shows the SEM and EDS image of the inside area of the coated sample. It can be observed from the Table 6.1 that, inside the specimen the weight percentage of the copper present is 16.93 percent and the percentage of the carbon present in the inside portion is high i.e. 63.14 percentage

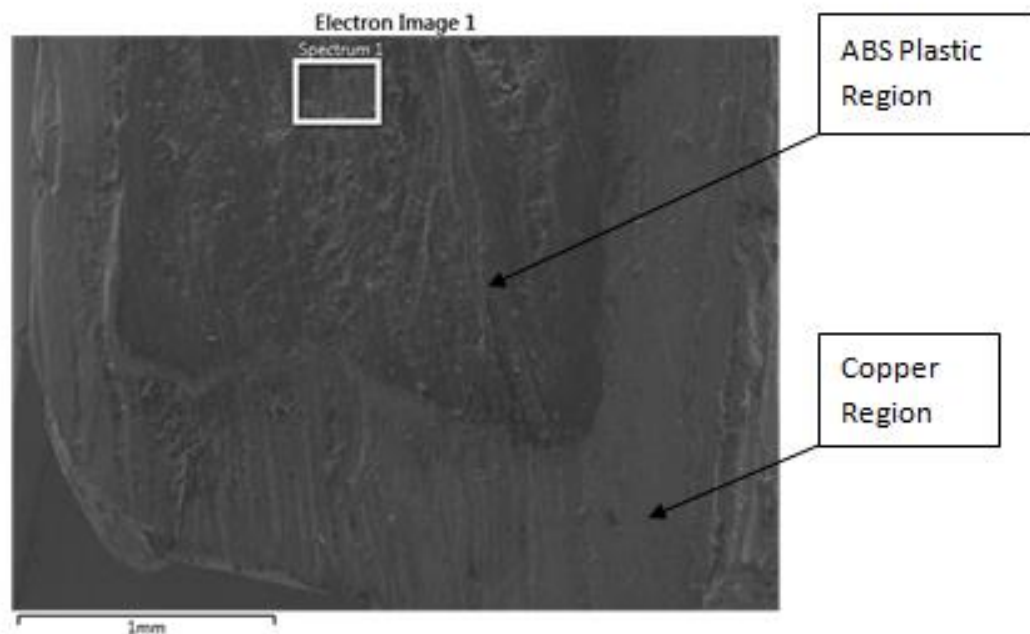


Figure 6.4 SEM Image of Specimen of Inside Area

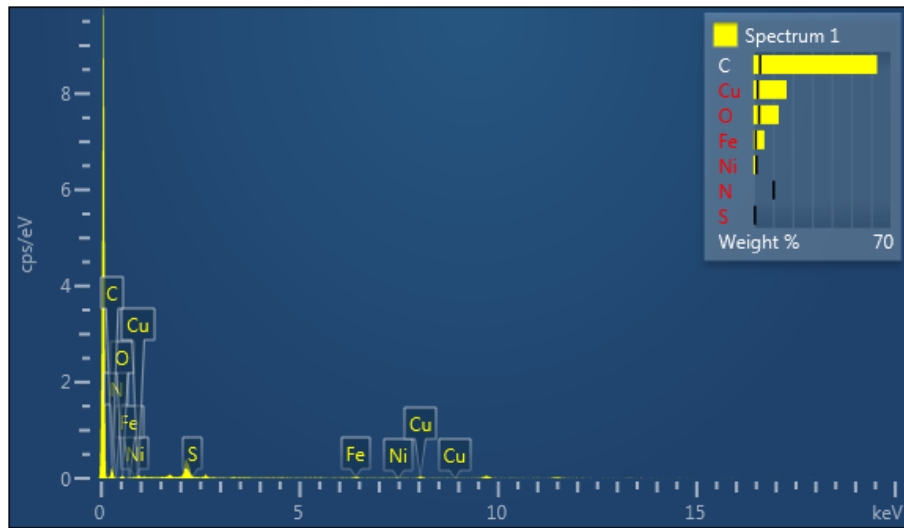


Figure 6.5 EDS Image of the Specimen of Inside Area

Table 6.1 Weight Percentage Distribution of the Element of Inside Area

Spectrum 1	Wt%
C	63.14
N	0.00
O	12.91
S	0.00
Fe	5.58
Ni	1.44
Cu	16.93
Total	100.00

Figure 6.6 and 6.7 shows the SEM and EDS image of the merging area of ABS over copper. It can be observed from the Table 6.2 that, inside the specimen the weight percentage of the copper present is 40.88 percent. And the percentage of the carbon present in the inside portion is high i.e. 50.53 percentage.

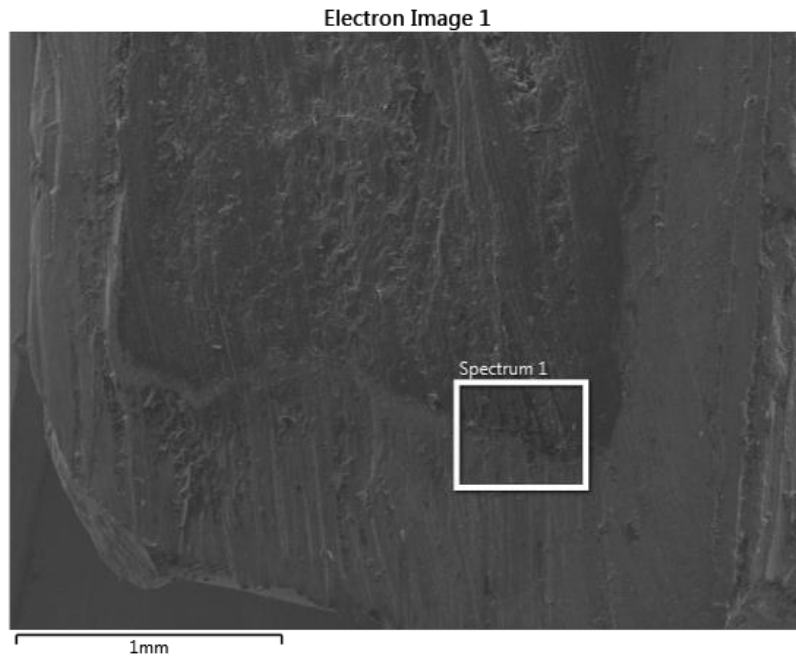


Figure 6.6 SEM Image of Specimen at the Merging Zone

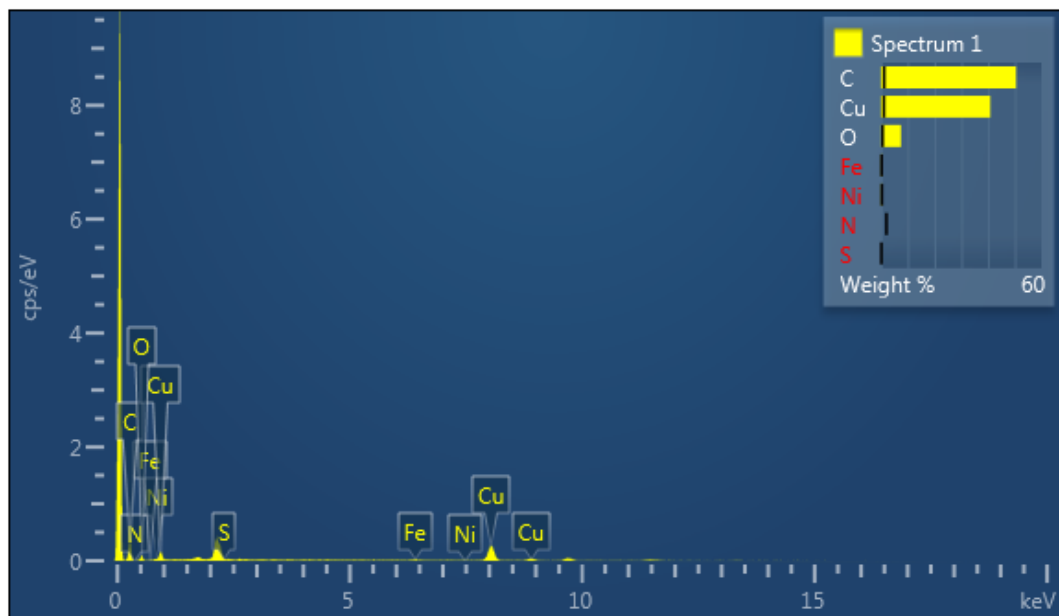


Figure 6.7 EDS Image of the Specimen of Merging Zone

Table 6.2 Weight Percentage Distribution of the Element of Merging Zone

Spectrum 1	Wt%
C	50.53
N	0.00
O	7.48
S	0.00
Fe	0.59
Ni	0.52
Cu	40.88
Total	100.00

Figure 6.8 and 6.9 shows the SEM and EDS image\*of the\*copper area of specimen. The Table 6.3 shows that, the presence of carbon percentage is less as compare to other two EDS result i.e., 13.53 percent. And the copper percentage present in this area is very high as compare to other EDS area i.e., 82.88 percentage.

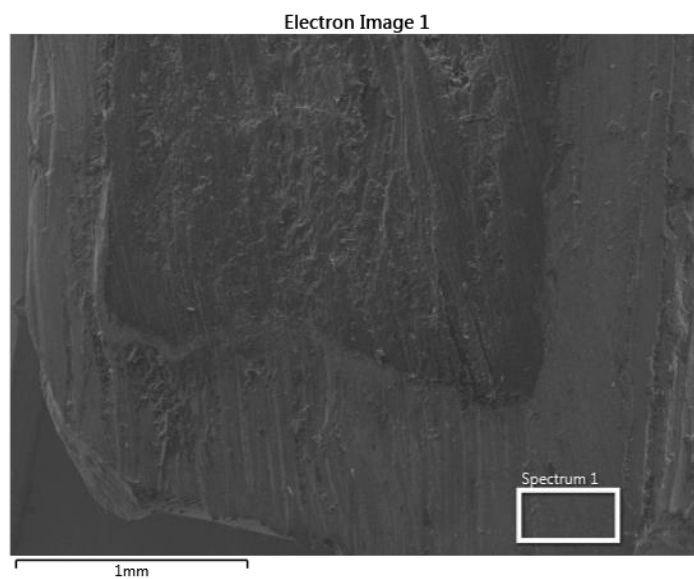


Figure 6.8 SEM Image of the Copper Area

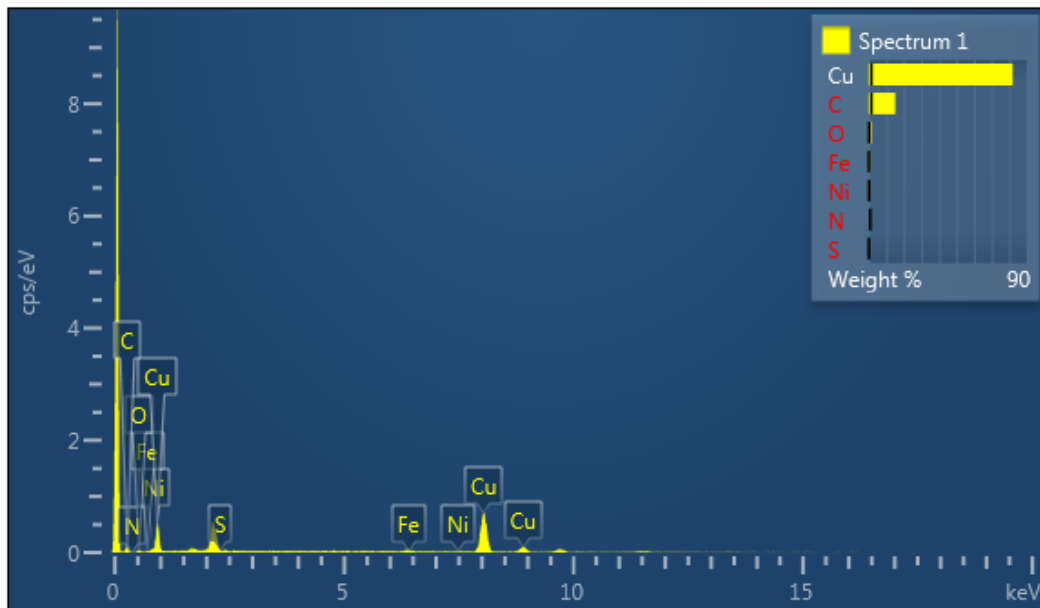


Figure 6.9 EDS Image of the Copper Area

Table 6.3 Weight Percentage Distribution of the Copper Area of Specimen

Spectrum 1	Wt%
C	13.53
N	0.00
O	2.48
S	0.00
Fe	0.59
Ni	0.52
Cu	82.88
Total	100.00

Figure 6.10 show the mapping of Elements present in the inside area of the specimen. It can be observed from the Figure that Carbon present in the specimen is high as compared to the copper.

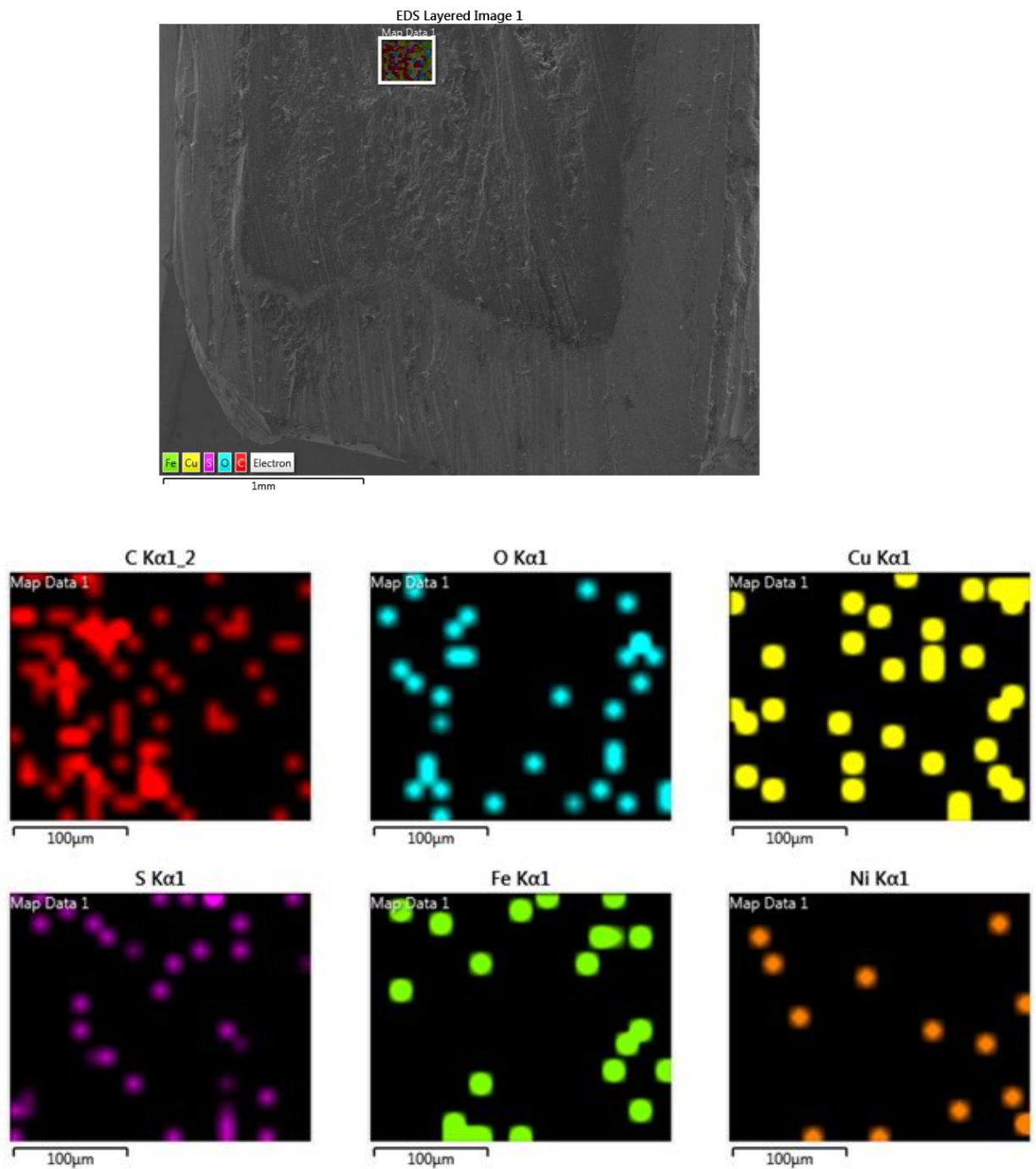


Figure 6.10 Mapping of the Elements in the Inside Area of the Specimen

Figure 6.10 show the mapping of Elements present in the inside area of the specimen. It can be observed from the Figure that Carbon present in the specimen is high as compared to the copper.



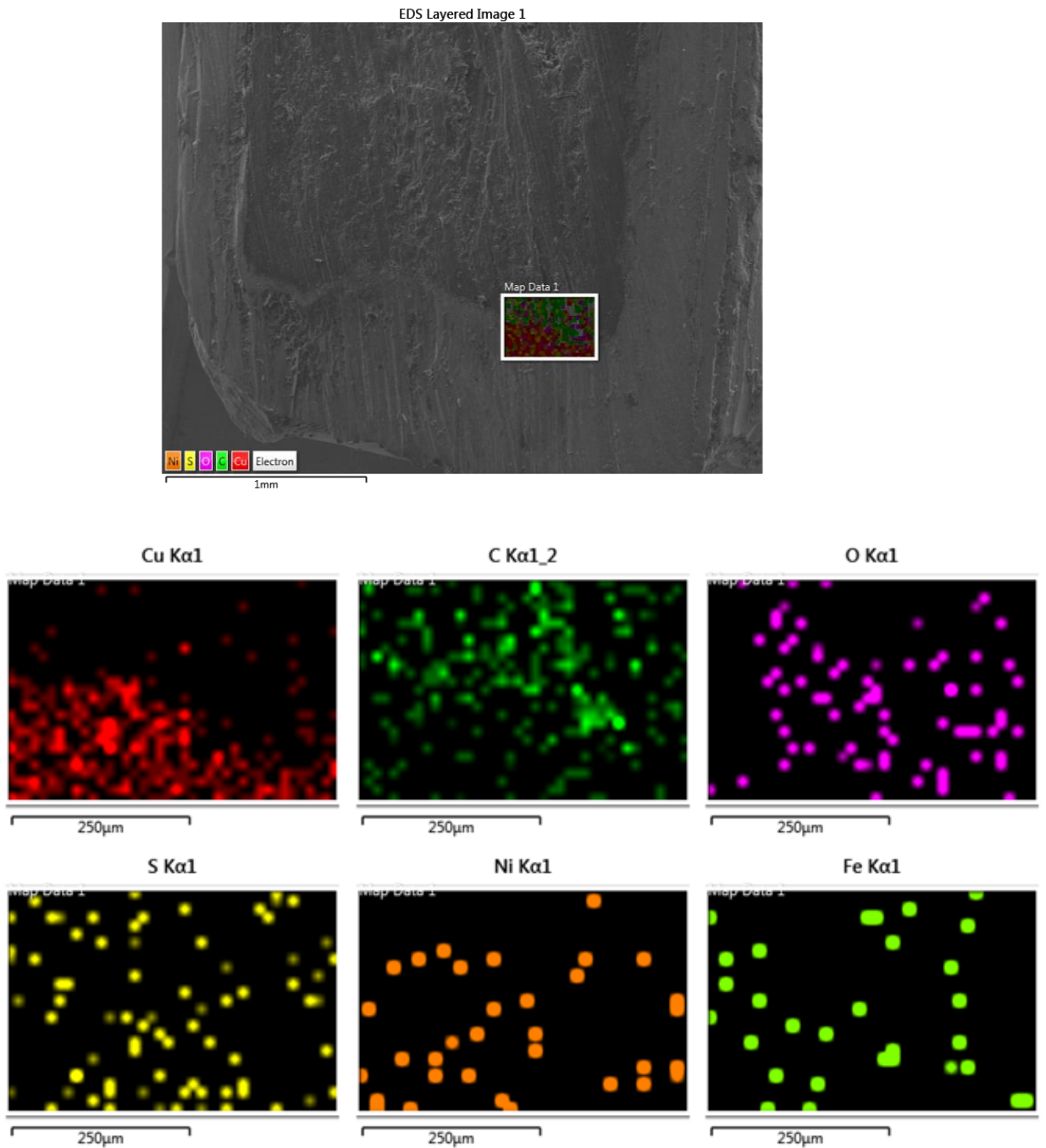


Figure 6.11 Mapping of the Element in the Merging Zone of the ABS Plastic and Copper

It can be observed from the Figure 6.11 that, the percentage of the carbon present is decreasing and the percentage change of the copper is increasing in this zone.

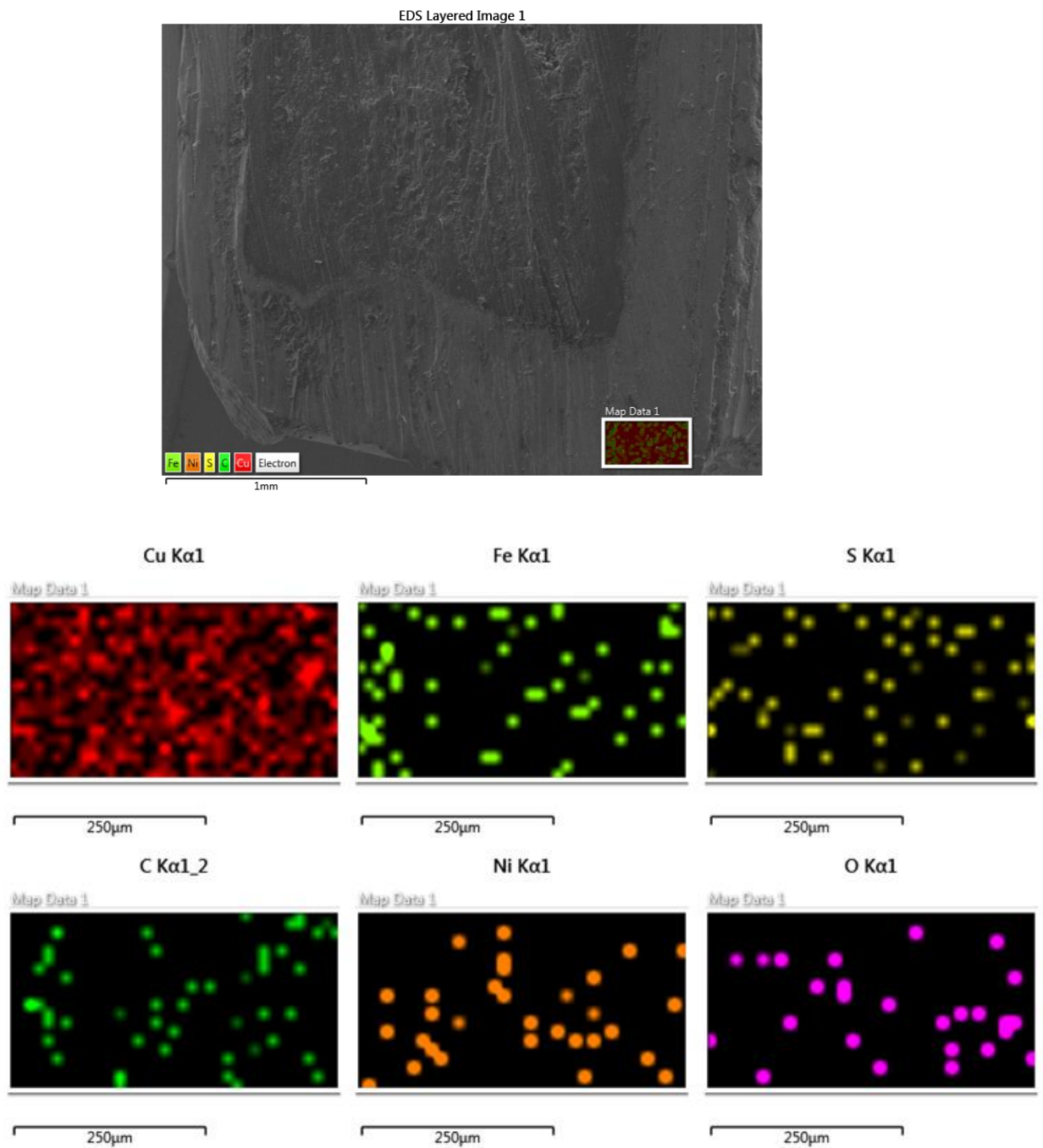


Figure 6.12 Mapping of Elements Present in the Copper Deposition Zone

Figure 6.12 show the mapping of the elements present in the electroplating area. It can be observed that the copper present in this area is very high and the present of carbon in the zone is very less.

From Figure 6.4 to Figure 6.12 it can be analyzed that the electroplating done on the ABS plastic is good. As the from all the figure it can be observed that the penetration of the copper inside the ABS plastic is also less. And the present of the carbon in the electroplating area is also less which show as good result of bonding between ABS and copper through electroplating operation.

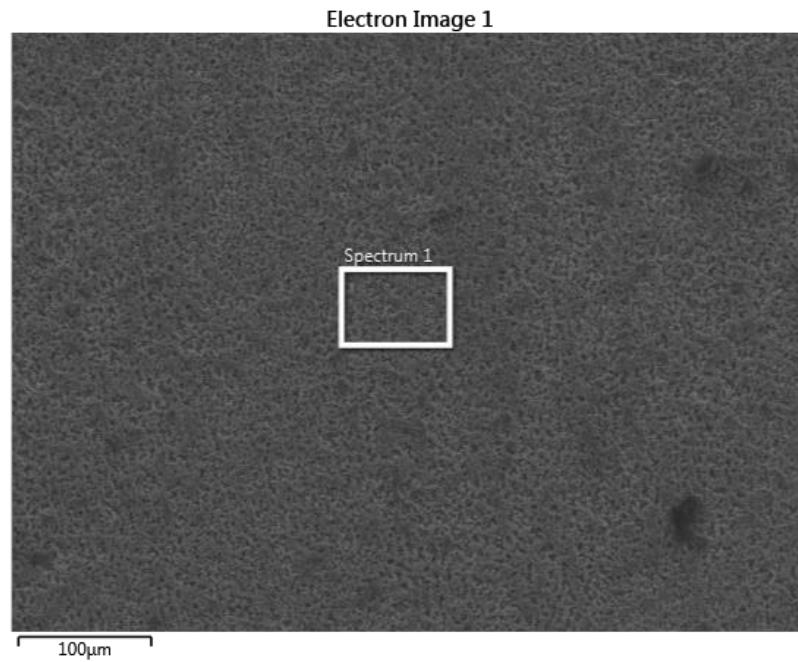


Figure 6.13 SEM Image of the Top Surface of the Electroplated Specimen

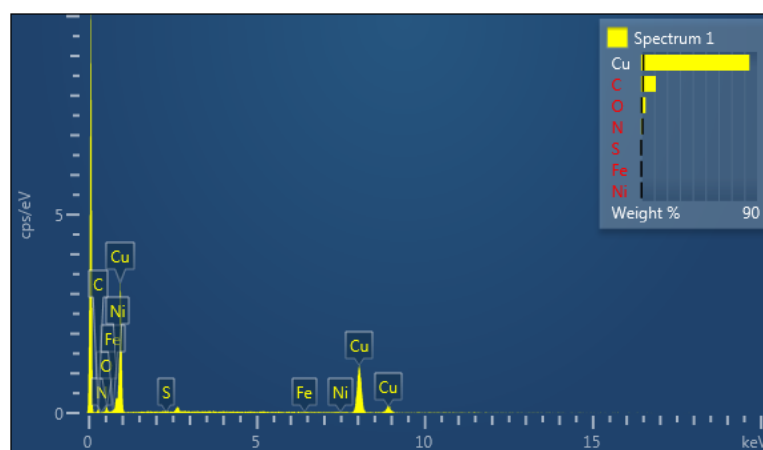
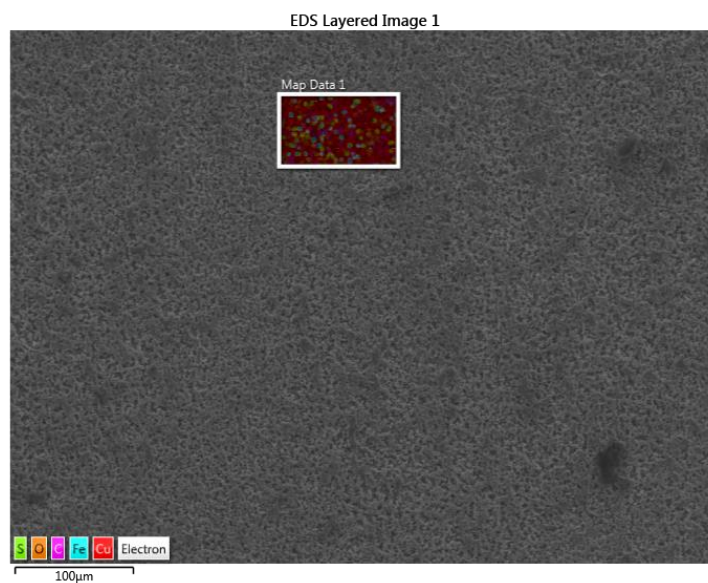


Figure 6.14 EDS of Top Surface of the Electroplated Specimen

Table 6.4 Weight Percentage distribution of the Elements on the Top Surface of the Specimen Electroplating Operation

Spectrum 1	Wt%
C	11.44
N	0.84
O	3.52
S	0.08
Fe	0.05
Ni	0.00
Cu	84.07
Total	100.00

It can be observed from the Figure 6.13 and 6.14 that, the carbon percentage present in the top surface is less and the copper present is high. Table 4 shows that carbon is present only 11.44 percent whereas the copper present in the top surface is high i.e. 84.07 percent.



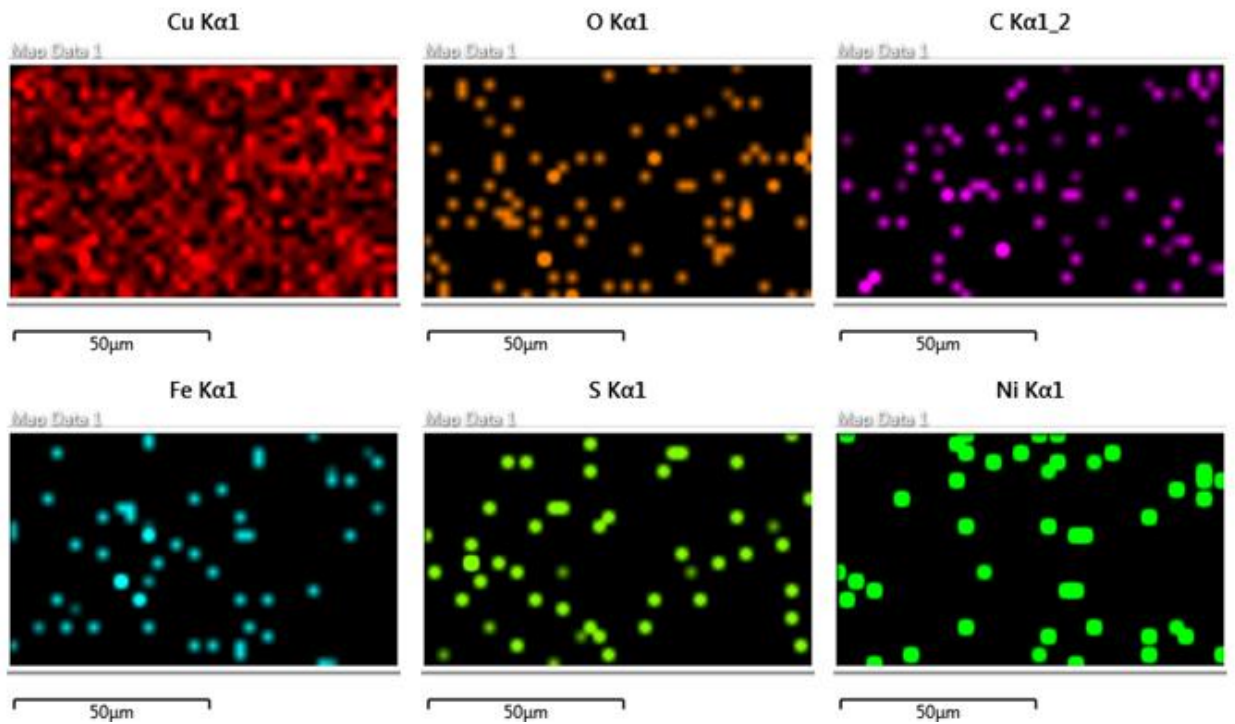
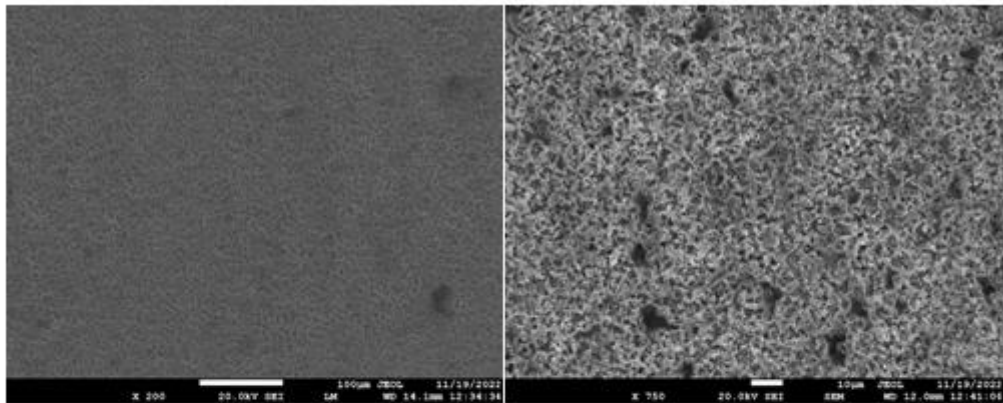


Figure 6.15: Mapping of the Element in the Top Surface of the Electroplated Specimen

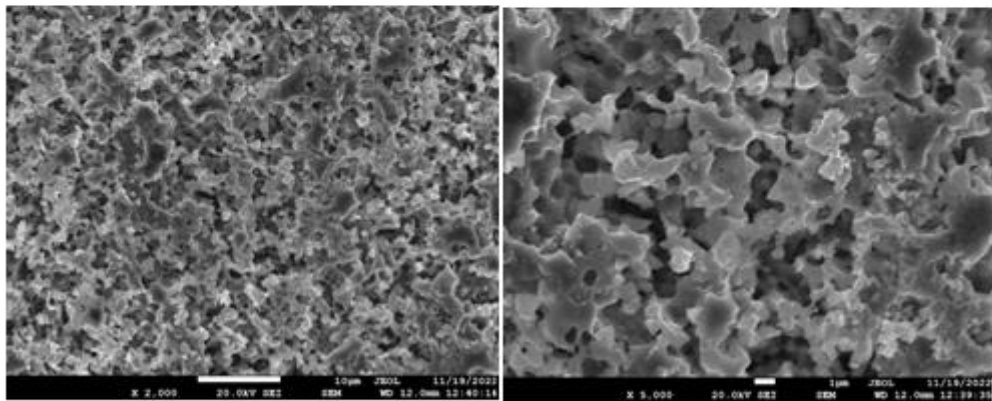
Figure 6.15 shows mapping of the element in the top surface of the specimen after electroplating operation. It can be visualized that, the accumulation of the copper in the top surface is very high as compare to the other element. This justify that the electroplating operation is successful.





(a) Top surface at 200X magnification

(b) Top surface at 750X magnification



(c) Top surface at 2000X magnification

(d) Top surface at 5000X magnification

Figure 6.16 SEM Image at Different Magnification of Top Surface of Electroplated Surface

Figure 6.16 (a) to (d) show the SEM image of the top surface of the copper during electroplating operation at different magnification. From Figure 6.16 (a) it can be observe that distribution of the copper is uniform through out the surface during electroplating operation. In Figure 6.16 (b) few voids were observed and at higher magnification i.e. 5000X the void can be seen clearly. Hence it can be said that the electroplating has been done on the ABS specimen successfully.

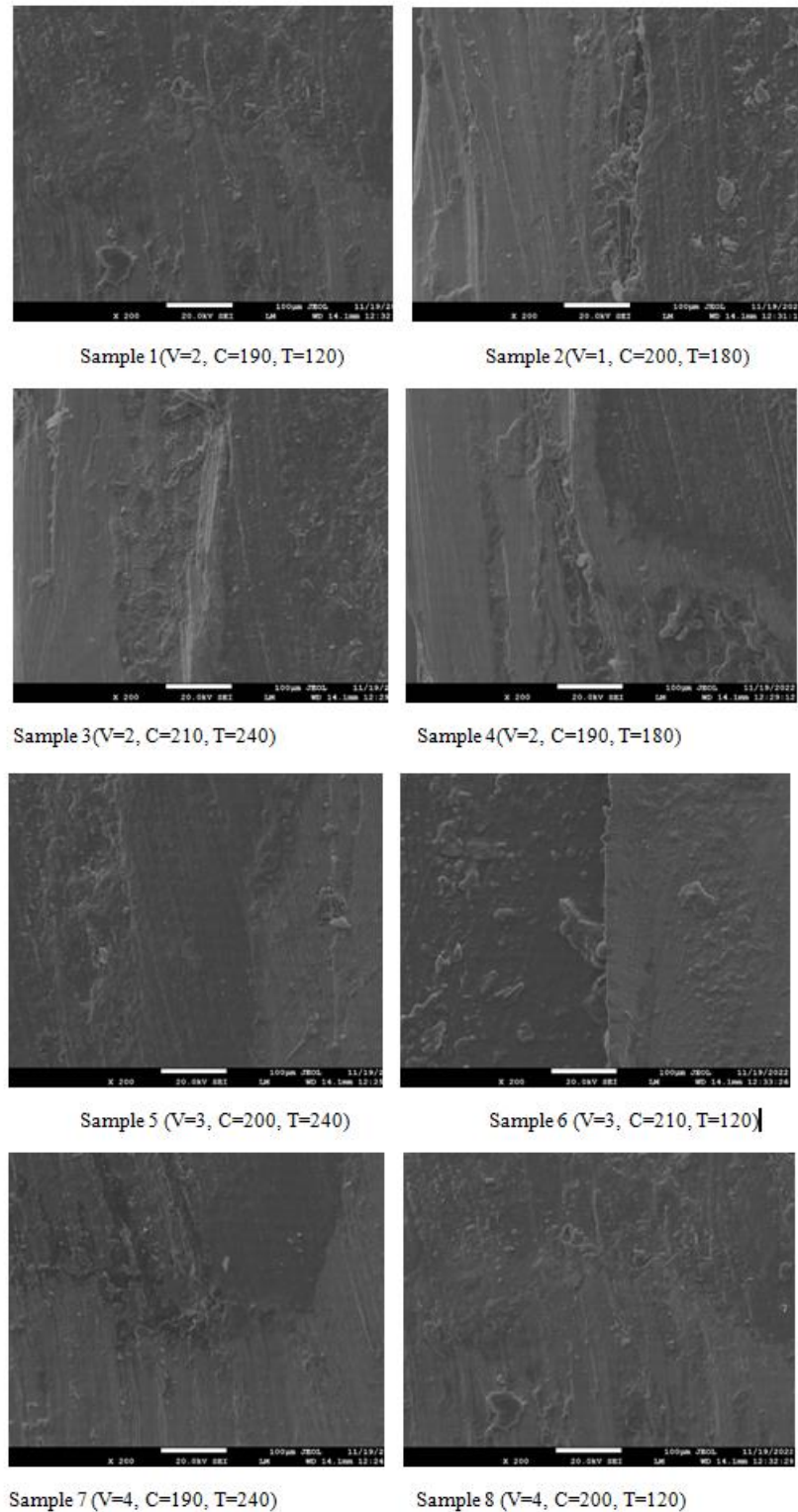


Figure 6.17 SEM Image of Samples at Interface Zone of Copper Plating and ABS

Figure 6.17 shows the interference zone of the ABS and Copper images after electroplating operation. The image was taken under 200X magnification. The image

shown at different electroplating condition. The interference zone of the ABS and copper can be clearly visualized. The debris of copper are were shown in the ABS plastic area this might be due to the different electroplating condition.

### 6.1.3 Surface Morphology of Copper Deposition Using Cold Spray Coating

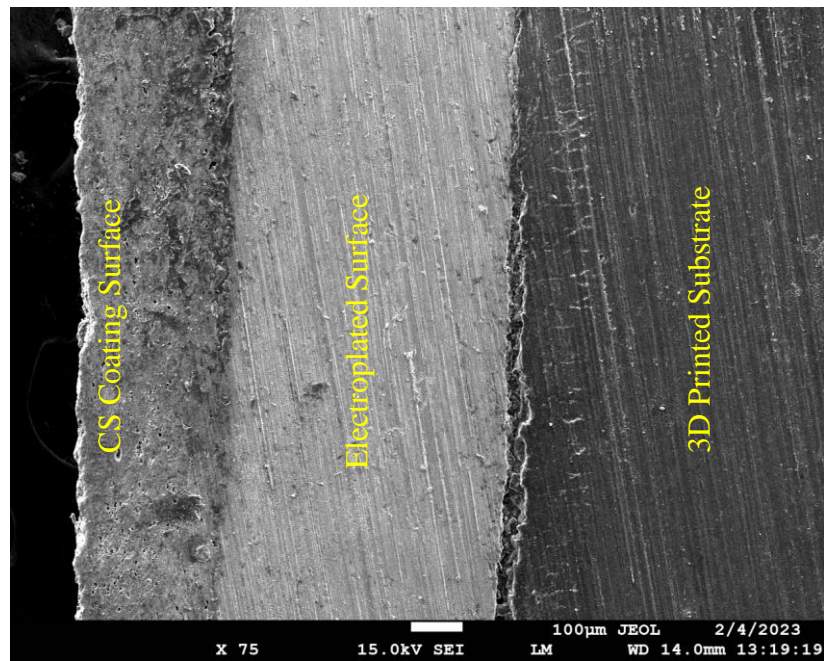


Figure 6.18 SEM Image of Cold Spray Copper Coating

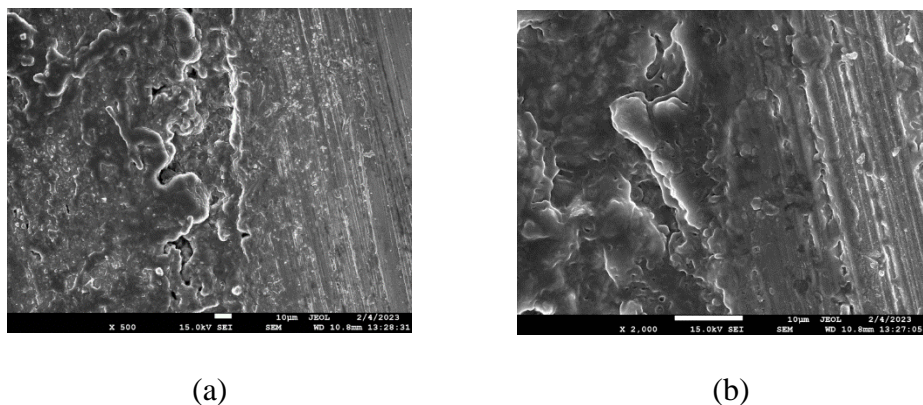


Figure 6.19(a), (b) SEM Images of Bonding between Cold Spray Copper Coating and Electroplated Interface

This figure 6.18 shows the intersection zone of the ABS, electroplating and cold spray. It can be seen that the bonding between the ABS and electroplating occurs



without crack or misalignment. Similarly, the bonding between the electroplating and cold spray surface was good, no void or inclusion is shown in the micrograph. From Figure 6.19(a) and 6.19(b) it can be observed that the deposition of the copper using the cold spray on the electroplated copper substrate a forced mixing occurred and that can only be attained by deep impact infiltration of copper particles on electroplated copper substrate are similar to finding of Champagne et al., 2005.

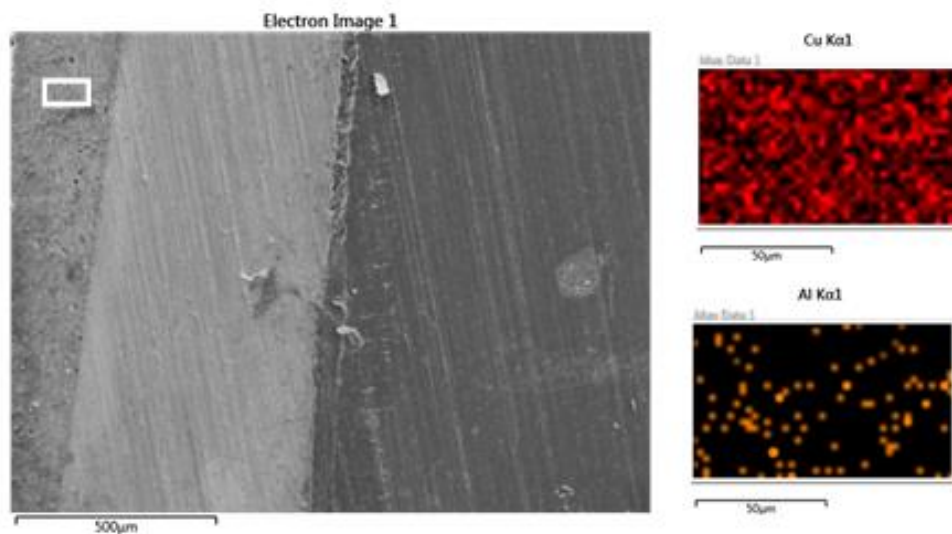


Figure 6.20 Mapping of the Element in the Cold Sprayed Region of the Specimen

Figure 6.20 show the mapping of elements present in the inside area of the cold spray region. It can be observed from the Figure 6.20 that copper present in this area is high and aluminum present in that area is very less.

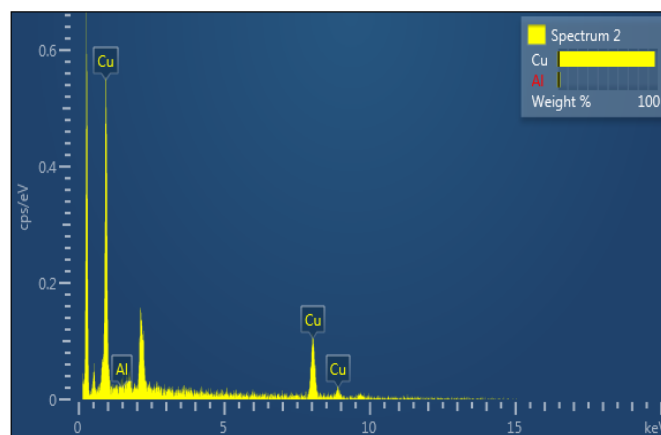


Figure 6.21 EDS of the Cold Sprayed Region of the Specimen

Table 6.5 Weight Percentage distribution of the Elements in the Cold Sprayed Surface

Spectrum 2	Wt%
Cu	97.14
Al	2.86
Total	100.00

It can be observed from the EDS figure 6.21 and table 6.5 that, the copper percentage present in the Cold Spray surface is 97.14% and aluminum present is 2.86%.

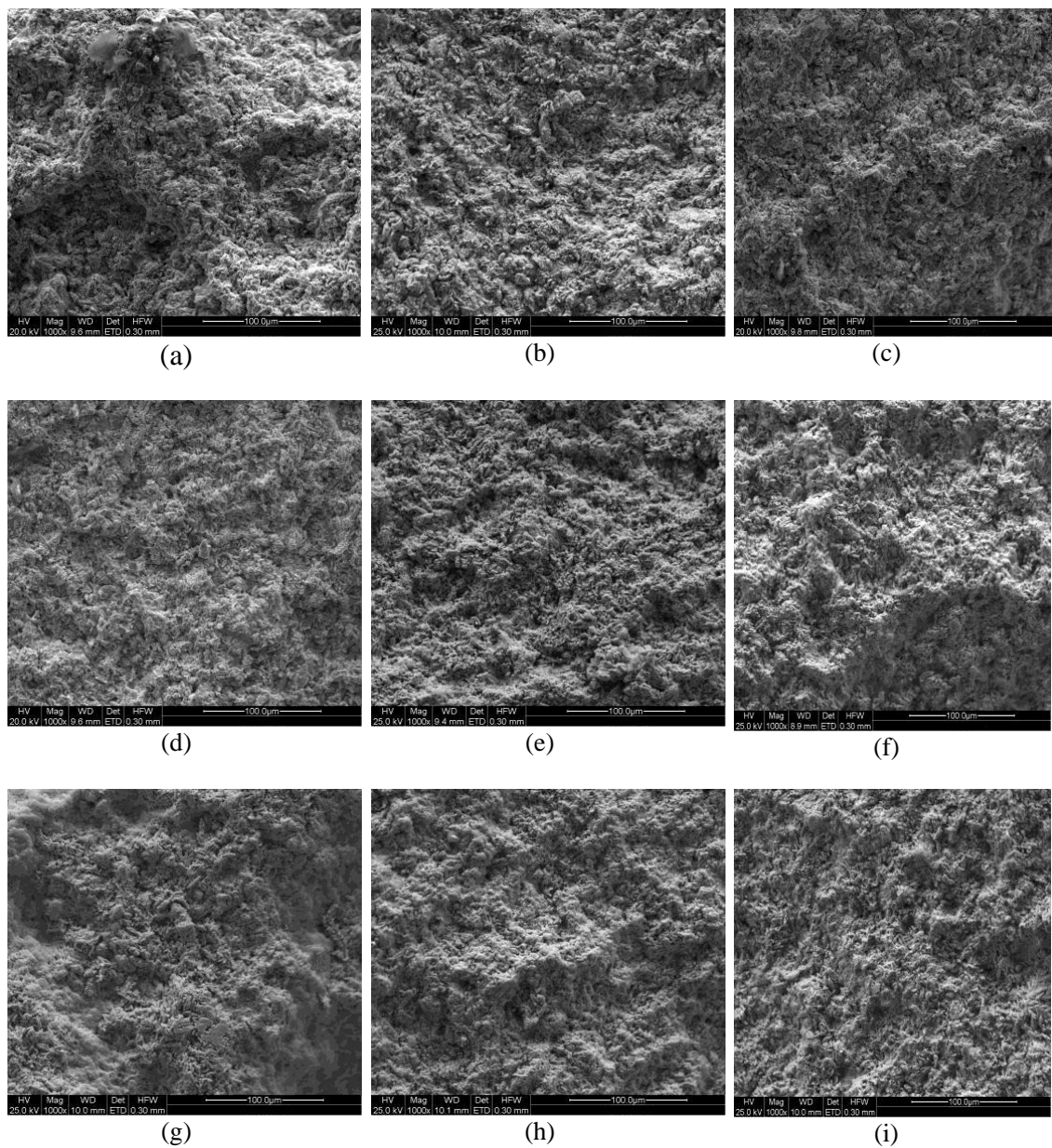


Figure 6.22 SEM Image of Top Surface of Different Cold Spray Coated Samples

The SEM microstructures shown in Figure 6.22(a) - (i) represent the set of 9 experiments conducted as per the design Table 5.12 respectively. The SEM microstructures were taken at CIF, LPU, Paghwara, India with help of a Scanning Electron Microscope. The micrographs were taken at following parameter values: HV 20kV, Magnification 1000X.

The pressure, standoff distance and gas temperature of the striking particles are the main factors influencing the quality of the coatings in regard to low surface roughness values. The effect of these factors can be noticed in the SEM micrographs shown in Figure 6.23(a) - (i). Microstructures observed in the present study are almost analogous with the findings of cold-sprayed coatings by McCune et al., 2000.

## **6.2 XRD ANALYSIS OF COPPER DEPOSITION:**

The information about the composition of the materials present in the test samples from experimentation is reported using the XRD analysis. The peak of copper metal as per the standard occurs for angle  $2\theta$  between  $0^{\circ}$  to  $80^{\circ}$ , so the samples were tested in this range using XRD equipment. The XRD graphs, peak list and pattern list is given in the Figure 6.6 (a), (b), and (c) for the samples taken from the experimentation and final mould. All the samples confirms the presence of pure nickel as the major constituent as a result of nickel electroforming process.

Figure 6.23 Show the XRD pattern of the specimen. It can be observed from the figure 6.23 that the copper is uniformly present throughout the top surface of the specimen. The peak formed during XRD analysis was done at a wavelength of 1.54060. The Two theta angle varies from 10 to 90 degree. Cubic lattice structure with a molecular weight of 63.55 and radiation of  $\text{MoK}\pm 1$ . It can be visualized that the peak formed at the angle 44.067 with count of 3918 and  $d$  ( $\text{\AA}$ ) is 2.05423, 51.269 with a count of 1204 and  $d$  ( $\text{\AA}$ ) is 1.78051 and 75.126 with a count of 811 and  $d$  ( $\text{\AA}$ ) is 1.26354 are same that occurred in the copper sample.

Counts **oTheta)**

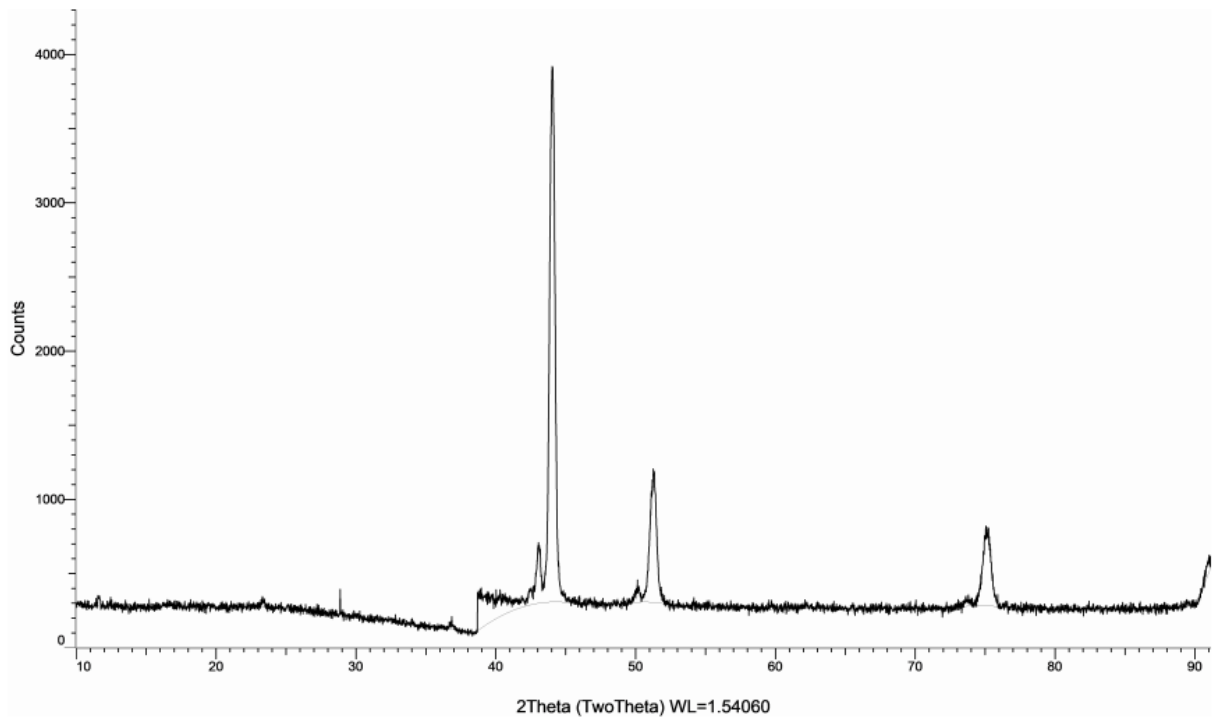


**Figure 6.23** XRD Image of Copper Deposition

### 7.1 CONCLUSIONS

The research delved into the hybrid technique involving cold spray coating of copper metal powder onto copper electroplated FDM plastic components. The investigation progressed sequentially from 3D printing nonconductive ABS plastic parts to rendering them conductive through steps encompassing conductive paint application, copper electroplating, and cold spray coating. Subsequently, comprehensive testing and surface characterization were carried out.

The present study has yielded significant findings of paramount importance:

The surface smoothing of FDM part surfaces was achieved through the utilization of cold vapor technique. However, this approach yielded a consistent and notably averaged improved surface finish ( $R_a=0.25 \mu\text{m}$ ).

The nonconductive ABS plastic can be made conductive by using either of the two techniques - chemical activation through electroless plating or by applying a coat of conductive paint. The silver conductive paint was used for the fabrication process as it is quicker and the surface finish is satisfactory.

The optimization of copper electroplating process parameters i.e voltage,  $\text{CuSO}_4$  concentration, and time was done for maximum deposition on FDM-produced ABS silver painted. An optimum mean thickness of  $349 \mu\text{m}$  materialized, accompanied by a deposition rate of  $1.454 \mu\text{m}/\text{min}$ . The two pivotal factors voltage and  $\text{CuSO}_4$  concentration exerting significant influence on the final deposition thickness, accounting for 45.24.8% and 39.65% respectively.

The optimized surface roughness of copper electroplating, adopting the criterion of smaller the better, are found at the initial level across the process parameters i.e voltage,  $\text{CuSO}_4$  concentration and time. The minimum surface roughness of  $1.85 \mu\text{m}$  was achieved. The  $\text{CuSO}_4$  concentration exert greatest influence i.e 68.75% among all the three parameters on the electroplated part surface roughness.

These optimized values for deposition thickness and surface roughness were used to produce metallized 3D printed samples to be used for cold spray coating. Uniform coating on all the samples were achieved.

The optimized of surface roughness of gas dynamic cold spray deposition of copper powder on metallized 3D printed, are found at the initial level across the process parameters i.e temperature, gas pressure and standoff distance. The minimum surface roughness of 3.27  $\mu\text{m}$  was achieved. Process parameters in descending order as per there contribution was pressure (37.25%), standoff distance (31.07%) and gas temperature (30.10%) respectively.

The optimization of gas dynamic cold spray coating process parameters i.e temperature, gas pressure and standoff distance for maximum copper coating hardness on metallized 3D printed parts was done and optimum surface hardness of 116 Hv was achieved. The standoff distance of the gun from the surface of metallized 3D printed parts is found to be the major contributing (75.06%) parameter.

The XRD analysis reveals that the final deposit confirms to the reference value as per the standard for copper.

Since these coatings have good mechanical properties and copper coating increase the components' working life by improving the thermal conductivity of the rapid tools. As a result, it is suggested that these coatings be tested on heat sinks, moulds and dies, and small electronic components involving in the conductive applications. When compared to carrier gases like nitrogen, helium, and others, air is readily available, inexpensive, and used successfully to deposit the coatings on the substrates by using LPCS process.

In conclusion, this research demonstrates that the hybrid fabrication method presents a viable alternative. Technically achievable, it holds promise as a cost-efficient and time-saving option for intricate shapes. The tools manufactured using this technology can be run for mass production.

## **7.2 SCOPE OF FUTURE WORK**

It was determined throughout this study project that the hybrid approach of cold spray coating on metal-coated 3D printed parts opens up a wide range of possibilities for additional research. Future research work is suggested:

The ranges of process parameters used for response optimization depend on the kind of powder sprayed. A wide range of powders may be used to create coatings by extending the range of the chosen parameters.

Numerous response parameters may be chosen for optimization depending on the application, and the methodologies described in the inquiry may be expanded to optimize both single and multiple answers.

The impact of the hybrid coating on mechanical properties such as surface finish, hardness, tensile strength, and wear resistance, with a focus on achieving improved component performance can be explored.

Conducting comprehensive adhesion tests and bonding analyses to assess the strength and durability of the hybrid coatings, ensuring their suitability for real-world applications.

In order to deposit advance materials onto electroplated surfaces with the least amount of heat penalty and expense, further advancements to the cold spray technique, such as pulsed gas dynamic spraying and laser aided cold spraying, may be investigated.

The thermal spray coating techniques of deposition can be combined with first two stages to fabricate a rigid workpiece even in low cost.

Investigating the scalability of the hybrid cold spray coating process for large-scale production, considering factors such as efficiency, cost-effectiveness, and reproducibility.

Application diversification of wide range of industries that could benefit from the hybrid-coated 3D printed parts, including aerospace, automotive, healthcare, biomedical implants and electronics can be explored.



## REFERENCES

- Abeykoon, C., Sri-Amphorn, P., & Fernando, A. (2020). Optimization of fused deposition modeling parameters for improved PLA and ABS 3D printed structures. *International Journal of Lightweight Materials and Manufacture*, 3(3), 284-297.
- Ajdelsztajn, L., Zuniga, A., Jodoin, B., & Lavernia, E. J. (2006). Cold gas dynamic spraying of a high temperature Al alloy. *Surface and Coatings Technology*, 201(6), 2109-2116.
- Ali, F., Chowdary, B. V., & Maharaj, J. (2014, September). Influence of some process parameters on build time, material consumption, and surface roughness of FDM processed parts: inferences based on the Taguchi design of experiments. In *Proceedings of the 2014 IACJ/ISAM Joint International Conference*.
- Alkhimov, A. P., Nesterovich, N. I., & Papyrin, A. N. (1982). Experimental investigation of supersonic two-phase flow over bodies. *Journal of Applied Mechanics and Technical Physics*, 23(2), 219-226.
- Alvarez C, K. L., Lagos C, R. F., & Aizpun, M. (2016). Investigating the influence of infill percentage on the mechanical properties of fused deposition modelled ABS parts. *Ingeniería e Investigación*, 36(3), 110-116.
- An, C. C., & Chen, R. H. (2007). Experimental study of demolding properties on stereolithography tooling, 129(4), 843-847.
- Ang, A. S. M., Berndt, C. C., & Cheang, P. (2011). Deposition effects of WC particle size on cold sprayed WC–Co coatings. *Surface and Coatings Technology*, 205(10), 3260-3267.
- Anitha, R., Arunachalam, S., & Radhakrishnan, P. (2001). Critical parameters influencing the quality of prototypes in fused deposition modelling. *Journal of Materials Processing Technology*, 118(1-3), 385-388.
- Baich, L., Manogharan, G., & Marie, H. (2015). Study of infill print design on production cost-time of 3D printed ABS parts. *International Journal of Rapid Manufacturing*, 5(3-4), 308-319.
- Balani, K., Laha, T., Agarwal, A., Karthikeyan, J., & Munroe, N. (2005). Effect of carrier gases on microstructural and electrochemical behavior of cold-sprayed 1100 aluminum coating. *Surface and Coatings Technology*, 195(2-3), 272-279.

- Baligheid, S., Kaup, V., Maharudresh, A. C., Kumar, G. C., & Elangovan, K. (2020). Quantitative analysis of surface treatment to enhance surface finish and mechanical characteristics of ABS parts. *Applied Physics A*, 126, 1-13.
- Bazzaoui, M., Martins, J. I., Bazzaoui, E. A., Albourine, A., Wang, R., & Hong, P. D. (2013). A simple method for acrylonitrile butadiene styrene metallization. *Surface and Coatings Technology*, 224, 71-76.
- Besterfield, D. H., Besterfield, C., Besterfield, G. H., Besterfield, M., Urdhwareshe, H., & Urdhwareshe, R. *Total Quality Management (TQM) 5e* by Pearson. Pearson Education India.
- Biglete, E. R., Manuel, M. C. E., Cruz, J. C. D., Verdadero, M. S., Diesta, J. M. B., Miralpez, D. N. G., ... & Picato, J. I. C. (2020, August). Surface Roughness Analysis of 3D Printed Parts Using Response Surface Modeling. In *2020 11th IEEE Control and System Graduate Research Colloquium (ICSGRC)* (pp. 191-196). IEEE.
- Bikulčius, G., Ignatjev, I., & Ručinskienė, A. (2014). Rapid method to determine suitability of ABS plastics for metallisation. *Transactions of the IMF*, 92(1), 47-51.
- Binder, K., Gottschalk, J., Kollenda, M., Gärtner, F., & Klassen, T. (2011). Influence of impact angle and gas temperature on mechanical properties of titanium cold spray deposits. *Journal of thermal spray technology*, 20, 234-242.
- Bolelli, G., Bonferroni, B., Koivuluoto, H., Lusvarghi, L., & Vuoristo, P. (2010). Depth-sensing indentation for assessing the mechanical properties of cold-sprayed Ta. *Surface and Coatings Technology*, 205(7), 2209-2217.
- Bonadei, A., & Marrocco, T. (2014). Cold sprayed MCrAlY+ X coating for gas turbine blades and vanes. *Surface and Coatings Technology*, 242, 200-206.
- Brischetto, S., Ferro, C. G., Maggiore, P., & Torre, R. (2017). Compression tests of ABS specimens for UAV components produced via the FDM technique. *Technologies*, 5(2), 20.
- Cai, L., Byrd, P., Zhang, H., Schlarman, K., Zhang, Y., Golub, M., & Zhang, J. (2016). Effect of printing orientation on strength of 3d printed abs plastics. In *TMS 2016 145 th Annual Meeting & Exhibition: Supplemental Proceedings* (pp. 199-204). Springer International Publishing.

- Cai, Z., Deng, S., Liao, H., Zeng, C., & Montavon, G. (2014). The effect of spray distance and scanning step on the coating thickness uniformity in cold spray process. *Journal of thermal spray technology*, 23, 354-362.
- Champagne, V. K., Helfritch, D., Leyman, P., Grendahl, S., & Klotz, B. (2005). Interface material mixing formed by the deposition of copper on aluminum by means of the cold spray process. *Journal of thermal spray technology*, 14, 330-334.
- Chan, S. F., Law, C. K., & Wong, T. T. (2003). Re-engineering the roto-casting mould making process. *Journal of materials processing technology*, 139(1-3), 527-534.
- Che, H., Chu, X., Vo, P., & Yue, S. (2018). Metallization of various polymers by cold spray. *Journal of Thermal Spray Technology*, 27, 169-178.
- Che, H., Chu, X., Vo, P., & Yue, S. (2018). Metallization of various polymers by cold spray. *Journal of Thermal Spray Technology*, 27, 169-178.
- Che, H., Vo, P., & Yue, S. (2019). Investigation of cold spray on polymers by single particle impact experiments. *Journal of Thermal Spray Technology*, 28, 135-143.
- Chen, X., Li, C., Xu, S., Hu, Y., Ji, G., & Wang, H. (2019). Microstructure and microhardness of Ni/Al-TiB<sub>2</sub> composite coatings prepared by cold spraying combined with postannealing treatment. *Coatings*, 9(9), 565.
- Chhabra, M., & Singh, R. (2011). Rapid casting solutions: a review. *Rapid Prototyping Journal*.
- Chohan, J. S., Singh, R., & Boparai, K. S. (2016). Parametric optimization of fused deposition modeling and vapour smoothing processes for surface finishing of biomedical implant replicas. *Measurement*, 94, 602-613.
- Chohan, J. S., Singh, R., & Boparai, K. S. (2020). Vapor smoothing process for surface finishing of FDM replicas. *Materials Today: Proceedings*, 26, 173-179.
- Choi, H. J., Lee, M., & Lee, J. Y. (2010). Application of a cold spray technique to the fabrication of a copper canister for the geological disposal of CANDU spent fuels. *Nuclear Engineering and Design*, 240(10), 2714-2720.
- Chua, C. K., Leong, K. F., & Lim, C. S. (2003). *Rapid Prototyping: Principal and Applications*.

- Chun, D. M., Choi, J. O., Lee, C. S., & Ahn, S. H. (2012). Effect of stand-off distance for cold gas spraying of fine ceramic particles (< 5  $\mu\text{m}$ ) under low vacuum and room temperature using nano-particle deposition system (NPDS). *Surface and Coatings Technology*, 206(8-9), 2125-2132.
- Chung Wang, C., Lin, T. W., & Hu, S. S. (2007). Optimizing the rapid prototyping process by integrating the Taguchi method with the Gray relational analysis. *Rapid prototyping journal*, 13(5), 304-315.
- Cinca, N., López, E., Dosta, S., & Guilemany, J. M. (2013). Study of stellite-6 deposition by cold gas spraying. *Surface and Coatings Technology*, 232, 891-898.
- Cizek, J., Kovarik, O., Siegl, J., Khor, K. A., & Dlouhy, I. (2013). Influence of plasma and cold spray deposited Ti Layers on high-cycle fatigue properties of Ti6Al4V substrates. *Surface and coatings technology*, 217, 23-33.
- Cobley, A. J., Abbas, B., & Hussain, A. (2014). Improved electroless copper coverage at low catalyst concentrations and reduced plating temperatures enabled by low frequency ultrasound. *International Journal of Electrochemical Science*, 9(12), 7795-7804.
- Coddet, P., Verdy, C., Coddet, C., Debray, F., & Lecouturier, F. (2015). Mechanical properties of thick 304L stainless steel deposits processed by He cold spray. *Surface and Coatings technology*, 277, 74-80.
- Coddet, P., Verdy, C., Coddet, C., Lecouturier, F., & Debray, F. (2013). Mechanical properties of cold spray deposited NARloy-Z copper alloy. *Surface and Coatings Technology*, 232, 652-657.
- Da Silva, F. S., Cinca, N., Dosta, S., Cano, I. G., Guilemany, J. M., Caires, C. S. A., ... & Benedetti, A. V. (2019). Corrosion resistance and antibacterial properties of copper coating deposited by cold gas spray. *Surface and Coatings Technology*, 361, 292-301.
- DeForce, B. S., Eden, T. J., & Potter, J. K. (2011). Cold spray Al-5% Mg coatings for the corrosion protection of magnesium alloys. *Journal of Thermal Spray Technology*, 20, 1352-1358.
- Denton, K. R., & Jacobs, P. F. (1994). QuickCast™ & rapid tooling: a case history at Ford Motor Company. In 1994 International Solid Freeform Fabrication Symposium.

- Dev, S., & Srivastava, R. (2020). Experimental investigation and optimization of FDM process parameters for material and mechanical strength. *Materials Today: Proceedings*, 26, 1995-1999.
- Dev, S., & Srivastava, R. (2021). Optimization of fused deposition modeling (FDM) process parameters for flexural strength. *Materials Today: Proceedings*, 44, 3012-3016.
- Ding, S., Zou, B., Wang, P., Huang, C., Liu, J., & Li, L. (2021). Geometric modeling and recycling of 3D printed fiber reinforced thermoplastic composite plain weft knitted structures. *Composites Part A: Applied Science and Manufacturing*, 149, 106528.
- Ding, Y., Lan, H., Hong, J., & Wu, D. (2004). An integrated manufacturing system for rapid tooling based on rapid prototyping. *Robotics and computer-integrated manufacturing*, 20(4), 281-288.
- Dong, G., Wijaya, G., Tang, Y., & Zhao, Y. F. (2018). Optimizing process parameters of fused deposition modeling by Taguchi method for the fabrication of lattice structures. *Additive Manufacturing*, 19, 62-72.
- Dosta, S., Couto, M., & Guilemany, J. M. (2013). Cold spray deposition of a WC-25Co cermet onto Al7075-T6 and carbon steel substrates. *Acta Materialia*, 61(2), 643-652.
- Dunne, P., Soe, S. P., Byrne, G., Venus, A., & Wheatley, A. R. (2004). Some demands on rapid prototypes used as master patterns in rapid tooling for injection moulding. *Journal of Materials Processing Technology*, 150(3), 201-207.
- Eason, P. D., Fewkes, J. A., Kennett, S. C., Eden, T. J., Tello, K., Kaufman, M. J., & Tiryakioğlu, M. (2011). On the characterization of bulk copper produced by cold gas dynamic spray processing in as fabricated and annealed conditions. *Materials Science and Engineering: A*, 528(28), 8174-8178.
- Equbal, A., & Sood, A. K. (2015). Investigations on metallization in FDM build ABS part using electroless deposition method. *Journal of Manufacturing Processes*, 19, 22-31.
- Equbal, A., Dixit, N. K., & Sood, A. K. (2013). Electroless plating on plastic. *Int. J. Sci. Eng. Res*, 8, 12-18.

- Faizan-Ur-Rab, M., Zahiri, S. H., Masood, S. H., Phan, T. D., Jahedi, M., & Nagarajah, R. (2016). Application of a holistic 3D model to estimate state of cold spray titanium particles. *Materials & Design*, 89, 1227-1241.
- Fallah, P., Rajagopalan, S., McDonald, A., & Yue, S. (2020). Development of hybrid metallic coatings on carbon fiber-reinforced polymers (CFRPs) by cold spray deposition of copper-assisted copper electroplating process. *Surface and Coatings Technology*, 400, 126231.
- Fernandez-Vicente, M., Calle, W., Ferrandiz, S., & Conejero, A. (2016). Effect of infill parameters on tensile mechanical behavior in desktop 3D printing. *3D printing and additive manufacturing*, 3(3), 183-192.
- Fukanuma, H., Ohno, N., Sun, B., & Huang, R. (2006). In-flight particle velocity measurements with DPV-2000 in cold spray. *Surface and Coatings Technology*, 201(5), 1935-1941.
- Fukumoto, M., Wada, H., Tanabe, K., Yamada, M., Yamaguchi, E., Niwa, A., ... & Izawa, M. (2007). Effect of substrate temperature on deposition behavior of copper particles on substrate surfaces in the cold spray process. *Journal of Thermal Spray Technology*, 16, 643-650.
- Gajdoš, I., Spišák, E., Kaščák, L., & Krasinskyi, V. (2015). Surface finish techniques for FDM parts. In *Materials science forum* (Vol. 818, pp. 45-48). Trans Tech Publications Ltd.
- Galantucci, L. M., Lavecchia, F., & Percoco, G. (2009). Experimental study aiming to enhance the surface finish of fused deposition modeled parts. *CIRP annals*, 58(1), 189-192.
- Galantucci, L. M., Lavecchia, F., & Percoco, G. (2010). Quantitative analysis of a chemical treatment to reduce roughness of parts fabricated using fused deposition modeling. *CIRP annals*, 59(1), 247-250.
- Ganesan, A., Affi, J., Yamada, M., & Fukumoto, M. (2012). Bonding behavior studies of cold sprayed copper coating on the PVC polymer substrate. *Surface and Coatings Technology*, 207, 262-269.
- Gardon, M., Latorre, A., Torrell, M., Dosta, S., Fernández, J., & Guilemany, J. M. (2013). Cold gas spray titanium coatings onto a biocompatible polymer. *Materials Letters*, 106, 97-99.

- Ghelichi, R., Bagherifard, S., Mac Donald, D., Brochu, M., Jahed, H., Jodoin, B., & Guagliano, M. (2014). Fatigue strength of Al alloy cold sprayed with nanocrystalline powders. *International Journal of Fatigue*, 65, 51-57.
- Ghelichi, R., MacDonald, D., Bagherifard, S., Jahed, H., Guagliano, M., & Jodoin, B. (2012). Microstructure and fatigue behavior of cold spray coated Al5052. *Acta Materialia*, 60(19), 6555-6561.
- Gillot, F., Mognol, P., & Furet, B. (2005). Dimensional accuracy studies of copper shells used for electro-discharge machining electrodes made with rapid prototyping and the electroforming process. *Journal of Materials Processing Technology*, 159(1), 33-39.
- Goyal, T., Sidhu, T. S., & Walia, R. S. (2012). Cold sprayed copper coatings on ASTM B 221 alloy—characterisation and corrosion study in simulated marine and industrial environment. *International Journal of Surface Science and Engineering*, 6(4), 306-337.
- Grigoriev, S., Okunkova, A., Sova, A., Bertrand, P., & Smurov, I. (2015). Cold spraying: From process fundamentals towards advanced applications. *Surface and coatings Technology*, 268, 77-84.
- Grujicic M, Zhao CL, Tong C, DeRosset WS, Helfritch D (2004) Analysis of the impact velocity of powder particles in the cold-gas dynamic-spray process. *Mater Sci Eng A368:222–230*
- Gui-Xiang, W., Ning, L., Hui-Li, H., & Yuan-Chun, Y. (2006). Process of direct copper plating on ABS plastics. *Applied Surface Science*, 253(2), 480-484.
- Grünberger, T., & Domröse, R. (2015). Direct Metal Laser Sintering: Identification of process phenomena by optical in-process monitoring. *Laser technik journal*, 12(1), 45-48.
- Guo, X., Zhang, G., Li, W. Y., Dembinski, L., Gao, Y., Liao, H., & Coddet, C. (2007). Microstructure, microhardness and dry friction behavior of cold-sprayed tin bronze coatings. *Applied Surface Science*, 254(5), 1482-1488.
- Hafsa, M. N., Ibrahim, M., Wahab, M. S., & Zahid, M. S. (2014). Evaluation of FDM pattern with ABS and PLA material. *Applied Mechanics and Materials*, 465, 55-59.

- Haidiezul, A. H. M., Aiman, A. F., & Bakar, B. (2018, March). Surface finish effects using coating method on 3D printing (FDM) parts. In IOP Conference Series: Materials Science and Engineering (Vol. 318, No. 1, p. 012065). IOP Publishing.
- Hamid, A., Frank, G., Thorsten, S., & Heinrich, K. (2003). Bonding mechanism in cold gas spraying. *Acta Materialia*, 51(15), 4379-4394.
- Harun, W. S. W., Safian, S., & Idris, M. H. (2009). Evaluation of ABS patterns produced from FDM for investment casting process. *WIT Trans. Eng. Sci*, 64(3), 319-328.
- Hashmi, M. S. J. (2014). *Comprehensive materials processing*. Newnes.
- Hernandez, R., Slaughter, D., Whaley, D., Tate, J., & Asiabanpour, B. (2016). Analyzing the tensile, compressive, and flexural properties of 3D printed ABS P430 plastic based on printing orientation using fused deposition modeling. In 2016 International Solid Freeform Fabrication Symposium. University of Texas at Austin.
- Heymann, K., Riedel, W., & Woldt, G. (1970). Electroplating of plastics in theory and practice. *Angewandte Chemie International Edition in English*, 9(6), 425-433.
- Himmer, T., Nakagawa, T., & Anzai, M. (1999). Lamination of metal sheets. *Computers in Industry*, 39(1), 27-33.
- Horvath, D., Noorani, R., & Mendelson, M. (2007). Improvement of surface roughness on ABS 400 polymer using design of experiments (DOE). In *Materials science forum* (Vol. 561, pp. 2389-2392). Trans Tech Publications Ltd.
- Hsu, C. Y., Chen, D. Y., Lai, M. Y., & Tzou, G. J. (2008). EDM electrode manufacturing using RP combining electroless plating with electroforming. *The International Journal of Advanced Manufacturing Technology*, 38, 915-924.
- <http://www.techok.com/rtv-molding.html>
- Huang, R., & Fukanuma, H. (2012). Study of the influence of particle velocity on adhesive strength of cold spray deposits. *Journal of thermal spray technology*, 21(3-4), 541-549.
- Huang, R., & Fukanuma, H. (2015). Future trends in cold spray techniques. In *Future development of thermal spray coatings* (pp. 143-162). Woodhead Publishing.



- Huang, R., Ma, W., & Fukanuma, H. (2014). Development of ultra-strong adhesive strength coatings using cold spray. *Surface and Coatings Technology*, 258, 832-841.
- Hussain, T. (2013). Cold spraying of titanium: a review of bonding mechanisms, microstructure and properties. *Key engineering materials*, 533, 53-90.
- Hussain, T., McCartney, D. G., & Shipway, P. H. (2011). Impact phenomena in cold-spraying of titanium onto various ferrous alloys. *Surface and Coatings Technology*, 205(21-22), 5021-5027.
- Hussain, T., McCartney, D. G., Shipway, P. H., & Zhang, D. (2009). Bonding mechanisms in cold spraying: the contributions of metallurgical and mechanical components. *Journal of Thermal Spray Technology*, 18, 364-379.
- Jahed, H., & Noban, M. (2009). Fatigue of Electroformed Nickel. *Journal of failure analysis and prevention*, 9, 549-557.
- Jayanth, N., Senthil, P., & Prakash, C. (2018). Effect of chemical treatment on tensile strength and surface roughness of 3D-printed ABS using the FDM process. *Virtual and Physical Prototyping*, 13(3), 155-163.
- Jayanthi, S., Bokuf, B., McConnel, R., Speer, R. J., & Fussell, P. S. (1997). Stereolithographic injection molds for direct tooling. In 1997 International Solid Freeform Fabrication Symposium.
- Jetley, S., & Low, D. K. (2006). A rapid tooling technique using a low melting point metal alloy for plastic injection molding. *Journal of Industrial Technology*, 22(3), 2-8.
- Ji, G. C., Wang, H. T., Chen, X., Bai, X. B., Dong, Z. X., & Yang, F. G. (2013). Characterization of cold-sprayed multimodal WC-12Co coating. *Surface and Coatings Technology*, 235, 536-543.
- Jodoin, B. (2002). Cold spray nozzle mach number limitation. *Journal of Thermal Spray Technology*, 11, 496-507.
- Jodoin, B., Ajdelsztajn, L., Sansoucy, E., Zúñiga, A., Richer, P., & Lavernia, E. J. (2006). Effect of particle size, morphology, and hardness on cold gas dynamic sprayed aluminum alloy coatings. *Surface and Coatings Technology*, 201(6), 3422-3429.
- Jones, D. A. (1996). Principles and prevention. *Corrosion*, 2, 168.

- Joshi, A., & James, S. (2018). Molecular dynamics simulation study on effect of process parameters on coatings during cold spray process. *Procedia Manufacturing*, 26, 190-197.
- Jung, H. B., Park, J. I., Park, S. H., Kim, H. J., Lee, C. H., & Han, J. W. (2009). Effect of the expansion ratio and length ratio on a gas-particle flow in a converging-diverging cold spray nozzle. *Metals and Materials International*, 15, 967-970.
- Kalyan, K., Singh, J., Phull, G. S., Soni, S., Singh, H., & Kaur, G. (2018). Integration of FDM and vapor smoothing process: Analyzing properties of fabricated ABS replicas. *Materials Today: Proceedings*, 5(14), 27902-27911.
- Kang, D. H., Choi, J. C., Choi, J. M., & Kim, T. W. (2010). An environment-friendly surface pretreatment of ABS plastic for electroless plating using chemical foaming agents. *Transactions on Electrical and electronic materials*, 11(4), 174-177.
- Kannan, S., & Senthilkumaran, D. (2014). Investigating the influence of electroplating layer thickness on the tensile strength for fused deposition processed ABS thermoplastics. *International Journal of Engineering and Technology*, 6(2), 1047-1052.
- Kaur, N., Kumar, M., Sharma, S. K., Kim, D. Y., Kumar, S., Chavan, N. M., & Singh, H. (2015). Study of mechanical properties and high temperature oxidation behavior of a novel cold-spray Ni-20Cr coating on boiler steels. *Applied Surface Science*, 328, 13-25.
- Kechagias, J., Iakovakis, V., Katsanos, M., & Maropoulos, S. (2008). Rapid electrode manufacture using Stereolithography models-A state of the art. *Technological Educational Institute of Larissa, Greece. RECENT*, 9(1), 22.
- Khan, M. S., & Dash, J. P. (2019). Enhancing surface finish of fused deposition modelling parts. *3D printing and additive manufacturing technologies*, 45-57.
- Khan, M. S., & Mishra, S. B. (2020). Minimizing surface roughness of ABS-FDM build parts: An experimental approach. *Materials Today: Proceedings*, 26, 1557-1566.
- Kim, H. J., Lee, C. H., & Hwang, S. Y. (2005). Fabrication of WC-Co coatings by cold spray deposition. *Surface and Coatings Technology*, 191(2-3), 335-340.

- King, D., & Tansey, T. (2002). Alternative materials for rapid tooling. *Journal of Materials Processing Technology*, 121(2-3), 313-317.
- Koivuluoto, H., & Vuoristo, P. (2014). Structure and corrosion properties of cold sprayed coatings: a review. *Surface engineering*, 30(6), 404-413.
- Kruth, J. P., Leu, M. C., & Nakagawa, T. (1998). Progress in additive manufacturing and rapid prototyping. *Cirp Annals*, 47(2), 525-540.
- Kulkarni, M. V., Elangovan, K., & Reddy, K. H. (2013). Development of electroplating process for plating polyamides. *Bangladesh Journal of Scientific and Industrial Research*, 48(3), 205-212.
- Kulkarni, M., Elangovan, K., & Reddy, K. H. (2012). Development of Electroplating setup for plating ABS plastics. *i-Manager's Journal on Mechanical Engineering*, 2(3), 53.
- Kumar, S., Bae, G., & Lee, C. (2016). Influence of substrate roughness on bonding mechanism in cold spray. *Surface and Coatings Technology*, 304, 592-605.
- Kumar, S., Kannan, V. N., & Sankaranarayanan, G. (2014). Parameter optimization of ABS-M30i parts produced by fused deposition modeling for minimum surface roughness. *International Journal of Current Engineering and Technology*, 3(3), 93-97.
- Lalehpour, A., Janeteas, C., & Barari, A. (2018). Surface roughness of FDM parts after post-processing with acetone vapor bath smoothing process. *The International Journal of Advanced Manufacturing Technology*, 95, 1505-1520.
- Lee, H., Shin, H., Lee, S., & Ko, K. (2008). Effect of gas pressure on Al coatings by cold gas dynamic spray. *Materials Letters*, 62(10-11), 1579-1581.
- Lee, M. W., Park, J. J., Kim, D. Y., Yoon, S. S., Kim, H. Y., James, S. C., ... & Coyle, T. (2011). Numerical studies on the effects of stagnation pressure and temperature on supersonic flow characteristics in cold spray applications. *Journal of thermal spray technology*, 20, 1085-1097.
- Lee, W. C., Wei, C. C., & Chung, S. C. (2014). Development of a hybrid rapid prototyping system using low-cost fused deposition modeling and five-axis machining. *Journal of Materials Processing Technology*, 214(11), 2366-2374.
- Lek, J. Y., Bhowmik, A., Tan, A. W. Y., Sun, W., Song, X., Zhai, W., ... & Boothroyd, C. B. (2018). Understanding the microstructural evolution of cold

- sprayed Ti-6Al-4V coatings on Ti-6Al-4V substrates. *Applied surface science*, 459, 492-504.
- Lemiale, V., King, P. C., Rudman, M., Prakash, M., Cleary, P. W., Jahedi, M. Z., & Gulizia, S. (2014). Temperature and strain rate effects in cold spray investigated by smoothed particle hydrodynamics. *Surface and Coatings Technology*, 254, 121-130.
  - Levasseur, D., Yue, S., & Brochu, M. (2012). Pressureless sintering of cold sprayed Inconel 718 deposit. *Materials Science and Engineering: A*, 556, 343-350.
  - Li, C. J., & Li, W. Y. (2003). Deposition characteristics of titanium coating in cold spraying. *Surface and Coatings Technology*, 167(2-3), 278-283.
  - Li, C. J., Li, W. Y., & Liao, H. (2006). Examination of the critical velocity for deposition of particles in cold spraying. *Journal of Thermal Spray Technology*, 15, 212-222.
  - Li, C. J., Li, W. Y., Wang, Y. Y., & Fukanuma, H. (2003). Effect of spray angle on deposition characteristics in cold spraying. *Thermal spray*, 91-96.
  - Li, C. J., Wang, H. T., Zhang, Q., Yang, G. J., Li, W. Y., & Liao, H. L. (2010). Influence of spray materials and their surface oxidation on the critical velocity in cold spraying. *Journal of Thermal Spray Technology*, 19, 95-101.
  - Li, S., Muddle, B., Jahedi, M., & Soria, J. (2012). A numerical investigation of the cold spray process using underexpanded and overexpanded jets. *Journal of thermal spray technology*, 21, 108-120.
  - Li, W. Y., & Li, C. J. (2005). Optimal design of a novel cold spray gun nozzle at a limited space. *Journal of Thermal Spray Technology*, 14, 391-396.
  - Li, W. Y., & Li, C. J. (2004). Optimization of spray conditions in cold spraying based on the numerical analysis of particle velocity. *Trans. Nonferrous Met. Soc. China*, 14(2), 43-48.
  - Li, W. Y., Li, C. J., & Yang, G. J. (2010). Effect of impact-induced melting on interface microstructure and bonding of cold-sprayed zinc coating. *Applied Surface Science*, 257(5), 1516-1523.
  - Li, W. Y., Li, C. J., Liao, H., & Coddet, C. (2007). Effect of heat treatment on the microstructure and microhardness of cold-sprayed tin bronze coating. *Applied surface science*, 253(14), 5967-5971.

- Li, W. Y., Zhang, C., Guo, X. P., Zhang, G., Liao, H. L., Li, C. J., & Coddet, C. (2008). Effect of standoff distance on coating deposition characteristics in cold spraying. *Materials & design*, 29(2), 297-304.
- Li, W. Y., Zhang, C., Wang, H. T., Guo, X. P., Liao, H. L., Li, C. J., & Coddet, C. (2007). Significant influences of metal reactivity and oxide films at particle surfaces on coating microstructure in cold spraying. *Applied Surface Science*, 253(7), 3557-3562.
- Li, W., Yang, K., Zhang, D., & Zhou, X. (2016). Residual stress analysis of cold-sprayed copper coatings by numerical simulation. *Journal of Thermal Spray Technology*, 25, 131-142.
- Lima, R. S., Kucuk, A., Berndt, C. C., Karthikeyan, J., Kay, C. M., & Lindemann, J. (2002). Deposition efficiency, mechanical properties and coating roughness in cold-sprayed titanium. *Journal of Materials Science Letters*, 21(21), 1687-1689.
- Liu, Y., Bai, W., Cheng, X., Tian, J., Wei, D., Sun, Y., & Di, P. (2021). Effects of printing layer thickness on mechanical properties of 3D-printed custom trays. *The Journal of Prosthetic Dentistry*, 126(5), 671-e1.
- Lokesh, K., & Jain, P. K. (2010). Selection of rapid prototyping technology. *Advances in Production Engineering & Management*, 5(2), 75-84.
- Lupoi, R. O. C. C. O., & O'Neill, W. (2010). Deposition of metallic coatings on polymer surfaces using cold spray. *Surface and Coatings Technology*, 205(7), 2167-2173.
- Ma, S. (2007). Rapid tooling with particulate reinforced epoxy composite for low volume production (Vol. 8, No. 1, pp. 11-17). *SIMTech Technical Reports*.
- Maamoun, A. H., Xue, Y. F., Elbestawi, M. A., & Veldhuis, S. C. (2018). Effect of selective laser melting process parameters on the quality of al alloy parts: Powder characterization, density, surface roughness, and dimensional accuracy. *Materials*, 11(12), 2343.
- Maev RGr, Leshchynsky V, (2008) Introduction to low pressure gas dynamic spray. In: *Physics and technology*. Wiley-VCH, Weinheim.
- Maidin, S., Muhamad, M. K., & Pei, E. (2015). Feasibility study of ultrasonic frequency application on fdm to improve parts surface finish.

- McCaskie, J. E. (2006). Plating on plastics: A survey of mechanisms for adhering metal films to plastic surfaces. *Metal finishing*, 104(5), 31-39.
- McGeough, J. A., Leu, M. C., Rajurkar, K. P., De Silva, A. K. M., & Liu, Q. (2001). Electroforming process and application to micro/macro manufacturing. *CIRP Annals*, 50(2), 499-514.
- Montgomery, D. C. (2017). *Design and analysis of experiments*. John Wiley & Sons.
- Monzon, M. D., Marrero, M. D., Benitez, A. N., Hernandez, P. M., & Cardenes, J. F. (2006). A technical note on the characterization of electroformed nickel shells for their application to injection molds. *Journal of materials processing technology*, 176(1-3), 273-277.
- Monzon, M., Benítez, A. N., Marrero, M. D., Hernandez, N., Hernandez, P., & Aisa, J. (2008). Validation of electrical discharge machining electrodes made with rapid tooling technologies. *Journal of Materials Processing Technology*, 196(1-3), 109-114.
- Mora, S. M., Gil, J. C., & López, A. M. C. (2019). Influence of manufacturing parameters in the dimensional characteristics of ABS parts obtained by FDM using reverse engineering techniques. *Procedia Manufacturing*, 41, 968-975.
- Morgan, R., Fox, P., Pattison, J., Sutcliffe, C., & O'Neill, W. (2004). Analysis of cold gas dynamically sprayed aluminium deposits. *Materials letters*, 58(7-8), 1317-1320.
- Moy, C. K., Cairney, J., Ranzi, G., Jahedi, M., & Ringer, S. P. (2010). Investigating the microstructure and composition of cold gas-dynamic spray (CGDS) Ti powder deposited on Al 6063 substrate. *Surface and Coatings Technology*, 204(23), 3739-3749.
- Nancharaiah, T. R. D. R. V., Raju, D. R., & Raju, V. R. (2010). An experimental investigation on surface quality and dimensional accuracy of FDM components. *International Journal on Emerging Technologies*, 1(2), 106-111.
- Neff, C., Trapuzzano, M., & Crane, N. B. (2016). Impact of vapor polishing on surface quality and mechanical properties of extruded ABS. *Rapid Prototyping Journal*, 24(2), 501-508.

- Nidagundi, V. B., Keshavamurthy, R., & Prakash, C. P. S. (2015). Studies on parametric optimization for fused deposition modelling process. *Materials Today: Proceedings*, 2(4-5), 1691-1699.
- Ning, X. J., Jang, J. H., Kim, H. J., Li, C. J., & Lee, C. (2008). Cold spraying of Al–Sn binary alloy: Coating characteristics and particle bonding features. *Surface and Coatings Technology*, 202(9), 1681-1687.
- Ning, X. J., Kim, J. H., Kim, H. J., & Lee, C. (2009). Characteristics and heat treatment of cold-sprayed Al–Sn binary alloy coatings. *Applied Surface Science*, 255(7), 3933-3939.
- Ning, X. J., Wang, Q. S., Ma, Z., & Kim, H. J. (2010). Numerical study of in-flight particle parameters in low-pressure cold spray process. *Journal of Thermal Spray Technology*, 19, 1211-1217.
- Noble, J., Walczak, K., & Dornfeld, D. (2014). Rapid tooling injection molded prototypes: a case study in artificial photosynthesis technology. *Procedia CIRP*, 14, 251-256.
- Nuñez, P. J., Rivas, A., García-Plaza, E., Beamud, E., & Sanz-Lobera, A. (2015). Dimensional and surface texture characterization in fused deposition modelling (FDM) with ABS plus. *Procedia Engineering*, 132, 856-863.
- Nuñez, P. J., Rivas, A., García-Plaza, E., Beamud, E., & Sanz-Lobera, A. (2015). Dimensional and surface texture characterization in fused deposition modelling (FDM) with ABS plus. *Procedia Engineering*, 132, 856-863.
- Olivera, S., Muralidhara, H. B., Venkatesh, K., Gopalakrishna, K., & Vivek, C. S. (2016). Plating on acrylonitrile–butadiene–styrene (ABS) plastic: a review. *Journal of materials science*, 51, 3657-3674.
- Onwubolu, G. C., & Rayegani, F. (2014). Characterization and optimization of mechanical properties of ABS parts manufactured by the fused deposition modelling process. *International Journal of Manufacturing Engineering*, 2014,1-13.
- Oyinbo, S. T., & Jen, T. C. (2019). A comparative review on cold gas dynamic spraying processes and technologies. *Manufacturing Review*, 6, 25.
- Pal, D. K., Ravi, B., Bhargava, L. S., & Chandrasekhar, U. (2004). Investment casting one-off intricate part using rapid prototyping technology. In *National Conference on Investment Casting, Durgapur* (pp. 150-169).

- Pal, D. K., Ravi, B., Bhargava, L. S., & Chandrasekhar, U. (2005). Rapid casting development using reverse engineering, rapid prototyping and process simulation. *Indian Foundry Journal*, 51(4), 23.
- Pal, D., & Ravi, B. (2007). Rapid tooling route selection and evaluation for sand and investment casting. *Virtual and Physical Prototyping*, 2(4), 197–207.
- Panda, S. K., Padhee, S., Anoop Kumar, S. O. O. D., & Mahapatra, S. S. (2009). Optimization of fused deposition modelling (FDM) process parameters using bacterial foraging technique. *Intelligent information management*, 1(02), 89.
- Pandey, P. M., Reddy, N. V., & Dhande, S. G. (2003). Improvement of surface finish by staircase machining in fused deposition modeling. *Journal of materials processing technology*, 132(1-3), 323-331.
- Pandey, V., & Suri, D. N. (2016). Copper Plating on ABS plastic. *Int Res J Eng Technol*, 3(04), 2726-8.
- Pandzic, A., Hodzic, D., & Milovanovic, A. (2019). Effect of infill type and density on tensile properties of PLA material for FDM process. *Annals of DAAAM & Proceedings*, 30.
- Pattison, J., Celotto, S., Morgan, R., Bray, M., & O’neill, W. (2007). Cold gas dynamic manufacturing: A non-thermal approach to freeform fabrication. *International Journal of Machine Tools and Manufacture*, 47(3-4), 627-634.
- Pattnaik, S., Karunakar, D. B., & Jha, P. K. (2012). Developments in investment casting process—a review. *Journal of Materials Processing Technology*, 212(11), 2332-2348.
- Pham, D. T., & Gault, R. S. (1998). A comparison of rapid prototyping technologies. *International Journal of machine tools and manufacture*, 38(10-11), 1257-1287.
- Poondla Vishnu Vikas, (2019). Experimental Evaluation Of Finding Optimum Process Parameters For ABS Material Using C300D Printer. *International Journal Of Scientific & Engineering Research*, 10(1), 617-630
- Polydoros, S., Polydoros, S. N., & Sfantsikopoulos, M. M. (2001). On the accuracy performance of the Laminated Object Manufacturing Technology. *National Technical University of Athens: Athens, Greece*.



- Pouzada, A. S. (2009). Hybrid moulds: a case of integration of alternative materials and rapid prototyping for tooling. *Virtual and Physical Prototyping*, 4(4), 195-202.
- Pramanik, D., Mandal, A., & Kuar, A. S. (2020). An experimental investigation on improvement of surface roughness of ABS on fused deposition modelling process. *Materials Today: Proceedings*, 26, 860-863.
- Radhwan, H., Shayfull, Z., Farizuan, M. R., Effendi, M. S. M., & Irfan, A. R. (2019, July). Optimization parameter effects on the quality surface finish of the three-dimensional printing (3D-printing) fused deposition modeling (FDM) using RSM. In *AIP conference proceedings* (Vol. 2129, No. 1, p. 020155). AIP Publishing LLC.
- Radhwan, H., Shayfull, Z., Nasir, S. M., & Irfan, A. R. (2020, May). Optimization parameter effects on the quality surface finish of 3D-printing process using taguchi method. In *IOP Conference Series: Materials Science and Engineering* (Vol. 864, No. 1, p. 012143). IOP Publishing.
- Rahman, H., John, T. D., Sivadasan, M., & Singh, N. K. (2018). Investigation on the Scale Factor applicable to ABS based FDM Additive Manufacturing. *Materials Today: Proceedings*, 5(1), 1640-1648.
- Rahmati, S. (2014). 10.12. Direct Rapid Tooling. *Comprehensive materials processing*, 10, 303-344.
- Rahmati, S., & Dickens, P. (2007). Rapid tooling analysis of Stereolithography injection mould tooling. *International Journal of Machine Tools and Manufacture*, 47(5), 740-747.
- Rahmati, S., Zúñiga, A., Jodoin, B., & Veiga, R. G. A. (2020). Deformation of copper particles upon impact: A molecular dynamics study of cold spray. *Computational Materials Science*, 171, 109219.
- Rajaguru, J., Duke, M., & Au, C. (2015). Development of rapid tooling by rapid prototyping technology and electroless nickel plating for low-volume production of plastic parts. *The International Journal of Advanced Manufacturing Technology*, 78, 31-40.
- Raju, M., Gupta, M. K., Bhanot, N., & Sharma, V. S. (2019). A hybrid PSO–BFO evolutionary algorithm for optimization of fused deposition modelling process parameters. *Journal of Intelligent Manufacturing*, 30, 2743-2758.

- Raletz, F., Vardelle, M., & Ezo'o, G. (2006). Critical particle velocity under cold spray conditions. *Surface and Coatings Technology*, 201(5), 1942-1947.
- Raletz, F., Vardelle, M., & Ezo'o, G. (2006). Critical particle velocity under cold spray conditions. *Surface and Coatings Technology*, 201(5), 1942-1947.
- Rankouhi, B., Javadpour, S., Delfanian, F., & Letcher, T. (2016). Failure analysis and mechanical characterization of 3D printed ABS with respect to layer thickness and orientation. *Journal of Failure Analysis and Prevention*, 16, 467-481.
- Raoelison, R. N., Xie, Y., Sapanathan, T., Planche, M. P., Kromer, R., Costil, S., & Langlade, C. (2018). Cold gas dynamic spray technology: A comprehensive review of processing conditions for various technological developments till to date. *Additive Manufacturing*, 19, 134-159.
- Raut, S., Jatti, V. S., Khedkar, N. K., & Singh, T. P. (2014). Investigation of the effect of built orientation on mechanical properties and total cost of FDM parts. *Procedia materials science*, 6, 1625-1630.
- Rech, S., Surpi, A., Vezzù, S., Patelli, A., Trentin, A., Glor, J., ... & Eklund, P. (2013). Cold-spray deposition of Ti<sub>2</sub>AlC coatings. *Vacuum*, 94, 69-73.
- Rennie, A. E., Bocking, C. E., & Bennett, G. R. (2001). Electroforming of rapid prototyping mandrels for electro-discharge machining electrodes. *Journal of Materials Processing Technology*, 110(2), 186-196.
- Richer, P., Jodoin, B., & Ajdelsztajn, L. (2006). Substrate roughness and thickness effects on cold spray nanocrystalline Al– Mg coatings. *Journal of thermal spray technology*, 15, 246-254.
- Richer, P., Yandouzi, M., Beauvais, L., & Jodoin, B. (2010). Oxidation behaviour of CoNiCrAlY bond coats produced by plasma, HVOF and cold gas dynamic spraying. *Surface and Coatings Technology*, 204(24), 3962-3974.
- Robitaille, F., Yandouzi, M., Hind, S., & Jodoin, B. (2009). Metallic coating of aerospace carbon/epoxy composites by the pulsed gas dynamic spraying process. *Surface and Coatings Technology*, 203(19), 2954-2960.
- Rokni, M. R., Nutt, S. R., Widener, C. A., Champagne, V. K., & Hrabe, R. H. (2017). Review of relationship between particle deformation, coating microstructure, and properties in high-pressure cold spray. *Journal of thermal spray technology*, 26, 1308-1355.

- Rokni, M. R., Widener, C. A., Crawford, G. A., & West, M. K. (2015). An investigation into microstructure and mechanical properties of cold sprayed 7075 Al deposition. *Materials Science and Engineering: A*, 625, 19-27.
- Rosochowski, A., & Matuszak, A. (2000). Rapid tooling: the state of the art. *Journal of materials processing technology*, 106(1-3), 191-198.
- Rosochowski, A., & Matuszak, A. (2000). Rapid tooling: the state of the art. *Journal of materials processing technology*, 106(1-3), 191-198.
- Saini, M. (2019). Optimization the process parameter of FDM 3D printer using Taguchi method for improving the tensile strength. *International Journal of All Research Education and Scientific Methods*, 7(4).
- Sakaki, K., & Shimizu, Y. (2001). Effect of the increase in the entrance convergent section length of the gun nozzle on the high-velocity oxygen fuel and cold spray process. *Journal of Thermal Spray Technology*, 10, 487-496.
- Sambu, S., Chen, Y., & Rosen, D. W. (2004, January). Geometric tailoring: A design for manufacturing method for rapid prototyping and rapid tooling. In *International Design Engineering Technical Conferences and Computers and Information in Engineering Conference* (Vol. 36231, pp. 149-161).
- Samykano, M., Selvamani, S. K., Kadirgama, K., Ngui, W. K., Kanagaraj, G., & Sudhakar, K. (2019). Mechanical property of FDM printed ABS: influence of printing parameters. *The International Journal of Advanced Manufacturing Technology*, 102, 2779-2796.
- Sansoucy, E., Kim, G. E., Moran, A. L., & Jodoin, B. (2007). Mechanical characteristics of Al-Co-Ce coatings produced by the cold spray process. *Journal of Thermal Spray Technology*, 16, 651-660.
- Santos da Silva, F., Cinca i Luis, N., Dosta Parras, S., García Cano, I., Guilemany, J. M., & Benedetti, A. V. (2017). Cold gas spray coatings: basic principles, corrosion protection and applications. *Eclética Química Journal*, 2017, vol. 42, num. 1, p. 9-32.
- Schmidt, T., Gärtner, F., Assadi, H., & Kreye, H. (2006). Development of a generalized parameter window for cold spray deposition. *Acta materialia*, 54(3), 729-742.

- Shahrubudin, N., Lee, T. C., & Ramlan, R. J. P. M. (2019). An overview on 3D printing technology: Technological, materials, and applications. *Procedia Manufacturing*, 35, 1286-1296.
- Sharma, V., & Singh, R. (2011). Investigations for modeling the silicon moulding process for plastic components. *Int J Mater Sci Eng*, 2(1-2), 250.
- Shayegan, G., Mahmoudi, H., Ghelichi, R. A. M. I. N., Villafuerte, J., Wang, J., Guagliano, M. A. R. I. O., & Jahed, H. (2014). Residual stress induced by cold spray coating of magnesium AZ31B extrusion. *Materials & Design*, 60, 72-84.
- Sheoran, A. J., & Kumar, H. (2020). Fused Deposition modeling process parameters optimization and effect on mechanical properties and part quality: Review and reflection on present research. *Materials Today: Proceedings*, 21, 1659-1672.
- Singamneni, S., Diegel, O., Singh, D., & McKenna, N. (2011). Rapid casting of light metals: an experimental investigation using taguchi methods. *International Journal of Metalcasting*, 5, 25-36.
- Singh, H., Sidhu, T. S., & Kalsi, S. B. S. (2012). Cold spray technology: future of coating deposition processes. *Frattura ed Integrità Strutturale*, 6(22), 69-84.
- Singh, H., Singh, S., & Prakash, C. (2020). Experimental investigation and parametric optimization of HA-TiO<sub>2</sub> plasma spray coating on  $\beta$ -phase titanium alloy. *Materials Today: Proceedings*, 28, 1340-1344.
- Singh, N.K., & Sood, A.K. (2012). Use of fused deposition modeling process in investment precision casting and risk of using selective laser sintering process.
- Singh, R., Singh, R., & Dureja, J. (2017) Comparison of post processing techniques for improving surface roughness of ABS replicas developed on FDM, 41-45.
- Singh, R., Singh, S., Singh, I. P., Fabbrocino, F., & Fraternali, F. (2017). Investigation for surface finish improvement of FDM parts by vapor smoothing process. *Composites Part B: Engineering*, 111, 228-234.
- Sivadasan, M., Singh, N. K., & Sood, A. K. (2012). Investment casting—rapid tooling approach. *International Journal of Mechanical and Industrial Engineering*, 1(4), 99-102.

- Song, Y., Yan, Y., Zhang, R., Xu, D., & Wang, F. (2002). Manufacture of the die of an automobile deck part based on rapid prototyping and rapid tooling technology. *Journal of materials processing technology*, 120(1-3), 237-242.
- Sood, A. K., Ohdar, R. K., & Mahapatra, S. S. (2009). Improving dimensional accuracy of fused deposition modelling processed part using grey Taguchi method. *Materials & design*, 30(10), 4243-4252.
- Sood, A. K., Ohdar, R. K., & Mahapatra, S. S. (2012). Experimental investigation and empirical modelling of FDM process for compressive strength improvement. *Journal of Advanced Research*, 3(1), 81-90.
- Sova, A., Grigoriev, S., Kochetkova, A., & Smurov, I. (2014). Influence of powder injection point position on efficiency of powder preheating in cold spray: Numerical study. *Surface and Coatings Technology*, 242, 226-231.
- Sova, A., Grigoriev, S., Okunkova, A., & Smurov, I. (2013). Cold spray deposition of 316L stainless steel coatings on aluminium surface with following laser post-treatment. *Surface and Coatings Technology*, 235, 283-289.
- Sova, A., Klinkov, S., Kosarev, V., Ryashin, N., & Smurov, I. (2013). Preliminary study on deposition of aluminium and copper powders by cold spray micronozzle using helium. *Surface and Coatings Technology*, 220, 98-101.
- Srikanth, A., Basha, G. M. T., & Venkateshwarlu, B. (2020). A brief review on cold spray coating process. *Materials Today: Proceedings*, 22, 1390-1397.
- Srikanth, A., Basha, G. M. T., & Venkateshwarlu, B. (2020). A brief review on cold spray coating process. *Materials Today: Proceedings*, 22, 1390-1397.
- Srikanth, A., Basha, G. M. T., & Venkateshwarlu, B. (2020). A brief review on cold spray coating process. *Materials Today: Proceedings*, 22, 1390-1397.
- Stein, B. (1996, March). A practical guide to understanding, measuring and controlling stress in electroformed metals. In *Proc. of AESF Electroforming Symposium*, Las Vegas.
- Stoltenhoff, T., Borchers, C., Gärtner, F., & Kreye, H. (2006). Microstructures and key properties of cold-sprayed and thermally sprayed copper coatings. *Surface and Coatings Technology*, 200(16-17), 4947-4960.
- Stoltenhoff, T., Kreye, H., & Richter, H. J. (2002). An analysis of the cold spray process and its coatings. *Journal of Thermal spray technology*, 11, 542-550.

- Subburaj, K., & Ravi, B. (2008). Computer aided rapid tooling process selection and manufacturability evaluation for injection mold development. *Computers in Industry*, 59(2-3), 262-276.
- Suo, X., Yin, S., Planche, M. P., Liu, T., & Liao, H. (2015). Strong effect of carrier gas species on particle velocity during cold spray processes. *Surface and Coatings Technology*, 268, 90-93.
- Tabbara, H., Gu, S., McCartney, D. G., Price, T. S., & Shipway, P. H. (2011). Study on process optimization of cold gas spraying. *Journal of thermal spray technology*, 20, 608-620.
- Taufik, M., & Jain, P. K. (2017). Laser assisted finishing process for improved surface finish of fused deposition modelled parts. *Journal of Manufacturing Processes*, 30, 161-177.
- Teixeira, L. A. C., & Santini, M. C. (2005). Surface conditioning of ABS for metallization without the use of chromium baths. *Journal of materials processing technology*, 170(1-2), 37-41.
- Uraz, C. (2019). The electroless metal plating process over ABS plastic by using ionic liquids.
- Van Steenkiste, T. H., Smith, J. R., Teets, R. E., Moleski, J. J., Gorkiewicz, D. W., Tison, R. P., ... & Barnett, K. J. (1999). Kinetic spray coatings. *Surface and Coatings Technology*, 111(1), 62-71.
- Venkatasubbareddy, O. Y., Siddikali, P., & Saleem, S. M. (2016). Improving the dimensional accuracy and surface roughness of FDM parts using optimization techniques. *IOSR Journal of Mechanical and Civil Engineering*, 16(053), 18-22.
- Vidaller, M. V., List, A., Gaertner, F., Klassen, T., Dosta, S., & Guilemany, J. M. (2015). Single impact bonding of cold sprayed Ti-6Al-4V powders on different substrates. *Journal of Thermal Spray Technology*, 24, 644-658.
- Villa, M., Dosta, S., & Guilemany, J. M. (2013). Optimization of 316L stainless steel coatings on light alloys using Cold Gas Spray. *Surface and Coatings Technology*, 235, 220-225.
- Wang, H. R., Li, W. Y., Ma, L., Wang, J., & Wang, Q. (2007). Corrosion behavior of cold sprayed titanium protective coating on 1Cr13 substrate in seawater. *Surface and Coatings Technology*, 201(9-11), 5203-5206.

- Wang, J., Wei, X. P., Christodoulou, P., & Hermanto, H. (2004). Rapid tooling for zinc spin casting using arc metal spray technology. *Journal of Materials Processing Technology*, 146(3), 283-288.
- Wang, Q., Birbilis, N., & Zhang, M. X. (2011). Interfacial structure between particles in an aluminum deposit produced by cold spray. *Materials Letters*, 65(11), 1576-1578.
- Watson, T. J., Nardi, A., Ernst, A. T., Cernatescu, I., Bedard, B. A., & Aindow, M. (2017). Cold spray deposition of an icosahedral-phase-strengthened aluminum alloy coating. *Surface and Coatings Technology*, 324, 57-63.
- Wu, H., Huang, C., Xie, X., Liu, S., Wu, T., Niendorf, T., & Deng, S. (2021). Influence of spray trajectories on characteristics of cold-sprayed copper deposits. *Surface and Coatings Technology*, 405, 126703.
- Yadav, D., Chhabra, D., Gupta, R. K., Phogat, A., & Ahlawat, A. (2020). Modeling and analysis of significant process parameters of FDM 3D printer using ANFIS. *Materials Today: Proceedings*, 21, 1592-1604.
- Yan, C., Shi, Y., Yang, J., & Liu, J. (2010). Multiphase polymeric materials for rapid prototyping and tooling technologies and their applications. *Composite Interfaces*, 17(2-3), 257-271.
- Yandouzi, M., Sansoucy, E., Ajdelsztajn, L., & Jodoin, B. (2007). WC-based cermet coatings produced by cold gas dynamic and pulsed gas dynamic spraying processes. *Surface and Coatings Technology*, 202(2), 382-390.
- Yang, Y., & Hannula, S. P. (2008). Development of precision spray forming for rapid tooling. *Materials Science and Engineering: A*, 477(1-2), 63-68.
- Yarlagadda, P. K., Ilyas, I. P., & Christodoulou, P. (2001). Development of rapid tooling for sheet metal drawing using nickel electroforming and stereolithography processes. *Journal of Materials Processing Technology*, 111(1-3), 286-294.
- Yin, S., Cavaliere, P., Aldwell, B., Jenkins, R., Liao, H., Li, W., & Lupoi, R. (2018). Cold spray additive manufacturing and repair: Fundamentals and applications. *Additive manufacturing*, 21, 628-650.
- Yin, S., Wang, X., Suo, X., Liao, H., Guo, Z., Li, W., & Coddet, C. (2013). Deposition behavior of thermally softened copper particles in cold spraying. *Acta Materialia*, 61(14), 5105-5118.

- Yin, S., Wang, X., Suo, X., Liao, H., Guo, Z., Li, W., & Coddet, C. (2013). Deposition behavior of thermally softened copper particles in cold spraying. *Acta Materialia*, 61(14), 5105-5118.
- Yu, Ning.(2005) Process parameter optimization for direct metal laser sintering (DMLS). PhD Diss.
- Zahiri, S. H., Antonio, C. I., & Jahedi, M. (2009). Elimination of porosity in directly fabricated titanium via cold gas dynamic spraying. *Journal of Materials Processing Technology*, 209(2), 922-929.
- Zahiri, S. H., Fraser, D., Gulizia, S., & Jahedi, M. (2006). Effect of processing conditions on porosity formation in cold gas dynamic spraying of copper. *Journal of thermal spray technology*, 15(3), 422.
- Zaragoza-Siqueiros, J., & Medellín-Castillo, H. I. (2014, November). Design for rapid prototyping, manufacturing and tooling: Guidelines. In *ASME International Mechanical Engineering Congress and Exposition* (Vol. 46438, p. V02AT02A013). American Society of Mechanical Engineers.
- Zhang, D., Shipway, P. H., & McCartney, D. G. (2005). Cold gas dynamic spraying of aluminum: the role of substrate characteristics in deposit formation. *Journal of thermal spray technology*, 14, 109-116.
- Zhao, Z. B., Gillispie, B. A., & Smith, J. R. (2006). Coating deposition by the kinetic spray process. *Surface and Coatings Technology*, 200(16-17), 4746-4754.
- Zhou, J. G., Kokkengada, M., He, Z., Kim, Y. S., & Tseng, A. A. (2004). Low temperature polymer infiltration for rapid tooling. *Materials & design*, 25(2), 145-154.
- Ziemian, C. W., Sharma, M. M., Bouffard, B. D., Nissley, T., & Eden, T. J. (2014). Effect of substrate surface roughening and cold spray coating on the fatigue life of AA2024 specimens. *Materials & Design* (1980-2015), 54, 212-221.
- Ziemian, C., Sharma, M., & Ziemian, S. (2012). Anisotropic mechanical properties of ABS parts fabricated by fused deposition modelling. *Mechanical engineering*, 23, 159-180.



**APPENDIX – A**

**TECHNICAL SPECIFICATIONS OF HVS-1000BVM HARDNESS TESTER**

---

Measuring range	5-3000 HV
Test force	10 to 1000 gmf
Hardness scale	HV0.01, HV0.025, HV0.05, HV0.1, HV0.2, HV0.3, HV0.5, HV1
Minimum scale value of the optical micrometer	0.01 $\mu$ m
Measuring range	200 $\mu$ m
Depth of throat	110 mm
Precision confirms	GB/T 4340.2, ISO 6507-2 and ASTM E384

## APPENDIX – B

### TECHNICAL SPECIFICATIONS OF SURFACE ROUGHNESS TESTER

---

#### Specifications of Surface Roughness Tester

<b>Speed</b>	<b>Measuring: 0.25mm/s, 0.5mm/s</b> <b>Returning: 0.8mm/s</b>
Measuring range	12.5 mm (x-axis)
Mass	190gm
Standard probe	Code No. 178-395
Type	Inductive
Stylus	Diamond cone
Skid radius	40 mm
Tip radius	2 $\mu$ m
Measuring force	0.75mN
Roughness parameters	R <sub>a</sub> , R <sub>y</sub> , R <sub>z</sub> , S, S <sub>m</sub> , P <sub>c</sub> , R <sub>3z</sub> , mr, R <sub>t</sub> , R <sub>p</sub> , R <sub>k</sub> , R <sub>pk</sub> , R <sub>vk</sub> , M <sub>r1</sub> , M <sub>r2</sub> , A <sub>1</sub> , A <sub>2</sub>
Roughness standards	JIS, DIN, ISO, ANSI
Evaluation length (L)	0.25mm, 0.8mm and 2.5mm

### Surface Roughness Measurement Conditions

<b>Output parameter</b>	<b>Average Surface roughness (<math>R_a</math>)</b>
Transverse length	1.5 mm
Sampling length	2.5 mm
Cut-off length	0.25 mm
Filter	Gaussian
Number of sampling lengths	5
Standard	ISO 4287 (1997)

## APPENDIX – C

### IMPORTANT PROPERTIES OF THE MATERIALS USED IN MOULD

Parameters/ Properties	Nickel	Copper	Aluminium
Symbol	Ni	Cu	Al
Atomic Number	28	29	13
Atomic Weight	58.69	63.54	26.97
Density g/cm <sup>3</sup>	8.90	8.96	2.699
Melting Point, °C	1455	1083	660
Boiling Point, °C	2730	2600	2060
Specific Heat cal/g/ °C	0.105	0.092	0.215
Heat of fusion cal/g	74	50.6	94.6
Thermal Conductivity W/m.°C	91	401	205
Thermal expansion coefficient (25 °C -100°C) m/m °C X 10 <sup>-6</sup>	13.3	17.10	23.10
Tensile Strength- MPa	320	224-314	180
Hardness	42-44 HRC	80-135 HV	51 HV